PolyU Design

# PhD

## THESIS SERIES

LAU MAN LUNG

Fractal Analysis on Movement Variability in Spinal Curvature

2016

# PhD

## 1999–2020 THESIS SHOWCASE

Human posture and movement sensing have become crucial practices in health monitoring, especially with the introduction of various types of wearable technology in the recent five years. Utilising computational techniques, this research explores human movement dynamics by using a fractal and multifractal approach. The study obtains knowledge from the movement data extracted from non-invasive optical motion capture techniques and analyses the representation of physiological signals on spinal curvature movement. Design criteria have been derived for the wearable sensing devices in monitoring applications. This thesis develops a framework that investigates the small and large local scale fluctuations within physiological signals' temporal dimension along the spine. The findings contribute to the understanding of human movement and demonstrate the implication of the technical results on wearable technology design. In general, this research provides insights into how computational techniques can be used to develop wearable design applications, with considerations of both technology and interaction design aspects.



School of Design,
The Hong Kong Polytechnic University
PhD 2020.

Original copy: https://theses.lib.polyu.edu.hk/handle/200/8553

# FRACTAL ANALYSIS ON MOVEMENT VARIABILITY IN SPINAL CURVATURE

LAU MAN LUNG

Ph.D

THE HONG KONG POLYTECHNIC UNIVERSITY

2016

The Hong Kong Polytechnic University

School of Design

# Fractal Analysis on Movement Variability in Spinal Curvature

LAU MAN LUNG

A thesis submitted in partial fulfillment of
the requirements for the degree of
Doctor of Philosophy

March 2015

# Certificate of Originality

I hereby declare that this thesis is my own work and that, to the best of my knowledge and belief, it reproduces no material previously published or written, nor material that has been accepted for the award of any other degree or diploma, except where due acknowledgement has been made in the text.

_____

Student Name: Lau Man Lung

Date: 30 MAR 2015

# Abstract

Human posture and movement sensing has become a crucial practice related to health monitoring, no matter for adults or children, especially with the introduction of various types of wearable technology in recent five years. The human movement acquisition process has become portable compared to traditional laboratory conditions. Although the business of wearable technology has an upward trend for the near future, research on human movement and the design requirements and criteria for using wearable technology remains limited.

Although it looks easy to sit in the upright position, numerous researchers have tried to understand the complexity of human posture behind. In static conditions, the human upright posture exhibits an everlasting oscillatory behavior of complex nature, called the postural sway. Variability exists in the movement patterns.

The exploration of the dynamics, physiology, and sensory motor control of human posture plays a crucial role in numerous areas of science. It is about the understanding of physiological signals generated by human movement. The understanding can then be applied to health, clinical, and medical applications. Issues related to pain are essential topics among those major applications. Through the understanding of human movement, preventive or monitoring measures are possible. Physiological signals have been extensively investigated to produce data

that enable various types of analysis. These analysis techniques can then be designed for use by consumers to manage their health through monitoring applications by using wearable sensing devices.

The conventional practice in analyzing human movement through the application of wearable sensing technology is to use descriptive statistical methods to describe the data. The methods summarize data samples, for example, central tendency and dispersion, rather than use the data to obtain further understanding. However, without the understanding of interdependency and the short- or long-range correlation of human movement, the conventional practice is inadequate to explain the complexity of physiological signals.

The analytical approach has also been used to reveal the complexity of the physiological system. This approach identifies appropriate sub systems to separate the physiological system into smaller components to reveal parts of the structure to understand it. Some examples of this approach include inverted pendulum modeling and impulsive muscle control. However, a complete representation of the whole complex physiological system is hardly possible. By contrast, many of these studies rely on invasive instruments, for example, X-ray, to extract measurements or data from the inner body structure of participants. The obvious disadvantage is the harmful effects of radiation when human bodies are exposed to these instruments. The other limitation is the time-varying factor that these instruments are unable to capture.

By realizing that the variability of human movement is an inevitable part of the research, the need for exploring the dynamics of complex human movement becomes essential. From the theoretical point of view, this study explores the dynamics of human movement and correspondingly associated to the motor control mechanism, which is affected by the human perception in sensation, processing, and the activation of movement. This study also contributes to the insight into the practical aspects of human movement in designing and engineering sensing devices. The process involves the design of a physiologically inspired information-processing model and then transforming it into design criteria for interactive technology and applications.

The objective of this study is to explore the dynamics of human movement by using a fractal and multifractal approach. In addition, the study also aims to initiate a nonanalytical framework to understand human movement. The nonanalytical approach on human movement is based on computational techniques to obtain knowledge from the movement data extracted using noninvasive optical motion capture techniques. Some examples of the computational techniques include artificial neural networks, inductive learning, and skill-based expert systems. In this study, the focus on the analysis is based on the representation of physiological signals on spinal curvature movement. Design criteria can then be derived for the wearable sensing devices targeting monitoring applications.

The research is conducted starting with the method and procedure in the collection of experimental human movement on the basis of the static upright sitting posture,

and then with the transformation of data for later analysis. The process then involves the in-depth analysis of the signals from structural investigation and evaluation regarding noise-like properties. The fractal analysis is adopted to reveal the existence of fractal structure and knowledge on the fluctuation of the underlying variations in movement performance. This is the first major achievement in this study. To our knowledge, this approach is the first attempt to be adopted in the analysis of static movement in spinal curvature.

The research then involves a multifractal analysis on the exploration of variation space. Multifractality structure can be identified based on the experimental set of participants. The structure is reflected by the multifractal spectrum with parameters on the scaling exponent and singularity dimension, together with the width, height, and shape. These parameters are the major research findings that describe the variation of the dynamic structure according to the movement performance. These findings are analyzed, compared, and ranked across participants within the experimental set. It can be found that there exists consistency and variation among participants. The consistency suggests that the multifractality structure is common among captured movement. The variation is applicable in differentiating various characteristics of participants.

To further investigate and validate the dynamic properties of cervical movement, correlation analysis is conducted in relation to neck performance and pain issues. The Neck Pain and Disability (NPAD) scale, which is a proven neck pain instrument for clinical use, is adopted. Results show that there exist groups of properties that

describe the correlation across various dimensions between the dynamic properties and the NPAD scale. The analysis findings are then described according to the variation of the level of spinal curvature movement. The variation is further associated with motor strategies and neural activities.

On the basis of the findings, the implication on the design criteria with regard to wearable sensing devices for monitoring purposes is explored. Core features are identified and further explained using a recent example, Fineck. Fineck is a wearable device on the neck to track the head movement. It identifies unfavorable habits and suggests exercises through gaming experience. On the basis of the 12 attributes defined in the fundamental guidelines for designing wearable systems, the applicability of the neck movement monitoring purpose is investigated. Criteria on the motion characteristics for the design of motion-sensing devices are considered by illustrating the analysis results qualitatively through neck movement sensing. Other design challenges from the aspects of interface and interaction experience in wearable technology are also investigated.

In this study, the major and original contribution is the framework developed to investigate the small and large local scale fluctuations within the temporal dimension of physiological signals along the spine. The findings contribute to the understanding of human movement. This study presents the implication of the technical results on the design of wearable technology. It includes the illustration of the design aspects of key features for interactive applications, wearability attributes, the criteria for sensing, and the experience in wearable interfaces. This research

provides insights into the guidelines on how computational techniques can be used for the development of wearable design applications, with considerations of both technology and interaction design aspects.

# List of Publications

[1] Lau, N., Choy, C., & Chow, D.H.K. (2012). Fractal analysis design for distinguishing subject characteristics on motor control of neck pain patients. In M. Alricsson (Ed.). Musculoskeletal Disorders (pp. 51-66). Croatia: Intech.

[2] Lau, N.M.L., Choy, C.S.T., & Chow, D.H.K. (2015). Identifying multifractality structure on postural sway. Journal of Ergonomics 5(2), 1000137.

[3] Lau, N.M.L., Choy, C.S.T., & Chow, D.H.K. (2015). Revealing control mechanism from multifractal analysis on physiological signals. IEEE International Conference on Fuzzy Systems and Knowledge Discovery, 1210-1216.

[4] Lau, N.M.L., & Chow, D.H.K. (2015). Dynamic characteristic analysis of spinal motor control between 11 and 15 year-old children. Motor Control. (in press)

[5] Lau, N.M.L., Choy, C.S.T., & Chow, D.H.K. (2016). Revealing control mechanism from multifractal analysis on physiological signals. Journal of Computational and Theoretical Nanoscience. (in press)

# Acknowledgement

I would like to express my special appreciation and thanks to my supervisor Dr. Clifford Choy; he has been a wonderful mentor to me. I thank him for encouraging me in my study and for allowing me to grow in the research path. His advice on this research and on my career is priceless. I also thank my cosupervisors, Prof. Daniel Chow and Dr. Jackie Kwok, for their continuous support and guidance in my research. I especially thank Mr. WS Leung for his engineering support at the motion capture studio during the experiments.

Special thanks to my family: Words cannot express how grateful I am to my sister, mother, father, mother-in-law, and father-in-law for all their sacrifices. Their care and prayers sustained me. I also thank all my friends who supported me in writing and encouraged me to strive for my goal. Finally, I express appreciation to my beloved wife, Debby Leung, and precious little son, Ives Lau, who gave me tremendous care and ongoing support.

# Table of Content

# List of Figures

# List of Tables

# Chapter 1.
# Introduction

Wearable technology has an upward trend now and for the near future. Human posture and movement sensing has become a crucial practice related to health monitoring. The human movement acquisition process has become portable compared to traditional laboratory conditions. However, the research on human movement in relation to motor control and the design requirements and criteria for using wearable technology remain limited.

Although it looks easy to sit in the upright position, researchers have tried to understand the complexity of human posture. Posture can be defined as the position of the body and limbs with respect to each other and the environment. Even in static conditions, the human upright posture exhibits an everlasting oscillatory behavior of complex nature, called the postural sway.

To stay in a static equilibrium position, the forces and moments acting on a body must be zero. However, a person cannot sit in static equilibrium; a person must sway. Both intrinsic and extrinsic factors may cause disruptions in the static equilibrium in sitting. Intrinsic factors include the mechanics of muscles, noise, delays, and nonlinearities in the motor control system. Extrinsic factors include external forces acting on the body.

The exploration of the dynamics, physiology, and sensory motor control of human posture emphasizes their importance in many areas of science, such as neuroscience and its clinical applications, physical education, sport, motor development, ergonomics, industrial design, ecology, and adaptive biology. The exploration is basically about the understanding of physiological signals generated

by human movement, and then associates the understanding with healthcare, clinical, or medical applications. A major topic is pain with regard to preventive or monitoring measures.

Physiological signals have been extensively investigated to produce data that enable further analysis; in turn, the data can be used by consumers to manage their health through the application of wearable devices. However, the nature of physiological signals is commonly irregular. A common practice is to use descriptive statistics by calculating the means and standard deviations. This method attempts to characterize the random properties. However, a major issue is the basic assumption. Signals may not be statistically independent of each other. The basic assumption appears to be the mechanism of numerous applications such as wearable sensing technology.

However, if the events are interdependent and have either a short- or long-range correlation, the descriptive statistical approach would be inadequate to explain the complexity of physiological signals. During upright sitting, the postural control system attempts to maintain the body in static posture, in an apparently irregular manner. Variability seems to exist across the movement patterns. Numerous attempts have been made to model the postural control system by using the analytical approach, for example, by using an inverted pendulum to model the postural body mechanism [134], impulsive muscle control activities [135], and a postural controller system with computational noise [136] or biomechanical feedback with scalable gains [137]. In these examples of modeling, the feedback is

continuous and exhibits a closed-loop control mechanism. By contrast, studies have shown that the feedback mechanism is not continuous in time; open- and closed-loop dynamics coexist for postural control [138]. With the realization that variability is an inevitable part of human behavior, the need for integrating this phenomenon of motion control into fractal analysis models by using a nonanalytical approach is essential.

In relation to the investigation of the dynamic properties of spinal movement, correlation analysis is also crucial in revealing the control performance and healthcare issues. The analysis can be described according to the variation in movement. In particular, the fluctuation within the temporal dimension is the major concern.

The technical findings have implications on the design criteria for wearable sensing devices for monitoring purposes and must be explored. Key features and considerations must be identified for guidelines on designing wearable systems for spinal movement monitoring. Criteria on motion characteristics for the design for sensing are also essential as an illustration of the applications, especially in preventive and monitoring healthcare measures, of the analysis results.

## 1.1. Significance of the Research

Statistical physics have been used to study the fluctuations and interactions that occur at the microscopic level. The present theoretical overview introduces fractal formalisms as a necessary extension. However, previous studies have often focused on the coarse movement, for example, stride and the center of pressure. There is no previous finding on the fine movement along the spine.

The significance of this study is to adopt a nonanalytic approach to describe the subtle fluctuations in the upright static sitting posture and to demonstrate the strong connection between static postural control and random walk. The investigation of the fine movement on the spine by using this approach provides insight into the neural control of posture.

In addition, the implication of the technical findings on design aspects is crucial. The objective of the research is to provide supplementary or new requirements and criteria for wearable technology on the basis of the computational framework of spinal movement. The investigation of motion sensing and the computational capability of physiological signals can also provide insights into potential design applications through the technical mechanism of sensory acquisition by using wearable interfaces and interaction.

## 1.2. Motivation of Study

The motivation of the research is two-fold. From the theoretical point of view, it is crucial to understand how complex human movement dynamics emerge across different scales and how these dynamics are related to neural and motor control mechanisms, which are thoroughly affected by the human perception in sensation, processing, and the activation of movement.

The practical aspect of human movement for wearable technology is a necessary topic and highly relevant for the future market as well. This study involves the design process of revealing a physiologically inspired information-processing model, and then transforms it into design criteria, including wearable sensing devices from the engineering perspective, for interactive technology and applications.

At the convergence of research areas, the investigation of mathematics for design and engineering is part of the concept in the recent context—STEM (science, technology, engineering, and mathematics). This research addresses the importance of academic multidisciplinary studies. This study is also about using basic mechanisms in complex analysis and further in design features and criteria for applications.

## 1.3. Aim of Study

The aim of this study include a few areas. First of all, it is to research on the dynamics and numerical modeling of the physiological signals on spinal curvature

during upright static sitting. The dynamics here represent the subtle movement, which is the postural sway, during a static body posture. The numerical modeling involves time-stepping procedure to obtain the modelling behavior of movement over time.

In addition, the study also aims to initiate a nonanalytical framework to understand human movement. The nonanalytical framework is the approach of giving rise to the knowledge about motor control by mathematics, specifically, fractal analysis, over the movement data.

Finally, using the technical findings, the aim is to apply the knowledge it the design aspects of wearable sensing technology and applications in monitoring movement for preventive measures in healthcare purposes.

## 1.4. Structure of the Thesis

This thesis is organized as follows:

Chapter 1 is the introduction on the research study. The topic is introduced from the research background. On the basis of the limitation of the present research areas, the importance of this study is identified. The motivation of this research is two-fold, with a theoretical point of view and the inspiration to design criteria for wearable applications. The aims of study are subsequently specified.

Chapter 2 is the literature review on the topics covered. The first section is a basic overview of the physiological signal of human movement. This section explains from the anatomical structure to the motor control mechanism, and then the characteristics of stability. Human movement data and the biomechanics behind are also introduced. From the studies, the importance of a numerical model for analyzing the signal is revealed.

The analysis is then introduced from the definition of fractal structure in relation to the human physiological signals. On the basis of the foundation of fractal analysis, a comparative study is conducted to distinguish particular features from various analysis techniques on the basis of mathematical models.

The implication of the research is then introduced by providing a solid background on wearable technology. This links the data collected and the analysis for application. The main focus is on motion-sensing modality in healthcare practice. On the basis of recent technological advances, the types and factors of devices and associated applications are covered. Design considerations on the basis of various technical factors and common user concerns are explained. Appropriate design priorities and settings for solutions during the product definition stage are considered. In the design and development cycle, validation and measurement for variables on the basis of an experimental and statistical setup are described.

In Chapter 3, the initial spinal movement acquisition and analysis are described. This involves the techniques in stabilogram diffusion analysis (SDA). The acquisition of movement data through an optical motion capture experiment is described. The

data are then prepared and adopted for the computational procedures. Numerical results are computed, visualized, and explained. To ascertain that the results from the analysis are dependent on the data acquired rather than on the nature of noise, parameters are evaluated individually to evaluate the influences. Particular fractal characteristics are then applied to differentiate various participant conditions. On the basis of the analysis, limitations of this technique are also identified.

Chapter 4 describes the revised experimental procedure and also the corresponding instruments. On the basis of multifractality and the degree of freedom, multifractal analysis is introduced and the cervical spine region is selected as the later focus. Neck pain assessment questionnaire on the basis of the Neck Pain and Disability (NPAD) scale is selected to evaluate the condition of participants. The procedure then adopts an optical motion session with markers attached to the cervical region. The detailed experimental procedure in capturing the subtle movement is described. The survey on neck pain assessment is then analyzed using descriptive statistics from the participant group on the basis of overall scores and various factors, namely pain, disability, neck-specific function, and emotion and cognitive influences. Results reveal the patterns and the characteristics of individuals from the participant group.

Chapter 5 is the core section on the multifractal fractal analysis on the captured cervical spine data. The beginning of the section defines the calculation in detail. The process starts with preparing the captured data into the appropriate data format in time series. Various characteristics of the data are revealed based on the

types of plots. One of the major concepts behind the computation of the residual is the root-mean-square (RMS) variation. RMS variation reveals the fluctuation with both large and small magnitudes. On the basis of the residual, local detrending is then applied to quantify the invariant structure in scale and to reveal the variations around these trends. Polynomial fitting and residuals are computed, and then detrended fluctuation analysis (DFA) is conducted. DFA reveals the Hurst exponent (H), which indicates the fractal structure of the time series in a single dimension. The characteristic of H is introduced using the association of various types of noise, from white noise to pink noise and to brown noise. The single-dimension fractal structure is subsequently considered in a multiple order statistical moment by the q-th order RMS, which arrives at the multifractal detrended fluctuation analysis (MFDFA). The concept, interpretation, and comparison relative to other noise structures are explained in detail. The multifractal spectrum is then defined as the formalism of multifractality by using various parameters revealed.

On the basis of the MFDFA computation, the results are generated from various perspectives related to participants, support conditions, and feature points. From the statistical analysis results, the ordered sequence of participants shows consistency across various multifractal variables. Subsequently, the results are compared between support groups with respect to whether there is low back support when sitting upright. Results show slight differences as observed from the plots and data; however, the differences are not significant. The calculation of inclined angles on the basis of feature points in cervical regions is compared. By

using the observed changes between these angles against various multifractal parameters, a summary of comparison is provided. Results show that general trends exist across the angles. The time series are validated using a few methods to ensure the accuracy, validity, and reliability of the results; in particular, the distinguished features of the multifractality structure are based on the characteristics of captured physiological data instead of the general phenomenon arising from noise property. The adoption of MFDFA on spine movement is explained. When applying the MFDFA computation process to this domain of physiological signals on cervical spine movement, there are numerous considerations in signal properties, parameter settings, and the interpretation of results. Most importantly, the process cannot be applied blindly without understanding the characteristics of the signals. The observed results, on the basis of various experimental parameters, are explained using the association of multifractality characteristics and possible physiological meaning in relation to human movement, motor control, and neural activity. Comparative analysis is also conducted on other promising examples to indicate the consistency.

Chapter 6 is about the correlation between the results on the multifractality structure and the patterns found in various neck pain assessment factors on the basis of the participant group. Initially, the correlation within the NPAD score factors is analyzed. A significant level of correlation is found between sets of bivariate. Similarly, the correlation within multifractal parameters is analyzed. Results also show correlated bivariate sets between the multifractal parameters. In sum, the

results of these correlations indicate that the parameters selected for analysis are related and consistent. By contrast, these parameters also exist with a considerable space of independency that exhibits various individual properties.

The data on the basis of the results of multifractal parameters and NPAD scores of various factors are put together for correlation analysis. The aim is to identify a possible relationship between neck pain issues and the fractal analysis parameters. This assists with the understanding on possible neck pain issues by using the numerical data captured and computed, and can further serve as a foundation for design and technical guidelines supporting the development of the method for capturing by using wearable devices. Results show that there are relationships between these two sets of variables. Each set of variables individually identifies the correlation value and significance value that can be used to define the priority in the importance or the weighting of each variable within the parameter set. These findings help to obtain the weighting factors for the extraction of variables from participants, that is, the trace of neck pain issues, for the purpose of a definite set of design criteria and movement monitoring by using wearable devices. In the discussion section, the physiological meanings are discussed to explain the findings obtained from the analysis. Limitations are also considered for the extension of analysis.

After the analysis, Chapter 7 explores the implication on the design criteria of wearable devices for health. Key features are identified and further illustrated using a recent example. In-depth design consideration is discussed based on the

fundamental guidelines for designing wearable systems. Considerations for accommodating the analysis results and the adoption of neck movement sensing are discussed in detail. Additional design challenges emerge from wearable technology dealing with human interaction when a computer is fitted in place. A number of major concerns in relation to the user interface, cognitive model, contextual awareness, and adaption to tasks is discussed.

Chapter 8 concludes the whole study by providing a summary on the basis of the research and findings.

# Chapter 2.
# Literature Review

In this chapter, the literature review is based on the topic of this thesis. The first section introduces the physiological signal of human movement. The anatomical structure is described. The motor control mechanism and biomechanical characteristics of movement are then explained. On the basis of the stability and variability of movement, the importance of a numerical model for analyzing the signal is revealed.

In the second section, fractal analysis is defined for applying to human physiological signals. Various promising analysis methods are described and compared to distinguish particular features.

In the third section, the implication of this research is introduced by providing a solid background on wearable sensing technology. This links the data collected and the analysis for application. The main focus is on motion-sensing modality in healthcare practice. Design consideration on the basis of various technical and user factors is explained. Appropriate design priorities and settings for solutions during the product definition stages are introduced. In addition, the systematic methods for the measurement and validation of variables on the basis of an experimental and statistical setup are described.

## 2.1. Physiological Signal

### 2.1.1. Characteristics of the Physiological Signal

Physiological signals from the body are based on the function performed by various physiological systems [10]. Because information is embedded inside the physiological signals, the functional performance and the status of those physiological systems can then be interpreted by extracting data from the signals. The accessibility to these signals is crucial because they directly reflect the internal status of the body (e.g., blood pressure), originating from the body (e.g., infrared radiation), or derived from a sample of tissue (e.g., skin).

Retrieving information can be simply achieved by feeling the pulse. The status on the heartbeat can then be identified. By contrast, it can also be a complex process that requires analysis by using sophisticated machines to reveal the structure of tissue. There are various types of physiological signal depending on the type of energy, namely bioelectrical, biomechanical, bioacoustics, biochemical, bioimpedence, and bio-optical signals. In particular for this study, biomechanical signals are the key components for analysis. This type of signal is generated from the physiological system through mechanical functions. Some mechanical functions include motion, displacement, and pressure, which can further be based on the movement of the chest and respiratory system functions.

### 2.1.2. Movement on Spinal Curvature

#### 2.1.2.1 Anatomical Structure

There are 33 individual bones along the spine. They align stably on top of each other. Connecting them together are ligaments and muscles, which in turn provide the main support for the body through the spinal column, allowing standing upright, bending, and twisting. By contrast, the spinal cord is protected inside the bones. It connects the body to the brain and signals the movement of arms and legs. A healthy spine usually contains sensitive nerves, flexible tendons, and strong muscles and bones.

In the lateral view of the body, the anatomical structure of the spine forms a natural S-shaped curve. Four regions are defined by the structure. The neck is the uppermost part, also called the cervical region. It consists of bones from C1 to C7. The next part is the upper back, also called the thoracic region. It consists of bones from T1 to T12. The lower part of the back is called the lumbar region, with bones L1 to L5. The last part, the lowest, is called the sacral region. It has bones from S1 to S5. Along the spine, the cervical region has a slight concave curve. The thoracic region has a gentle convex curve. The lumbar region has a slight concave curve as well. Finally, the sacral region has a gentle convex curve at the end (Figure 2.1) [139].

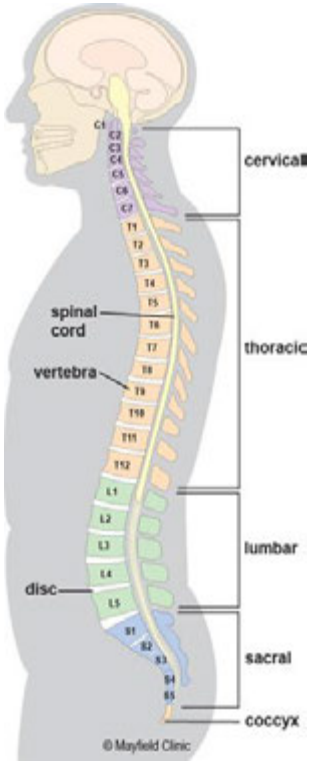


Figure 2.1. Five regions of the spinal column.

The curvature of the spine is then divided into various major regions (Figure 2.2), namely cervical lordosis (OC & C7), upper thoracic kyphosis (C7 & T7), lower thoracic kyphosis (T7 & T12), lower lumber lordosis (T12 & L3), and the pelvic tilt (S1 & vertical).

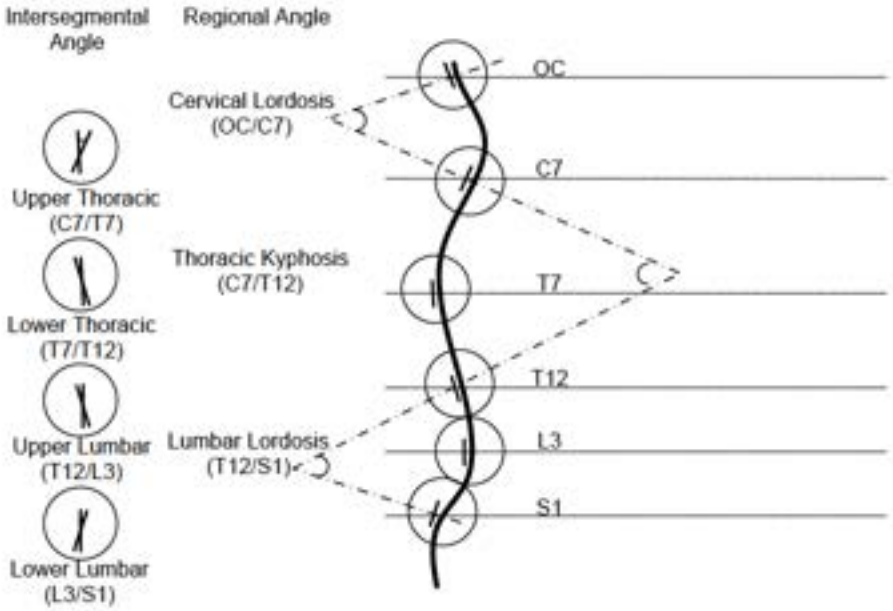


Figure 2.2. Curvature of the spine in various regions.

The weight of the head is supported by the neck. The nerves coming from the brain are protected by the neck and then go to the rest of the body. There are seven bones compose this cervical section of the spine. They are called vertebral bodies. The size of bones gets bigger when they are further away from the base of the skull. The top two segments are responsible for most of the rotation of the cervical spine. The C5-C6 and C6-C7 vertebral bodies at the lower part are responsible for most of the flexion and extension movement.

The upper back has 12 vertebral bodies that make up the thoracic spine. The rib cage is firmly attached to each of the levels. The main function of the attachments is to provide stability while allowing little motion. The rib cage is a strong cage that protects the vital organs inside the upper back, for example, the heart and lung.

Further down is the lumbar spine in the lower back region. Compared with the thoracic spine, it has substantially more motion. There are five vertebral bodies in the lumbar spine, called L1 to L5. These vertebral bodies are the biggest unfused bones along the spinal column. They carry all the weight of the torso. Because of the heavy weight support, this area of the spine has a high risk of injury. In the lower segments, there is a disproportionate amount of motion between L3¬–L4 and L4–L5. Therefore, wear and tear happens often between these two segments. They are the most likely parts to breakdown. The two lowest ends of the lumbar spine, L4–L5 and L5–S1, carry most of the weight, and the risk of degradation and injury is also high here. At the lumbosacral joint, L5–S1, the lumbar spine connects to the sacrum. This joint allows for considerable rotation. It contributes to the swing of the pelvis and hips when walking and running.

Below the lumbar spine is the sacral region. It composes the back part of the pelvis. This bone is shaped like a triangle that fits between the two halves of the pelvis, connecting the spine to the lower half of the body.

#### 2.1.2.2 Motor Control

Motor control is determined by sensory inputs, which involves the somatosensory, visual, and vestibular system. The sensory inputs serve as the stimuli to initiate movements and also provide feedback to modulate movements. The somatosensory system provides positional information of the body and limbs. Kinematic and kinetic

information about joints and muscles are also included. As a result, proprioception of the body can function in place. In addition, the visual system also plays a crucial role to provide necessary information for the correctness in proprioception. Methods for quantifying spinal proprioception have been proposed in recent years. These include the examination of spinal coordination by using a forward-reaching test or stability challenging task [11-14], and a repositioning error [15-17] and electromyographic assessment with perturbation tasks [18-22]. These measurements can provide substantial information on the motor feedback in response to the sensory inputs. Motor control learning is concerned with the changes in the coordination of movement due to pathological issues and ageing. By contrast, the vestibular system provides the information about directional changes on the basis of the movement of the head.

The nervous system, including the brain and spinal cord, interprets the sensory information and commands the musculoskeletal systems to move various body parts. Postural control then attempts to maintain the body in a balanced state. Several analyses have represented it as the balance of a multijoint inverted pendulum [23-25]. The basic idea is to keep the center of mass over the base of support. However, the human postural control system is highly complex with complex interactions between the sensory, nervous, and motor systems. The organization of the feedback control mechanism has been questioned. During postural control, the question is whether the feedback control mechanism is crucial dominantly or only playing a minor role. Some previous studies have suggested that

the feedback control mechanism alone can explain human postural control sufficiently [26]. Others have concluded the importance of the role of predictive mechanisms [27, 28]. Some studies about stance control have concluded that nonlinear mechanisms combining open- and closed-loop control exist [29, 131].

The open-loop system contains instructions for movements that are structured in advance and are executed without regard to the effects they may have on the environment. This control system involves involuntary movements that are not sensitive to feedback or the mechanism for error regulation. One of the key features is that it produces rapid movement, or movements under the condition in which normal feedback sources have been eliminated or disrupted. Attention is not normally allocated to ensure correction in this type of movement. The closed-loop system has feedback, error detection, and error correction as key elements in control. This is usually a voluntary and self-regulating movement by compensating for deviations from the reference position. This control system requires the feedback mechanism that operates from the receptors to the control unit for determining the instruction of movements. It is usually taken place after the open-loop control because the pathway of signals transmitted is substantially longer than that in the open-loop control mechanism. Further analysis has suggested that stochastically driven dynamics can be presented in the system [30].

Previous studies and experiments have found that the human body has various types of response systems, which results in different response times. The reaction can be quick on some types of responses, whereas some may require longer periods

of time. From the literature, there are four types of responses that pass through different response pathways and result in different latency times, as shown in Table 2.1 and Figures 2.3 and 2.4 [132].

Table 2.1. Four types of responses.

| | |
|---|---|
| **M1 response** | 30 to 50 ms latency |
| **M2 response** | 50 to 80 ms latency |
| **Triggered reaction** | 80 to 120 ms latency |
| **Reaction-time response (M3)** | 120 to 180 ms latency |

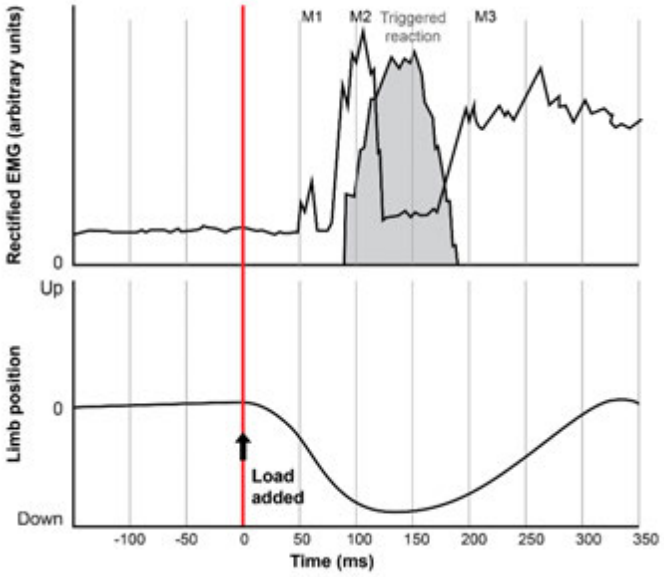


Figure 2.3. Plot on the latency time on the basis of responses.

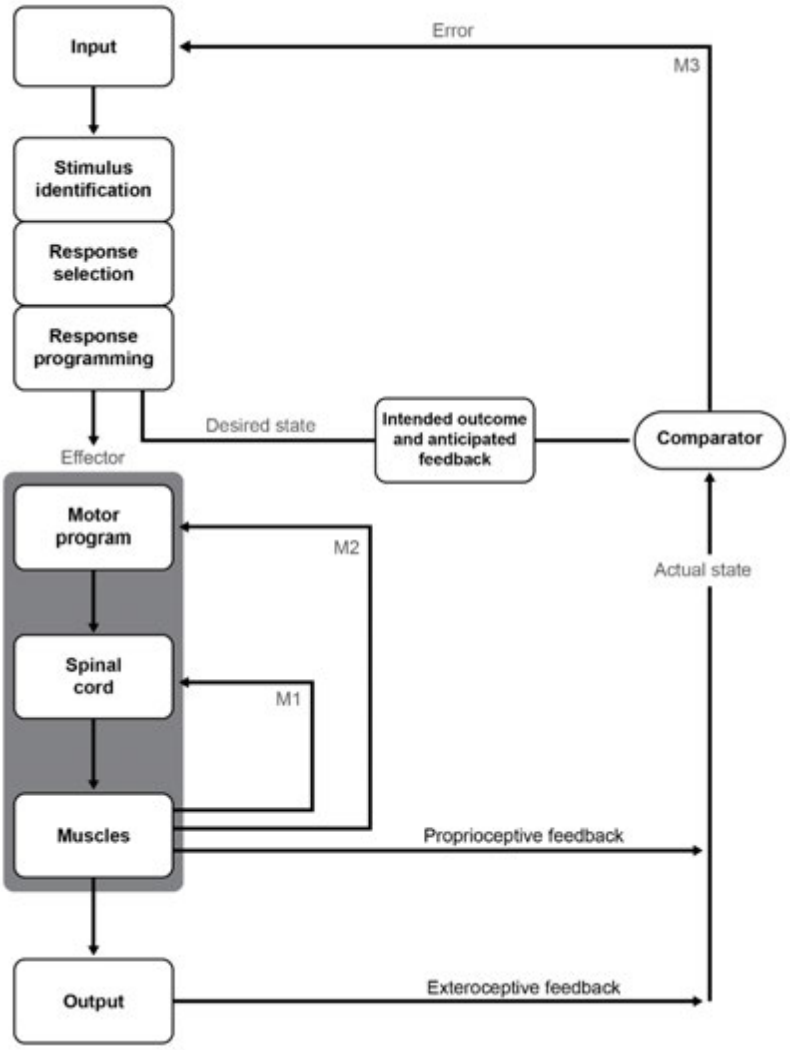


Figure 2.4. Different response pathways.

### 2.1.2.3 Spinal Curvature and Kinematic Measurement

Studies have been conducted to develop various biomechanical models. The spinal curvature has been predicted and quantified. The spine is not a rigid body. It contains nonlinear geometry combining into a multijoint structure. This must be considered when studying the spinal model in a biomechanical approach.

The biomechanical model suggests that there are six degrees of freedom along three dimensions, which are up or down, forward or backward, and left or right. The movement can also be referred to as rotation, translation, flexion or extension, and compression or distraction. Figure 2.5 shows the complete motion segments along the three-dimensional system. It illustrates the displacement and directions of the load by labels. Along the y-axis, the motion segments are (1) compression, (2) tension, (3) left axial rotation, and (4) right axial rotation. Along the z-axis, these are (5) anterior shear, (6) posterior shear, (7) left lateral bending, and (8) right lateral bending. Along the x-axis, these are (9) left lateral shear, (10) right lateral shear, (11) flexion, and (12) extension. Basically, there are two types of movement, namely rotation and translation. Rotation consists of the three axial rotations, that is, (3) and (4) along the y-axis, (7) and (8) along the z-axis, and (11) and (12) along the x-axis. Translation consists of the movement toward or away from the axis, that is, (1) and (2) along the y-axis, (5) and (6) along the z-axis, and (9) and (10) along the x-axis.

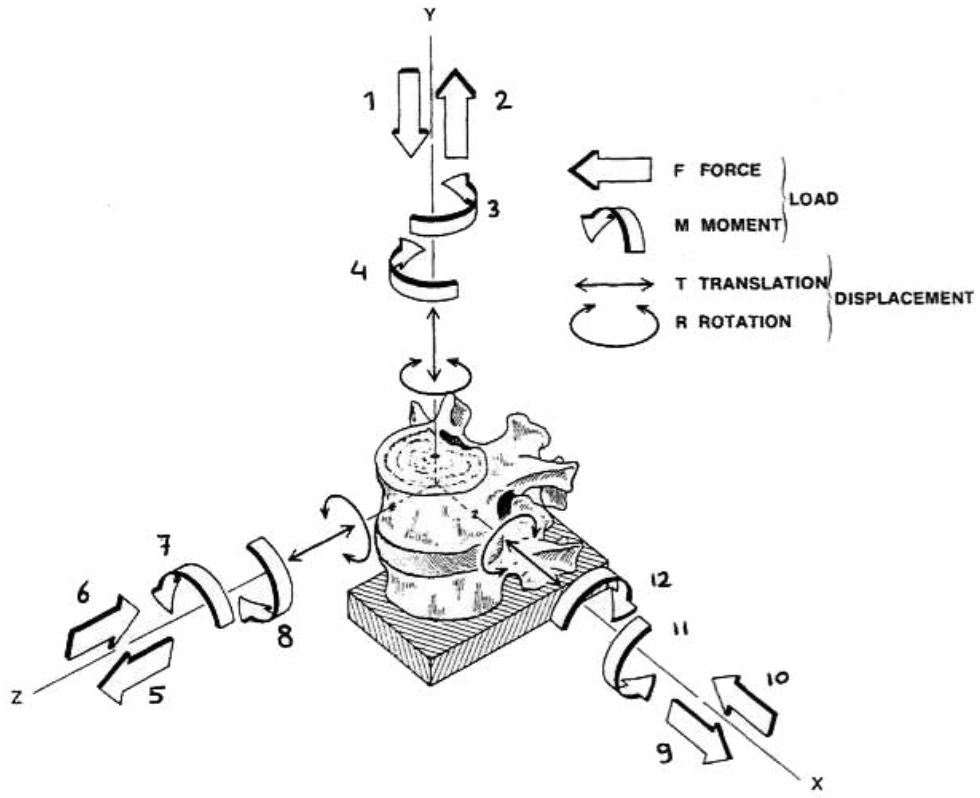


Figure 2.5. Motion segments defined in three dimensional space.

The most common practice for obtaining spinal geometry is to use imaging techniques. These include magnetic resonance imaging (MRI), computer tomography (CT), and X-ray. However, all participants are not recommended for prolonged and repeated exposure because it is invasive. Licensed technicians are needed for the operation of this equipment. For field measurements, these methods are costly and inappropriate.

By contrast, the noninvasive method has the advantage of easily obtaining the measurement of the trunk posture. The measurement can be used for evaluating the spinal geometry. As described in the literature, evaluation of spinal curvature

can be conducted using noninvasive methods. The methods include measurement by using flexible tape or an ultrasonic digitizer, photography or videography on external markers or skin markers, and devices such as an electrogoniometer, accelerometer, or electromagnetic devices. The benefits of noninvasive methods are apparent when compared to invasive methods such as CT and MRI. The noninvasive methods can be used for spinal curvature prediction provided that the accuracy of the device can be ensured. Another criterion is whether these tools or devices can be applicable to the working environment or laboratory settings. Quick measurements that permit screenings of participant groups would be an advantage.

#### 2.1.2.4 Stability and Variability

Spinal stability is the ability for the vertebrae to maintain their posture and limit their relative displacements during physiological loads without producing initial or additional incapacitating, neurological deficit, and deformity [140]. This depends on three functionally interdependent subsystems that limit the excursion of spinal motion segments and maintain the appropriate ratio of neutral-to-elastic zone motion. The three subsystems are the passive subsystem, active subsystem, and neutral subsystem, which can be associated with the schematic view of the musculoskeletal system, the spinal column, and the activation of the active system through neurological control, respectively [141].

Muscular contraction of the trunk and spine muscles provides the active part of stability. The control process is operated under the postural reflexes, which are the neural control subsystem [140]. Regarding the passive part of stability, vertebral bodies, facet joints and their capsules, spinal ligaments, and the passive tension work together to form the musculotendinous units [140]. Derek [142] defined spinal stability as the instance when it is under physiologic loading, when there is neither abnormal strain nor excessive motion in the functional spinal unit. Spinal stability can be maintained by the functional spinal unit, muscular tension, abdominal and thoracic pressure, and rib cage support. It is also a supporting structure of the three-column theory: the anterior, middle, and posterior column.

There is no unified definition of lumbar spinal instability because it has different meanings to different individuals and specialists, for example, bioengineers, clinicians, and radiologists. Some reasonable definitions have been proposed. Holdsworth [143] defined spinal instability as the rupture of the posterior ligamentous complex. It has also been supported and confirmed that spinal instability is the study of the mechanics of spinal injuries in which the rupture of normal spinal ligaments could not be produced by excessive extension or flexion. The implication is that the rupture of the posterior ligamentous complex is not compatible with a stable compression fracture but is pathognomonic of instability initiated by either rotation or translation [144]. Instability has been proposed as an abnormal behavior [144]. Beyond normal constraints, abnormal movement in the motion segment can be characterized through kinematics. The abnormal behavior is

the response to the applied loads. There is damage to the restraining structures, that is, facet joints, discs, ligaments, and muscles. The damage causes the abnormal movement to occur. If any of these structures are damaged, the equilibrium is altered, thus resulting in instability [145]. Studies have also suggested that instability results from the loss of motion segment stiffness [140].

There are two types of postural stability in general. They maintain a state of balance through dynamic or static equilibrium, in which all forces are acting on the body [31]. While progressing through an intended movement, dynamic equilibrium maintains balance. While the body is at rest, static equilibrium maintains the intended position. When the concept of stability is applied to the spine, the intervertebral and global torso can maintain equilibrium [32]. In relation to postural stability, kinematic variability of postural control has also been researched in many studies. The kinematic variance is defined as the disturbances caused by neuromotor or small biomechanical changes that are continuously perturbing the system. Therefore, measured kinematics can be observed as an association with the posture of static equilibrium, related to stability. Substantial information about the postural changes and kinematic variability can then be provided using the previously mentioned measurements on motor feedback. However, in the investigation of motor control, the dynamic features along the time series, particularly the correlation between time points and the kinematic outcomes through serial ordering, are not well considered.

In addition to the concept of stability, regarding the wide range of perceptual and motor functions, all physiological signals exhibit some degree of variability [149]. This variability is often considered as related with stability or the ability of offsetting an applied perturbation. This point of view is also particularly relevant in the studies of patient populations, where a high amount of variability in various motoric functions has been observed. The variability observed in the patient populations is believed to have a negative effect as a result of the pathology in reducing stability. By contrast, the dynamical system perspective has changed the understanding on variability. For example, a healthy norm is observed when the heart rate exhibits variability. The variability causes the body system to be flexible and stable, allowing the heart to recover from applied perturbations. Therefore, a high incidence of death rate is directly related to the high degree of consistency between heartbeats [150].

Studies on variability in the movement sciences have been inspired by the dynamical models and their stochastic extension [151]. On the basis of these theoretical contributions, between the modes of coordination, it is necessary to view normal changes as elements in variability. In a study on the oscillation of fingers, variability was also indicated to maintain the stability of the system. The experiment started with antiphase oscillation at a low frequency. The frequency of oscillation was then gradually increased. The oscillation was found to shift abruptly to the in-phase at a certain critical frequency. By observation, the increase in variability was found to occur before the model phase transition.

Measurements of kinematic variability have been researched in the case of center-of-pressure (COP), including the study of the total path length, root mean square, and ellipsoid area travelled per time unit. It is generally assumed that these measurements on the representation of stability can be used to identify healthy controls from pathological cases [33].

## 2.2. Fractal Analysis

### 2.2.1. Fractal Structure

The term “fractal” was first mentioned by mathematics in the 17th century [37]. The term is based on the Latin adjective “fractus,” meaning “broken” or “fractured.” The geometry in a fractal structure features irregularity at all scales mathematically. In other words, if a small portion of a model were magnified, it would show the same complexity as the entire model.

Fractals can be further classified into two categories, namely monofractals and multifractals, which are characterized by fractal dimension. Fractal dimension is the index that describes the complexity of fractal patterns between changes in detail against scales. Monofractal systems have scaling properties that stay the same across different regions. Multifractal systems consist of differently weighted fractals of different noninteger dimensions, which make them self-similar but in a complex

manner. They are the generalized version of a fractal system with multiple scaling exponents to describe its dynamics. In this case, there exists a continuous spectrum of exponents, also named as a singularity spectrum. The multifractal spectrum identifies the deviations in a fractal structure that consists of large and small fluctuations within the time series.

What does the static spinal curvature movement have to do with fractals? During a static posture, the nervous system, including the brain and spinal cord, interprets the sensory information and commands the musculoskeletal systems to move different body parts. Postural control then attempts to maintain the body in a balanced state. In a static posture, the spinal curvature apparently stays in a definite position (Figure 2.6).

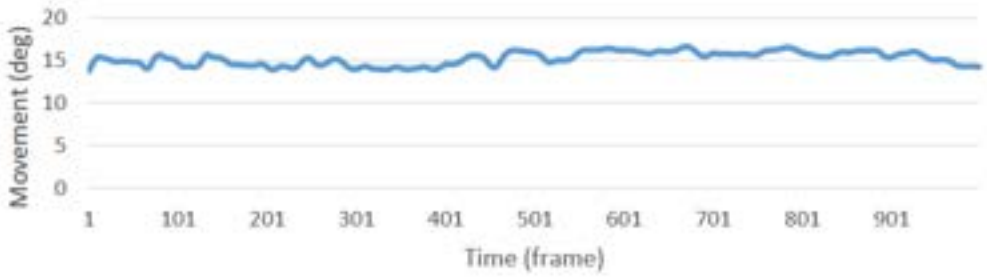


Figure 2.6. Spinal curvature in a balanced state.

At first inspection, the posture along the spine appears to be a static and stationary process. However, when we look into it at the microscopic level of movement, as

shown in Figure 2.7, statistics show that there is variance and subtle fluctuation along the time.

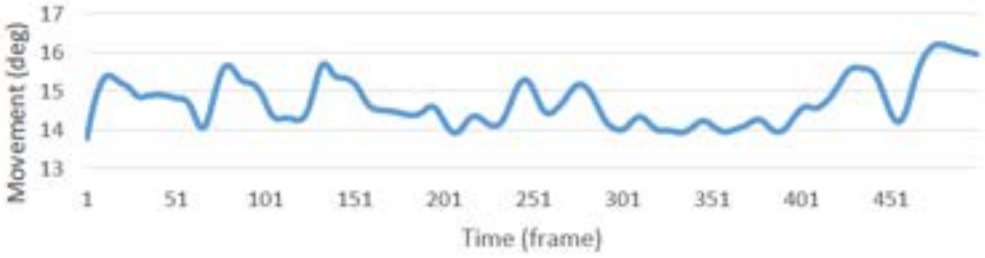


Figure 2.7. Microscopic level of spinal movement.

The variations within a static posture may be considered as only the representation of uncorrelated white noise combined on a static and stationary series of data. This assumes that these large and small fluctuations are noise. The other possible explanation is that there exist finite range correlations in space. In other words, the current data are influenced by the near and most recent data. However, the fluctuations are random in the long term. Similarly, the fluctuations in the spinal curvature consist of long-range correlations. In this case, the spinal curvature data at any instant are influenced by relatively remote intervals, and the influence would decay in a scale-free manner.

Several biomechanical studies have evaluated postural sway by using descriptive statistics. The dynamic characteristics are ignored, for example, correlations between adjacent data in terms of the magnitude and direction of displacements, and the temporal ordering of the data series. Most of the postural control

investigations for scientific and clinical purposes have usually focused on analyzing the variety of external perturbations and the corresponding response by the human body. Although this approach in analyzing the response enables the examination of the characteristics and relationship between the input and output of different closed-loop feedback systems, the stabilizing mechanism or the steady-state behavior from the possible open-loop control schemes of the human body under an undistributed condition is not explicitly considered.

### 2.2.2. Detrended Fluctuation Analysis

In biomedical time series, fractal structures often can be revealed within a wide range of physiological phenomena. Detrended fluctuation analysis (DFA is a useful method to extract the range correlations and determine the fractal scaling properties in time series of noisy and nonstationary characteristics. It has been widely applied to diverse fields such as heart rate dynamics [38, 51], human gait [39, 52], neuron spiking [40], DNA sequences [41], economic time-series [42], and earthquake signals [43]. DFA has limitation in accounting for a single scaling exponent, which corresponds to monofractal scaling behavior.

An accumulated difference from the mean value is represented as follow:

$$X(k) = \sum_{i=1}^{k} [x(i) - \bar{x}]$$

where x(i) is the time series with N numbers of data points; and $\bar{x}$ is the mean value of the time series.

This integration turns the original time series into a self-similar process. The measurement on the vertical characteristic scale is computed based on the integrated time series. The integrated series is divided into nonoverlapping intervals, each with a length of n. A least square line is then fit to the data of each n length interval. This represents the trend in each particular interval. The detrending process is completed by subtracting the local trend $X_n(t)$ given by the regression from the integrated time series X(t). Regarding this integrated and detrended time series, the characteristic size of fluctuation is given by

$$F(n) = \sqrt{\frac{1}{N}\sum_{k=1}^{N}[\,X(k) - X_n(k)\,]^2}$$

The computation is based on each given interval length n, and is repeated over all possible interval lengths. This is to provide a relationship between interval length n and F(n). By convention, approximately 10 data points are suggested to be the shortest length, and N/2 is selected to be the largest. In general cases, when the interval length n increases, F(n) increases and has a power law relationship with n.

$$F(n) = a\, n^{\alpha}$$

where a is a constant and α is the scaling exponent. By taking log at both sides, it becomes

$$\log F(n) = \alpha \log n + k$$

where k is a constant. In general, it has a value between 0 and 1.5. In an uncorrelated random process, α has a value of 0.5. It is also denoted as white noise. A value of 1.0 represents pink or 1/f noise. This is a boundary value between stationarity and nonstationarity, represented by having α smaller than 1.0 and larger than 1.0, respectively. A value of 1.5 represents a Brownian motion. Mathematically, a higher value is also possible. For persistent series, the value can reach an upper bound at 2.0. However, the reliability regarding the high exponents is yet to be confirmed. The relationship between exponent H and α is as follows:

$$H = \frac{(2\,\alpha - 1)}{4}$$

### 2.2.3. Multifractal Detrended Fluctuation Analysis

Numerous geophysical and medical patterns do not exhibit only in a monofractal structure. Different scaling exponents must be extracted for different parts of the series [44] to reveal the details of the system structure. Therefore, multifractal analysis is used. The difference between monofractal and multifractal time series is illustrated in Figure 2.8 [68]. In the monofractal time series (top), there are three consecutive segments of data. The three segments have the same strength of temporal correlation, and the size of the scaling exponent is the same. In the multifractal time series (bottom), the scaling exponent varies over time. It reflects

the changing levels of correlation among the participating processes in each segment.

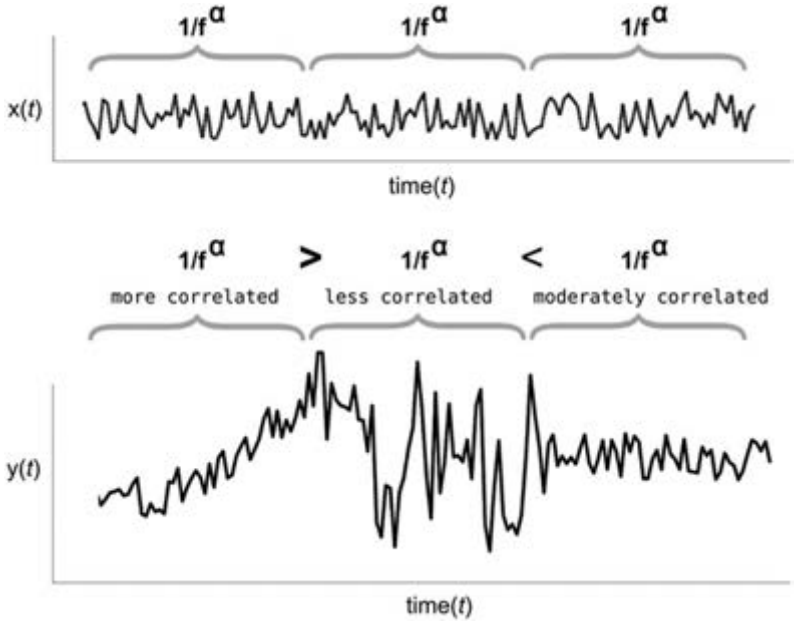


Figure 2.8. Difference between monofractal (top) and multifractal (bottom) time series.

Multifractal detrended fluctuation analysis (MFDFA is used to estimate the multifractal structure within a time series. As a generalization of the standard DFA, it was first formulated by Kantelhardt et al. [45]. It has been applied successfully to study the multifractal scaling behavior of various nonstationary time series [46-48]. During upright standing, it has been suggested that fluctuations of COP are multifractal, not monofractal [29, 69, 70]. The implication of multifractality suggests that intended quiet standing and purposeful dynamic touch are alike in that both involve interactions across many different time scales. The movement by itself relies

on a nested structure of motions in which larger motions contain small motions and smaller motions support and constrain larger motions [71, 72]. Postural sway is the term to describe movement in the case of quiet standing. This sway comprises nested fluctuations at multiple time scales [70]. The nesting of COP fluctuations shapes the manner in which mechanical perturbations or deformations propagate through the body's tissues. Mechanical information is grounded in the correlation of fluctuations over shorter time scales with fluctuations over longer time scales. Perceptual intention can be interpreted as the long-range fluctuation of the haptic perceptual system that spreads across scales into the scales of COP fluctuations. In other words, whether the perception is intentional or unintentional, it is understood to produce a particular variation as a nested dependence of short-scale fluctuations within long-scale fluctuations. Analysis also suggests that human movement exhibits multifractality in gait [58, 74].

In the study of human movement variability, the multifractal spectrum is identified from the temporal variation of local scaling exponents. It is illustrated by the COP variations during quiet and relaxed standing. Another research successfully demonstrated the difference in multifractal parameters in time series of human gait between normal and pathological participant sets. It was observed that the origin of multifractality is primarily about the long-range correlation. The normal participant set exhibited a higher degree of multifractality than did the pathological participant set. This infers that neurodegenerative diseases can cause an alteration in the human gait in terms of fractal dynamics. This explains the weakening and

impairment of neural control on locomotion. The results are also consistent with previous studies on gait rhythm, stride interval, and alterations in physiology correlated with aging and disease [75-77]. Because of neuronal deterioration, a network of neurons controlling the human gait is expected to be less correlated in a diseased set than in a healthy neuronal network [78].

The multifractal analysis is useful in the investigation of variability in the recurrence time of cyclical movement such as the human gait, the bimanual coordination of multiple limbs, segments or joints, and variability in the performance parameter of a movement task. On the basis of these previous studies on multifractal analysis on human movement, this study attempts to extend the application to human movement variability in spinal movement during quite sitting. The variability behavior is similar to that of COP during quite standing. The objective is to introduce and adopt the multifractal analysis method to define the multifractal parameters between temporal scales in spinal movement variability.

### 2.2.4. Comparison to Other Analysis Models

Regarding biological time series, various research analyses have been attempted to reveal the dynamic features [49, 50]. To extract the hidden fractal properties, there are other sets of analysis methods. In general, the various methods attempt to access the dispersion or displacement of variables in multiple temporal intervals of various lengths. Various methods are different in a number of aspects.

#### 2.2.4.1 Hurst Rescaled Range Analysis

Hurst rescaled range analysis (HRRA) is one of the most classical methods. It has been commonly used to extract fractal features in economics [154], geophysics [155], biology [156], and motor control [157]. Similar to the previous method mentioned, this approach also starts from locally integrated time series for each interval. The assessment is then based on the range of displacement. Given a time series with an N number of data, x(t) is the function retrieving the data at any particular time t. The time series are divided into nonoverlapping intervals of length n. The integrated series X(t, n) can then be calculated as follows:

$$X(t,n) = \sum_{k=1}^{t} \{x(k) - \langle x \rangle_n\}$$

where $\langle x \rangle_n$ is the local average of data at the interval of length n:

$$\langle x \rangle_n = \frac{1}{n} \sum_{t=1}^{n} x(t)$$

The range $R_n$ for each interval is then defined as the difference between the maximum and minimum values of the integrated series X(t, n):

$$R_n = \max[\, X(t,n) \,] - \min[\, X(t,n) \,] \quad \text{where } 1 \le t \le n$$

The local standard deviation $S_n$ of the entire time series is computed as

$$S_n = \sqrt{\frac{1}{n}\sum_{t=1}^{n}[x(t) - m_n]^2}$$

where $m_n$ is the mean for each interval with length n:

$$m_n = \frac{1}{n}\sum_{t=1}^{n} x(t)$$

The normalization process then has the range divided by the local standard deviation. This computation is conducted using the possible interval lengths. Ten data points are suggested for the shortest length, and N/2 is the largest. At the final stage, the average of the rescaled range R/S is taken for each interval length n. Power law is then the relationship between R/S and n, as follows:

$$R / S = (k\, n)^{H_{R/S}}$$

where k is a constant, and n is the length of interval.

The slope of the log-log plot on R/S is then estimated using $H_{R/S}$ as a function of n. The value of $H_{R/S}$ falls between 0.0 and 1.0. A white noise is indicated by an $H_{R/S}$ value of 0.5, and Brownian motion is represented by an $H_{R/S}$ value of 1. Compared to the SDA mentioned in the next section, there is a 0.5 shift in the value. Therefore, the exponent H and $H_{R/S}$ have a relationship as follows:

$$H = H_{R/S} - 0.5$$

The interpretation of the exponent H of HRRA has a 0.5 value shift compared to the exponent H of SDA. For antipersistent behavior, it can be represented by H < 0.5. However, because the HR/S value falls between 0.0 and 1.0, H is bounded by 0.5 as

the highest. Therefore, HRRA cannot be used to represent persistent biological series.

#### 2.2.4.2 Stabilogram Diffusion Analysis

Stabilogram diffusion analysis (SDA) has been proposed for analysis during unperturbed stance by using COP trajectories [29]. This method follows the Brownian motion study by Einstein (1905). The main concept is the relationship of paired points separated in time (Figure 2.9) [29]. In relation to the time interval Δt, the mean square displacement $\langle \Delta i^2 \rangle$ is defined as follows:

$$\langle \Delta i^2 \rangle = \langle \Delta x^2 \rangle + \langle \Delta y^2 \rangle$$

where Δi is the displacement between two data points with x and y coordinates, and $\langle \dots \rangle$ represents the method of obtaining the average over time. $\langle \Delta i^2 \rangle$ is computed by obtaining the average on the square of the displacement between pairs of data points. These points are separated in time with a particular time interval Δt.

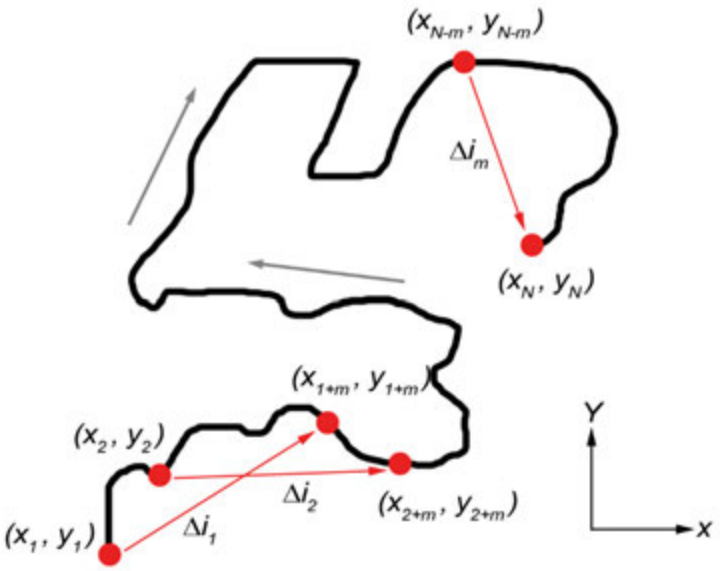


Figure 2.9. Relationship of paired points separated in time.

For each time interval, the mean square displacement calculated as

$$\langle \Delta i^2 \rangle_{\Delta t} = \frac{\sum_{j=1}^{N-m} \left(\Delta i_j\right)^2}{N - m}$$

where Δt indicates the time span over an m number of data, and N is the total number of data points. It can then be plotted against the time interval.

$$\langle \Delta i^2 \rangle = 2\, D\, \Delta t$$

where D is defined as the diffusion coefficient. The concept from Einstein has been further generalized in relation to stochastic processes [53]. This specific process is named as fractal Brownian motion (fBm). By putting forward the relationship between the mean square displacement and time interval into a scaling law, it becomes

$$\langle \Delta i^2 \rangle \sim \Delta t^{2H}$$

where H is defined as the scaling exponent. It has a value between 0.0 and 1.0. Subject to the log-log plot of the mean square displacement against the time interval, the scaling exponent H can then be calculated. One of the essential features of fBm is its exhibition of long-memory processes. There exists a long-term correlation between past and future movement. That means each data value has a dependency on the past history of the data in the series. In statistical analysis on the correlation, the fluctuation on average at various time scales is similar. Regarding the interpretation of the scaling exponent H, white noise is indicated by a value of 0.0. It consists of a random signal with a flat power spectral density. The Brownian motion is represented by a value of 0.5. For H > 0.5, this indicates the phenomenon in which the movement direction of the current and future tends to be positively correlated. This exhibits persistent behavior. A value of H < 0.5 exhibits antipersistent behavior. This means the movement direction of the current and future tends to be negatively correlated.

By contrast, there is a bilinear behavior as observed from the plot. It consists of a short-term and long-term value of the scaling exponent H, named as $H_s$ and $H_l$. The transition point distinguishing the two is named as critical point. It represents a particular time interval $\Delta t_c$ and is defined as the intersection between the two lines in the two regions of the plot. An automatic determination method has been proposed to identify this critical time point [54]. The method is based on the logarithmic plot of a pure stochastic process, which is presented as a straight line,

and the logarithm of the resultant curvature-diffusion plot. The distance between the two plots initially increases if the signal variability exhibits persistent behavior. By contrast, the distance between the two decreases when the signal variability exhibits antipersistent behavior. Between the short-term and long-term region, there is a maximum difference between the two plots. It indicates the transition separating the signal into persistent and antipersistent behavior. Therefore, this point is named as the transition point in the plots.

Referring to the analysis of COP trajectories during unperturbed stance, it has been found that the critical time is approximately at one second. This result is consistent with the findings obtained from analytical analysis by using an inverted pendulum model on the basis of active balance experiments [55].

The plot on SDA features a two-region structure, which exhibits the persistent and antipersistent behavior. This, in turn, is associated with the open- and closed-loop control mechanism. The short-term region is suggested to consider persistency as information gathering during exploratory processes, whereas the long-term region is suggested to consider antipersistency as the adjustment on the basis of obtained information during performance processes [56]. Later studies have also shown the evolution and association of the parameters within this analysis model by using its exhibition of short- and long-term regions and coordinates of the inflexion point. This can be observed from studies on human factors such as vision, learning, and haptic touch [56, 57].

#### 2.2.4.3 Adaptive Fractal Analysis

A recent fractal analysis technique is called adaptive fractal analysis (AFA) [118, 119]. It uses an adaptive detrending algorithm to extract globally smooth trend signals from the data and then analyzes the scaling of the residuals to the fit as a function of the time scale at which the fit is computed. There are many aspects of AFA that are more similar to DFA than other methods; for example, H estimated using DFA and AFA does not saturate at 1. Despite the similarities between the methods, AFA exhibits some advantages over DFA. For example, AFA can deal with arbitrary, strong nonlinear trends, whereas DFA cannot. As such, AFA has a more favorable resolution of fractal scaling behavior for short time series.

A crucial first step in fractal analysis is to determine the basic type of signal. Simple plotting along time series can help to serve a first pass on whether a preprocessing stage of integrating the data is required. Integration is required if the data are a stationary, noisy increment process, such as fractional Gaussian noise, or called white noise. Integration is not suggested if the data are a nonstationary random-walk process, such as fractional Brownian motion, or called brown noise. The consequence is crucial with respect to the Hurst exponent (H). H estimates can be artificially inflated by the integration of a signal that should not be integrated. For example, a lack of integration when it should be performed could suggest the appearance of multiple scaling regions separated by a crossover point when only one scaling region actually exists.

Given the time series signal, we first identify a globally smooth trend signal, illustrated in Figure 2.10, which is created by patching together local polynomial fits [120]. This is one of the primary differences between DFA and AFA. DFA does not involve the creation of a globally smooth trend, and instead relies on discontinuous, piece-wise linear fits. This procedure means that local features of the data are created using a simple polynomial function. Small segments of the time series can be approximated reasonably by adjusting the parameters of a polynomial regression model. The optimal fitting polynomial of order M is identified based on standard least squares regression in which the coefficients of the polynomial model are adjusted until the polynomial fits the data with the least amount of residual error. Typically, M should be 1 or 2, that is, a linear or quadratic function. The goal is to capture any relatively global trends in the data while leaving enough residual variability for further analysis.

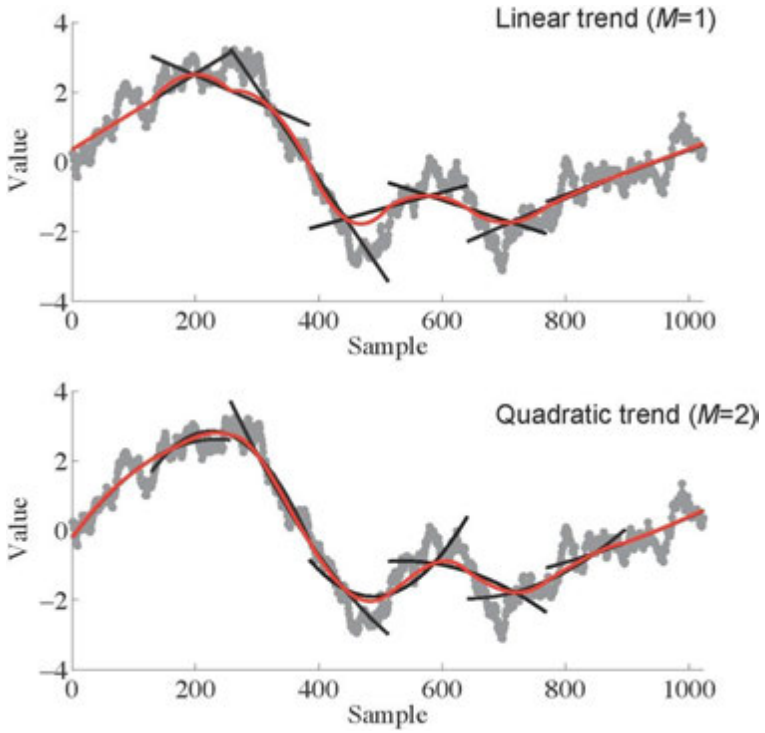


Figure 2.10. Illustration of a globally smooth trend signal.

The local fits must then be stitched together to provide a smooth global fit for the time series. This is another major difference from DFA, in which local polynomial fits are disconnected with each other. The fit to overlapping regions is created by taking a weighted combination of two adjacent regions to ensure that the local fits are continuous and differentiable:

$$y^{(c)}(l) = w_1\, y^{(i)}(l+n) + w_2\, y^{(i+i)}(l)$$

where l = 1, 2, …, n + 1; $w_1$ = [ 1 – (l – 1) / n ]; and $w_2$ = (l – 1) / n. According to this weighted combination, the weights decrease linearly with the distance between the point and the center of the segment. This ascertains that the boundary points are smooth and without any jumps or discontinuities around neighboring regions.

Moreover, this can enable the derivatives to occur at both the left and right hand side of the boundary. Moreover, this scheme can work with any arbitrary signal without any prior knowledge of the trends in the data, which is the reason that it can deal with arbitrary, nonlinear trends.

The data are then detrended by removing the global trend signal that was created. The detrending method in both AFA and DFA is achieved locally over windows of varying lengths but not on the entire time series. The residuals of the fit of the data to the trend signal are identified by subtracting the global trend from the original time series. These steps are then repeated for a range of time scale values, with a chosen minimum and maximum, as well as a chosen size of time steps.

The relation between the variance of the magnitude of the residuals and the window size is then examined. For a fractal process, the variance of the residuals scales with the window size.

$$F(w) = \left[ \frac{1}{N} \sum_{i=1}^{N} ( u(i) - v(i) )^2 \right]^{1/2} \sim w^H$$

where F(w) is the variance of the residuals, w is the window size, u(i) is the original trend, v(i) is the global trend, and H is the power raised by w and is proportional to F(w).

Fractal scaling can be qualified using the slope of a linear relation in the logarithmic plot of both functions.

$$\log_2 F(w) = H \ \log_2 w$$

This slope provides an estimate of H. When applying to the data, if fractal scaling is present, it may be limited to a range of time scales. This is to identify regions where linear scaling might by present in the logarithmic plot. As often occurs with empirical data, some of the time series yield slightly curved functions and have cut-off edge effects. Visual inspection may suggest two or even three distinct regions of linear scaling. The first region denotes the fast time scale. The second region denotes the intermediate. The last region denotes the slow time scale. This is illustrated in Figure 2.11 as AFA plots for the time series by using an experimental example [120]. Briefly, the experiment was conducted by a single participant who repeatedly performed a cognitive task over the course of multiple experimental sessions. The duration of the temporal interval was estimated. Visual inspection of the AFA plots suggested two distinct regions of linear scaling. One shorter region was for a low w and fast time scales; a longer region was for a higher w and slow time scale. This occurred in both with and without feedback conditions. The finding was expected based on previous studies that have revealed $H < 0.5$ on the fast scales and $H > 0.5$ on the slow scales.

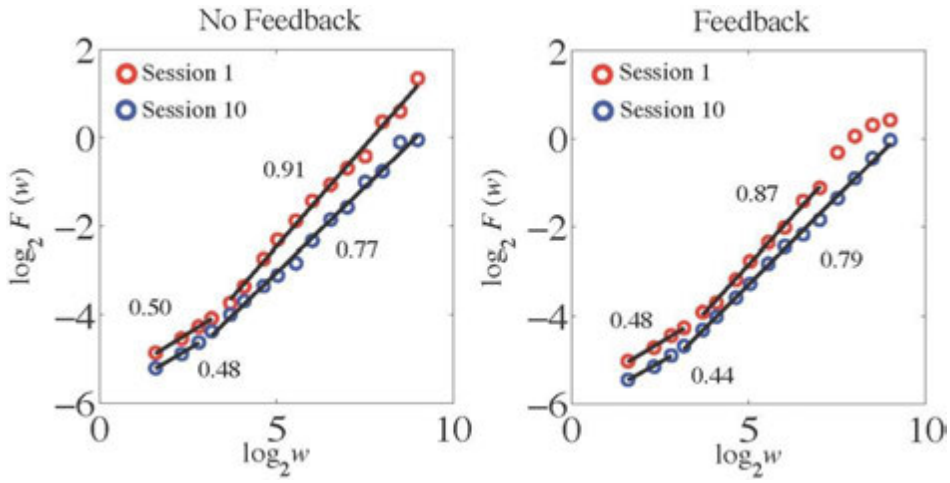


Figure 2.11. AFA plots for time series by using an experiment.

The application of AFA to data reveals some of the complexities in applying fractal analysis, particularly the identification of linear scaling regions in this project. These findings raise crucial questions about the nature of data signals and the type of models and methods that are most suitable for understanding postural control. The data may be characterized by on and off intermittency.

#### 2.2.4.4 Wavelet Based Multifractal Analysis

Another well-known method to investigate the multifractal scaling properties is wavelet transform modulus maxima (WTMM). The essence of wavelet-based multifractal analysis is similar to that of AFA. Given the presence of nonstationarities, it is an analysis method to extract fractal and self-affine objects [146]. The wavelet transform of a signal x(t) is initially defined as a convolution

integral. In case of a discrete time series $x_i$ , where i = 1, … N, it is then replaced by a summation as follows:

$$L_\psi(\tau, s) = \frac{1}{s}\int_{-\infty}^{\infty} x(t)\,\psi\left[\frac{(t-\tau)}{s}\right] dt$$

$$= \frac{1}{s}\sum_{i=1}^{N} x_i\,\psi\left[\frac{(i-\tau)}{s}\right]$$

where ψ(t) is called mother wavelet, and $\psi_{\tau,s}(t) = \psi[(t-\tau)/s]$ are daughter wavelets. The daughter wavelets come from the mother wavelet by evolution through the shift and stretch of the time axis. Therefore, they have a dependency on both time position τ and scale s. An appropriate time resolution is used to describe the local frequency decomposition of the signal. It is chosen for the considered frequency f = 1 / s. All wavelets ψ(t) must have a zero mean and are usually selected to be orthogonal to the polynomial trends. In that case, the analysis through the use of wavelets is not sensitive to any possible trends in the data. The m-th derivative of a Gaussian is often and most frequently chosen as the family of wavelets to be used:

$$\psi^{(m)}(s) = \frac{d^m}{dx^m}\left(e^{-\frac{x^2}{2}}\right)$$

Within the modulus maxima method, the average is taken only once for every local maxima of $|L_\psi(\tau, s)|$, instead of using all wavelet coefficients $L_\psi(\tau, s)$ for obtaining the average. $|W(\tau, s)|$ is defined by a given scale s and as a function of τ. The local maxima of $|W(\tau, s)|$ is then located at the position $\tau_j$ so that

$$|L_\psi(\tau_{j-1}, s)| < |L_\psi(\tau, s)| \geq |L_\psi(\tau_{j+1}, s)|$$

for j = 1, … $j_{max}$ . Then, the m-th power of the maxima is summed as follows:

$$Z\ (q,s)\ =\ \sum_{j=1}^{j_{max}} \left|L_\psi\ (\tau_j\ ,s)\right|^q$$

The absolute wavelet coefficient $|L_\psi\ (\tau, s)|$ can become arbitrarily small; that is the reason why the maxima procedure is needed. Because the analyzing wavelet $\psi(t)$ must be orthogonal to possible constant trends, it must always have both positive values and negative values for some and other t respectively. These positive and negative terms might cancel each other in the summation equation during the calculation of $L_\psi\ (\tau, s)$. $|L_\psi\ (\tau, s)|$ can then be small or even close to zero. In the calculation of the m-th power summation, such small terms could affect the negative moments. Hence, the maxima procedure is needed for eliminating the small terms.

In the previous mentioned fluctuation analysis, only positive terms are subjected to summation in the calculation of variance $F^2(v, s)$. The variances do not happen to be arbitrarily small, so there is no need to use the maximum procedure on the time series. In addition, the variances increase with an increasing length of the segment. This is because the fit usually becomes less favorable for a longer segment.

By contrast, in the WTMM analysis, given an increasing scale s, the absolute wavelet coefficients $|L_\psi\ (\tau, s)|$ do not increase accordingly. This stays the same even though only the maxima are included. In case there are more positive and negative terms canceling each other during the summation, the value $|L_\psi\ (\tau, s)|$ might even become smaller for increasing s. Therefore, in the WTMM method, the supremum procedure is additionally introduced. The purpose is to maintain the dependence of

partition function Z(q, s) on s monotonous. This is achieved by replacing $L_\psi$ (τ, s) by $L_\psi$ (τ', s'). For a given scale s, the replacement occurs if there is a maximum that appears at a certain position $\tau_j$ and happens to be smaller than the maximum at $\tau_j' \approx \tau_j$ for a lower scale s' < s.

For a signal with fractal structure, the scaling behavior is observed for Z(q, s) scales with s:

$$Z\ (q,s) \sim s^{\tau\,(q)}$$

The exponent τ(q) characterizes the multifractal properties of the series under investigation. The singularity spectrum f(q) can now be obtained according to the following:

$$\alpha = \tau'(q) \quad and \quad f(\alpha) = q\,\alpha - \tau\,(q)$$

In addition, there is a relation between τ (q) and the Hurst exponents:

$$\tau\,(q) = q\,h(q) - 1$$

The linear behavior of τ (q) indicates monofractality. A nonlinear τ (q) suggests that the signal under investigation is multifractal.

The MFDFA results are found to be slightly more reliable than the WTMM results [45, 147]. The MFDFA has slight advantages, in particular, for short series and negative q values. In other cases, the results are equivalent by using both of the methods. Nevertheless, the key advantage of the MFDFA method over WTMM is the simplicity of the computational process.

## 2.3. Design Issue

### 2.3.1. Background on Wearable Application

Wearable technology is not necessary in people's lives. However, in the US, approximately one out of five people own a piece such as a fitness band. The survey results suggest the interest of the consumer, especially in fitness bands and in receiving health information from wearable devices (Figure 2.12) [129]. During the survey, nearly one in every two consumers said that they are very or somewhat likely to buy one wearable device in the following year.

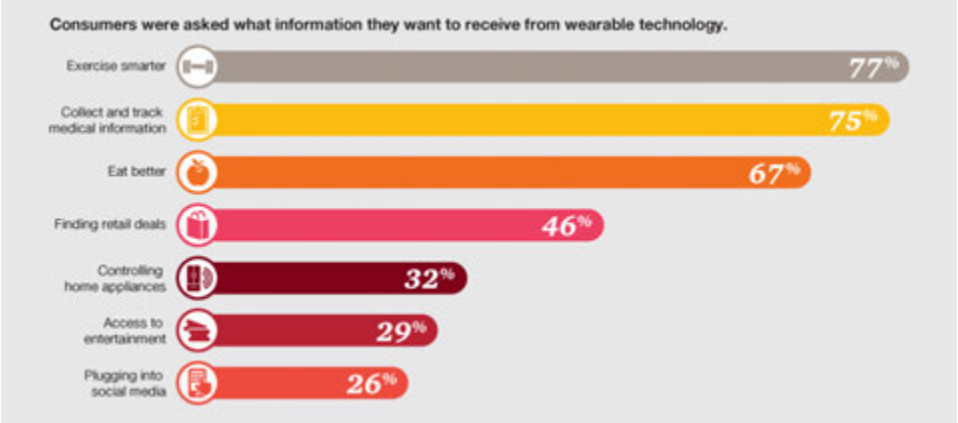


Figure 2.12. List of the top information that US consumers want from wearable devices.

Motion sensing plays a crucial role and is critical for supporting the findings in health practice. There are two essential phases in relation to sensing modality. The

first one is definitely the acquisition of human physiological data. The second is the computational modules that give meaning to data. In practice, this is a new frontier for intervention. To benefit from the analysis and intervention techniques, there are two major concerns, namely portability and variability. Wearable systems are defined as portable devices that enable acquiring various physiological signals, for example, movement. Because wearable computational devices that work with smartphones have become popular among consumers, the cost of sensing and actuation components has decreased. At the same time, the trend pushes technological development forward to enable long-term, continuous usage for hours and days. Therefore, wearable sensing and feedback systems have increasing potential to provide substantial benefits to consumers, especially in the health-related domain. The application also involves clinical practices to complement and extend interventions, and to contribute to additional values.

Several outstanding commercially available wearable systems have been distributed in the market, such as Nike + Fuelband, FitBit, Jawbone UP, and Google Glass. They have spread across various applications. In the wider population, they are moving toward a standard related to walking, working, eating, and sleeping, in which daily information is tracked with sensitive feedback. Again, one of the major aspects of this technological transformation is the interest in using wearable systems for clinical assessment and intervention.

In the consumer market, measuring human movement by using wearable sensing has been suggested as a practical means. Some of the major expectations about the

sensing devices include small in size, light in weight, more robust in measurement, combination with the computation in smartphones, and the variety of application [79]. The development of accelerometers, gyroscopes, and magnetometers has enabled small and light weighted components that can fit conveniently and practically inside mobile phones for measurement. Integrating and taking advantage of individual components are also possible. For example, combining accelerometers and gyroscopes can improve inertial measurement. Integrating the accelerometers, gyroscopes, and magnetometers has further facilitated the accuracy in measurement and the ease-of-use. The advancement of technology not only opens up new opportunities but also enables feasibility that is previously not possible, for example, the portable manner of monitoring, analyzing, and intervening human movement. Regarding measurement, wearable systems with a simple accelerometer or switch have been designed to detect various spatiotemporal parameters, such as step count, stride length, cadence, and walking speed in relation to the application on gait [80]. In more complex systems, arrays of accelerometers, gyroscopes, and magnetometers have been created to fit the body for the measurement of joint and segment kinematics [81]. On the application side, self-management, self-monitoring of health status, and remote monitoring of patients have been designed and developed for viable solutions for managing the progress of chronic diseases or for preventive measurements [82].

Although increasing people and research are incorporating wearable systems into daily lives, the design for clinical application that provides benefit to the society by

using these systems is unclear. In this research, the design criteria for possible clinical application in monitoring the kinematics of the spine are analyzed and concluded by implying the target usage of wearable devices for kinematic measurements. The primary target is based on electronics of small and lightweight accelerometers, gyroscopes, and magnetometers.

### 2.3.2. Design Consideration on Sensing Movement

In the domain of noninvasive motion sensing, recent, current, and reliable clinical solutions are to use camera imaging techniques on the basis of a motion capture system. Body motion is derived from the movement of multiple feature points attached on the body. Although this is effective and accurate in capturing human movement, this technique is expensive and has its limitation when applied. For example, in optical motion-sensing techniques, a clear line of sight is required from the feature points on the body to the cameras, and at least two or more cameras must be visible at any instant. In other words, the feature points cannot be covered by any clothing. In addition, the motion capture system is usually bulky and requires a certain amount of time and space to setup. This makes portable application not possible, in addition to the daily monitoring tasks.

With the advancement of small and lightweight electronics in motion-sensing devices, microscale motion-sensing technology has advanced substantially, benefiting the development of various domains and extending the types of

movement sensing, for example, human balance prosthesis, sports medicine, and biomechanical research. In particular for body motion sensing, the advancement in micro-electro-mechanical systems, together with features of high accuracy, high reliability, and multiple functionalities, has provided a powerful tool set.

Generally, the design for motion-sensing devices includes the acquisition of the motion characteristics of an object in three-dimensional space. The motion characteristics, in geometrical perspective, can be described by six independent variables. Three of those are linear movements along the three axes defined in perpendicular to each other, also as coordinate axes in space. The other three are the rotational movements with respect to the three perpendicular directions. To accurately measure the motion characteristics of an object in space, a sensing system is required to have the six degrees of freedom in sensing capability.

The portable device market is becoming increasingly competitive. A number of electronic technologies are able to capture motion and its corresponding characteristics. Therefore, device suppliers now focus on products that have a distinct advantage or product differentiation that sets them apart from competitors. These advantages or differentiators are primarily derived from customer feedback and market research about existing applications and products, current product limitations, and unfilled market needs. From the feedback and studies reviewed, the design must be based on crucial decisions. Prioritizing design requirements and criteria is a crucial step in selecting affordable components and ensuring functionality. The goal is to meet the most critical product priorities and satisfy

business objectives. In general, a portable device for the clinical and medical industry is typically evaluated using the following criteria: weight and size, resolution, frequency or speed, accuracy, cost, power consumption, and electromagnetic interference.

The term portable implies that the device should be easily carried around. In comparison to many other systems that are set up inside a laboratory, the consideration of weight and size is essential in this aspect of portability. For example, in the market, the wristband is a popular accessory for capturing human movement. It has a weight and size that ensures the consumer's comfort in attaching it to the wrist, and it is also flexible in movement. However, if the same components are used in an application for measuring neck movement, the design may not be appropriate. If the measurement involves measuring the kinematics of each spinal section, the size of the wristband sensor would not fit. Weight and size are critical and also challenging in product design because the designer has limited space and weight allowance for electronic components. In relation to this, functionality then becomes a tradeoff because of the limited number of components that can be assembled together. In a bulk size system, the space can accommodate the interaction between numerous electronic components and the main control unit; hence, the system is functional for various tasks. However, the smaller the size, the fewer electronic components can be accommodated, and the less functional the system is. The choice of components is therefore a crucial

decision on the basis of this rationale. This is why microscale technology is the major contributing advancement that synergizes the portable device market.

Another crucial criteria in selecting the right motion-sensing device is resolution. The resolution determines how sensitive the device is in capturing. In other words, given minimal human movement, can the device capture the change? For example, when comparing the resolution of a high-resolution camera to a low-resolution camera, it is obvious that even when there is minimal movement occurring at the feature points attached on the body, the high-resolution camera can detect the changes because it has a high number of sensor units per each standard distance unit. By contrast, the low-resolution camera can only sense changes when there is a considerable amount of movement. In comparison to the previous case, three steps of movement may be required here before the sensor can capture the change, versus one step for the high-resolution camera. By contrast, the motion characteristics describe not only linear movement; there is also three rotational movements along the X-, Y- and Z-axis, also called angular movements. The term “resolution” is also used to describe the angle of change per unit time interval. In other words, the sensing of the device is described as how much an angle of an object is moved with respect to the capture that occurs in the previous interval. Moreover, the resolution also relates to how many steps or intervals the device can resolve or represent in the output signal when there is a movement. However, a higher resolution does not necessarily imply that improved accuracy in the design

can be achieved. It only provides more counts per unit distance for the application and does not reveal details about the potential measurement error.

The frequency rating of a device determines how fast the sensing process can be. The measurement per sensing process is usually called a frame. The frequency describes the number of frames that can be acquired per unit time; usually, the unit is in seconds. For example, if a motion-sensing device has a frequency of 30 frames per second, it would mean that the device could capture 30 times the movement of any object in every one-second interval. Because the sensing only occurs at a specific frame interval, the sensing output between two intervals is usually connected by a spline, which can be a simple straight line or a curve that puts into consideration the trend from the previous data point or several intervals to the later data point or several intervals. The same analogy is applied in the case of angular movement. The frequency of human movement is usually limited to 10 or fewer frames per second. However, if the data outputs are only limited to 10 frames per second, there is a considerable distance between two consecutive sensing outputs. In that case, the in-betweens of the two outputs must be estimated using a spline, either a straight line or a curve. Therefore, usually for a device that is used to capture human movement for analysis in short time series, the capture cannot be set to a low frequency. This is because the movement of interest in the analysis usually concerns the details that occur within short time intervals, but not the trend across a long time period. For example, in the case of the captures that are described in subsequent chapters, some of them are 180 frames per second with 30

seconds as the length of time series. By contrast, if the target of analysis occurs in long time series, the frequency can usually be set to a lower frequency because the data change of interest usually concerns the trend of movement across a long time period, but not the exact detail of movement between short time intervals.

Accuracy is the criterion that determines the reliability of the data output in measurement. In other words, it describes the amount of error in the capture. Theoretically, the sensing output is proportional to the change in the movement of an object in space. There are both internal and external factors that interfere with the output. In a typical case of internal interference, there is electronic or digital noise. This alters the electronic output and usually happens at random, typically in the frequency and magnitude of interference. External interference occurs when the device is sensitive to an external source, for example, electromagnetic fields. This alters the output in a similar manner. Therefore, the output may not be proportional to the change in the movement of an object in space. For a high accuracy device, the change in the output signal is considered less noticeable, both in magnitude and frequency. However, for a low accuracy device, for a constant change in movement, the output signal may have many variations. Hence, before analysis, accuracy should take into account the output measurement. A low accuracy device leads to unreliable and unstable values in the signal that eventually cause the analysis on the data to be unreliable. In usual practice, a controlled or manipulated condition is set to capture a constant movement. The output should happen in a constant manner. In that case, the output data can be analyzed to observe the accuracy of the data.

Cost is always a parameter for device manufacturers to consider, including design and manufacturing perspectives and also the acceptability in the consumer market. Consumers are often cost-conscious in acquiring portable devices for health or clinical practice while striving to maintain a high level of effective care. Often, engineers are challenged to find the correct component at a suitable price. Motion-sensing products require a large portion of the design budget because precision motion-sensing component choices are limited and traditionally expensive. In addition, the mounting of the device is another concern. Nowadays, design appearance, look and feel, and style are all considerations in the consumer psychology. A lack of design in a device can affect the branding and the sales to recover the cost.

Another consideration in selecting an appropriate motion-sensing solution is the immunity against electromagnetic interference. Electromagnetic interference problems have increased significantly in recent years because devices now use more sensitive electronic components. Another reason could be because of the extensive adoption of wireless communication devices such as smartphones, WIFI networks, and radio transmitters. To avoid device failures or accuracy issues related to electromagnetic interference, engineers should adopt optical-based solutions as an alternative to magnetic-based solutions.

A suitable design and solution during the product definition stage can simplify the work and increase the product’s chance of success and quick market entry.

### 2.3.3. Systematic Methods for Measuring Continuous Variables

In this study, the source data for analysis are derived from the acquisition of human movement by using feature points attached to the human body. The motion-sensing technique is a complex setup of camera arrays arranged in a ring-shaped rack. The cameras are carefully adjusted to align the effective capture area. The capture system is an optical one, which is equipped in a laboratory environment. The optical system consists of feature points attached on the human body and measured using camera image sensors. Red spectrum light is emitted from the camera. Through the reflective surface on the feature points, the movement of the human is captured using the camera image.

Because this is an optical system, the feature points attached on the body are not affected by the electromagnetic interference mentioned in the previous section. However, the major issue here is the line of sight between the feature points and the camera sensors. If anything obstructs the line of sight, the feature points would not be visible to the camera sensor. Hence, the data would be lost in that particular frame or time period if the feature points remain invisible.

Because the camera and the image sensor are typically an electronic device, digital noise could occur to interfere the electronic components. Therefore, a control experiment must be conducted to verify and validate the data captured. The other major issue in the field of image processing is that the digitalization and transformation processes occur between the data acquired by the image sensor and

the final numerical movement output. Between these processes, sampling of images happen and the pixels are determined by their visibility in depth and corresponding positions across the eight adjacent pixels. Here, accuracy or error issues arise. After the digitalization of the image data, mathematical transformation occurs across images captured by various cameras. This involves transforming the planar images into three-dimensional coordinates. The accuracy issue is then reinforced in another layer of error. In sum, the test on the data measurement is necessary to ascertain that the accuracy is under control and to determine the accuracy required of the data for them to be usable and representative of the actual movement. The purpose is to quantify random error or control the noise level at a manageable level so as to not affect the data for analysis. The smaller the random error is, the more accurate the measurement is.

In relation to accuracy, reliability is another crucial parameter in determining the quality of an instrument and its measurement. Reliability measures the precision or the extent to which test results can be replicated. Almost all crucial variables measured using instruments or devices appear to be numerical and continuous in nature. As for the motion-sensing method, the numerical values represent the six degrees of movement, both in linear and angular measurement. Various statistical methods have been used to assess the reliability of instruments with quantitative or continuous outcomes [83].

Within participant variation is the random variation in an individual over trials. As mentioned previously, random errors exist in each measurement. The analysis based

on within participant variation is to quantify the variation that happens when comparing between the trials captured by a single participant performing under the same condition. Standard deviation is a typical statistical parameter that represents the within participant variation, also called standard error of measurement. It captures the notion of the random variability of a single individual's values on repeated testing. In other words, it represents the typical error in a measurement. Because this is a value representing the error in measurement, the value increases when the data of measurement are in a large scale. Therefore, it is expressed in percentage, dividing the standard deviation by the respective mean value. This form of typical error is called the coefficient of variation. Because it is represented in percentage, there is no specific dimension dependent on the measurement. Therefore, it allows direct comparison of reliability.

The variation represented by typical error comes from several sources. The main source is usually biological. The measurement depends on the reputability of an individual to perform exactly the same movement. However, as a matter of fact, there exists variation in between trials because of changes in physical state. Equipment also contributes noise to the measurements, and is usually tested and described by the manufacturer. When the same individual is retested on different capture setting or equipment or at different period of time, additional error due to difference in the calibration or functioning of the equipment.

The other popular method is based on the change in the mean value as a measure of reliability. It is to compare the means of two sets of measurements. Typically, it

represents the random change caused by sampling error. The random change is caused by the random error of measurement. As a result, the mean value of each trial is inevitably different. Statistically, the random changes become smaller when there is a larger sample size. This happens because the random errors tend to cancel each other when more sample measurements are used during the calculation of means. In the case of longitudinal studies, systematic change occurs due to the effect of time span, for example, learning effects, fatigue, and lack of motivation or training effects. Typically, participants perform more favorably in the second trial than in the first because they benefit from the experience of the first trial. Fatigue could also affect the performance in the second trial and increase in a series of trials, causing the loss of motivation. The change of mean in this case is a nonrandom change in the value. Therefore, for each capture, the participants must be given sufficient training and have energy to perform the experiment.

To explore the relationship among variables, correlational techniques are often used as the basis. Correlation is used when the strength and direction of the relationship between two variables, usually continuous, are aimed to be described. The relationship described here is linear. High correlation values between two variables means that the two sets of variables are highly correlated, whereas low correlation values between two variables means that the two sets do not have substantial relationship. However, it is not a method to measure reliability, detect any systematic or fixed errors. It is possible to have two sets of highly correlated variables, but the measurements are not often repeatable. For instance, in one

measurement, the correlation coefficient for the data is high. However, the second measurement may not be close to the first one because of the variability between the two occasions of measurements. Therefore, the correlation coefficient should be used together with other techniques mentioned previously in measuring reliability.

By contrast, estimates of reliability and correlation should also be accompanied by confidence limits for the true value. Confidence limits are the precision range within which the true value of the outcome is likely to occur. The typical confidence limit in practice is 95%.

# Chapter 3.
# Methodology on Developing SDA Model for the Spinal Curvature

This chapter describes the initial spinal movement acquisition and analysis on the basis of the techniques in SDA. In the first section, the acquisition of movement data through the optical motion capture experiment is described. The computational procedures are then illustrated to analyze the data. The numerical results are described, visualized, and explained.

In the second section, the results from analysis are evaluated by adjusting the parameters one after the other to illustrate the influences. The evaluation is to ascertain that the results from the analysis are dependent on the data acquired, rather than from the nature of noise.

In the third section, particular fractal characteristics are applied to differentiate the participant conditions, namely, between patient and normal participants, and also between age groups. Various parameters are described to illustrate the difference.

In the fourth section, the limitations of this technique are identified and eventually brought forward for the later approach in the study using multifractal analysis. The cervical spine region is selected as the focus for the subsequent analysis.

In the last section, the structure of the cervical spine is illustrated. Neck pain, as one of the major issues, is described. The biomechanics and corresponding characteristics in measurement are explained.

## 3.1. Research Design on the SDA Model Development

In this chapter, the SDA model for spinal curvature is purposed. The target is to develop a suitable and valid methodology for analyzing spinal curvature by using the SDA model. In the literature on COP, results have been found related to the control mechanism. In this study, attempts were made in analyzing spinal curvature to determine whether similar results can be found. The whole development was divided into several phases. At the beginning, an experimental setup was used to acquire participant data inside the laboratory environment. The participant, with markers attached to the skin, was asked to perform upright sitting following a set of instructions during the experiment. Data of the markers were captured and computed to determine the spinal curvature. After the acquisition of spinal curvature data from the participant, computational procedures were implemented for SDA. Fractional Brownian motion (fBm) characteristics with a number of graphical representations of data were then extracted. The extracted results were then compared with the results of the COP data from the literature. The aim was to determine the validity of the purposed method of developing the SDA model for spinal curvature by comparison to the dynamic features exhibited during body sway at the static posture of sitting upright.

### 3.1.1. Experiment Setup

An optical motion capture system was set up for acquiring the data of participant movement. The system used was the Eagle digital system manufactured by Motion

Analysis Corporation (USA), containing five cameras (out of 12) particularly having the field of views set to focus on the participant (Figure 3.1). Each camera had a visible red LED ring-light attached in front with a stable 60-Hz frequency customized by the capturing software. For each second, 60 frames of the image that appeared within the view of the camera were captured by the system. The movement of the participant was recorded using the spherical markers with 3M Scotchlite (USA) optical reflective material taped on the surface, which was attached on the skin proximal to bony prominences. The image resolution of each frame was 1280 pixels in width with 1024 pixels in height. The consecutive image frame sequences captured by the system were used to determine the trajectories of markers. Through calculation of various camera angles, the three-dimensional coordination of the markers in space was determined in the form of X, Y, and Z coordinates. With a control setup of a dummy subject, an accuracy of 0.3 mm of the marker trajectories in three-dimensional space was determined.

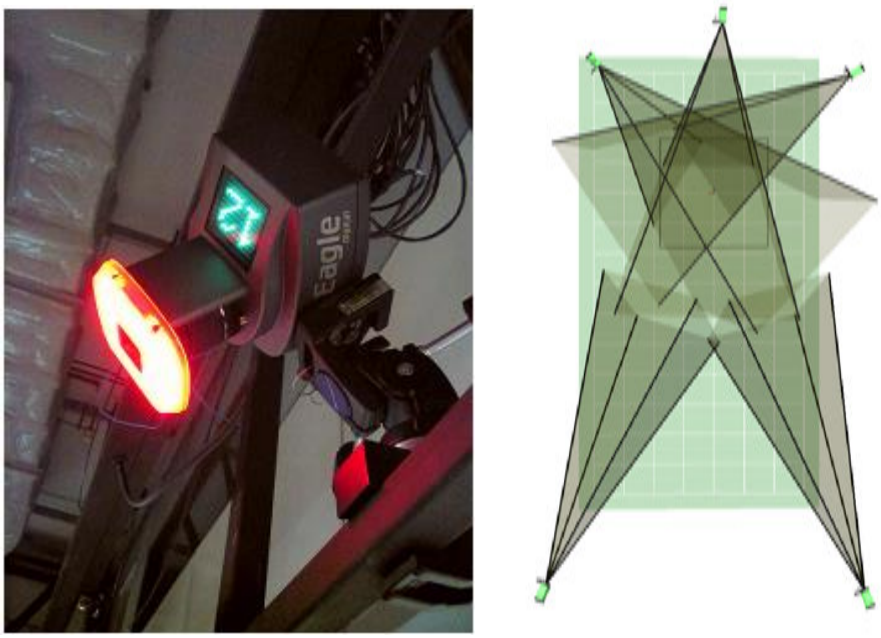


Figure 3.1. Eagle digital motion capture camera.

The participant was instructed to sit upright (Figure 3.2) on a medium foam-base with a thickness of 10 cm and a density of 50 kg/m$^3$ [148]. The participant was requested to have the arm across the chest to eliminate any lateral support to the trunk. The feet positions were standardized at a natural and comfortable position where heels were kept at a distance of approximately 10 cm in separation, and both feet pointing 10 degrees outward. During the measurement, the participant was requested to close the eyes with the head facing forward at a horizontal eye level to eliminate the visual feedback for postural control. He was asked to maintain the upright sitting posture for 30 seconds as steadily as possible for data acquisition. The foam base was used to increase the challenge for sitting balance.

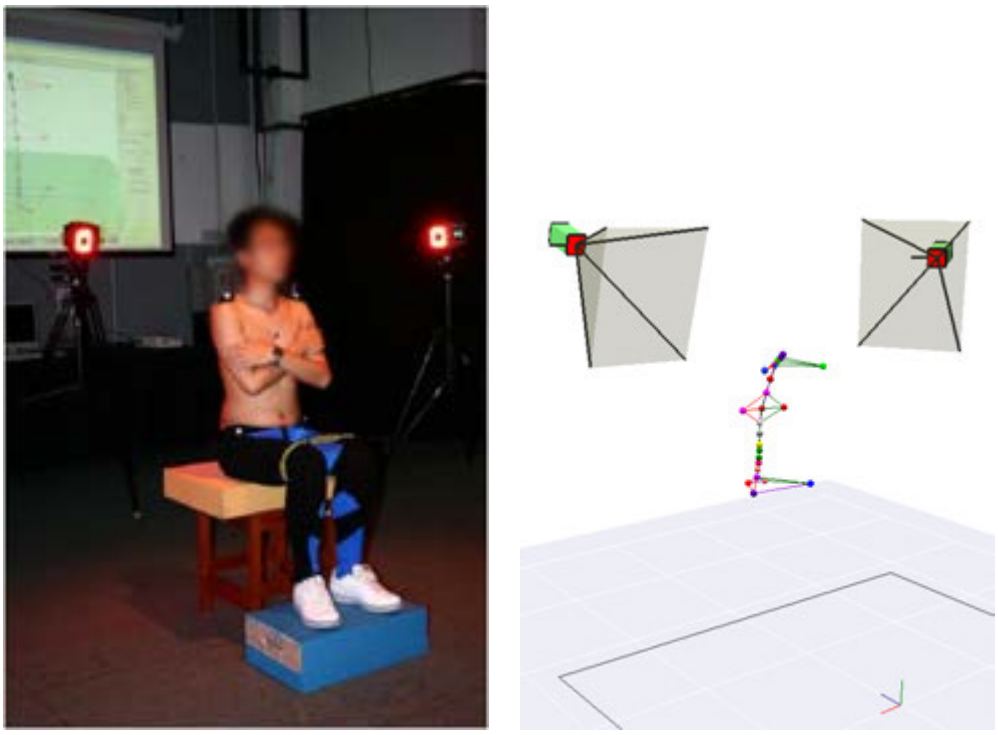

Figure 3.2. Sitting posture of the participant for data acquisition.

### 3.1.2. Kinematic Data Capture

On the participant, a total of 23 markers were attached to the skin proximal to bony prominences as shown in Figure 3.3 for measurement. Among those markers, 15 were placed along the spine (C4, C5, C6, T1, T3, T5, T7, T9, T11, L1, L2, L3, L4, L5, S1), four were used to determine the orientation of the pelvis by the left and right sides of anterior superior iliac spines (ASIS) and posterior superioriliac spines (PSIS), two were used to determine the orientation of the shoulder, and two were attached to the left and right sides of T7 for assisting the system in rectifying the marker sequence and determining the trunk orientation. The X, Y, and Z coordinates of each

marker were captured according to the physical space location in the standard unit of millimeter. A dummy object (Figure 3.4 and 3.5) with the same number and positions of markers attached as those on the participant body was set up to evaluate the digital noise characteristics of the system relative to the participant data captured. Because the participant was asked to sit facing one orthogonal plane, in the analysis, the marker data were extracted in the sagittal plane (Y- and Z-axis of the system).

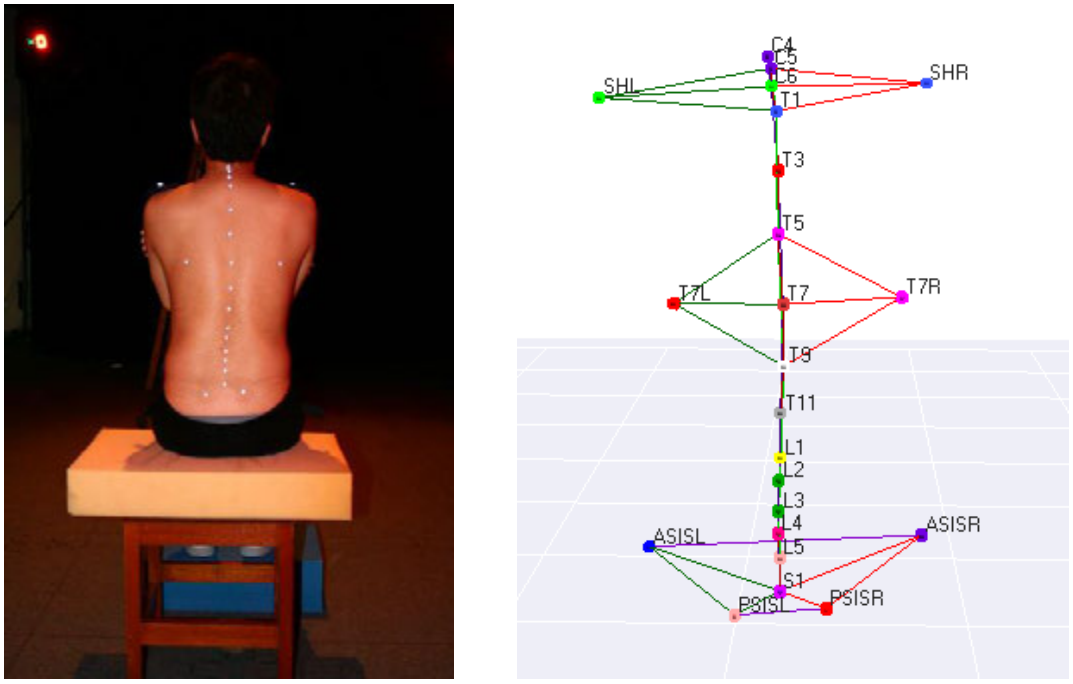


Figure 3.3. A total of 23 markers attached to the skin proximal to bony prominences on the participant.

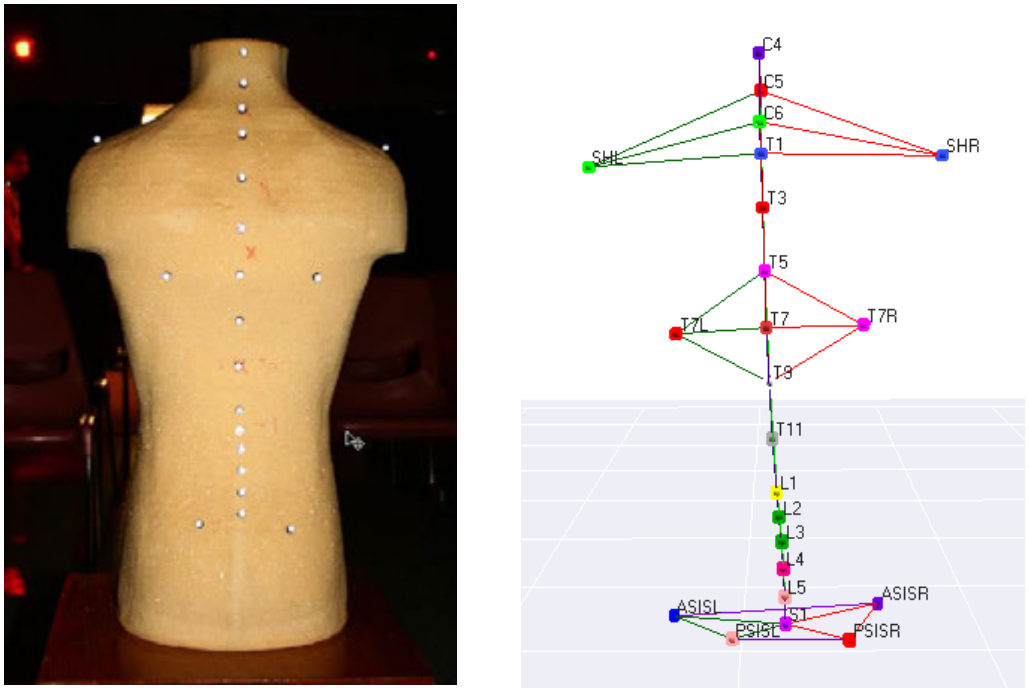


Figure 3.4. A total of 23 markers attached to the dummy with similar positions as those on the participant.

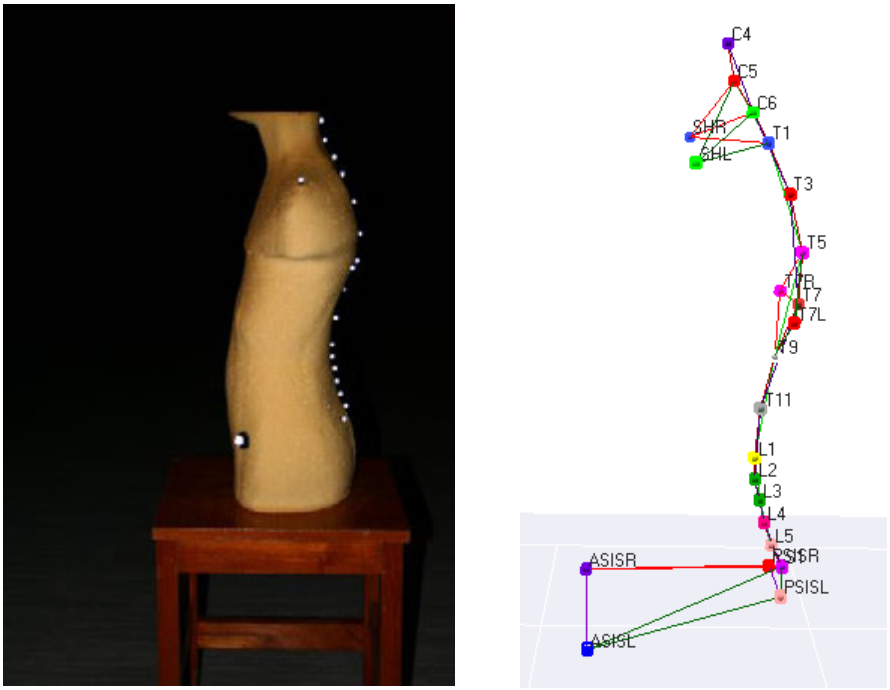


Figure 3.5. Side view of the markers on the dummy.

EVaRT was used to control the data acquisition. It is a utility software with an interface for the visualization of data in real-time from Motion Analysis Corporation (USA). The data were then exported to a plain text format called TRC, in which each row represents the number of frames during the data acquisition, and each column represents the individual position according to the label of each marker. The visualization of data in three-dimensional space is shown in Figure 3.6.

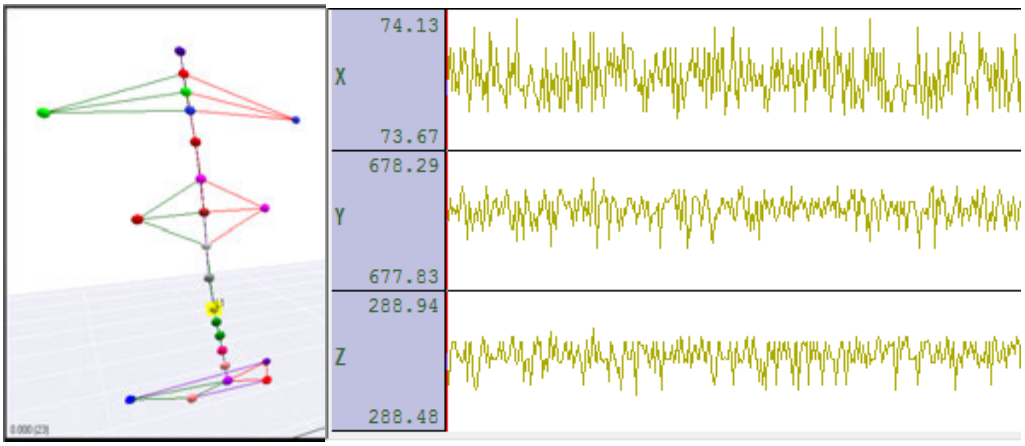


Figure 3.6. Visualization of captured data.

Following the experimental method of [29] on COP for SDA, 10 trials were captured on a participant with a 30-second duration for each trial. In between each consecutive trial, the participant was allowed to take a one-minute break. The participant was requested to sit as steadily as possible in the upright position during each 30-second data acquisition.

### 3.1.3. Calculation of Inter-segmental Spinal Curvature

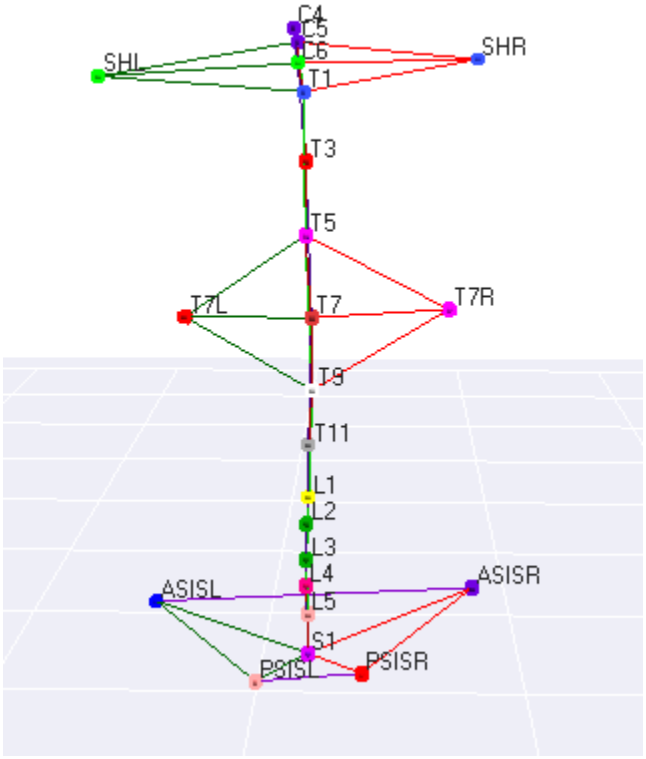


Figure 3.7. Markers link together along the shoulder, spine, and pelvis.

There were 15 markers altogether attached along the spine, as visualized in software (Figure 3.7). With any three ordered marker data along the spine, two vectors ( $\overrightarrow{v_{OA}}$ , $\overrightarrow{v_{OB}}$ ) were developed from the two sides of the origin of angle. The

two vectors were then used to calculate the inclined angle, A, according to trigonometry.

$$A = \cos^{-1}\left(\frac{|\vec{v}_{OA}|^2 + |\vec{v}_{OB}|^2 - |\vec{v}_{AB}|^2}{2 \cdot |\vec{v}_{OA}| \cdot |\vec{v}_{OB}|}\right) / (\pi \cdot 180)$$

The flexion and extension of the spine in different regions were represented by the corresponding angles extracted. Angle values were either taken in consecutive order or spanning an equal number of markers on both sides of the origin of angle.

In this analysis, the spinal curvature was considered as having different data intervals between ordered markers from one to seven. As a result, there were 49 intersegmental angles extracted along the spinal curvature. There were 13 angles extracted from consecutive data intervals; 11 angles were ordered with two data intervals in between. For example, if L3 was taken as the origin of angle during analysis, the inclined angle of one data interval would be L2, L3, and L4, whereas two data intervals would be the angle between L1, L3, and L5. There were nine, seven, five, and three angles corresponding to three, four, five, and six data intervals. Finally, there was one angle with seven data intervals calculated using C4, T9, and S1.

### 3.1.4. SDA Model Computation Procedure

The MATLAB (MathWorks Inc., USA) platform was used to develop the implementation of SDA model computation. Through a built-in MATLAB function

named butter(order, $w_n$), where $w_n$ was calculated from the cut-off frequency $f_c$ and sampling rate of data $f_s$, the third-order Butterworth low-pass filter was applied to the positional data of markers.

$$w_n = \frac{2f_c}{f_s} \qquad \text{where } 0.0 < w_n < 1.0$$

In this case, the sampling rate of data was 60 Hz and the cut-off frequency was 4 Hz. Another built-in MATLAB function named filtfilt( ) was performed with zero phase digital filtering.

From the filtered raw data of each marker position, the inclined angle was calculated. The inclined angle is the representation of spinal curvature. According to the time dimension, it could be illustrated in a time plot (Figure 3.8).

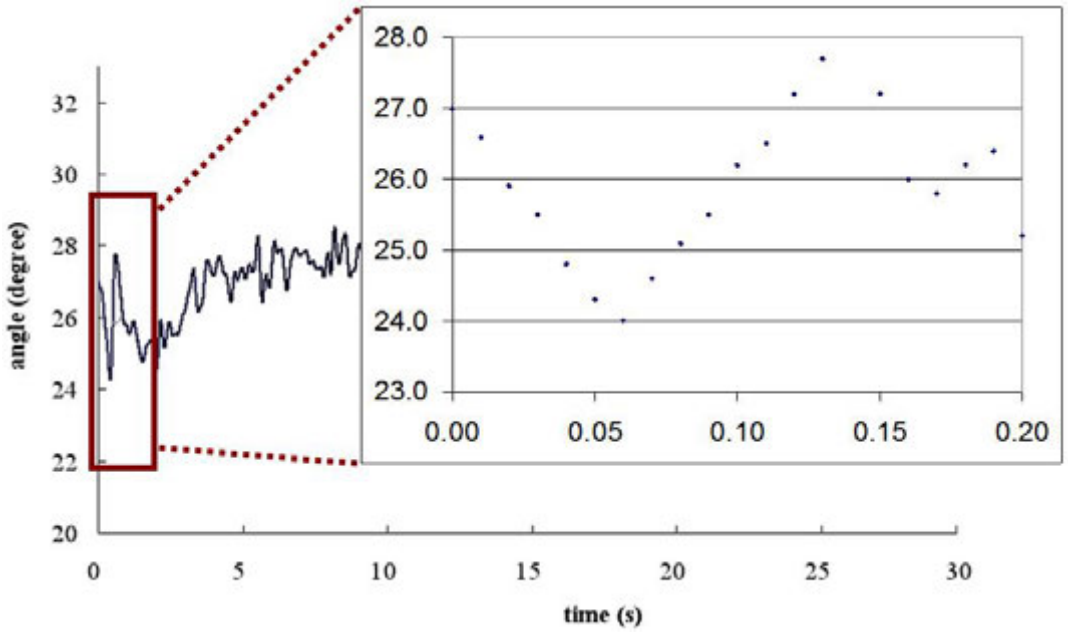


Figure 3.8. Spinal curvature in terms of inclined angles, illustrated in a time plot.

### 3.1.5. Curvature Diffusion Plot

The data were then studied with the assumption of a stochastic process as a one-dimensional random walk. According to the time difference between data points, a time interval $\Delta$t was initially defined. It was found that the shortest length of two adjacent intervals is 1/60 second, and the longest is 10 seconds. On the basis of various data intervals, the squared difference between any two data values was calculated. According to each data interval, groups of squared differences were defined. By averaging the number of entries composing the group, the mean square angle $\langle \Delta X^2 \rangle$ was then calculated. For example,

For $\Delta t$ = 0.017, $\langle \Delta X^2 \rangle = average(x_1^2 + x_2^2 + \cdots + x_{1799}^2)$

For $\Delta t$ = 0.033, $\langle \Delta X^2 \rangle = average(x_1^2 + x_3^2 + \cdots + x_{1798}^2)$

A stabilogram-diffusion plot is defined here to illustrate the mean square angle $\langle \Delta X^2 \rangle$ against time interval $\Delta$t, as shown in Figure 3.9.

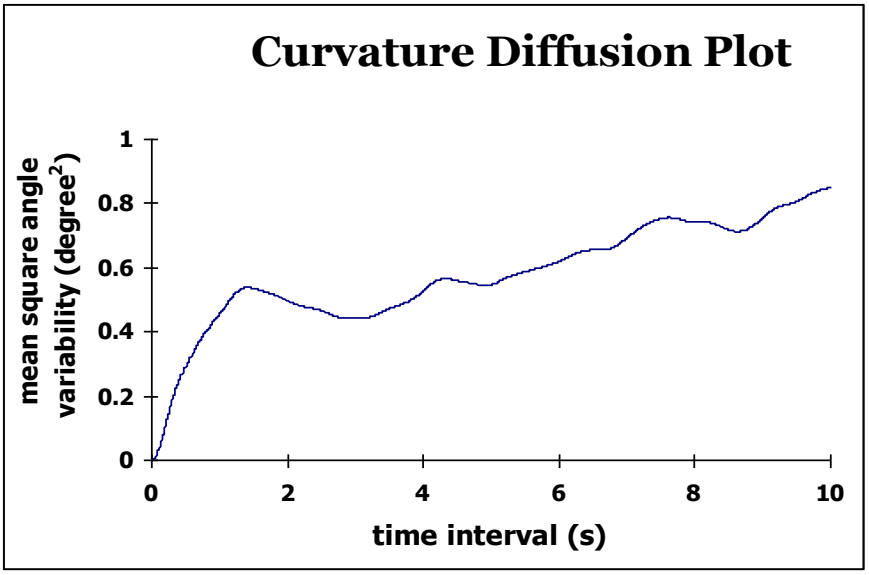


Figure 3.9. Curvature diffusion plot with the mean square angle against the time interval.

### 3.1.6. Diffusion Coefficient

In posturographic investigation, having participants perform for extended periods of time is impractical because physiological factors such as fatigue would affect the results. In this study, each participant was asked to perform 10 trials and the averaged sets of results derived from the 10 trials were analyzed. Specifically, the stabilogram diffusion plots were computed to extract the parameters. These were then subjected to further analysis for a particular participant.

To provide a quantified measurement of evenness, a nonfinite integer or factional space dimension could be used to quantify the trajectories. In the case of one-dimensional random walk with stepwise displacement X, the slopes of the resultant

linear-linear plots of the mean square angle against time interval curves, that is, $\langle \Delta X^2 \rangle$ vs $\Delta t$, are defined as related to a diffusion coefficient D.

$$\langle \Delta X^2 \rangle = 2D\Delta t$$

where $\langle \Delta X^2 \rangle$ is the arithmetic mean of $\Delta X^2$, named as the mean square angle; and D is the half slope of the curvature diffusion plot, representing the level of stochastic activity, as illustrated in Figure 3.10.

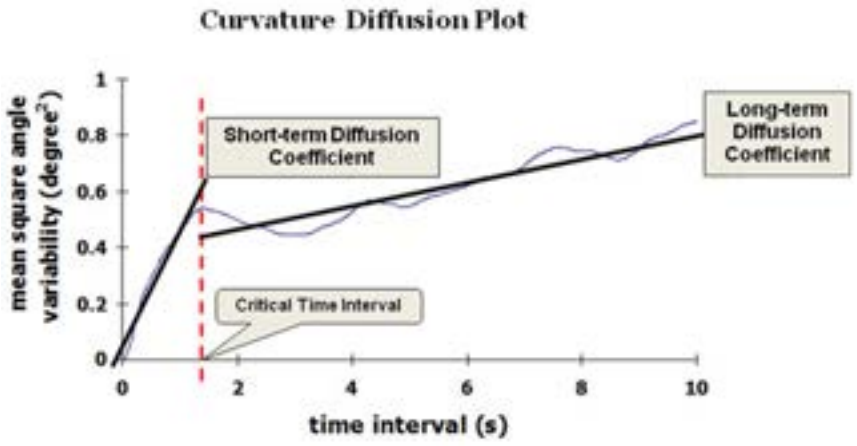


Figure 3.10. Diffusion coefficient defined on the curvature diffusion plot.

### 3.1.7. Critical Time

There were two diffusion coefficients $D_s$ and $D_l$ computed from the slops of the lines fitted to the short-term and long-term regions, respectively. The critical point ( $\Delta t_c$ , $\langle \Delta X^2 \rangle_c$ ) is defined by the intersection of the lines fitted to the two regions of the plot. . According to another study [54], the intersection can be determined by the

difference between the logarithmic plot of the curvature diffusion curve and the logarithmic plot of a pure stochastic process (Figure 3.11). The difference varies along the time interval. The maximum is then defined as the critical time (Figure 3.12).

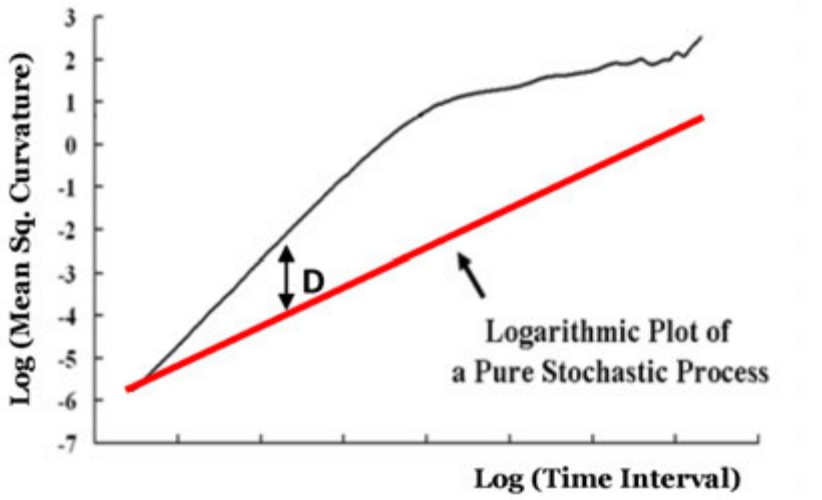


Figure 3.11. Difference between the logarithmic plot of a curvature diffusion curve and the logarithmic plot of a pure stochastic process.

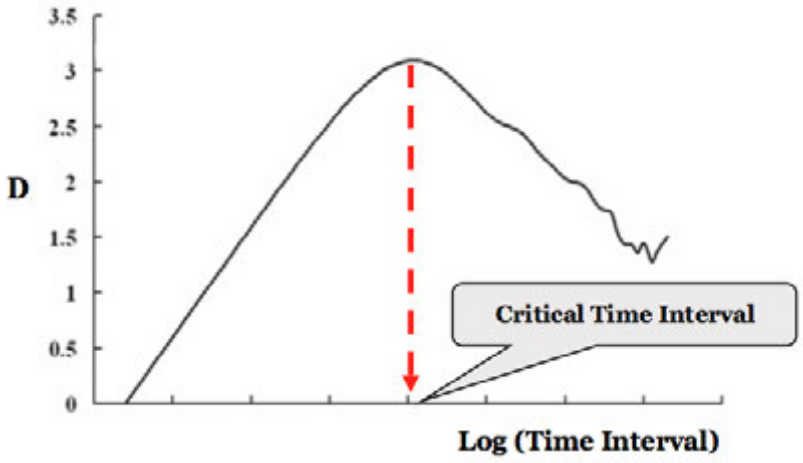


Figure 3.12. Critical time interval extracted.

### 3.1.8. Hurst Exponent

From the resultant log-log plot of the aforementioned curvature diffusion curve, scaling exponents $H_s$ and $H_l$ were computed. The least squares method was used to fit straight lines through the particular regions of the plots. The two regions were defined to represent the two scaling exponents respectively. In all of the previously mentioned cases, the slopes could then be determined.

$$\langle \Delta X^2 \rangle = \Delta t^{2H}$$
$$\log \langle \Delta X^2 \rangle = 2\,H \log \Delta t$$

The two regions as defined by H indicate the level of correlation between past and future increments (Figure 3.13). Regarding the interpretation of the scaling exponent H, white noise is indicated by a value of 0.0. It consists of a random signal with a flat power spectral density. The Brownian motion is represented by a value of 0.5. For H > 0.5, the phenomenon in which the movement direction of the current

and future tends to be positively correlated is indicated. This exhibits persistent behavior. With H < 0.5, antipersistent behavior is exhibited. This means that the movement direction of the current and future tends to be negatively correlated.

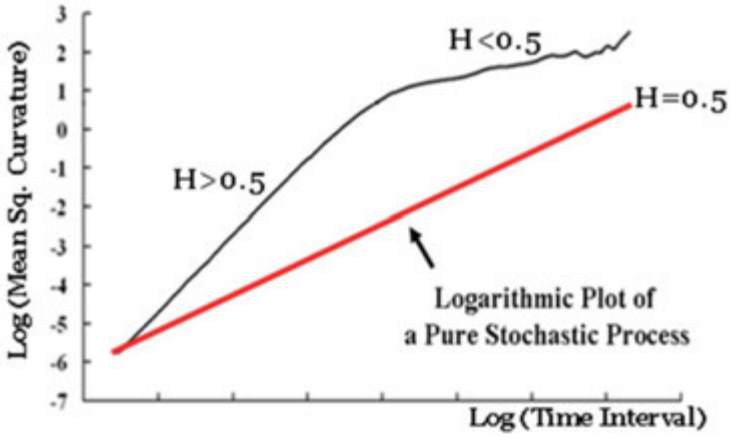


Figure 3.13. Hurst exponents illustrated on the curvature diffusion curve.

### 3.1.9. Result Analysis

This study modeled the physiological data through SDA by using the fractional Brownian motion method, and the hypothesis was that the dynamic features, and both open- and closed-loop control behavior were exhibited in the movement of spinal curvature. Moreover, different regions of the spine had different control mechanisms that resulted in different dynamic characteristics.

To verify the hypothesis, the first dynamic feature was taken as the critical time point. It was a crucial feature in which the curvature diffusion plot was divided into

two regions. In this study, most of the spinal angles were found to have a critical time point dividing the plot into open- and closed-loop regions. Only two out of 49 spinal angles were found without it. These were the ones with seven data intervals spanning, and one with six. From those 47 spinal angles, a consistent bounded value was found between 0.15 and 0.20 (Figure 3.14) with a mean value of 0.18 and a standard deviation of 0.02.

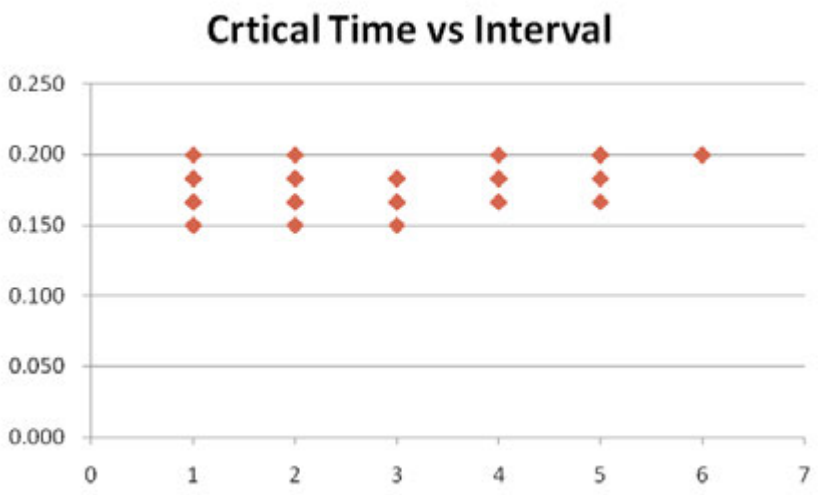


Figure 3.14. Critical time extracted from the curvature diffusion plot against spinal angle intervals.

A common behavior found in COP research is the dynamic feature in diffusion coefficients $D_s$ and $D_l$. Literature shows that $D_s$ is larger than $D_l$ in exhibiting control behavior. In this study, all the spinal angles were found to have a short-term diffusion coefficient larger than that of the long-term, except two without critical time points. Some statistical properties are shown in Table 3.1. The plots on

diffusion coefficient values against spinal angle intervals are shown in Figure 3.15 and 3.16. There were two outliers on $D_s$ at the angles of one data interval, and one on $D_l$. These outliers were those with values beyond the two standard deviations.

Table 3.1. Statistical properties of $D_s$ and $D_l$ .

| | **Mean** | **Standard Deviation** | **Minimum** | **Maximum** |
|---|---|---|---|---|
| **$D_s$** | 0.232 | 0.395 | 0.013 | 2.143 |
| **$D_l$** | 0.008 | 0.010 | 0.001 | 0.073 |

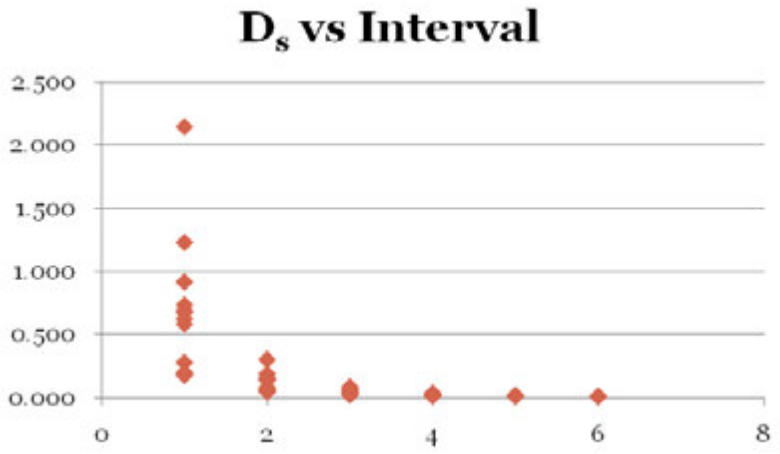


Figure 3.15. Short-term diffusion coefficients against spinal angle intervals.

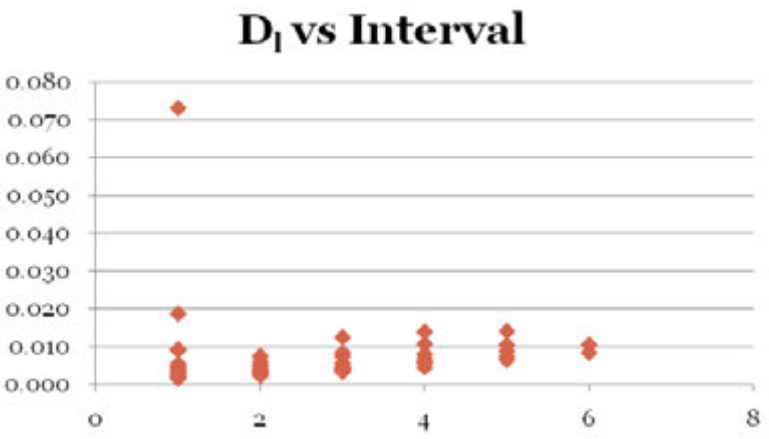


Figure 3.16. Long-term diffusion coefficients against spinal angle intervals.

Moreover, the short-term Hurst exponents were found to be greater than 0.5, except two without critical time points. The values of this exponent were found to consistently fall between 0.675 and 0.868 (Figure 3.17) with a mean value of 0.830 and a standard deviation of 0.051. This indicated that the control behavior in the open-loop region exhibited persistency and was positively correlated.

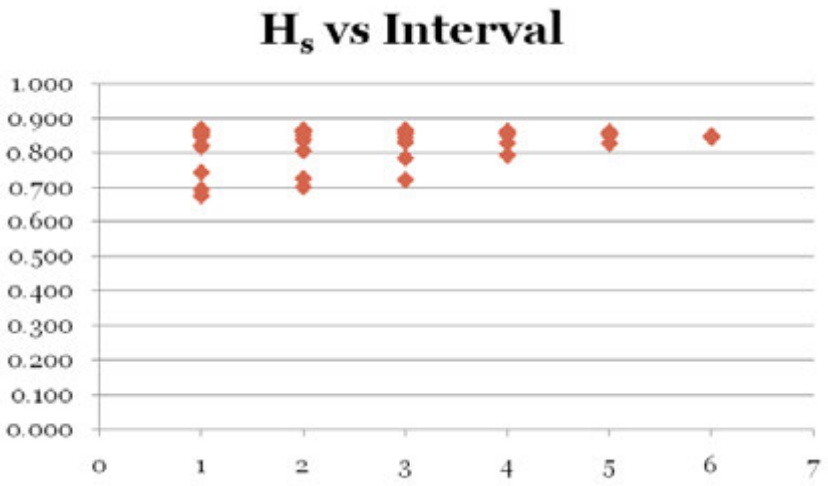


Figure 3.17. Short-term Hurst exponents against spinal angle intervals.

By contrast, the long-term Hurst exponents were found to be smaller than 0.5, except two without critical time points. This also indicated that the short-term Hurst exponents were larger than those of the long-term. The values of this exponent were found to have an increasing trend when the number of spanning data intervals increased, as shown in Figure 3.18. Some statistical properties are shown in Table 3.2.

Table 3.2. Statistical properties of short-term Hurst exponents.

| Mean | Standard Deviation | Minimum | Maximum |
|---|---|---|---|
| 0.231 | 0.148 | 0.041 | 0.514 |

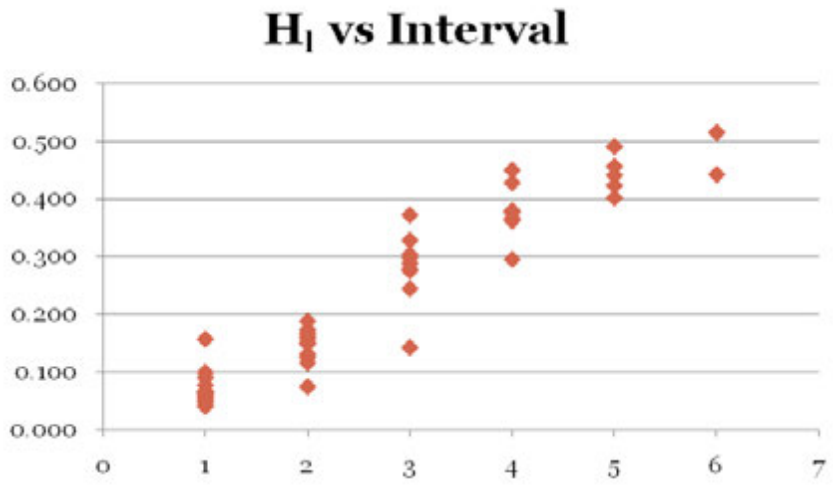


Figure 3.18. Long-term Hurst exponents against spinal angle intervals.

In conclusion, the spinal angles captured and calculated had dynamic features. These included the critical time point, values of diffusion coefficient, and Hurst exponent, which were found to be larger in the short-term larger than in the long-term. Short-term Hurst exponents were larger than 0.5, and long-term Hurst exponents were smaller than 0.5. The spinal curvature data also had two regions of open- and closed-loop control behavior. This is consistent with the literature on analyzing COP during body sway at stance.

## 3.2. Evaluation of Protocol

In this section, the parameters and procedural steps of the SDA model are evaluated in detail. The objective is to determine whether any deviation is necessary to fine-

tune the model for spinal curvature analysis. Regarding the trial acquisition, there were parameters on the trial duration and the number of trials needed for a significant illustration and computation on the results. In the later stage, the averaging method of computing the resultant plot of trials on a single participant could be evaluated. During the computation of diffusion data, whether a digital filter was necessary and the suitable cut-off frequency were considered. The implication of the sampling frequency on raw data in relation to the dynamic features was also considered. After the data were prepared, the time interval was needed for consistent results.

### 3.2.1. Trial Duration

According to the literature, the trial duration was usually 30 seconds for each trial on a participant. However, in the data acquisition conducted in this study, 30 seconds of holding a steady posture in cervical training was found to be difficult because of fatigue, which obscured the results. The objective was to evaluate whether a 10-second trial duration was feasible for fBm analysis.

In this study, three normal participants were invited to conduct the data acquisition. The data were acquired using a VICON (USA) optical motion capture system with passive markers attached to the skin proximal to bony prominences of participants. Positional changes of each marker were acquired along the cervical spine and around the head. Before the neck retraction training exercise, one 30-second

capture trial was conducted. Subsequently, the participant was requested to conduct the retraction training exercise. After the training, another 30-second capture trial was conducted. Both before and after capture sessions required the participant to have 30 seconds of holding time on the cervical spine.

The raw data captured were in the format of X, Y, and Z coordinates in three-dimensional space. Calculation was completed to convert the positional data into angular data to reflect the flexion and extension of the cervical spine. The angular data were then passed to undergo a zero-phase third-order Butterworth filter at 10-Hz cut-off frequency. To conduct the evaluation, different lengths of trial duration were taken from the angular data at 0 second onward. The range varied from 4 seconds to 30 seconds in every one-second increment. In other words, there were a total of 27 different trial durations under investigation.

### 3.2.2. Effect on the Critical Time

Among those three captures before and three captures after the retraction training exercise, most of the values showed stability with a trial duration of 8 seconds and longer. The comparison of plots of critical time against the trial duration of all three participants for both before and after training is shown in Figure 3.19 to 3.21. Exception was found in the capture of participant 3 before training. The stable critical time value could only be revealed after 12 seconds. Another exception was found with participant 1 after training. Initially, the critical time showed stability

after a trial duration of 7 seconds. However, there was a step increment after 22 seconds.

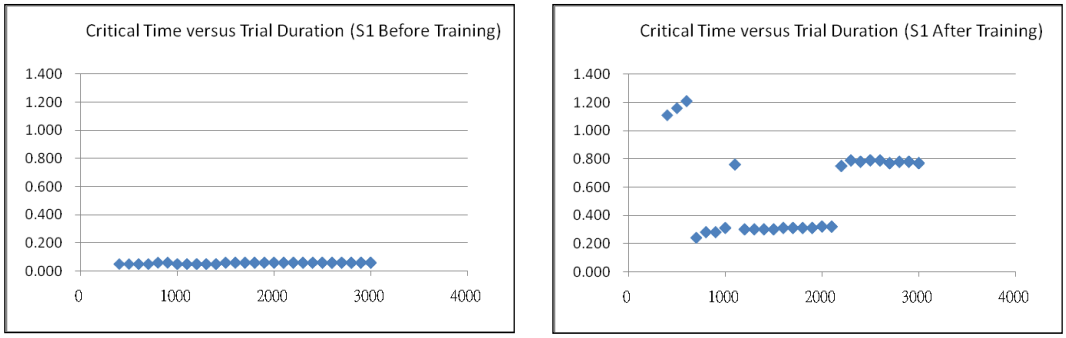


Figure 3.19. Comparison on plots of the critical time against the trial duration of participant 1 before and after training.

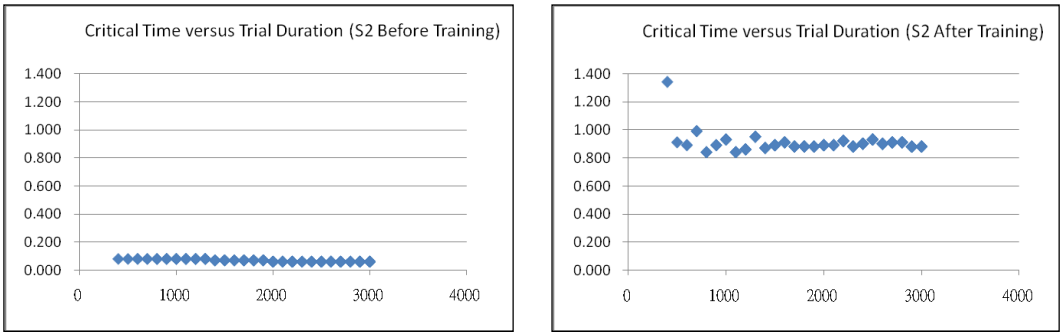


Figure 3.20. Comparison on plots of the critical time against the trial duration of participant 2 before and after training.

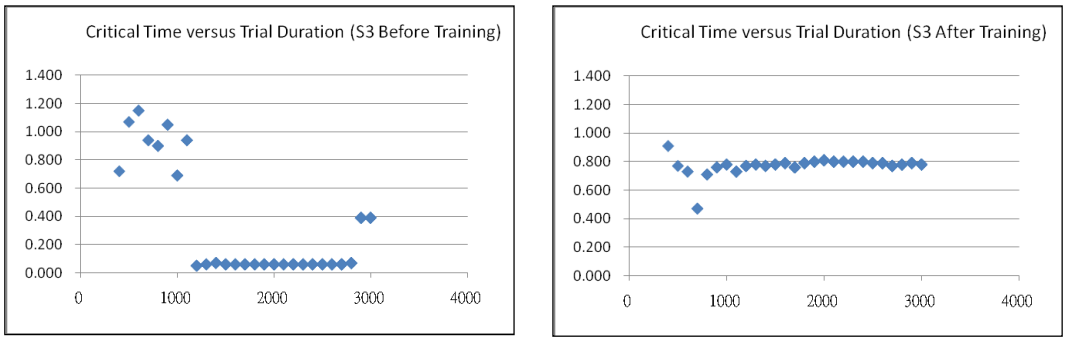

Figure 3.21. Comparison on plots of the critical time against the trial duration of participant 3 before and after training.

### 3.2.3. Effect on the Mean Square Angle at Critical Time

Almost all the values computed showed stability with a trial duration of 5 seconds and longer. The comparison of plots of the mean square angle against the trial duration of all three participants for both before and after training is shown in Figure 3.22 to 3.24. Again, exceptions were found at participant 3 before training and participant 1 after training. Regarding the case of participant 3 before training, the stability of the mean square angle was found from 12 seconds onward. For participant 1 after training, the first stability was found after seven seconds, whereas the other one with a step of 0.15 was found after 22 seconds.

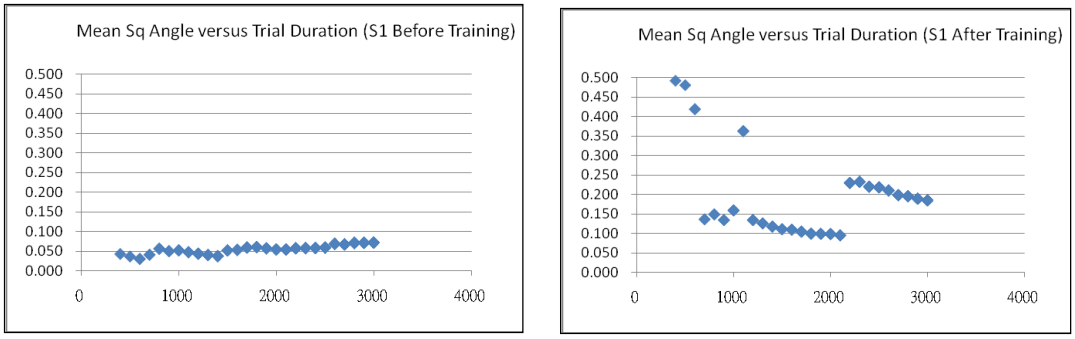


Figure 3.22. Comparison on plots of the mean square angle against the trial duration of participant 1 before and after training.

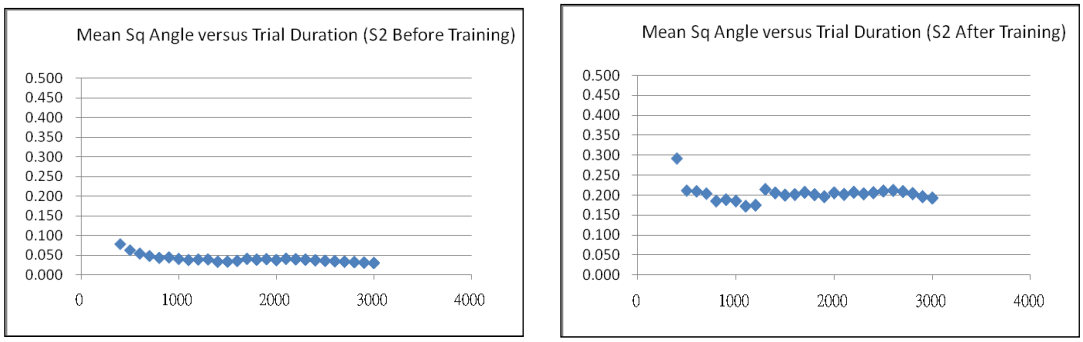


Figure 3.23. Comparison on plots of the mean square angle against the trial duration of participant 2 before and after training.

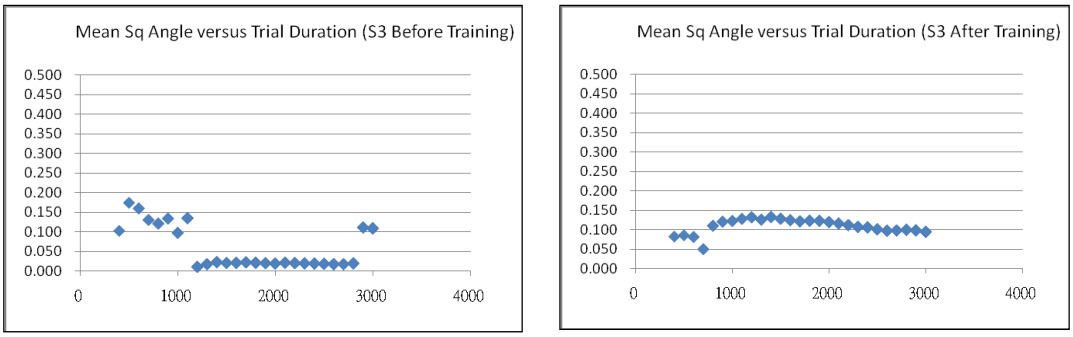


Figure 3.24. Comparison on plots of the mean square angle against the trial duration of participant 3 before and after training.

### 3.2.4. Effect on the Short-term Diffusion Coefficient

All of the short-term diffusion coefficient values were found to have stability within ±0.1 after approximately 7 seconds onward. By contrast, regarding this dynamic feature, some increasing and decreasing trends could also be found in some data captured when the trial duration was longer. The comparison of plots of the short-term diffusion coefficient against the trial duration of all three participants for both before and after training are shown in Figure 3.25 to 3.27.

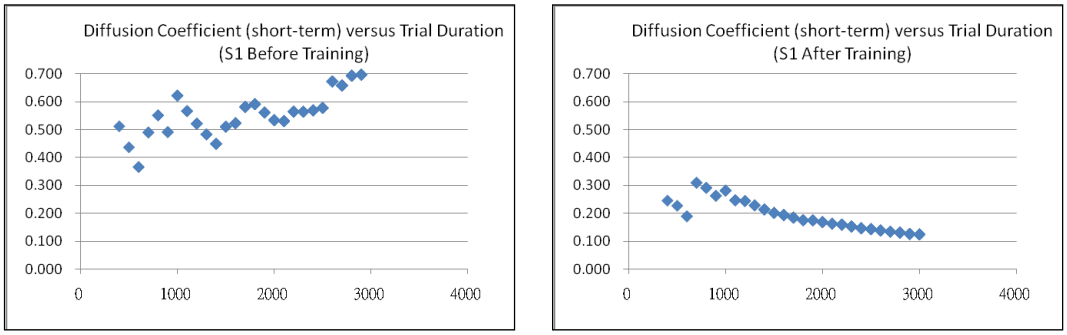


Figure 3.25. Comparison on plots of the short-term diffusion coefficient against the trial duration of participant 1 before and after training.

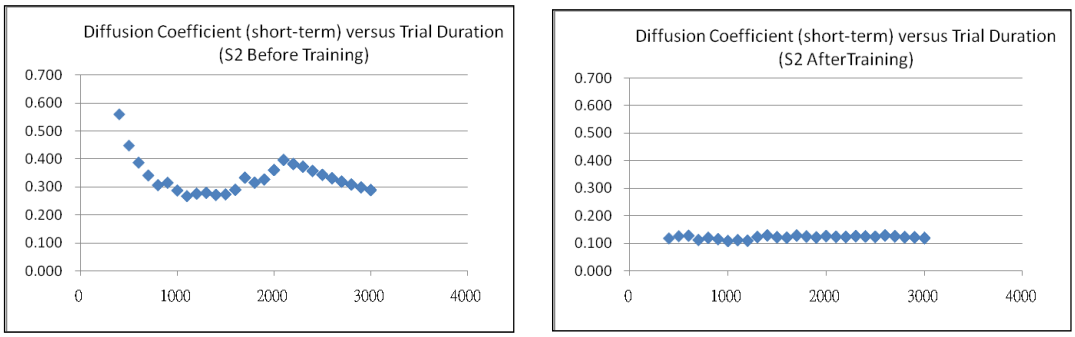


Figure 3.26. Comparison on plots of the short-term diffusion coefficient against the trial duration of participant 2 before and after training.

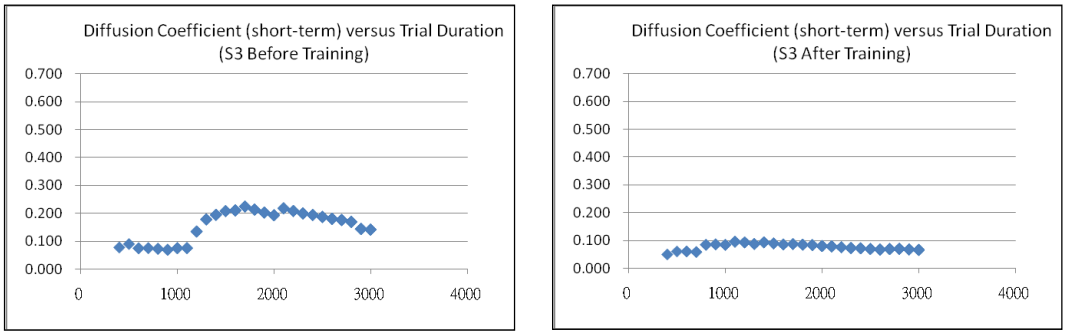


Figure 3.27. Comparison on plots of the short-term diffusion coefficient against the trial duration of participant 3 before and after training.

### 3.2.5. Effect on the Short-term Hurst Exponent

The comparison of plots of the short-term Hurst exponent against the trial duration of all three participants for both before and after training are shown in Figure 3.28 to 3.30. Most of the capture showed stability with a trial duration from four seconds onward. However, in the capture of participant 3 before training, a stable value could only be found after 12 seconds. In addition, in the capture of participant 1 after training, there was a step decrement of 1.5 after 22 seconds.

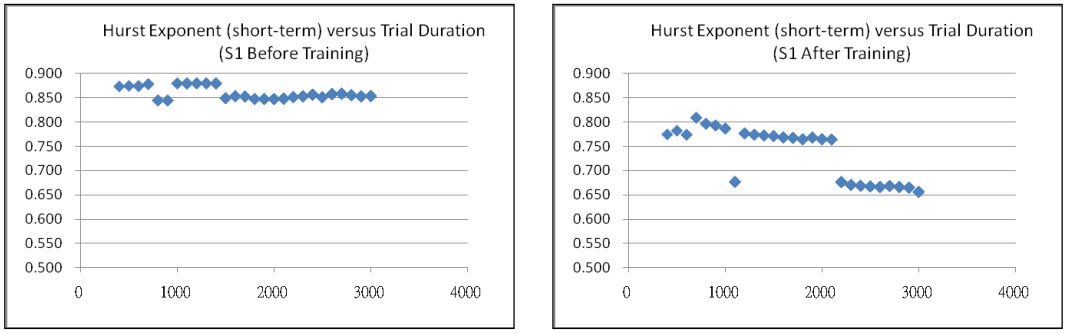


Figure 3.28. Comparison on plots of the short-term Hurst exponent against the trial duration of participant 1 before and after training.

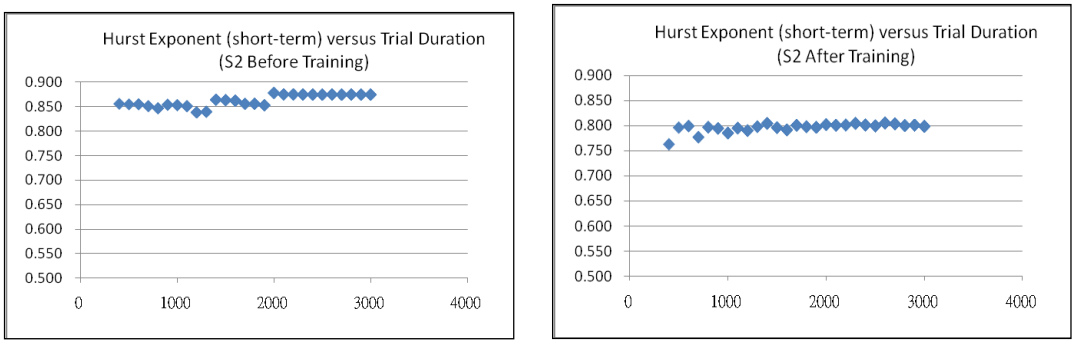


Figure 3.29. Comparison on plots of the short-term Hurst exponent against the trial duration of participant 2 before and after training.

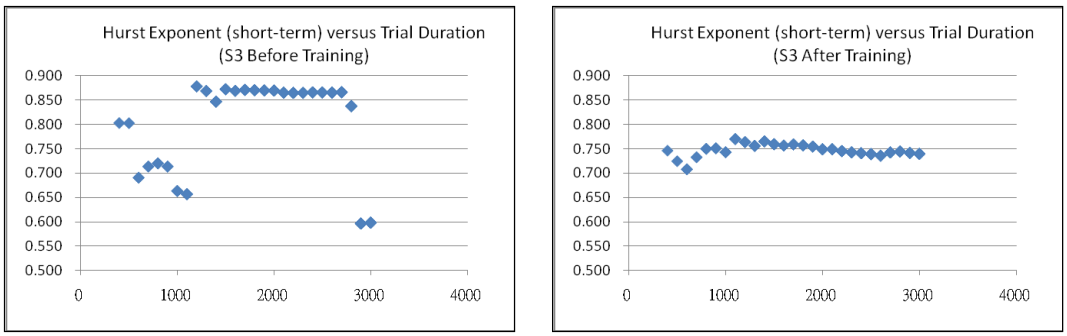


Figure 3.30. Comparison on plots of the short-term Hurst exponent against the trial duration of participant 3 before and after training.

In short, there were various definite values of the trial duration that signified the stability of the dynamic features (Table 3.3). Considering the Brownian characteristics across the critical time, mean square angle, short-term diffusion coefficient, and short-term Hurst exponent, a stable and consistent value could be obtained with a trial duration of eight seconds or longer. In this case, the accuracy was within ±0.1. If the exception cases were also considered, a trial duration of 12 seconds or longer could be obtained.

Table 3.3. Definite values of the trial duration that signified the stability of the dynamic features.

| Duration | Stability on Brownian Characteristics |
|---|---|
| 4s | (short-term Hurst) most values showed the stability |
| 5s | (mean sq angle) most values showed the stability |
| 7s | (short-term diffusion) most values showed the stability |
| 8s | (critical time) most values showed the stability |
| 12s | (critical time) exception on trial 3 before training<br>(mean sq angle) exception on trial 3 before training<br>(mean sq angle) exception on trial 1 after training<br>(short-term Hurst) exception on trial 3 before training |
| 22s | (critical time) exception on trial 1 after training<br>(short-term Hurst) exception on trial 1 after training |

### 3.2.6. Trial Averaging

Several trial data acquisitions resulted in capturing the movement of a participant. In the analysis process, these trials were usually computed for a resultant output to describe the data from a single participant. In this section, the objective is to determine which averaging method for the integration of the trial data is more consistent with an individual trial in terms of Brownian characteristics. Three types of computation were attempted. The first and most primitive method of dealing with raw data was the averaging method applied to the positional data captured using the data acquisition system. The second method considered the diffusion characteristics of which every trial was computed. Subsequently, the average was

applied across the diffusion data after the mean square angle was calculated. The third method was a control set of which every single trial was used to perform the computation, and the results were compared to those of the previous two methods. The analysis was conducted in the upright sitting experiment mentioned in previous sections. The data acquisition was achieved using an optical motion capture system operating at 60 Hz. Passive markers were attached to the skin proximal to bony prominences along the spine and around the participant body. There were a total of 16 markers along the spine that were considered for the analysis of this section. These markers included C5, C6, C7, T1, T3, T5, T7, T9, T11, L1, L2, L3, L4, L5 and S1. The participant was requested to maintain the upright position for 30 seconds in each trial. The data of 10 trials were collected. In between consecutive trials, the participant was allowed to take a one-minute break to eliminate the influence of fatigue.

In the process of preparing the curvature information, the position data of markers were filtered using a zero-phase third-order Butterworth low-pass digital filter at 4-Hz cut-off frequency. The angle data in unit of degree were then calculated from the selection of three ordered markers along the spine. The ordered markers were either taken in consecutive order or spanning an equal number of markers on both sides of the origin of angle.

### 3.2.7. Method of Averaging Position Data

Given 10 trials of low-pass filtered position data, the average was taken for each position value across different trials. Subsequently, the angles were calculated along the spine and according to different configurations of spanning data intervals. The mean square angles were computed afterward according to SDA. The Brownian characteristics were later extracted from the curvature diffusion plot for analysis. Results showed that 16 out of 49 specifications of spinal curvature were unable to determine the critical time (Table 3.4). These angles happened to be around the longer spanning data interval area. The angles at spanning data intervals 3 and 4 were found in the lower thoracic and lumbar regions.

Table 3.4. Spinal angle intervals found unable to determine the critical time.

| |
|---|
| 3 out of 9 at spanning data interval 3 |
| 4 out of 7 at spanning data interval 4 |
| 5 out of 5 at spanning data interval 5 |
| 3 out of 3 at spanning data interval 6 |
| 1 out of 1 at spanning data interval 7 |
| Total: 16 out of 49 |

### 3.2.8. Method of Averaging Diffusion Plot

The second method of averaging the data of the 10 trials was to consider the averaging step after the diffusion characteristics were computed for each individual trial. Given 10 trials of low-pass filtered position data, the angles were calculated along the spine and according to different configurations of spanning data intervals.

The mean square angles were then computed according to SDA. The major difference from the previous method was that the averaging step occurred here at the mean square angles corresponding to the time interval dimension. This became a resultant diffusion plot of a participant combining the data of 10 trials. Finally, the Brownian characteristics were extracted from the resultant plot for analysis.

From the resultant plot, only two angles out of 49 were found to be unable to determine the critical time. One was found in the lower region of the spine under spanning data interval 6, and the other one was interval 7, which described the overall superimposed curvature of the whole spine.

### 3.2.9. Individual Trial Data

As a control method for comparison, individual trial data were computed to extract the Brownian characteristics. The angles were calculated directly from the low-pass filtered position data. The mean square angles were then computed according to SDA. Finally, the Brownian characteristics were extracted.

According to different trials, there were various angles in which the critical time was unable to be determined. This phenomenon was also found in the previous two averaging methods. However, the number of angles was different. For the control set, this number was within the range of 0 to 7, with a mean value of 2.4 and a standard deviation of 2.0. This number was similar to that of the method of averaging diffusion plot. The dynamic features of that method were used for the

averaging of mean square angles. As a result, the control behavior retained. By contrast, the method of averaging position data showed a large discrepancy compared to the control method. In conclusion, the method of averaging diffusion plot is more suitable for the integration of various trial data.

### 3.2.10. Butterworth Filtering

Raw data captured using the digital system through the acquisition process are usually subjected to noise introduced. Digital processing includes a step of filtering to eliminate the noise with special characteristics from the useful raw data. In handling human motion data through the acquisition process, Butterworth low-pass filtering is often used as a tool to eliminate high-frequency noise introduced by the digital system. In this section, the objective is to extract the relationship between different frequencies of the Butterworth filter and the Brownian characteristics. An appropriate frequency was found to be more suitable for the captured data under SDA.

The analysis was based on the data acquired from the experiment of upright sitting. The data acquisition was completed using the optical motion capture system operating at 60 Hz. Passive markers were attached to the skin proximal to bony prominences along the spine and around the participant body. The marker on T11 was used as the origin of angle. With T11 at the center, the marker positions of T9 and L1 were collected with one spanning data interval. A zero-phase third-order

Butterworth low-pass digital filter was used by adapting the built-in function inside MATLAB software.

Different cut-off frequencies of the Butterworth low-pass digital filter were applied to the position data. These included 29Hz, 20Hz, 10Hz, 8Hz, 6Hz, 5Hz, 4Hz, 3Hz, 2.5Hz, 2Hz, 1.5Hz, and 1Hz. Angles were then calculated based on the filtered position data of different cut-off frequencies. The data were verified using selected statistical properties to ensure that there was no outstanding value within the data source (Table 3.5).

Table 3.5. Statistical properties on the data source subjected to various low-pass filters.

| Filter Applied | MIN | MAX | MEAN | STDEV |
|---|---|---|---|---|
| NA | 169.550 | 172.830 | 171.110 | 0.491 |
| 29 Hz BW | 169.430 | 172.780 | 171.110 | 0.488 |
| 20 Hz BW | 169.460 | 172.460 | 171.110 | 0.464 |
| 10 Hz BW | 169.720 | 172.290 | 171.110 | 0.436 |
| 8 Hz BW | 169.840 | 172.290 | 171.110 | 0.429 |
| 6 Hz BW | 169.970 | 172.260 | 171.110 | 0.422 |
| 5 Hz BW | 169.980 | 172.280 | 171.110 | 0.417 |
| 4 Hz BW | 169.990 | 172.280 | 171.110 | 0.411 |
| 3 Hz BW | 170.100 | 172.260 | 171.110 | 0.403 |
| 2.5 Hz BW | 170.210 | 172.230 | 171.110 | 0.396 |
| 2 Hz BW | 170.350 | 172.160 | 171.110 | 0.386 |
| 1.5 Hz BW | 170.360 | 172.070 | 171.110 | 0.372 |
| 1 Hz BW | 170.390 | 172.010 | 171.110 | 0.352 |

Brownian characteristics were then extracted using a self-developed procedure on the MATHLAB platform, as shown in Table 3.6. In the cases of having no filter applied and a cut-off frequency of 29 Hz, the critical time was not found. For the

other cases, the critical time increased with decreasing cut-off frequencies. It changed from the value of 0.017 to 0.633. In relation to the critical time point, the mean square angle at critical time maintained a consistent value within the range of 0.09 and 0.12, except 29 Hz and the one without filter, which were 0.132 and 0.143, respectively. With decreasing frequencies, there was a turning point at 3 Hz signifying the increasing and decreasing trend of the mean square value at the critical time point. By contrast, the short-term diffusion coefficients decreased with decreasing frequencies. With the same decreasing frequencies, the short-term Hurst exponent signified an increasing and decreasing trend at a turning point of 2.5 Hz cut-off frequency. Except for the two cases without critical time, all the short-term Hurst exponents had values larger than 0.5. Regarding the long-term diffusion coefficient, it had a stable value of approximately 0.01 at all frequencies. The long-term Hurst exponents also exhibited a consistent range of 0.09 to 0.15 at all frequencies. In addition, the values increased with decreasing frequencies.

Table 3.6. Brownian characteristics of data subjected to various low-pass filters.

| Filter Applied | $\Delta t_c$ | $\langle \Delta X^2 \rangle_c$ | $D_s$ | $D_l$ | $H_s$ | $H_l$ |
|---|---|---|---|---|---|---|
| N/A | 0.017 | 0.143 | 0.000 | 0.011 | 0.237 | 0.088 |
| 29 Hz BW | 0.017 | 0.132 | 0.000 | 0.011 | 0.247 | 0.090 |
| 20 Hz BW | 0.033 | 0.123 | 2.076 | 0.011 | 0.595 | 0.099 |
| 10 Hz BW | 0.067 | 0.091 | 0.817 | 0.010 | 0.787 | 0.112 |
| 8 Hz BW | 0.083 | 0.091 | 0.650 | 0.010 | 0.820 | 0.114 |
| 6 Hz BW | 0.117 | 0.105 | 0.525 | 0.010 | 0.841 | 0.115 |
| 5 Hz BW | 0.133 | 0.108 | 0.467 | 0.010 | 0.860 | 0.117 |
| 4 Hz BW | 0.167 | 0.118 | 0.406 | 0.010 | 0.862 | 0.119 |
| 3 Hz BW | 0.217 | 0.125 | 0.329 | 0.010 | 0.866 | 0.123 |
| 2.5 Hz BW | 0.250 | 0.124 | 0.281 | 0.010 | 0.868 | 0.127 |

| | | | | | | |
|---|---|---|---|---|---|---|
| 2 Hz BW | 0.300 | 0.120 | 0.226 | 0.009 | 0.867 | 0.132 |
| 1.5 Hz BW | 0.400 | 0.117 | 0.164 | 0.009 | 0.859 | 0.141 |
| 1 Hz BW | 0.633 | 0.124 | 0.109 | 0.009 | 0.840 | 0.150 |

Combining all the aforementioned features, the data exhibited significant Brownian characteristics at cut-off frequencies of 2.5 Hz to 3 Hz.

### 3.2.11. Time Interval

The objective of this section is to evaluate the independency of the time interval with the other dynamic features when applied in the curvature diffusion plot. Experimental data from the previous setup of cervical spine retraction training were used. A zero-phase third-order Butterworth low-pass digital filter at 10-Hz cut-off frequency was applied to the angle data calculated. To enhance the consistency while using different time intervals, various trial durations were also used. The time intervals used here ranged from 2s to a time which is half of the trial duration. Regarding the Brownian characteristics of critical time, the mean square angle at the critical time point, the short-term diffusion coefficient, and the short-term Hurst exponent, there was no change in value with any fixed trial duration between 4 and 30 seconds. Because almost all the critical time occurred under one second, the critical time fell within the range of the time interval applied, which was set from 2 seconds onward. The values of the mean square angle at critical time, short-term diffusion coefficient, and short-term Hurst exponent all substantially depended on the location of critical time. Because the location of critical time did not change with

different time intervals, these dynamic features were not affected by any time intervals set at a fixed trial duration.

By contrast, the long-term Brownian characteristics of the diffusion coefficient and Hurst exponent were affected by varying the time interval with any fixed trial duration (Figure 3.31 to 3.36). In these figures, the vertical axis illustrates the values of the long-term diffusion coefficient. The horizontal axis going from front to back represents the particular fixed trial duration as a reference parameter. The duration ranges from 400 mille-seconds to 3000 mille-seconds. The horizontal axis going from right to left illustrates the varying time interval for evaluation. For any particular fixed trial duration, the time interval ranges from 200 mille-seconds to a time which is half of the trial duration by rounding down to hundred unit of mille-seconds. In general, the diffusion coefficient and Hurst exponent showed a more favorable stability in values with a time interval at 8 seconds or longer.

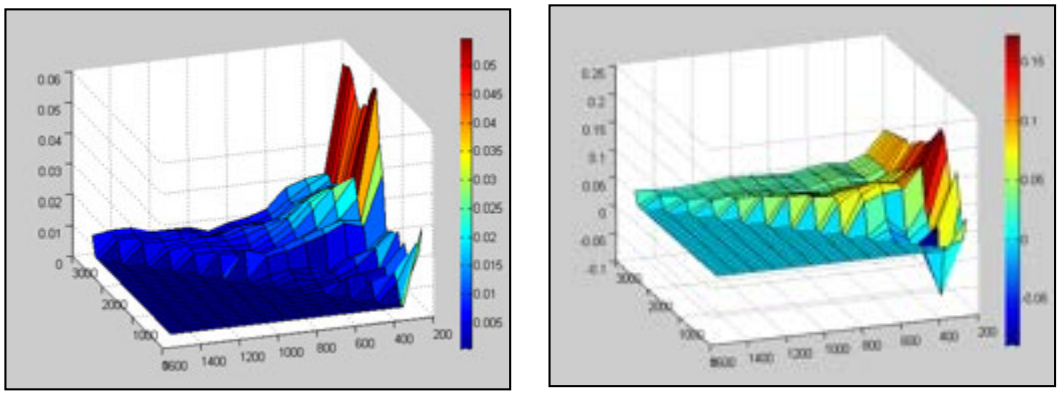

Figure 3.31. Comparison of the long-term diffusion coefficients of participant 1 before and after retraction training.

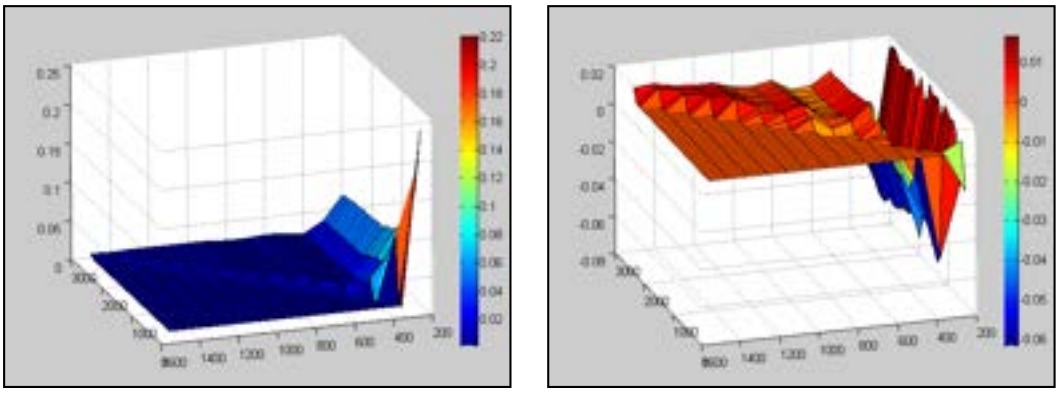

Figure 3.32. Comparison of the long-term diffusion coefficients of participant 2 before and after retraction training.

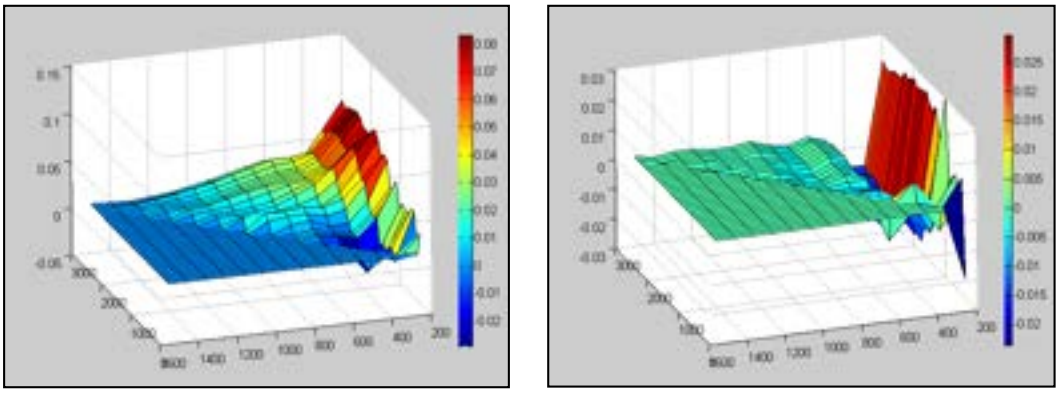

Figure 3.33. Comparison of the long-term diffusion coefficients of participant 3 before and after retraction training.

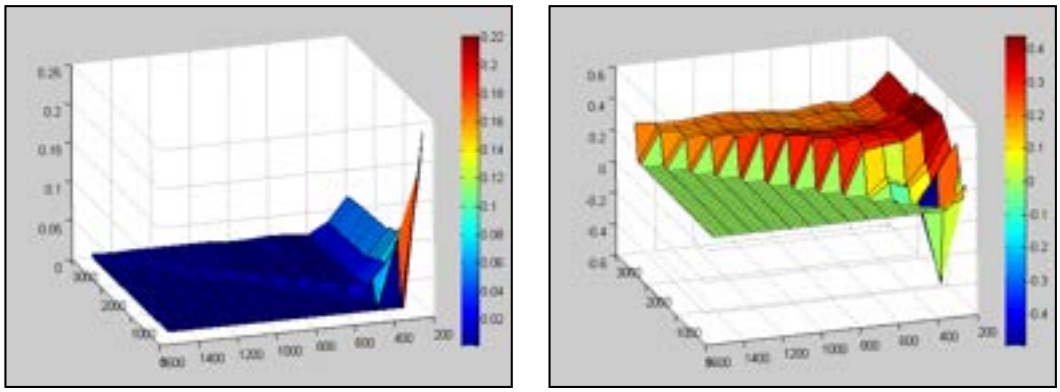

Figure 3.34. Comparison of the long-term Hurst exponent of participant 1 before and after retraction training.

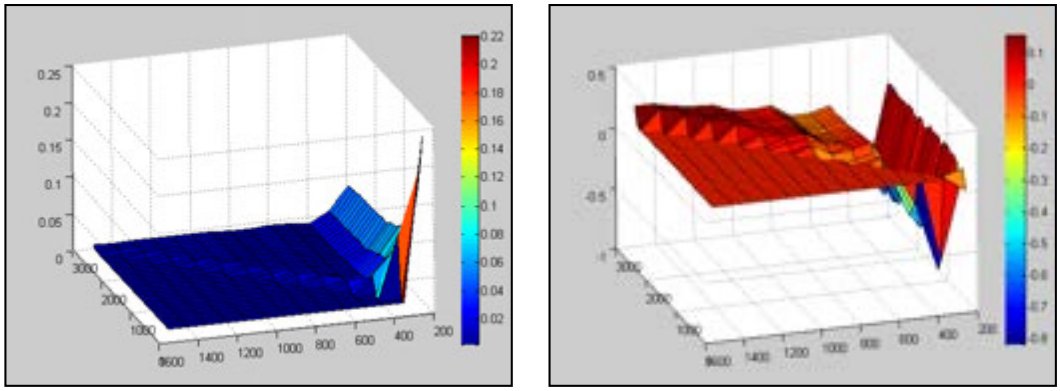

Figure 3.35. Comparison of the long-term Hurst exponent of participant 2 before and after retraction training.

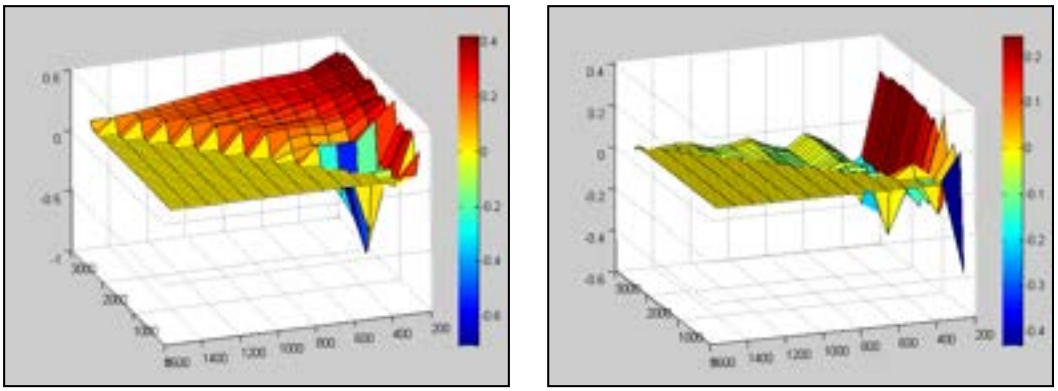

Figure 3.36. Comparison of the long-term Hurst exponent of participant 3 before and after retraction training.

In conclusion, because critical time usually appeared between 0 and 2 seconds, any time interval longer than 2 seconds was suitable for analysis on Brownian characteristics, except for long-term dynamic features. An 8-second time interval was suitable for analyzing long-term characteristics.

## 3.3. Differentiation of Participant Characteristics

After the development of the analysis model and the assessment of the protocol, the methodology was applied for potential practical contribution. Conclusion, by means of the dynamic features, was reached after computation and analysis. The objective was to differentiate various participant characteristics. The hypothesis was that participants with various characteristics would exhibit various dynamic features in control. The first experiment distinguished the features of spinal control in the

cervical region between patients and normal participants. This was the first step in applying the research outcomes to clinical use for preliminary inspection or differentiation. The second experiment was about the developmental changes of children. The experiment was conducted on schoolchildren of ages 11 and 15 years. Attempts were made to reveal their spinal motor control development and the effects of age and gender. The evaluation assessed their sensitivity for spinal motion control measurement and also explored the development of spinal motion control.

### 3.3.1. Distinguish between Patients and Normal Participants

In this experiment, the objective was to distinguish the dynamic features of patients and of normal participants with respect to cervical spinal control by means of SDA. The setup of the experiment refers to commonly used cervical spine retraction training. One normal participant and one neck pain patient were involved in the data acquisition. The normal participant was reported as having no neck pain history that lasted for more than three days in the last year. The patient had mechanical neck pain that lasted for at least six weeks, including myofascial neck pain and degenerative changes, with no radiating symptom.

Four stages, namely S – self-adopted posture, I – upright posture before training, T – training stage, and F – upright posture after training, were defined as the acquisition sequence. In the “S” phase, participants were asked to maintain a daily sitting posture for at least ten seconds per trial during data capturing. A rest of 15 seconds

was provided between consecutive trials, and the data of 10 trials were collected. During the “I” phase, participants were requested to perform an upright sitting posture as steadily as possible. The capture lasted for 10 seconds per trial. A total of 10 trials were conducted with 10 seconds of rest between consecutive trials. A neck retraction exercise was taught before entering the “T” phase. The capture in that stage was of their performance during the exercise. The capture time and regulation were the same as those in the previous phase. At the final stage, the participants were requested to maintain an upright sitting posture as they did in the “I” stage as steadily as possible. The capture lasted 10 seconds, and the data of 10 trials were acquired with 15 seconds of rest between each consecutive trial.

Regarding the marker placement, there were nine markers attached to the skin of participants, as shown in Table 3.7. The markers at the “Head” and “Shoulder” sections were used for the calculation of kinematic data. The markers at the “Skull” section were used for the rectification and estimation of virtual markers during the post-processing of motion capture data.

Table 3.7. Nine markers attached to the participant.

| **Head** | **Shoulder** | **Skull** |
|---|---|---|
| RTRA - Right tragus | RAPR - Right acromion process | FHD - Forehead (with hair band) |
| LTRA - Left tragus | LAPR - Left acromion process | BHD - Back-head (with hair band) |
| LORB - Left orbital | C7 - Spinous process | C4 - Spinous process |

Position data were filtered using a zero-phase third-order Butterworth low-pass digital filter with 4-Hz cut-off frequency applied. Subsequently, the angular flexion and extension on the cervical spine were calculated.

The hypothesis was made on the dynamic features between the patient and normal participant. Initially, a patient had a larger value of critical time than did a normal participant. As shown in Table 3.8, the experimental results proved that the critical time of a patient was consistently larger than that of a normal participant in all four phases.

Table 3.8. Comparing the critical time in four phases between a patient and a normal participant.

| **Participant** | **Phase** | **$\Delta t_c$** |
|---|---|---|
| **Patient** | S | 1.07 |
| | I | 0.99 |
| | T | 0.87 |
| | F | 0.78 |
| **Normal** | S | 0.94 |
| | I | 0.87 |
| | T | 0.81 |
| | F | 0.48 |

The other dynamic feature is about the diffusion coefficient. It was hypothesized that a patient would have a larger value than would a normal participant. As shown in Table 3.9, except the short-term diffusion coefficient of phases “S” and “F,” most of the data are consistent with the hypothesis that a patient has a larger value than

does a normal participant. The long-term diffusion coefficients are similar in value across the table and do not show any major difference.

Table 3.9. Comparing the diffusion coefficient in four phases between a patient and a normal participant.

| Participant | Phase | $D_s$ | $D_l$ |
|---|---|---|---|
| **Patient** | S | 0.05 | 0.03 |
| | I | 0.14 | 0.03 |
| | T | 0.11 | 0.04 |
| | F | 0.14 | 0.07 |
| **Normal** | S | 0.07 | -0.03 |
| | I | 0.07 | -0.02 |
| | T | 0.06 | -0.01 |
| | F | 0.17 | 0.02 |

Regarding the short-term Hurst exponent, it was hypothesized that both a patient and a normal participant would have values larger than 0.5, and a patient would have a smaller value than normal. As the experimental results show in Table 3.10, the values matched with the hypothesis in all four phases.

Table 3.10. Comparing the Hurst exponent in four phases between a patient and a normal participant.

| Participant | Phase | $H_s$ |
|---|---|---|
| **Patient** | S | 0.73 |
| | I | 0.81 |
| | T | 0.76 |
| | F | 0.82 |
| **Normal** | S | 0.78 |
| | I | 0.85 |

| | | |
|---|---|---|
| | T | 0.83 |
| | F | 0.86 |

The difference between a patient and a normal participant with respect to the selected dynamic properties is shown in Table 3.11. The experimental results show that the two types of participants who carried different characteristics exhibited different dynamic features.

Table 3.11. Results of the dynamic features between a patient and a normal participant.

| **Dynamic Features** | **Patient** | **Normal** |
|---|---|---|
| Critical Time | Longer | Shorter |
| Diffusion Coefficient (short- and long-term) | Larger | Smaller |
| Hurst Exponent (short-term) | > 0.5 | >0.5 |
| Hurst Exponent (short-term) | Smaller | Larger |
| Hurst Exponent (long-term) | < 0.5 | < 0.5 |

### 3.3.2. Significance in the Spinal Motor Control between Age Groups

In this section, the study focuses on the exploration of dynamic features of spinal postural control by using fractional Brownian motion (fBm) analysis for the effects of age and gender in relation to the development of children. We recruited four target groups of children. A total of 64 schoolchildren were divided equally among girls aged 11 years, boys aged 11 years, girls aged 15 years, and boys aged 15 years. All of

them were reported healthy without any known history of back pain or neurological or musculoskeletal disorders in the previous 12 months.

Participants were asked to stand upright as steadily as possible on a foam base with their eyes closed. The foam was of 10-cm thickness and 50-kg/$m^3$ density. It was used to increase the challenge for stance balance. The duration of data acquisition in each trial was 30 seconds. A total of three trials were conducted with at least 30 seconds of rest between consecutive trials. Six gravitationally referenced accelerometers (ADXL311, Analog Devices Inc., USA) were used to measure the spinal curvature. The signal was captured using an analogue-to-digital converter (DAQ6225, National Instruments Corporation, USA) at a sampling frequency of 100 Hz. The acquisition of the data was controlled using a self-developed program on a LabVIEW (National Instruments Corporation, USA) platform. Calibration was conducted on all the accelerometers prior to the experiments. The root mean square error of the devices was between 0.4 and 0.7 degree.

The accelerometers were attached to the skin proximal to bony prominences of the occiput (OC) and the spinous processes of C7, T7, T12, L3, and S1 (as shown in Figure 3.37). The participants were asked to slightly flex their trunks when positioning the accelerometers to minimize possible sensor displacement during trunk movements. Spinal curvatures of different regions were determined.

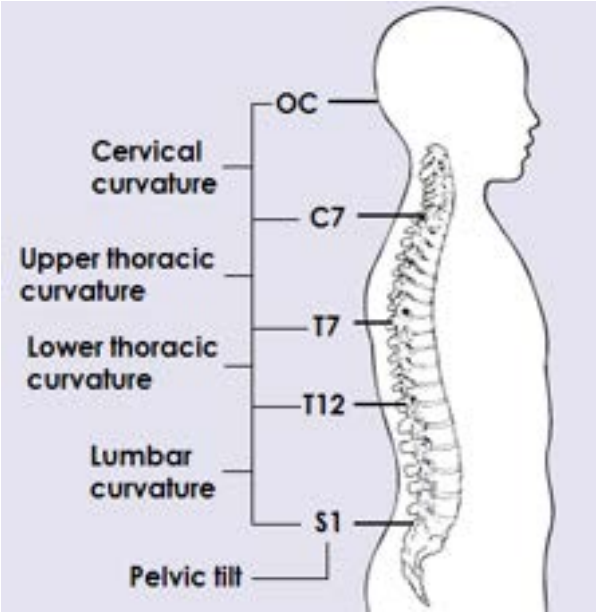


Figure 3.37. Spinal curvatures of different regions and accelerometer positions.

The data captured were filtered using a fourth-order Butterworth low-pass filter with a cut-off frequency of 4 Hz. In this case, the cut-off frequency was determined using the residual analysis technique [158]. MATLAB was used as the computation platform for filtering and obtaining fBm characteristics. The averaging was achieved in two phases. The first phase applied the averaging method for each individual participant by using the mean square angles computed across various trials. Subsequently, the dynamic features were computed for each participant. The second phase applied the averaging of each dynamic feature of all participants contained in each group.

### 3.3.3. Difference in the Critical Time

Almost all critical time values of 11-year-old children were larger than those of 15-year-old children (Table 3.12 and Figure 3.38). However, by observation, 37 out of 384 data values across all spinal regions of individual participant were found to be substantially greater than the grand average. They ranged from 2 to 7 standard deviations above the mean value.

Table 3.12. Statistics of the critical time values in different spinal regions of participant groups.

| | **OC & C7** | **C7 & T7** | **T7 & T12** | **T12 & L1** | **L1 & L3** | **S1** |
|---|---|---|---|---|---|---|
| | **Critical Time (Mean)** | | | | | |
| **M 11** | 0.26 | 0.70 | 0.48 | 0.36 | 0.63 | 0.47 |
| **M 15** | 0.25 | 0.53 | 0.34 | 0.35 | 0.48 | 0.43 |
| **F 11** | 0.28 | 0.56 | 0.53 | 0.45 | 0.64 | 0.48 |
| **F 15** | 0.26 | 0.52 | 0.38 | 0.50 | 0.66 | 0.46 |
| | **Critical Time (Standard Deviation)** | | | | | |
| **M 11** | 0.02 | 0.55 | 0.33 | 0.07 | 0.39 | 0.24 |
| **M 15** | 0.02 | 0.38 | 0.18 | 0.04 | 0.40 | 0.11 |
| **F 11** | 0.04 | 0.33 | 0.36 | 0.25 | 0.28 | 0.22 |
| **F 15** | 0.02 | 0.34 | 0.24 | 0.33 | 0.35 | 0.19 |

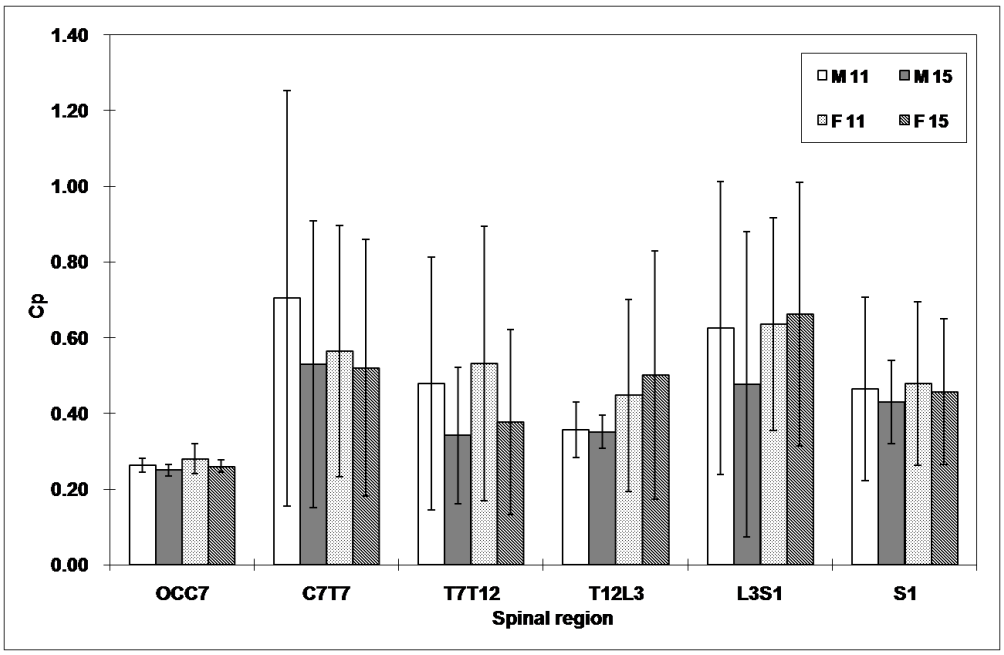


Figure 3.38. Statistics of the critical time values in different spinal regions of participant groups.

### 3.3.4. Difference in the Diffusion Coefficient

From the computation results, both short-term (Table 3.13 and Figure 3.39) and long-term (Table 3.14 and Figure 3.40) diffusion coefficients were found to be significantly larger in 11-year-old children than in 15-year-old children. Exception was only found in one female participant aged 15 years who had a substantially large value of the long-term diffusion coefficient at 1.17, compared to the mean of 0.14 for others in the same group.

Table 3.13. Statistics of the short-term diffusion coefficient values in different spinal regions of participant groups.

| | OC & C7 | C7 & T7 | T7 & T12 | T12 & L1 | L1 & L3 | S1 |
|---|---|---|---|---|---|---|
| | **Short-term Diffusion Coefficients (Mean)** | | | | | |
| **M 11** | 2.06 | 0.34 | 0.35 | 0.63 | 0.29 | 0.47 |
| **M 15** | 1.64 | 0.11 | 0.24 | 0.51 | 0.22 | 0.39 |
| **F 11** | 2.26 | 0.33 | 0.50 | 0.93 | 0.33 | 0.63 |
| **F 15** | 1.19 | 0.17 | 0.14 | 0.35 | 0.27 | 0.34 |
| | **Short-term Diffusion Coefficients (Standard Deviation)** | | | | | |
| **M 11** | 1.09 | 0.40 | 0.50 | 0.70 | 0.18 | 0.26 |
| **M 15** | 0.97 | 0.06 | 0.25 | 0.52 | 0.17 | 0.23 |
| **F 11** | 0.89 | 0.25 | 0.46 | 0.87 | 0.29 | 0.51 |
| **F 15** | 1.01 | 0.41 | 0.15 | 0.32 | 0.49 | 0.16 |

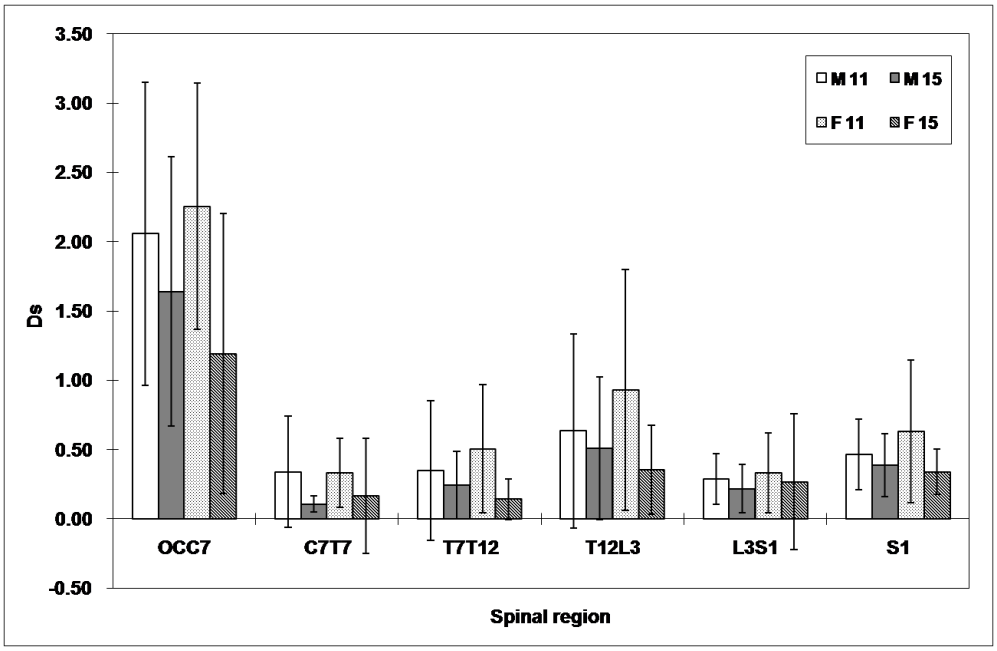


Figure 3.39. Statistics of the short-term diffusion coefficient values in different spinal regions of participant groups.

Table 3.14. Statistics of the long-term diffusion coefficient values in different spinal regions of participant groups.

| | OC & C7 | C7 & T7 | T7 & T12 | T12 & L1 | L1 & L3 | S1 |
|---|---|---|---|---|---|---|
| | **Long-term Diffusion Coefficients (Mean)** | | | | | |

| | | | | | | |
|---|---|---|---|---|---|---|
| **M 11** | 0.29 | 0.07 | 0.06 | 0.11 | 0.07 | 0.08 |
| **M 15** | 0.17 | 0.02 | 0.04 | 0.06 | 0.05 | 0.06 |
| **F 11** | 0.40 | 0.07 | 0.12 | 0.16 | 0.07 | 0.11 |
| **F 15** | 0.15 | 0.02 | 0.03 | 0.18 | 0.05 | 0.05 |
| | **Long-term Diffusion Coefficients (Standard Deviation)** | | | | | |
| **M 11** | 0.29 | 0.07 | 0.05 | 0.11 | 0.04 | 0.04 |
| **M 15** | 0.17 | 0.03 | 0.04 | 0.06 | 0.04 | 0.03 |
| **F 11** | 0.31 | 0.06 | 0.14 | 0.18 | 0.04 | 0.08 |
| **F 15** | 0.11 | 0.03 | 0.04 | 0.27 | 0.05 | 0.05 |

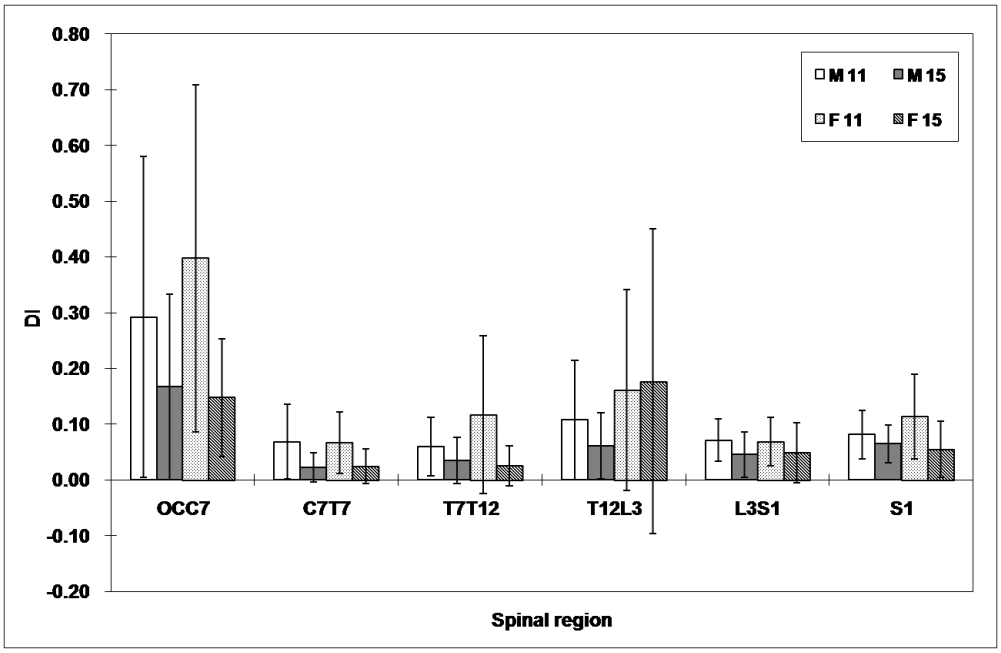


Figure 3.40. Statistics of the long-term diffusion coefficient values in different spinal regions of participant groups.

### 3.3.5. Difference in the Mean Square Angle at Critical Time

Regarding the mean square angle at the critical time point, all the values of 11-year-old children were larger than those of 15-year-old children (Table 3.15 and Figure

3.41). However, 32 out of 384 values across all spinal regions of individual participant data were found to be substantially larger than the grand average. They ranged from 2 to 9 standard deviations above the mean value.

Table 3.15. Statistics of the mean square angle at critical time point in different spinal regions of participant groups.

| | **OC & C7** | **C7 & T7** | **T7 & T12** | **T12 & L1** | **L1 & L3** | **S1** |
|---|---|---|---|---|---|---|
| | **Mean Square Angle at Critical Time (Mean)** | | | | | |
| **M 11** | 0.96 | 0.56 | 0.25 | 0.48 | 0.31 | 0.42 |
| **M 15** | 0.73 | 0.09 | 0.13 | 0.31 | 0.23 | 0.28 |
| **F 11** | 1.13 | 0.37 | 0.39 | 0.69 | 0.35 | 0.61 |
| **F 15** | 0.55 | 0.14 | 0.10 | 0.44 | 0.31 | 0.28 |
| | **Mean Square Angle at Critical Time (Standard Deviation)** | | | | | |
| **M 11** | 0.50 | 1.02 | 0.27 | 0.68 | 0.22 | 0.39 |
| **M 15** | 0.44 | 0.07 | 0.13 | 0.33 | 0.44 | 0.15 |
| **F 11** | 0.46 | 0.41 | 0.36 | 0.54 | 0.30 | 0.72 |
| **F 15** | 0.46 | 0.31 | 0.11 | 0.61 | 0.57 | 0.22 |

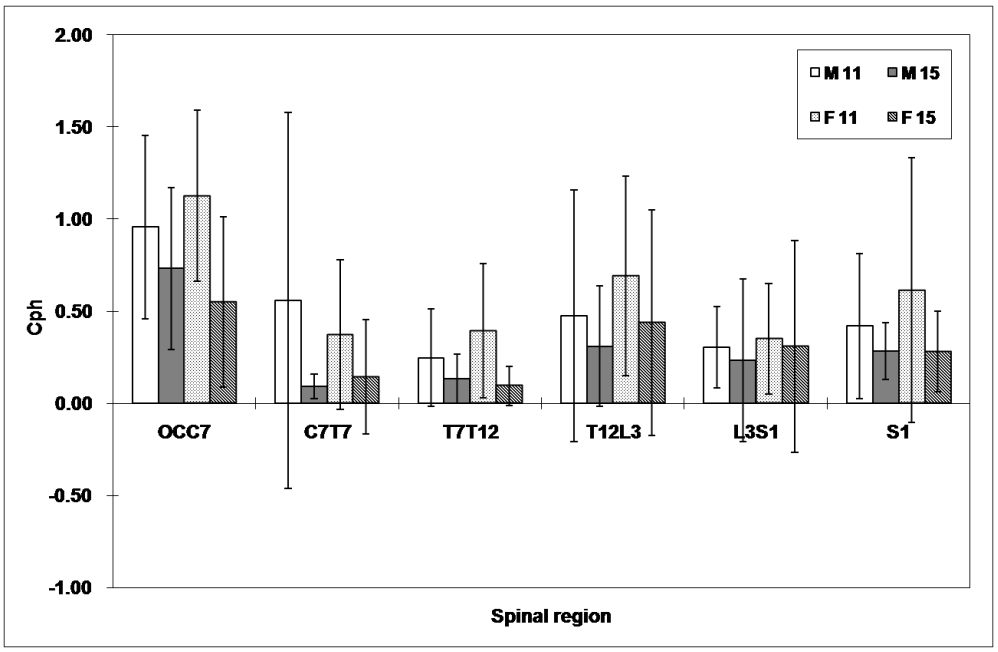


Figure 3.41. Statistics of the mean square angle at critical time point in different spinal regions of participant groups.

### 3.3.6. Difference in the Hurst Exponent

The mean and standard deviation of the short-term Hurst exponent of different spinal regions were determined (Table 3.16). For the short-term region, the Hurst exponents of all spinal regions were larger than 0.5.

Table 3.16. Means and standard deviations of short-term Hurst exponents in different spinal regions.

| | OC & C7 | C7 & T7 | T7 & T12 | T12 & L1 | L1 & L3 | S1 |
|---|---|---|---|---|---|---|
| | **Short-term Hurst Exponent (Mean)** | | | | | |
| **M 11** | 0.89 | 0.86 | 0.87 | 0.90 | 0.86 | 0.89 |
| **M 15** | 0.88 | 0.88 | 0.89 | 0.89 | 0.91 | 0.90 |
| **F 11** | 0.89 | 0.87 | 0.86 | 0.88 | 0.86 | 0.89 |

| | | | | | | |
|---|---|---|---|---|---|---|
| **F 15** | 0.87 | 0.86 | 0.89 | 0.88 | 0.87 | 0.90 |
| | **Short-term Hurst Exponent (Standard Deviation)** | | | | | |
| **M 11** | 0.03 | 0.07 | 0.07 | 0.02 | 0.07 | 0.05 |
| **M 15** | 0.04 | 0.06 | 0.04 | 0.03 | 0.01 | 0.02 |
| **F 11** | 0.03 | 0.06 | 0.07 | 0.05 | 0.05 | 0.04 |
| **F 15** | 0.05 | 0.07 | 0.05 | 0.05 | 0.06 | 0.02 |

### 3.3.7. Discussion

In conclusion, as shown in Table 3.17, features of the smaller diffusion coefficient, shorter critical time, and smaller mean square angle, a preliminary statement could indicate that the spinal motor control of 15-year-old children was more favorable than that of 11-year-old children. Although the variation of the participant group was statistically diverse, it reflected the evidence that the variability of this participant group was large. The curvature variability during upright stance in children of 11 years old was larger than that in children of 15 years old. In addition, the 11-year-old children also required larger curvature deformation and a longer response time for triggering the open-loop feedback control. The spinal curvature was independent of age and gender, while the spinal postural control was affected by age. The findings revealed that the spinal motor control is associated with age and the spinal motor control in 11-year-old children might be underdeveloped.

Table 3.17. Overall results of dynamic features comparing 11- and 15-year-old children.

| **Dynamic Parameters** | **11 years old** | **15 years old** |
|---|---|---|
| Diffusion Coefficient (short- and long-term) | Larger | Smaller |
| Critical Time | Larger | Smaller |
| Mean Square Angle | Larger | Smaller |
| Hurst Exponent (short-term) | > 0.5 | > 0.5 |
| Hurst Exponent (long-term) | < 0.5 | < 0.5 |

According to the experimental procedure, the participant was instructed to stand on the foam base with closed eyes during the measurement. The sensory information from the vision and vestibular apparatus was challenged, and therefore the outcomes mainly reflected the closed-loop proprioceptive feedback control. Moreover, the diffusion coefficient of the short-term region was determined. Similar to the study by Collins and De Luca [29], the diffusion coefficient of the persistent motion was larger compared to the region after the critical time point, which showed that the curvature variability (postural instability) of persistent movement was large with open-loop feedback control. In addition, with the transition point automatic determination method [54], the transition point, that is, the boundary between the short-term and subsequent regions, could be consistently determined. Physiologically, the transition point indicates the region of the open-loop behaviors [29]. The coordinates, denoted by critical time and critical mean square curvature, can indicate the average response time and the average curvature deformation required for triggering the open-loop feedback control system. Moreover, the response time ranged between 0.26s and 0.66s, which indicated that the control of

the spine in maintaining upright stance was M3 response, that is, voluntary reaction [132]. The findings confirmed that this analytical method could be applied for studying spinal motor control, which could be used to further investigate the neurological control of the spine. In addition, it also provides a new approach for deepening our understanding of spinal motor control, for example critical time, which could not be determined using conventional assessments.

Through this experiment, the spinal motor control was quantified by the spinal postural control ability. The spinal postural control ability represented the ability to maintain the upright stance by computing the changes in the magnitude and direction of the spinal curvature within the 30-second upright stance, including control characteristics (i.e., open-loop feedback control), the variation of movement, as well as the requirement of response time and curvature deformation for open-loop feedback control. Therefore, the dynamic characteristics of the spinal postural control ability could be reflected by the parameters with more apparent clinical relevance, which could be useful for clinical diagnosis and evaluation.

## 3.4. Limitation

The fractal model for spinal curvature has been developed. Evaluation on various technical parameters has been attempted to verify the consistency and choice of

values while applying the model. Those technical details about the protocol include the trial duration, trial averaging method, Butterworth filtering, and time interval. The model has also been applied to further experiment to differentiate participant characteristics. The first experiment successfully identified the dynamic features between pathological and normal participants. The second one extracted the significance in motor control development between 11- and 15-year-old children. Some dynamic features, namely the diffusion coefficient, critical time, and mean square angle at critical time, showed the difference between participant groups.

The SDA showed promising results on the fundamental fractal features on the physiological signal of spinal curvature. Along the spinal structure from the cervical to lumbar, multisectional consistency is also shown.

However, because of the high degree of freedom and the exhibition of different motion control behaviours in various spinal regions, further investigation is required for the analysis of the intersegmental relationship of the spine in limited segments, that is, the cervical spine as described in the later chapters. This limits the analysis on the degree of freedom on intersegmental angles which are extracted by large data intervals, which is assumed not to be the primary factor affecting the control on spinal curvature as compared to those data points located in close proximity to the point of focus.

Regarding the development of the fractal analysis model, due to the limited parameters we can extract from SDA, additional exploration is needed in order to explain more about the features of the motor control. Numerical methods in MFDFA

is attempted to refine the model for demonstrating the fractal features and conditions that are related to the biological series of spinal curvature.

# Chapter 4.
# Methodology on Research Analysis of the Cervical Spine Region

In this chapter, the revised experimental procedure is introduced to focus on the cervical spine region. The analysis focuses on extracting and adopting the multifractal analysis model. The biomechanics and measurement of the cervical spine are described in the first section.

In the second section, detail on the capture was recorded. The setup was again inside the optical motion capture studio. The capture focused on the cervical region. Participants were recruited to participate in the experiment. A convenient participant group of 11 girls aged 19–25 years was recruited from The Hong Kong Polytechnic University. They all shared a common characteristic of working behavior in research and study.

In the third section, neck pain assessment questionnaires were adopted for the self-report of neck problems from each individual participant. The survey on neck pain assessment was then analyzed using descriptive statistics from the participant group on the basis of overall scores and various factors, namely pain, disability, neck-specific function, and emotion and cognitive influences. Patterns as extracted from the characteristics of individuals in the participant group were revealed from the results.

## 4.1. Focus on the Cervical Spine Region

Given the aforementioned limitation on the basis of the previous analysis, the cervical spine is selected for the fractal analysis model. The analysis can then be focused to extract and adopt the multifractal analysis model. This leads to the numerical and technical consideration and criteria for designing wearable devices for capturing spinal movement. The analysis results are to be correlated to clinical data and also the neck pain problem of the general population. This eventually contributes to health-monitoring aspects and the wellness of humans. Although the spinal structure is complex in deriving the factors to account for the neck pain problem, the attempt to extract information on the trace of motor control on the cervical spine movement is one method to further understand the problem.

Statistics show that neck pain affects 10% of the population each year. Approximately two-thirds of the population experience neck pain at some point in their lives, especially in middle age. People of age 25–45 years commonly have occupational diseases; 72% experience pain on the shoulder muscles, 11% on the cervical nerves, and 4% on the cervical artery. Neck pain may occur slightly more frequently in women than in men [62]. Particularly in recent years, by the introduction of mobile device usage and also the issues in ergonomics of using computers in the workplace, neck and shoulder pain has gained increasing attention, especially for office workers. After back pain, neck pain has become the most frequent musculoskeletal cause of consultation in primary care worldwide. It also causes heavy burden on healthcare services, employers, and individuals.

### 4.1.1. Neck Structure

A survey showed that, in general, in daily life we move our neck more than 600 times per hour, whether a person is awake or asleep [96]. This requires substantial mobility and stability in the neck control mechanism. In particular, it requires the flexibility to move the head via the cervical spine. The biomechanics require substantial endurance of the musculoskeletal system.

The neck begins from the base of the skull and extends down to a series of seven vertebral segments. The vertebral segments connect to the thoracic spine, the upper back. They are called the cervical vertebrae, which are the bony building blocks of the spine in the neck. Between these vertebrae are the discs, and nearby are the nerves of the neck that pass by. The seven vertebrae are named as C1, C2, C3, C4, C5, C6, and C7, and often noted as C1–C7, based from the skull and extending down to the thoracic spine in sequential order. The positions of the vertebrae are shown in Figure 4.1 [61, 67].

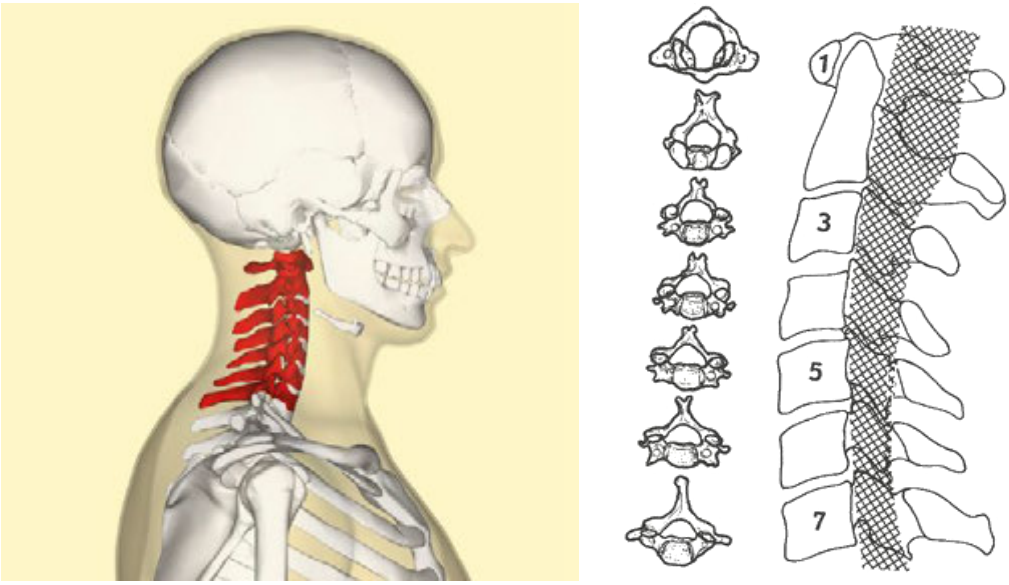


Figure 4.1. Position and shape of cervical vertebrae of C1–C7 (from top to bottom).

The first cervical vertebra is different from others in that it is a ring rotating around the second vertebral body called odontoid. The last five cervical vertebrae, C3 through C7, are also constructed differently from the first two. They have three joints, a disc in the front and two facets joints in the back to compose each vertebral segment, which is more similar to the rest of the spine. Regarding the size, the cervical vertebrae located closest to the skull are the smallest. The vertebrae in the thoracic spine and the lumbar spine are all bigger than the cervical vertebrae.

The function of the cervical vertebrae is to provide support, structure, and stabilization to the neck, especially for certain types of movement. Together with muscles, joints, ligaments, and tendons, cervical vertebrae are essential for movement with two vertebral bodies connected. The movement includes rotation, flexion, and extension. Rotation denotes the movement of the head from side to

side. Most of the rotation occurs in the first two segments of the cervical spine, especially the atlas (C1) and the axis (C2). Flexion denotes the head moving forward, whereas extension denotes the backward movement. The C5–C6 and C6–C7 segments of the spine contribute to the flexion and extension movements most of the time.

To maintain the center of gravity in a functional position, the architecture of the axial skeleton is well designed in maintaining a perfect balance between stability and mobility in biomechanics. The cervical spine is part of the whole spinal system, and is the furthest from the center of gravity. Its composition can be divided into several functional units. Each functional unit can be divided into contiguous vertebrae that are divided into anterior and posterior anatomically. The anterior column consists of the vertebral body, longitudinal ligaments, and intervertebral disc. The anterior view of the cervical spine is shown in Figure 4.2 [97]. It shows the anterior segment of C4 through C6 vertebral bodies. The structure of this anterior column is mainly weight bearing, shock absorbing, and providing flexibility of the intervertebral discs for maximum movement control. The posterior column is composed of the osseous canal, zygapophyseal joints, and erector spinae muscles. The posterior view is shown in Figure 4.2 [2] with the whole cervical spine from C1 to C7 vertebral bodies. The structure of this posterior column mainly provides protection to neural elements, acts as fulcrum, and guides movement for the functional unit.

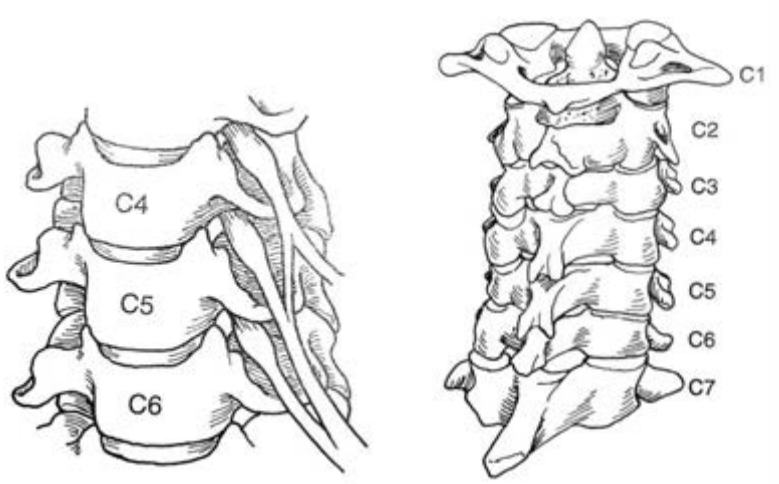


Figure 4.2. Anterior and posterior columns of the cervical spine.

The function of the cervical spine can be divided into upper and lower segments. The upper segment is the region above C3. There are five articulations: two between the occiput and atlas, two between the atlas and axis, and one between the dens and atlas. The occipitoatlantoaxial complex is the most complex articulation series in the whole body. The occipitocervical angle is sharp so as to hold the head in a horizontal plane. A total of 23 degrees of movement is resulted at the occipitoatlantoaxial complex. There are approximately 13 degrees of flexion and extension from the occipitoatlantal joint, and approximately 10 degrees of flexion and extension at the atlantoaxial joint [98]. Most of the axial rotation in the upper segment occurs at the atlantoaxial joint with an average of 47 degrees. [99] The lower segment is the region from C3 to C7. The motion of this segment constitutes flexion, extension, lateral flexion, and rotation. There is no motion that occurs in a single plane here, and the motion requires a certain deformation of the

intervertebral disc. As a whole range of motion considering both the upper and lower segments, they both contribute approximately 50% of axial rotation. Table 4.1 is a summary of the normal range of motion at various cervical segments measured in degrees.

Table 4.1. Summary of the normal range of motion at cervical segments.

| Level | 0-C1 | C1-C2 | C2-C3 | C3-C4 | C4-C5 | C5-C6 | C6-C7 | C7-T1 |
|---|---|---|---|---|---|---|---|---|
| **Flexion / Extension** | 13 | 10 | 8 | 13 | 12 | 17 | 16 | 9 |
| **Lateral Bending** | 8 | 0 | 10 | 11 | 11 | 8 | 7 | 4 |
| **Rotation** | 0 | 47 | 9 | 11 | 12 | 10 | 9 | 8 |

With this range of motion, studies have found abnormality if the movement goes beyond it. From survey and clinical studies, when there is an angulation greater than 11 degrees between two cervical segments on the lateral side, it is considered abnormal. Other abnormal conditions include the maximum anteroposterior translation of 3.5 mm, or the intervertebral disc space increases with traction of more than 1.7 mm. These are considered abnormal [100, 101].

The cervical spine maintains several crucial roles. The first crucial role is to house and protect the spinal cord. A bundle of nerves extends from the brain. They, in turn, run through the cervical spine and thoracic spine and end just before the lumbar spine. The brain sends messages out and relays them through the spinal cord, arriving at different parts of the body.

The other crucial role of the cervical spine is to provide support to the head and its movement. Because the head weighs between 10 and 13 pounds on average, it actually imposes a large load to the cervical spine. Compared to the whole body mass, that is not too much weight. However, this weight is only supported by the relatively small structure around the region of the cervical spine and muscles attached. Moreover, the cervical spine supports also the rotation, flexion, extension, and lateral bending movements of the head, not just the weight.

Facilitating the flow of blood to the brain is also crucial. With the passageway provided by the vertebral foramen in the cervical spine, the vertebral arteries are able to pass and ensure proper blood flow to the brain. Only the vertebrae of the cervical spine have this type of opening. In relation to the spinal system, the neck is complemented with other functions such as visual coordination, vestibular balance, and auditory direction for the control mechanism. These together result in precise control, which is necessary for normal functioning.

Recognition of any biomechanical deviation from the aforementioned normal function, such as a hypermobile segment and excessive cervical kyphosis, may help in explaining the source of pain in a person, provided that there is no specific anatomic abnormality. Therefore, an understanding of the basic biomechanics of the cervical spine is necessary for investigation on the sources and causes of pain, and further leading to assessment and treatment.

The structure of the neck is complex, including the skin, muscles, arteries, veins, lymph nodes, thyroid gland, parathyroid glands, esophagus, larynx, and trachea

[159]. Any changes affecting these tissues due to diseases or conditions can lead to pain in the neck.

### 4.1.2. Neck Pain

Neck pain in general means the pain located in the neck. It is also referred to as cervical pain. From the International Association for the Study of Pain, cervical spinal pain is defined as follows [103]:

"Pain perceived as arising from anywhere within the region bounded superiorly by the superior nuchal line, inferiorly by an imaginary transverse line through the tip of the first thoracic spinous process, and laterally by sagittal planes tangential to the lateral borders of the neck."

Pain can happen in two ways: one is the localization of pain at the cervical spine, and the other one is the radiation of pain down to other parts of the body, such as the arm. Neck pain can develop in all age groups. In recent years, because of the extensive use of computers and mobile phones, neck pain has become the most common pain for people who sit and stare at screens for long periods. These people usually experience a certain level of neck pain. Any disorders and diseases affect the tissues in the neck and can cause pain, such as degenerative disc disease, neck strain, and neck injury. Infections, for example, virus infection of the throat, can lead to neck pain because of the lymph node swelling. Improper body posture in the

workplace, which directly affects the muscles of the neck, is also a common cause of neck pain.

Neck pain is commonly associated with numerous other symptoms including dull aching, numbness, tingling, tenderness, sharp shooting pain, fullness, difficulty swallowing, pulsations, swishing sounds in the head, dizziness or lightheadedness, and lymph node swelling [159]. Headache, facial pain, shoulder pain, and arm numbness or upper extremity paresthesias could also be associated with neck pain. These related symptoms are usually caused by the nerves becoming pinched in the neck [159]. Neck pain could sometimes occur with upper back and/or lower back pain, depending on the conditions.

Neck pain is usually referred by most patients pointing to the pain perceived in the posterior region of the cervical spine. The region starts from the top at the superior nuchal line to the bottom until the first thoracic spinous process, as illustrated in Figure 4.3 [104]. The pain perceived in the anterior region of the cervical spine is usually referred to as the throat, but not neck pain. Although it is not defined by an international authority, practitioners recognize this as pain occurring in/from the “anterior” of the neck. It is defined as pain perceived anteriorly and ostensibly stemming from the cervical spine. It arises from the evidence of a special, but not unusual, type of pain that cannot be adequately described by the term “neck pain” alone.

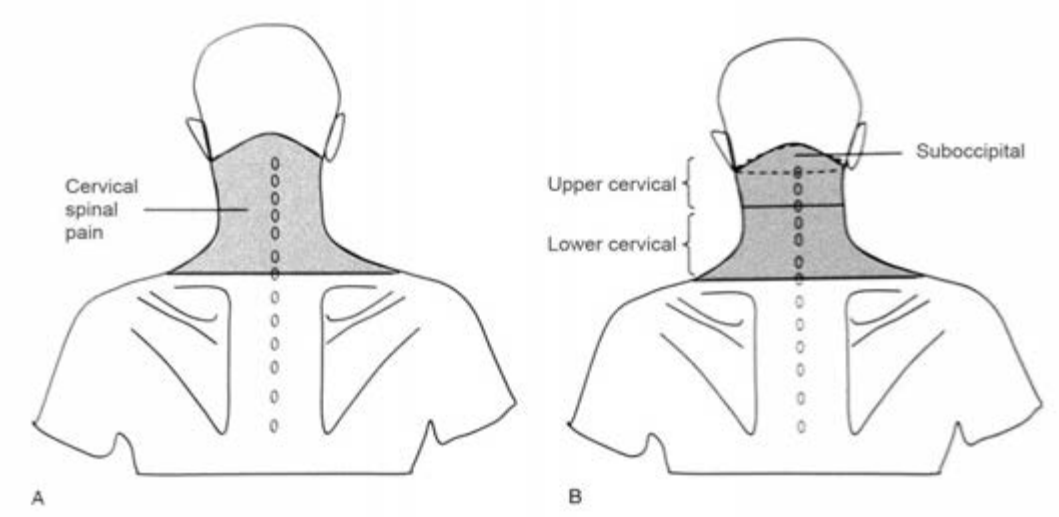


Figure 4.3. Posterior and anterior neck pain.

The pain can be further classified as upper and lower cervical spinal pain. Two equal halves of the cervical spinal region is divided by a boundary above and below an imaginary transverse line. Suboccipital pain is also defined separately. The pain is located between the superior nuchal line and an imaginary transverse line passing through the tip of the second cervical spinous process [104]. It introduces headache, in particular, cervicogenic headache.

Cervical radicular pain refers to the pain perceived in the upper limb, although neck pain may also be associated. This term is different from neck pain; however, it is usually misused by practitioners and students. Cervical radicular pain has distinct causes, diagnosis, and management from neck pain [105-107]. Investigations and treatments that are appropriate for one may be inappropriate for the other.

Somatic referred pain is the pain perceived by the nerves of a region that is different from the source of the pain, as illustrated in Figure 4.4 [103]. Originating from the

cervical spine, referred pain can be perceived in various regions such as the head, upper limb, interscapular region, and anterior chest wall.

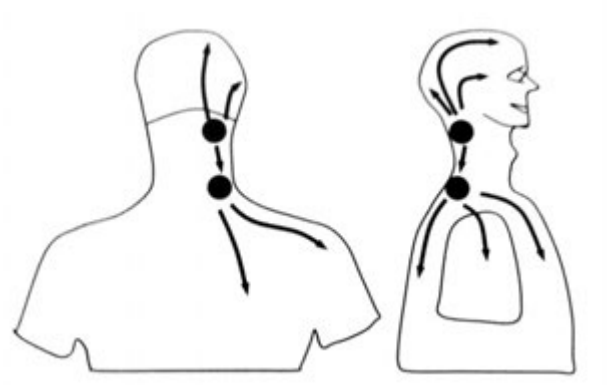

Figure 4.4. Illustration of referred pain.

The referred locations are usually segmental subjected to a function of the primary source of pain. In the case that pain is perceived in the head, further investigation reveals that it is referred from upper cervical segments. Pain in the anterior chest wall, interscapular region, or upper limb is usually referred from lower cervical segments. Various patterns of referred pain (Figure 4.5) are stimulated from the interspinous muscles at the segments indicated distally and away from the cervical spine into the upper limb [111]. Another study conducted a stimulation of pain from the cervical zygapophysial joints [109, 112]. Results revealed that the patterns of pain are localized only within the upper limb girdle. At most, the pain spreads into the proximal arm. Similar patterns can also be found in pain simulated at the cervical intervertebral discs [108, 113].

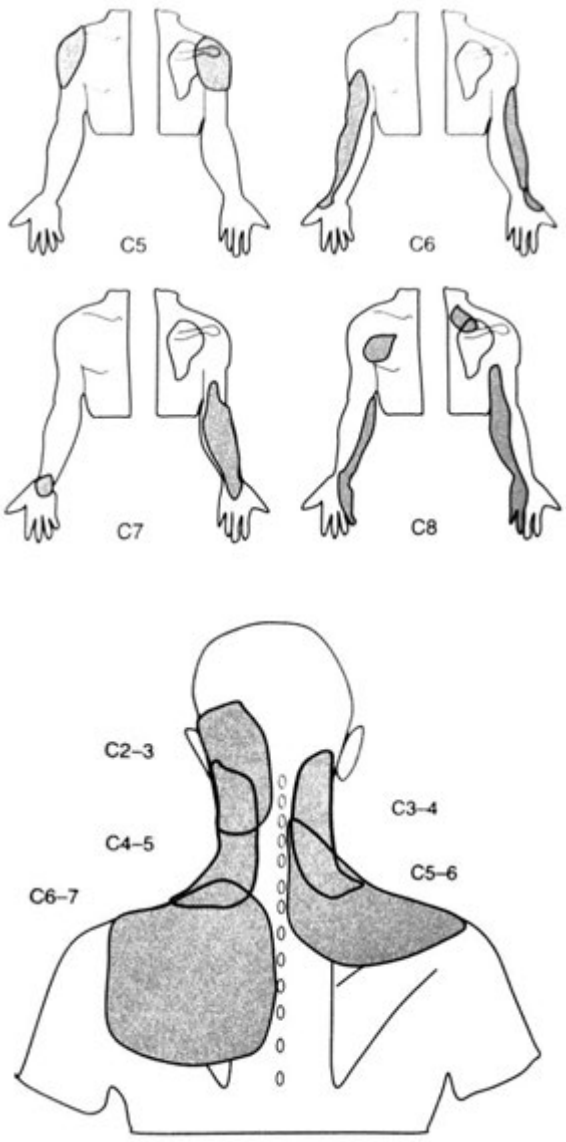


Figure 4.5. Various patterns of referred pain.

As shown in several studies, referred pain is indicated by its segmental location and nerve perception rather than the structure that is associated. This means that all structures perceived by the same segmental nerves can result in a relatively specific territory of referred pain. Other segmental relationships have also been revealed in

various research studies. Lower cervical intervertebral discs can result in pain perceived at the chest wall [108]. Headache perceived can be referred from various joints, namely C2-3 zygapophysial joints [109], lateral atlanto-axial joints [110], and atlanto-occipital joints [110].

According to the convention by the International Association for the Study of Pain [161], pain is also defined from a temporal basis. The causes of neck pain are generally categorized into two types: acute and chronic neck pain. A three-month period is usually adopted as a convenient point to distinguish the types of pain, assuming that it is not due to cancer. Acute pain is defined as pain that occurs for less than 3 months. Chronic pain is defined as pain that occurs for longer than 3 months. Subacute pain may also be referred for pain that occurs for less than 3 months but more than 7 weeks. The convention is taken from the context of low back pain. However, it is not common in the context of neck pain because there is no distinct intervention and treatment identified.

Acute neck pain is usually caused by whiplash injury, for example, car accidents or sports injuries, to the cervical region [160]. Impulsive stretching of the spine, such as a sudden force directed at the patient's back, would lead to whiplash or whiplash-associated disorders. This sudden force snaps the head and neck backward and then forward. Neck pain is one of the major symptoms of whiplash-associated disorders. It may also extend to the upper and/or lower back, as well as pins and needles and/or numbness in the arms and fingers. Whiplash-associated disorders are graded

from mild subjective pain and stiffness to fracture, dislocation, and injuries to the spinal cord [160].

Chronic neck pain is often the result of muscle tension. Some of the common causes are prolonged sitting, poor working posture, poor circulation, and lack of exercise [160]. As a result, muscle tension develops in the upper back, shoulders, and neck areas. Symptoms are not only limited to muscle aching but also to spinal joint movements. After a certain period, because of the poor joint mechanics, disc problems may arise, as well as nerve impingement [160].

For most neck disorders, there is an absence of an identifiable underlying disease or abnormal anatomical structure. As a consequence, they are classified as nonspecific [62]. This causes a lack of standard assessment for nonspecific neck pain (NS-NP). From this perspective, NS-NP is mainly diagnosed based on clinical grounds, provided there are no features to suggest a specific or more serious condition. The natural cause of NS-NP remains unclear; as a consequence, a heavy burden is placed on individuals, employers, and health care services [63, 64]. The literature reveals numerous diverse treatment approaches for NS-NP. However, for most patients with NS-NP, definitive pathology cannot be identified; the medical model fails to provide direct treatment. A change can be observed in the international literature, with an increasing amount of clinical research on neck disorders being directed toward understanding the pathophysiology of neck pain [65, 66]. This fits the clinical reasoning model used by physiotherapists in their physical examination of patients with neck pain.

### 4.1.3. Biomechanics of the Cervical Spine

The weight of the occiput contributes largely to the weight of the head. One of the major functions of the vertebral column is to support the weight by means of the ligaments and muscles. In biomechanical terms, the structure must counter balance the moment of inertia involved, as illustrated in Figure 4.6 [114]. Therefore, most weight is placed on relatively small bones, the cervical vertebrae. This demands a strong interplay between ligaments and the neuromuscular system to maintain the system in the equilibrium state.

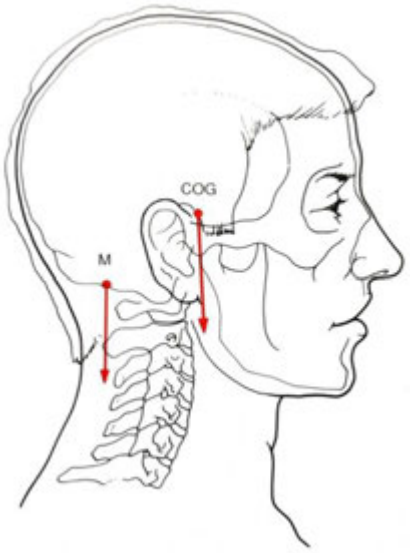


Figure 4.6. Counter balancing the moment of occiput.

There are several organ systems that are closely related to the upper quarter. These include the vertebral artery, internal jugular vein, sympathetic chain of the autonomic nervous system, and components of organ systems, such as respiratory and digestive tissues. In addition, the cervical vertebra protects the spinal cord, nerve roots, and also the brain stem; the upper cervical vertebrae are especially directly involved. Stability of the region is essential to provide a degree of protection to vital structures. However, a degree of mobility must also be provided.

The root of the muscles attached to the occiput and cervical vertebrae is connected to the bones of the shoulder girdle. This provides anchors for the muscles and supports effectively the force exerted from the cervical spine to the scapula. Particularly in the case of referred and radicular pain patterns, tissues of the girdle must be closely examined to investigate the source of pain.

To maintain the previously mentioned equilibrium, musculoskeletal tissues must be subjected to a nondestructive force while keeping an optimal state of health. The biomechanical forces usually include tension, compression, and shear. A theoretical physiological loading capacity of musculoskeletal tissues is shown in Figure 4.7 [114]. The area under the curve represents the loading that the musculoskeletal tissues are subjected to. The region at the top of the diagram denotes the area with excessive loading on the tissues. Under such condition, the tissues are subjected to a destructive force. At the bottom, the region denotes the area with too little loading. Under such condition, the tissues no longer have adequate stress, resulting in a state of weakness. In both these two regions, the tissues may result in

breakdown, either through injury or the catabolic effects of inactivity. The interpretation of this graph can also be extended to characterize various tissues. Because different tissues may have different mechanical properties, the resulting ability in supporting load capacity is different. In other words, the tolerance of force as represented by the area of the two regions is different. Hence, the optimal loading zone can also be characterized and unique. The middle zone represents the physiological loading capacity of tissues that are subjected to forces such as tension, compression, and shear. Under any circumstances, maintaining the tissues loaded within the optimal zone can maintain the tissues in favorable health condition. Although the optimal loading area is characterized and unique for various tissues, the area cannot be kept constant at all times.

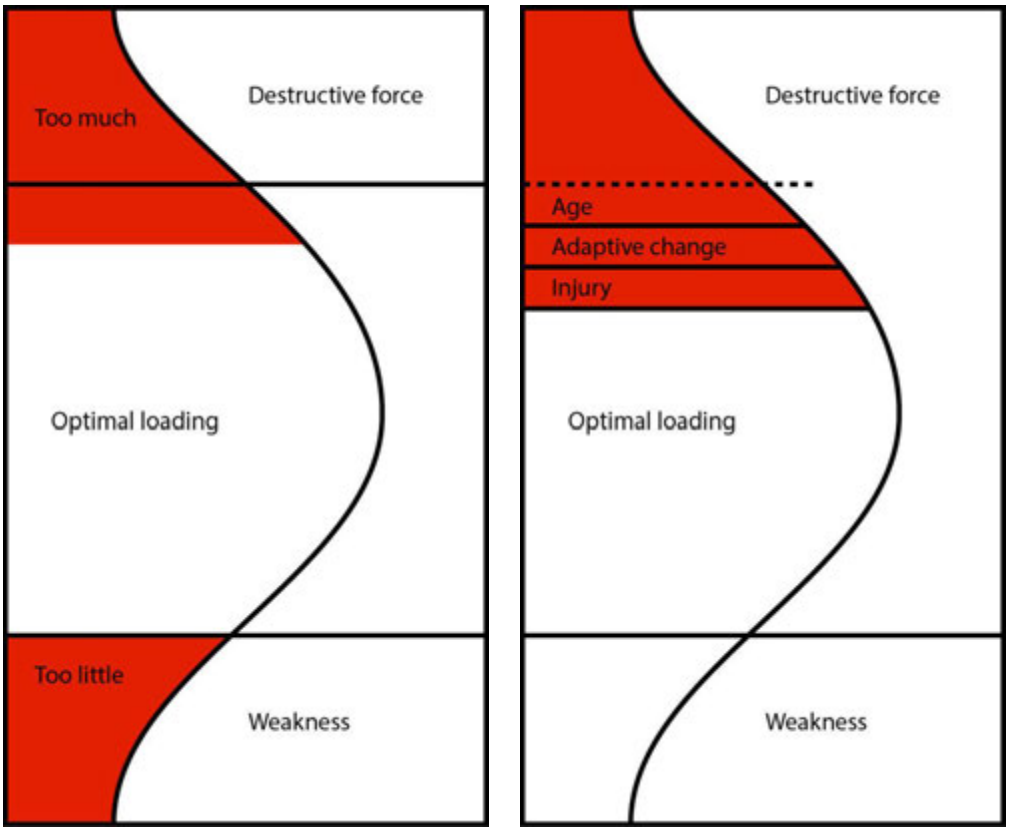


Figure 4.7. Theoretical physiological loading capacity of musculoskeletal tissues.

There are factors that alter the boundary of the optimal loading regions, both the upper and lower regions. The change of boundary means that the tolerance for subjective force changes, as shown in Figure 4.8 [114]. Age is one of the major factors in changes to the tissue ability to attenuate stresses. With age increases, the chemical composition inside the tissues changes [115, 116], resulting in decreases in the availability of binding sites for water. As a result, the tissues become less hydrous and, subsequently, less resilient. Therefore, the physiological loading capacity is reduced.

Injury and adaptive change are other factors that alter the area of loading capacity. Acceleration injury of the neck is an example of the effects on the future load-bearing capacity of tissues after an incidence. The body has effective compliance in responding to external stresses exerted on the tissues. However, changes in function may still occur when there is unyielding stress under condition, such as prolonged posture and general inactivity.

The aforementioned factors reduce the physiological loading capacity boundary of musculoskeletal tissues. They reduce the load-bearing and force attenuation ability of the musculoskeletal system. When forces exceed the upper boundary or impact the understressed tissues, damage of tissue occurs and triggers the response of pain caused by mechanical or chemical activation of the nerve system.

Another major effect as a result of age changes is the changes on the stress-strain curve of tissues. With increasing age, the curve becomes steeper. This implies that the tissues are more vulnerable to breakage by loading force, as shown in Figure 4.8 [114]. At point 1, the fibers of tissues are lengthened because of the increased force applied. Between points 1 and 2, the fibers encounter the elastic range, which is linear in behavior and obey Hooke's law. With an increased force applied, the length is then directly proportionally increased. Between points 2 and 3, ruptures begin and happen at individual fibers. At point 3, the rupture goes beyond the yield, and the breakage of tissue occurs.

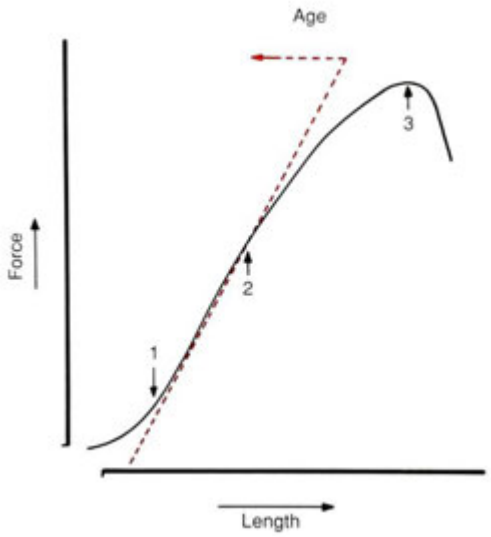


Figure 4.8. Implication of age on stress-strain curve.

The function of noncontractile supporting tissues is to provide stability between bones and mobility in specific direction for the range of motion. The support for this stability is grounded by the viscoelastic characteristic of the tissues. This characteristic provides the primary and major support. To understand the mechanism, viscoelasticity is often modeled using a spring-and-dashpot mechanism as illustrated in Figure 4.9 [114]. The model allows a specified range of stress exerted to the system. The tissue has the ability to resist the deformation. It also has the elasticity for returning to its original shape.

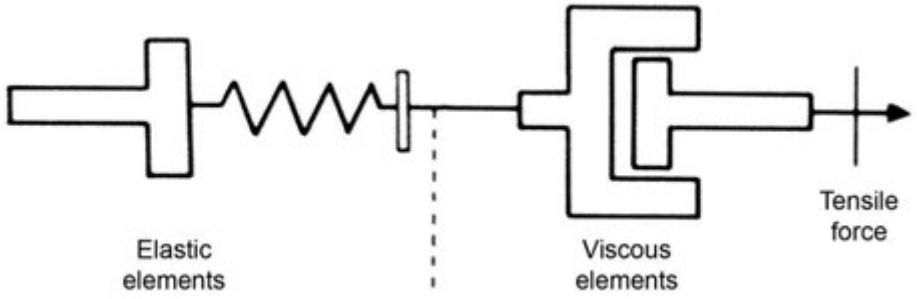


Figure 4.9. Spring-and-dashpot model on viscoelasticity.

Regarding the stress-strain curve, unloading the tissue may not return the loading pattern into its original place. This is often the case when the restoration after stretch occurs at a lower rate and smaller extent than elongation. Hysteresis is defined as the loss of energy between the lengthening and recovery activity of tissues. With a change in viscoelasticity property, the strain change with increasing stress does not allow the tissue to return to its original length, as illustrated in Figure 4.10 [114].

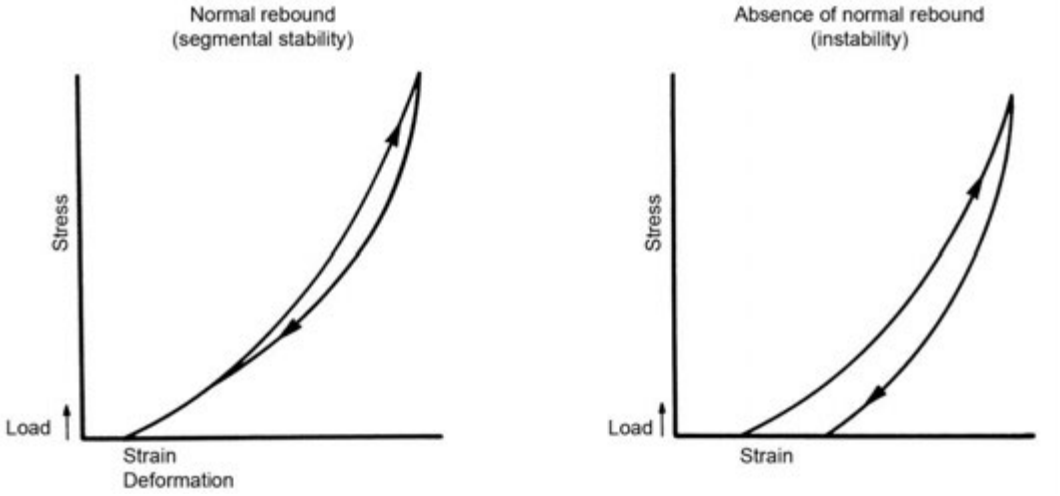


Figure 4.10. Illustration of hysteresis.

In addition to the aforementioned stress and strain properties of tissues as subjected by mechanical forces, the position of the cervical spine also affects the intradiscal pressure. In the supine position, the least pressure is experienced. The greatest pressure is encountered in the extension position of the cervical spine, as shown in Figure 4.11 [117].

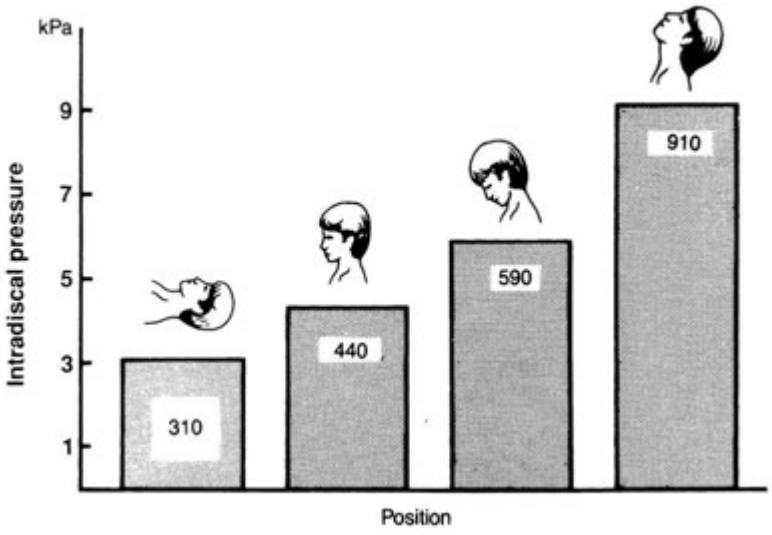


Figure 4.11. Pressure at various cervical spine positions.

Considering another example of a forward head posture, Figure 4.12 shows the compressive force on the articular cartilage [114]. This results in the loss of the compression–decompression cycle needed for maintaining the health of the articular cartilage.

Figure 4.12. Compressive force on the articular cartilage in a forward head posture.

The radiography diagram in Figure 4.13 shows a case in which stress increases on the subchondral bone in place of the degeneration of the articular cartilage [114]. As the articular cartilage becomes thinner, the elasticity of it decreases. There is a loss of apophyseal joint space, resulting in bone spurs. The subchondral bone then takes the role in case of increased load.

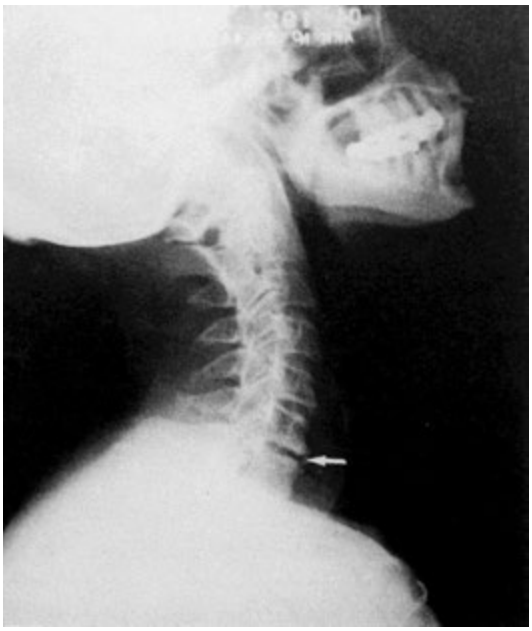

Figure 4.13. Radiography diagram showing a loss of apophyseal joint space resulting in bone spurs.

### 4.1.4. Measurement on the Cervical Spine

Measurement on the cervical spine usually involves assessment and treatment. Some of the major parameters include strength, endurance, range of motion, and proprioception [84-88]. During investigation on the cause of both neck pain and headache, the core in evaluating the cervical range of motion (CROM) was recognized by the American Medical Association [89]. There are various types of noninvasive methods for the measurement on neck motion. These include the CROM device [90], ultrasonography [91], electromagnetic tracking systems [92], electrogoniometry [93], and the optical-based system [94]. Many of these studies have aimed to quantify CROM during activities of daily living. Among them, optical-

based video systems enable highly accurate recording of movements as a function of time. However, its application restricts the capture to be conducted in a laboratory environment because of the complex system and specific illumination condition. Electromagnetic systems are also highly effective for use in specific applications.

The characteristics of the range of normal cervical spine movement and daily living performance of adults have been investigated. In relation to the head and neck motion, the parameters on magnitude and frequency over a long period of time are unknown. If the characteristics or patterns of these parameters can be acquired during daily activities, this can help to construct the normal behavior and progressive changes that may lead to pain or disease. This information may help to define the treatment goals and support the choice of appropriate treatment methods. This is essential information supporting specialists to deliver treatments related to cervical spine disorders. The magnitude, frequency, and range of motion in daily activities are also beneficial for addressing ergonomic issues in occupational environment settings. Moreover, the quantified values on cervical spine movement can serve as a benchmark for disability determination. Therefore, methods for measuring the frequency and magnitude of neck movement over a long period of time are necessary. Commercially available systems have been produced to measure changes in energy expenditure and daily human activities as a whole [95]. These could possibly be adapted and modified for use on the cervical spine.

In biomechanical studies regarding the cervical spine, there are two major areas that are usually concentrated. One is clinical stability and the other is kinematics. When applying to the spine, stability can be defined as the ability to undergo physiologic loads in limiting the patterns of movement. The basic requirement is to prevent damaging or irritating the spinal cord and nerve roots. In addition is to prevent incapacitating deformity or pain due to structural change [102]. The range of motion can then occur in the subaxial cervical spine. This can be helpful in making decisions about instability. Kinematics is the examination of movement in body parts. Numerous studies have used a three-dimensional measurement system for capturing the cervical spine movement. However, many of them have focused on primary movements only. In a typical experimental setup, the neck can have movement in maximal flexion and extension, maximal right and left lateral bending, and maximal right and left axial rotation, as illustrated in Figure 4.14 [133]. There are two major factors determining the kinematics of vertebral motion. They are the geometry of the articulating surface and the mechanical characteristics of the connecting structures. Fractal analysis techniques, by contrast, focus on understanding the movement and dynamic behavior, which aligns the reasoning of motor control from a nonanalytical approach. In the following chapters, the analysis attempts to reveal the inner mechanism behind the spinal curvature movement, with focus on the cervical spinal region.

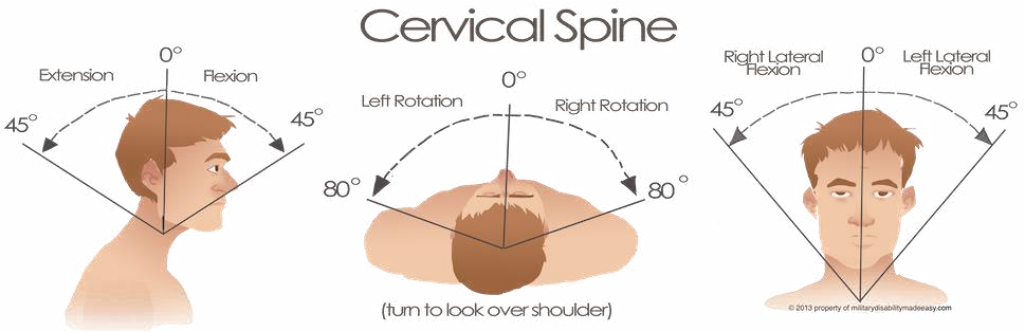


Figure 4.14. Range of motion for the cervical spine.

## 4.2. Survey Analysis on Neck Pain

### 4.2.1. NPAD Instrument

In clinical assessment convention, a few instruments are often used for assessing neck pain, including the Neck Pain and Disability Scale (NPAD) [2-4], Neck Disability Index [4, 5], short form McGill Pain Questionnaire [6], Functional Rating Index [7], and Northwick Park Neck Pain Questionnaire [8]. Among these, NPAD is considered to have the optimal psychometric properties [1], and, therefore, was adopted to assess the neck problem of the participants in this experiment.

Inside the NPAD instrument are 20 items to answer, as shown in Table 4.3. This enables a comprehensive measurement on neck pain. According to an initial study [2], the NPAD instrument covers four aspects in relation to neck pain. They are pain, neck function, interference in life activities, and emotional and cognitive effects.

Each question has a six-point scale (0–5). The participants select the one choice that most closely describes their neck problem.

Table 4.2. NPAD questionnaire.

**NECK PAIN AND DISABILITY SCALE**

Please answer the following questions according to your current level of neck pain.

**1.) How bad is your neck pain today?**

No Pain  Very Little Pain  Some Pain  Moderate Pain  Severe Pain  Highest Possible Pain

**2.) How bad is your neck pain on average?**

No Pain  Very Little Pain  Some Pain  Moderate Pain  Severe Pain  Highest Possible Pain

**3.) How bad is your neck pain at its worst?**

No Pain  Very Little Pain  Some Pain  Moderate Pain  Severe Pain  Highest Possible Pain

**4.) Does your neck pain interfere with your sleep?**

Not at All  Seldom  Some  Moderately  Severely  Can't Sleep

**5.) How bad is your neck pain with standing?**

No Pain  Little Pain  Some Pain  Moderate Pain  Severe Pain  Highest Possible Pain

**6.) How bad is your neck pain with walking?**

No Pain  Little Pain  Some Pain  Moderate Pain  Severe Pain  Highest Possible Pain

**7.) Does your neck pain interfere with driving or riding in a car?**

Not at All  Seldom  Some  Moderately  Severely  Can't Drive or Ride

**8.) Does your neck pain interfere with social activities?**

Not at All  Seldom  Some  Moderately  Severely  Always

**9.) Does your neck pain interfere with recreational activities?**

Not at All  Seldom  Some  Moderately  Severely  Always

**10.) Does your neck pain interfere with work activities?**

Not at All Seldom Some Moderately Severely Can't Work

**11.) Does your neck pain interfere with your personal care (Hygiene, Bathing, Eating, Dressing)?**

Not at All Seldom Some Moderately Severely Always

**12.) Does your neck pain interfere with personal relationships (Family, Friends, Sex, etc.)?**

Not at All Seldom Some Moderately Severely Always

**13.) How has your neck pain changed your outlook on life and the future (Depression, Hopelessness)?**

No Change Very Little Some Moderately Severely Complete Change

**14.) How has your neck pain affected your emotions?**

Not at All Very Little Some Moderately Severely Completely

**15.) Does your neck pain affect your ability to think or concentrate?**

Not at All Seldom Sometimes Moderately Severely Completely

**16.) How stiff is your neck?**

No Trouble Light Stiffness Some Moderate Severe Can't Move Neck

**17.) How much trouble do you have turning your neck?**

No Trouble Little Trouble Some Moderate Severe Can't Move Neck

**18.) How much trouble do you have looking up or down?**

No Trouble Little Trouble Some Moderate Severe Can't Look Up or Down

**19.) How much trouble do you have working overhead?**

No Trouble Little Trouble Some Moderate Severe Can't Work Overhead

**20.) How much do pain pills help?**

N/A Complete Relief Severe Relief Moderate Relief Some Relief Very Little Relief No Relief

Total Score _____ %

The total NPAD score is calculated by summing up the scores from all 20 questions. This produces a range between 0 and 100. The higher the total NPAD score is, the greater the disability is. The maximum number of missing answers that is acceptable in one participant case is four. That means if there were any participant case with more than four missing answers, the case would be excluded from any analysis. If there were only a few values missing, within a maximum of four questions, the missing values would be extrapolated using the remaining completed items. For outcome assessment, scores can be directly compared across participants. A change of 10% or greater is considered clinically significant.

In this study, the answers of the NPAD as provided by the participants were further cross checked by focused conversation immediately after the questionnaire. The aim was to maintain a consistency of standard across participants in answering the questions by providing a similar level of scales. Results found out that the scores and the health conditions as described by each individual participant were consistently documented.

### 4.2.2. Descriptive Statistics on Results

Of the 11 participants, 100% responded to the NPAD without any missing answers. The distribution of scores is shown in Figure 4.15. The pain score ranges from the lowest of 4 to a highest of 70. After the sorting process, a distribution of a linear

scale from the lowest to highest is shown. The mean of 30.27 is approximately at the center of distribution. There is one outlier score of 70 at the end.

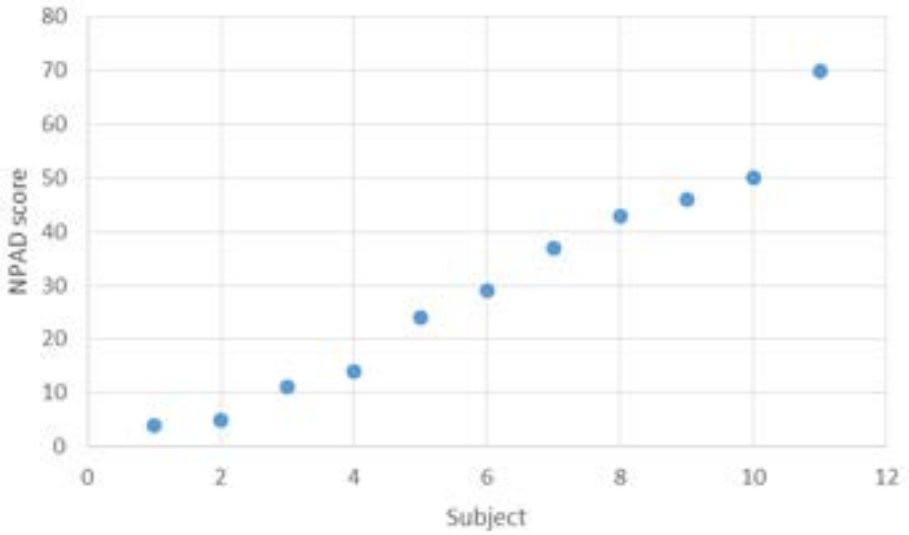


Figure 4.15. Distribution of NPAD scores of the participant group.

According to the factor analysis on the 20 questions, there are four significant factors [1]. They represent “pain” (questions 1–3, 5, 7, 20), “disability” (question 4, 6, 8–11, 15), “neck-specific function” (question 16–19), and “emotional and cognitive influences” (question 12–14). Table 4.3 shows the descriptive statistics on the overall NPAD scores and also the individual factors on the basis of the participant group. Because the ceiling value of each factor is not equal, Table 4.4 shows the normalized score with respect to 100 for the ease of comparison. Among the mean values of the four factors, there is no significant difference, even between the maximum (33.18) and minimum (25.45). By contrast, the score of “neck-specific

function" is highest, whereas the effects on the basis of "emotional and cognitive influences" are the lowest. After the normalization process, the standard deviation can then be compared. The "pain" factor has the lowest standard deviation, whereas the "neck-specific function" factor has the highest. In addition, the variation on the range can also be indicated by the minimum at the "pain" factor, with a value of 56.67, and the maximum at "neck-specific function," with a value of 80.00. The statistics on the range can provide a hint on how the participant group can further be distinguished. A trend line can be drawn among the set. The higher the range and standard deviation are, the more possible it is for the participants to be broken down into a trend line. On the basis of the results on the standard deviation and range values, the "neck-specific function" factor is the most possible to distinguish the trend in the participant group. The next factors are "disability" and "emotional and cognitive influences", of which "emotional and cognitive influences" has a higher standard deviation than the other, whereas "disability" has a higher range than the other. Next is the overall summary on the scores, and the least possible factor is "pain," which has the lowest normalized value in both the standard deviation and range.

Table 4.3. Descriptive statistics on the NPAD scores (n = 11).

| | **Overall** | **Pain** | **Disability** | **Neck-specific Function** | **Emotional and Cognitive Influences** |
|---|---|---|---|---|---|
| **Ceiling Value** | 100 | 30 | 35 | 20 | 15 |
| **Mean** | 30.27 | 9.73 | 10.09 | 6.64 | 3.82 |

| | | | | | |
|---|---|---|---|---|---|
| **Standard Deviation** | 21.04 | 6.21 | 7.83 | 5.03 | 3.57 |
| **Minimum** | 4 | 1 | 1 | 0 | 0 |
| **Maximum** | 70 | 18 | 26 | 16 | 10 |
| **Range** | 66 | 17 | 25 | 16 | 10 |

Table 4.4. Normalized descriptive statistics on the NPAD scores (n = 11).

| | **Overall** | **Pain** | **Disability** | **Neck-specific Function** | **Emotional and Cognitive Influences** |
|---|---|---|---|---|---|
| **Ceiling Value** | 100 | 100 | 100 | 100 | 100 |
| **Mean** | 30.27 | 32.42 | 28.83 | 33.18 | 25.45 |
| **Standard Deviation** | 21.04 | 20.71 | 22.37 | 25.13 | 23.82 |
| **Minimum** | 4 | 3.33 | 2.86 | 0.00 | 0.00 |
| **Maximum** | 70 | 60.00 | 74.29 | 80.00 | 66.67 |
| **Range** | 66 | 56.67 | 71.43 | 80.00 | 66.67 |

Figures 4.16 to 4.20 show the sorted scores of each factor in the participant group. It can be observed that individual participant can be sequenced within each factor. The order can be seen clearly and an obvious trend line can be drawn. In other words, in the participant group is an approximately equal distribution of the neck pain score in each factor. In this case, the variation among participants on the basis of each factor can be adapted in the later stage to distinguish participant characteristics and the correlation to the fractal analysis.

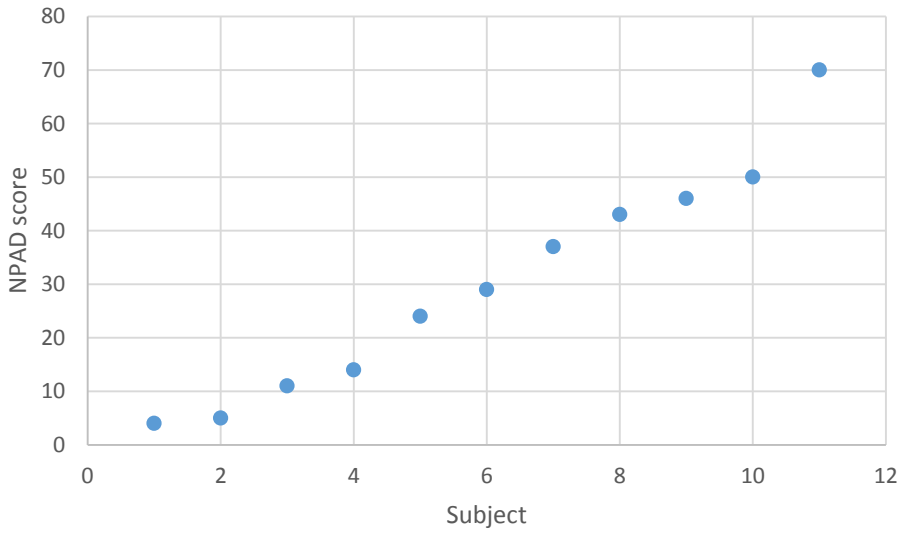


Figure 4.16. Distribution of overall NPAD score summary of the participant group.

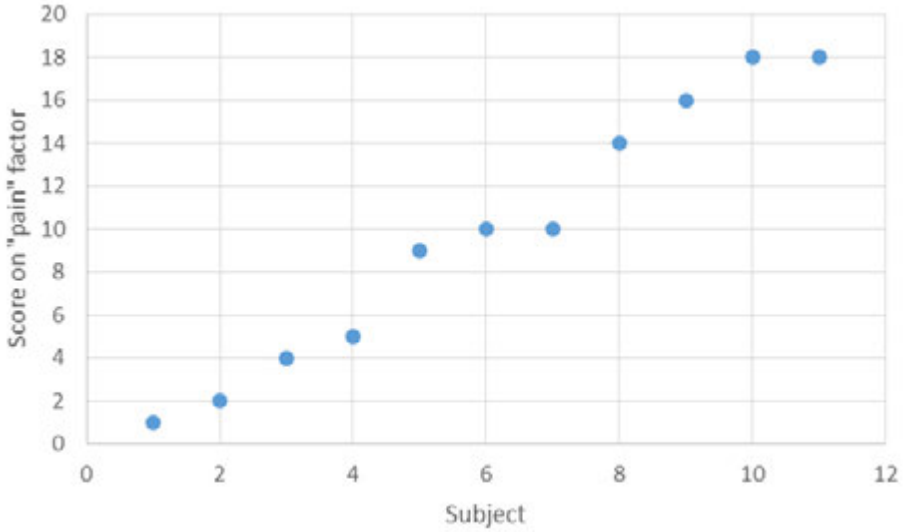


Figure 4.17. Distribution of the score on the “pain” factor of the participant group.

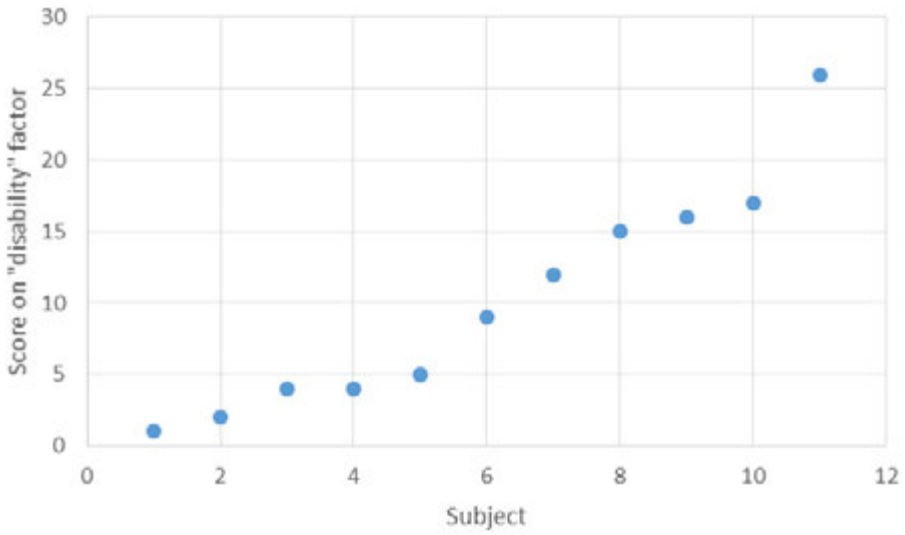


Figure 4.18. Distribution of the score on the “disability” factor of the participant group.

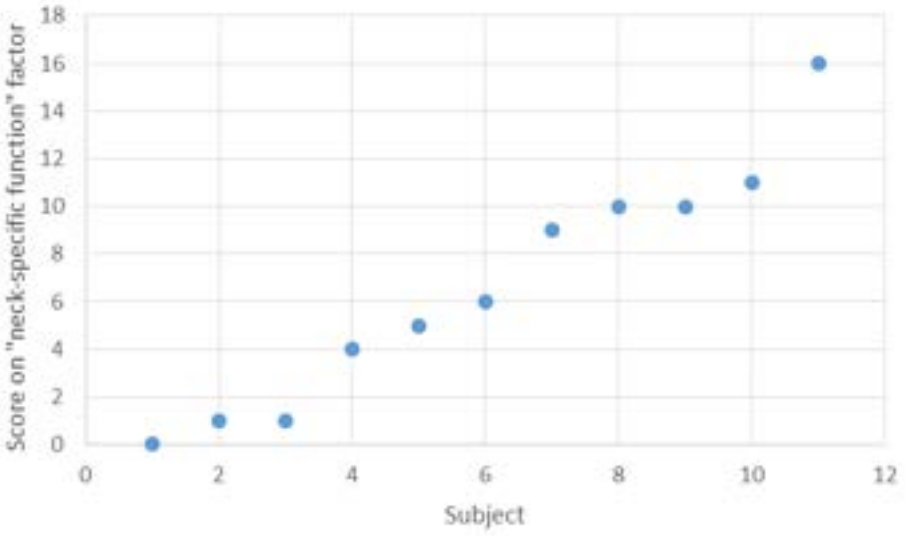


Figure 4.19. Distribution of the score on the “neck-specific function” factor of the participant group.

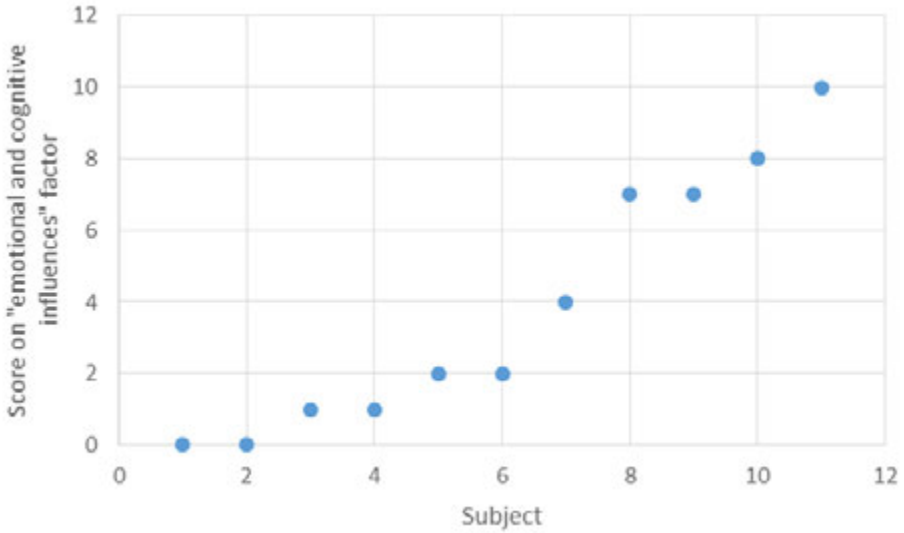


Figure 4.20. Distribution of the score on the “emotional and cognitive influences” factor of the participant group.

Table 4.5 indicates the participant sequences on the basis of each factor in ascending score order, from top to bottom. There is consistency in their occurrence along the sequence and across the factors. For example, regarding the overall summary, the lowest NPAD score appears at participant S01, whereas the highest score appears at participant S10. Across the table, participant S01 appears with the lowest score across various other factors, namely “neck-specific function” and “emotion and cognitive influences.” Another obvious case is that participant S10 has the highest score across all factors, appearing at the bottommost position across all columns.

Table 4.5. Ascending order (from top to bottom) of participant sequence with respect to each factor.

| Overall summary | Pain | Disability | Neck-specific function | Emotion and Cognitive Influences |
|---|---|---|---|---|
| S01 | S09 | S09 | S01 | S01 |
| S09 | S01 | S01 | S09 | S04 |
| S11 | S11 | S02 | S11 | S11 |
| S02 | S02 | S04 | S02 | S02 |
| S04 | S07 | S11 | S05 | S09 |
| S07 | S04 | S07 | S03 | S07 |
| S05 | S08 | S05 | S07 | S05 |
| S08 | S06 | S03 | S04 | S03 |
| S03 | S05 | S08 | S08 | S08 |
| S06 | S03 | S06 | S06 | S06 |
| S10 | S10 | S10 | S10 | S10 |

To investigate the consistency, the occurrence is further quantified. According to the order of occurrence as per participant within the participant sequence, Table 4.6 shows the sequence of occurrence. It shows the percentage of a participant that appears in the ranked order. The order is based on the ascending order from the top to bottom. For example, participant S01 has 60% of its score as the lowest score across all the factors, and 40% of the score appears at the second ranked position. At the other end, participant S10 has a 100% occurrence at the highest score. By using the same mechanism, all the 11 participants can have quantified percentages that correspond to their occurrences along the sequence according to various factors.

Table 4.6. Percentage of occurrence per each participant in ascending order (from top to bottom) according to the participant sequences.

| S01 | S02 | S03 | S04 | S05 | S06 | S07 | S08 | S09 | S10 | S11 |
|---|---|---|---|---|---|---|---|---|---|---|
| 60% | 0% | 0% | 0% | 0% | 0% | 0% | 0% | 40% | 0% | 0% |
| 40% | 0% | 0% | 20% | 0% | 0% | 0% | 0% | 40% | 0% | 0% |
| 0% | 20% | 0% | 0% | 0% | 0% | 0% | 0% | 0% | 0% | 80% |
| 0% | 80% | 0% | 20% | 0% | 0% | 0% | 0% | 0% | 0% | 0% |
| 0% | 0% | 0% | 20% | 20% | 0% | 20% | 0% | 20% | 0% | 20% |
| 0% | 0% | 20% | 20% | 0% | 0% | 60% | 0% | 0% | 0% | 0% |
| 0% | 0% | 0% | 0% | 60% | 0% | 20% | 20% | 0% | 0% | 0% |
| 0% | 0% | 40% | 20% | 0% | 20% | 0% | 20% | 0% | 0% | 0% |
| 0% | 0% | 20% | 0% | 20% | 0% | 0% | 60% | 0% | 0% | 0% |
| 0% | 0% | 20% | 0% | 0% | 80% | 0% | 0% | 0% | 0% | 0% |
| 0% | 0% | 0% | 0% | 0% | 0% | 0% | 0% | 0% | 100% | 0% |

To summarize the quantified sequence, the participants are then sorted according to the sum of percentages with respect to the ranking. Table 4.7 illustrates the sorted order of participants in ascending scores, from left to right. It is a summary considering all the factors in computation for ranking the participant order. In other words, after considering the overall NPAD score and the factors on “pain,” “disability,” “neck-specific function,” and “emotion and cognitive influences,” participant S01 appears to have the lowest possibility of neck-related problems and participant S10 appears to have the most serious neck-related problem in the experimental participant set.

Table 4.7. Sorted order of the sequence of participants in ascending order (from left to right) with consideration of occurrence among different factors.

| S01 | S09 | S11 | S02 | S04 | S07 | S05 | S03 | S08 | S06 | S10 |
|---|---|---|---|---|---|---|---|---|---|---|
| 60% | 40% | | | | | | | | | |
| 40% | 40% | | | 20% | | | | | | |
| | | 80% | 20% | | | | | | | |

| | | | | | | | | | | |
|---|---|---|---|---|---|---|---|---|---|---|
| | | | 80% | 20% | | | | | | |
| | 20% | 20% | | 20% | 20% | 20% | | | | |
| | | | | 20% | 60% | | 20% | | | |
| | | | | | 20% | 60% | | 20% | | |
| | | | | 20% | | | 40% | 20% | 20% | |
| | | | | | | 20% | 20% | 60% | | |
| | | | | | | | 20% | | 80% | |
| | | | | | | | | | | 100% |

## 4.3. Experiment Setup on Motion Capture

After the questionnaires were completed, the motion capture session was arranged. A seat with low back support was prepared to allow the participants to sit upright. First, the sitting posture was adjusted to allow an upright condition. The legs of the seat could be adjusted to allow 90$^{o}$ flexion at the knee. The feet pointed forward and were separated by shoulder width. The torso was upright with the arms across in front of the chest. Data were captured in two sitting conditions: with and without low back support. Before starting the capture, a reference point was placed approximately five feet in front of the participants at eye level. After this was set, the participants were asked to close the eyes. The capture was then conducted for 30 seconds. Two trials were conducted with the same sitting condition. A randomized sequence on the basis of low back support was assigned to each participant. This was to minimize the cross effect between the two sitting support

conditions. Altogether, there were four trials, each of 30 seconds, captured from each participant.

A total of six retro reflective markers of 2.5mm radius were attached to the skin surface at the cervical spine region, as shown in Figure 4.21. To locate the cervical spine region, two markers were placed on C2 and C7 on the basis of their anatomical features. In between the two markers, four markers, named M3, M4, M5, and M6, were placed at approximately equal distance from each other. The x, y, and z coordinates were captured using the optical motion capture system (Motion Analysis Corporation, USA) with 12 cameras of image resolution 1280 × 1024. Data were acquired at 180 Hz by using EVaRT software, which came with the optical motion capture system. For each 30-second trial, there were 5400 (30 × 180) frames along the time dimension. Because there were a total of six markers, each with three coordinates, for each time frame, there were 18 floating point values. These numeric data were captured in a TRC file format, an ASCII format that is readable in a text editor and MS Excel for data preparation. A snapshot of the data format is shown in Table 4.8. All the numbers were measured in millimeters.

Figure 4.21. Marker placement on the cervical region of participant.

Table 4.8. Snapshot of the motion capture data format.

| Frame# | Time | C7 | | | M6 | | |
|---|---|---|---|---|---|---|---|
| | | X1 | Y1 | Z1 | X2 | Y2 | Z2 |
| 1 | 0 | 140.11 | 1419.05 | 10.84 | 141.85 | 1425.76 | 3.23 |
| 2 | 0.006 | 140.14 | 1419.03 | 10.80 | 141.82 | 1425.76 | 3.34 |
| 3 | 0.011 | 140.109 | 1419.03 | 10.719 | 141.83 | 1425.78 | 3.22 |

# Chapter 5.
# Results of Fractal Analysis on the Cervical Spine

In this chapter, the dynamic properties of spinal curvature are characterized during static posture by adapting MFDFA. The aim is to develop a framework to model, examine, and interpret the data series on the captured cervical spine data.

The first section defines the calculation in detail. The process starts from preparing the captured data into an appropriate data format in time series. Various characteristics of the data are revealed based on the types of plots. One of the major concepts behind the computation of the residual is the RMS variation. It reveals the fluctuation with both large and small magnitudes. On the basis of the residual, local detrending is then applied to quantify the invariant structure in scale and to reveal the variations around these trends. By proceeding to DFA, various parameters are defined. These parameters are then further considered into a multiple order statistical moment by q-th order RMS, which comes to MFDFA.

The second section describes the overall results on the basis of MFDFA. The multifractal spectrum is interpreted as the formalism of multifractality, and together with various parameters defined.

In the next three sections, analysis results are generated from various perspectives related to participant, support conditions, and feature points. Results show consistency, differences, and trends across comparison groups.

In the sixth section, the time series are validated using a few methods to ensure the accuracy, validity, and reliability of the results; in particular, the distinguished features of the multifractality structure is based on the characteristics of captured physiological data instead of the general nature of noise property.

In the seventh section, the adoption of MFDFA to spine movement is illustrated by several careful considerations of signal properties, parameter settings, and interpretation of results. The observed results, on the basis of various experimental parameters, are explained by the association of multifractality characteristics and possible physiological meaning in relation to human movement, motor control, and neural activity. Comparative analysis is also conducted on other promising examples to indicate the consistency.

## 5.1. Calculation in Detail

### 5.1.1. Preparation of Data in Time Series

The format of captured data was in TRC, which is a native data format recording the x, y, and z coordinates per time frame on the basis of the position of each marker according to the global coordination system with reference to the origin (0, 0, 0), the ground center of the capture area. Because each trial was captured for 30 seconds at 180 Hz, there were 5400 data frames altogether in each data clip.

The position data of the markers were then set to calculate the angles representing the curvature cervical spine. Angles were calculated based on every three adjacent markers. This allows four angles to be calculated based on vertices at M3, M4, M5, and M6. Figures 5.1 to 5.4 show examples of angle data calculated along the

temporal dimension from one participant on the basis of M3, M4, M5, and M6, respectively.

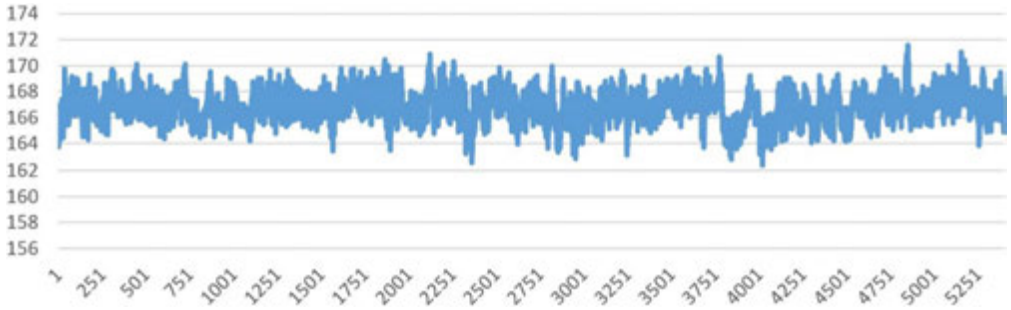


Figure 5.1. Angles on the cervical spine at vertex M3.

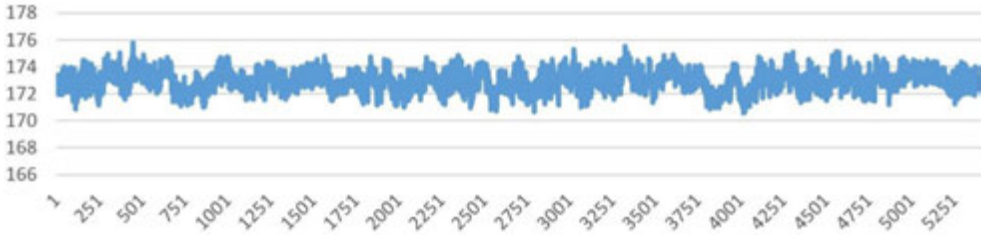


Figure 5.2. Angles on the cervical spine at vertex M4.

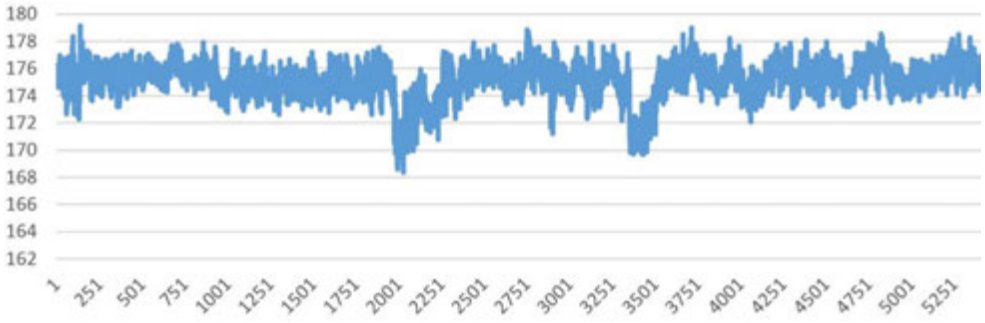


Figure 5.3. Angles on the cervical spine at vertex M5.

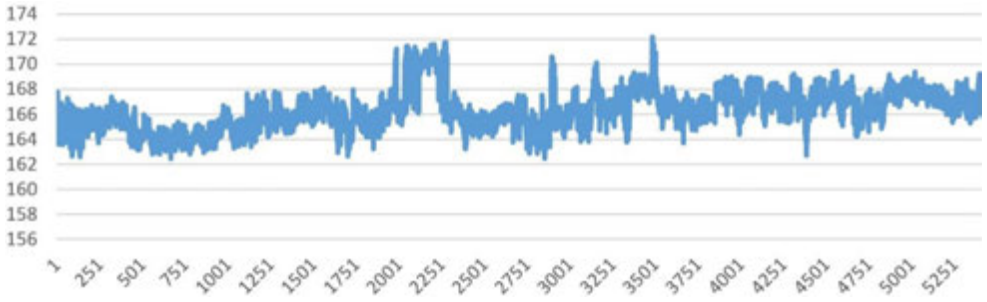


Figure 5.4. Angles on the cervical spine at vertex M6.

On the basis of the angles extracted from the four vertices along the cervical spine, descriptive statistics are summarized in Table 5.1.

Table 5.1. Descriptive statistics summary of the four cervical spine vertices.

| Vertex | Mean | Standard Deviation | Minimum | Maximum | Range |
|---|---|---|---|---|---|
| **M3** | 166.87 | 1.22 | 162.39 | 171.57 | 9.18 |
| **M4** | 172.98 | 0.76 | 170.57 | 175.78 | 5.22 |
| **M5** | 175.14 | 1.38 | 168.38 | 179.12 | 10.74 |
| **M6** | 166.30 | 1.56 | 162.42 | 172.17 | 9.75 |

### 5.1.2. Random Walk Characteristics

Along the temporal dimension, the angle data show the noise characteristics of the physiological signal. The fluctuation appears similar to the plot of white noise as shown in Figure 5.5.

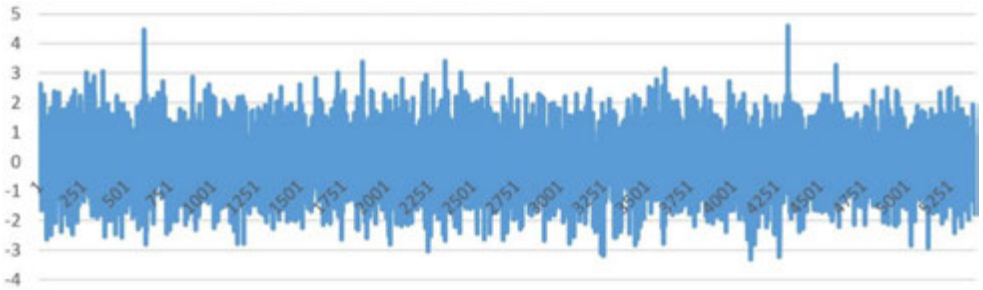


Figure 5.5. Plot of white noise.

The mean amplitude of the white noise is 0.00 with a standard deviation of 1.00. The minimum and maximum amplitudes of this data clip are -3.29 and 4.60, respectively, which produce a range of 7.89.

Most biomedical time series usually consist of property similar to the increments of random walks. To convert the noise signal into a random walk-like time series, the data are subtracted by the overall mean value and then integrated along the time series.

$$Y(i) = \sum_{k=1}^{i} [\, x_k - \langle x \rangle \,]$$

where i = 1, … , N; Y(i) is the random walk signal at frame i of the time series; $X_k$ is the original data signal; and <x> is the overall mean value of the time series, given by

$$\langle x \rangle = \frac{1}{N} \sum_{i=1}^{N} x_i$$

After subtracting the angle data of the cervical signal by its overall mean, the plot is shown in Figure 5.6.

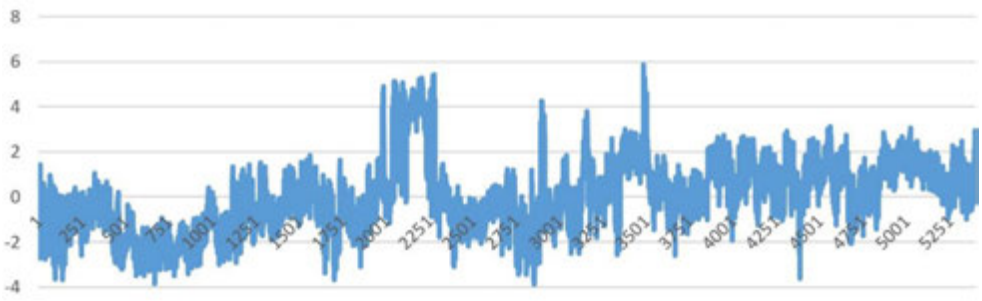


Figure 5.6. Plot after subtracting the angle data of the cervical signal by its overall mean.

After the integration along the time series, a random walk like-structure can be observed (Figure 5.7). It shows the subtle changes in spinal curvature along the time in near intervals attempting to stabilize the human body.

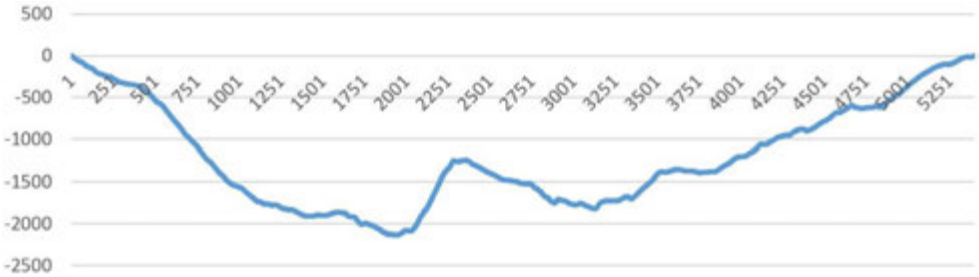


Figure 5.7. Random walk-like structure of the cervical spine time series.

When applying the same random walk computation to the white noise, the plot (Figure 5.8) does not fluctuate as observed in the previous plot.

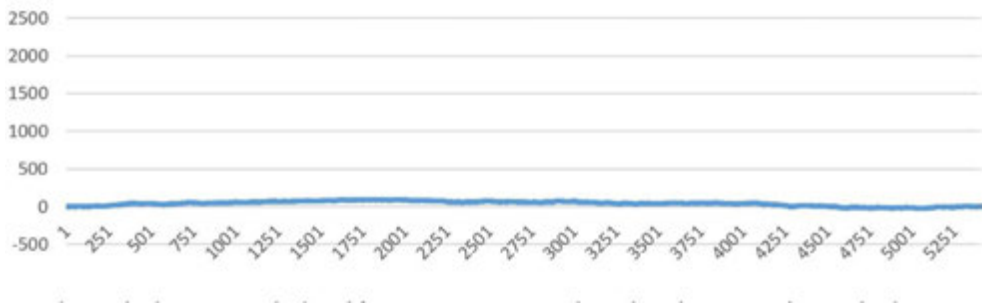


Figure 5.8. Plot of white noise after the application of the random walk computation.

Because the angle data were calculated using motion capture data, digital noise could overlap the actual movement. Under the assumption that the markers do not move faster than 10 Hz when attached to the human skin surface, Butterworth low-pass filtering can usually be applied to the raw marker position data with a cut-off frequency at 10 Hz. After the application of the low-pass filter with an order set of three, the angle data are then as shown in Figure 5.9.

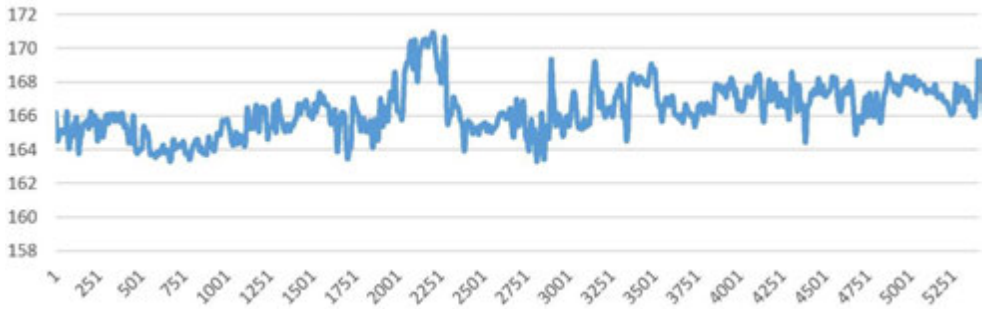


Figure 5.9. Angle data after the application of the low-pass filter with an order set of three.

After filtering, the density of the signal plot does not appear as intense as the original one. On the basis of this filtered signal, the random walk plot is then as shown in Figure 5.10.

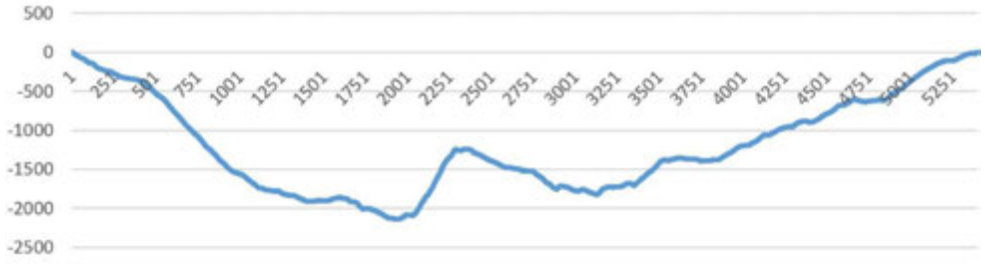


Figure 5.10. Random walk plot on the basis of the filtered signal.

For improved sign handling at the later step, the angles are then calculated using the complement of 180$^{o}$ (Figure 5.11), which represents the spinal curvature deviation with respect to a straight line in three adjacent markers. The signal plot and random walk plot is as shown in Figure 5.12. This is then the experimental signal for studying the subsequent computational steps.

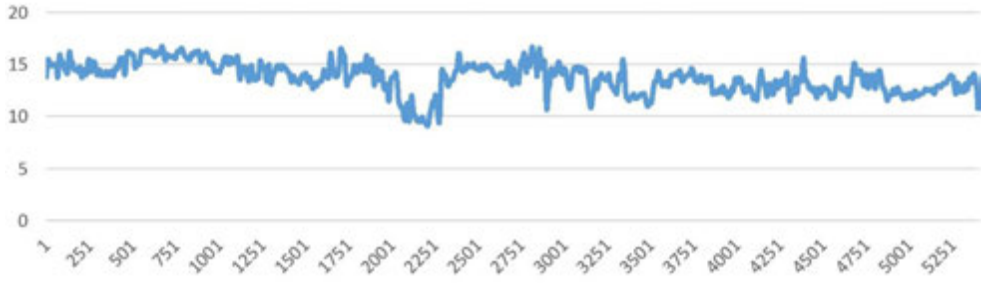


Figure 5.11. Signal plot after 180$^{o}$ complement.

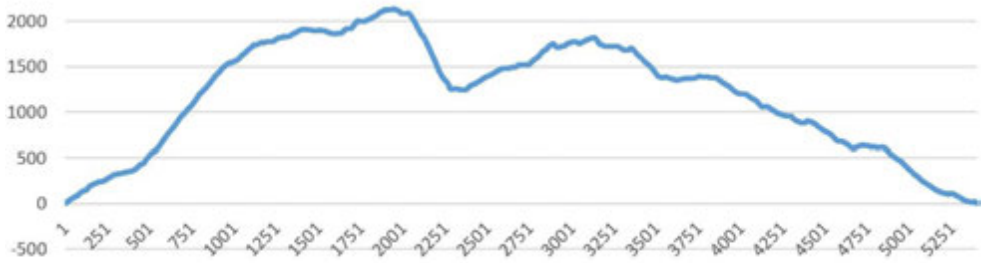


Figure 5.12. Random walk plot on signal after 180$^{o}$ complement.

### 5.1.3. RMS Variation

Given the experimental plot as in biomedical time series, a conventional method to analyze the variation is to measure the average as RMS, as follows:

$$rms_{overall} = \sqrt{\frac{1}{N}\sum_{i=1}^{N} x_i^2}$$

where N is the total number of frames in the time series, and $x_i$ is the signal at a particular frame i.

Figure 5.13 illustrates the experimental time series and white noise. Both of them have a zero average (red dashed line) and a similar RMS value of one (+/- 1 RMS in red solid lines). However, they are of quite different structures. The RMS here is sensitive to the differences in the amplitude of variation, but not to the differentiation in the structure of variation.

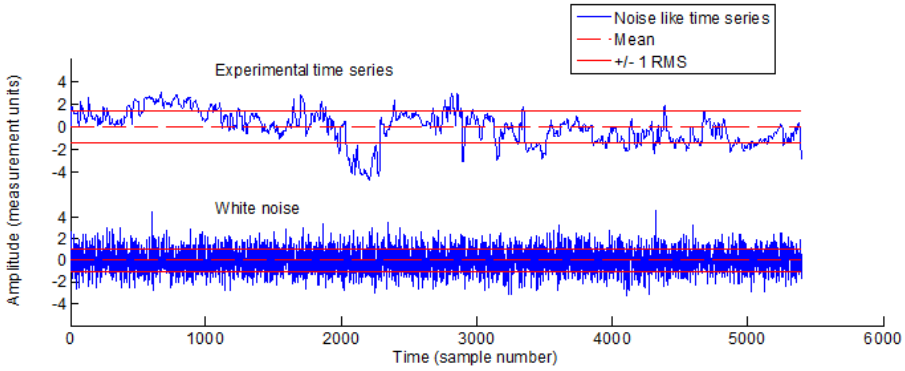


Figure 5.13. RMS value of experimental time series and white noise.

In the experimental time series, there are local fluctuations with both large and small magnitudes. The method to analyze this local structural variation is to divide the time series into segments and compute the local RMS corresponding to each segment. The process is to divide the time series into nonoverlapping segments of equal size.

$$N_s = int\left(\frac{N}{s}\right)$$

where $N_s$ is the number of segments in a scale of s; N is the total number of frames; s is the length of equal-sized nonoverlapping segments; and int( ) is a function to obtain the floor value after the division.

Our experimental time series has a total of 5400 frames. When the segment length is set to 600, it results in nine segments, hence, nine local RMS values (Table 5.2).

Table 5.2. RMS value of nine segments.

| **Segment** | **1** | **2** | **3** | **4** | **5** | **6** | **7** | **8** | **9** |
|---|---|---|---|---|---|---|---|---|---|

| | | | | | | | | | |
|---|---|---|---|---|---|---|---|---|---|
| **Local RMS** | 33.21 | 45.30 | 31.53 | 127.42 | 24.77 | 55.31 | 48.46 | 29.04 | 37.48 |

### 5.1.4. Local Detrending

In biomedical time series, slow varying trends exist. Therefore, detrending the data is necessary to quantify the invariant structure in scale and to reveal the variations around these trends. A polynomial fitting is applied to extract the trend of each segment. Linear, quadratic, cubic, or even higher order polynomials can be used in this fitting procedure. The local fluctuation can then be computed for the residual variation when comparing to the fitting.

$$F^2\,(s,v) = \frac{1}{s}\sum_{i=1}^{s}\{\,Y\,[\,(v-1)\,s\ +i\,]-\ y_v\,(i)\,\}^2$$

where $F^2(s, v)$ is the square of the RMS on the basis of the local trend; s is the segment length; v is the segment 1, … , $N_s$ ; Y [ (v - 1) s + i ] is the time series signal at a particular frame [ (v – 1) s + I ]; and $y_v$ is the fitting polynomial in segment v. Because the detrending is achieved by subtracting the polynomial fits to the time series, different order DFA differ in their capability of eliminating the trends. In Figure 5.14, the red dashed line is the fitting trend of three orders within nine segments of a sample size of 600. The distance between the red dashed trend line and the red solid lines represents +/- 1 local RMS.

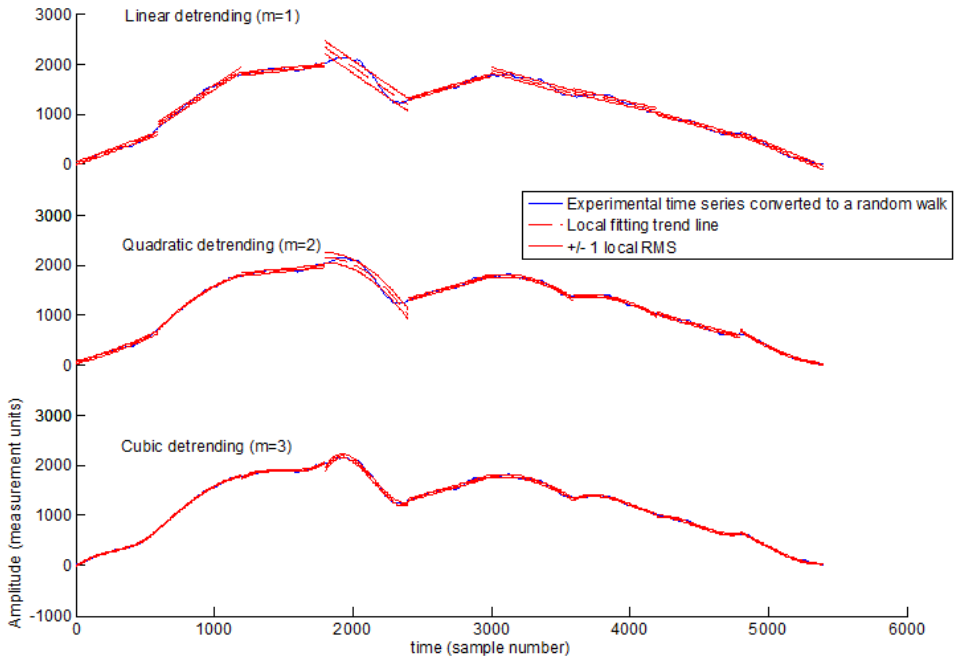


Figure 5.14. Fitting trend of three orders within segments of a sample size of 600.

The detrending process applied on the experimental time series is to distinguish the local fluctuations of the spinal movement within each divided segment. The regression lines are the trend lines that represent the local tendency of spinal movement. The RMS computation measures how much the local fluctuations are different from the local tendency on the movement.

### 5.1.5. Detrended Fluctuation Analysis

The time series has both fast- and slow-changing fluctuation characteristics. The overall RMS is influenced by the choice on the length of segment. Fast-changing

fluctuation is influenced by the segment with a shorter sample length, whereas slow-changing fluctuation is influenced by the segment with a longer sample length. The scaling function of the overall RMS should then be computed for multiple segment sizes. It features both the fast- and slow-changing fluctuations that influence the structure of the time series.

$$F_2\,(s) = \sqrt{\frac{1}{N_s}\sum_{v=1}^{N_s} F^2\,(\,s, v\,)}$$

where $F_2(s)$ is the standard detrended fluctuation function at time scale s; s is the segment length; $N_s$ is the number of segments in a scale of s; $F^2(s, v)$ is the square of the RMS on the basis of the local trend; and v is the segment 1, … , $N_s$ .

In this case, the time scale is chosen with a segment length [16, 32, 64, 128, 256, 512, 1024]. There are a total of seven scales that compose the overall scaling function.

Different segment lengths within the experimental time series represent how long the period of time is under investigation. A shorter period reveals more local fluctuation in spinal movement. A longer period compares the fluctuation to a relatively more stabilized posture. This is because when the period is long, there is an averaging effect that averages the large and small magnitudes of fluctuations, which eventually results in a stabilized posture.

The fitting polynomial is chosen to be the first order. DFA identifies the fractal structure as the power law relation among the RMS computed for multiple scales.

The power law relation is represented by the slope of the regression line. Figure 5.15 illustrates the log-log plot of the local fluctuations and overall RMS versus multiple scales.

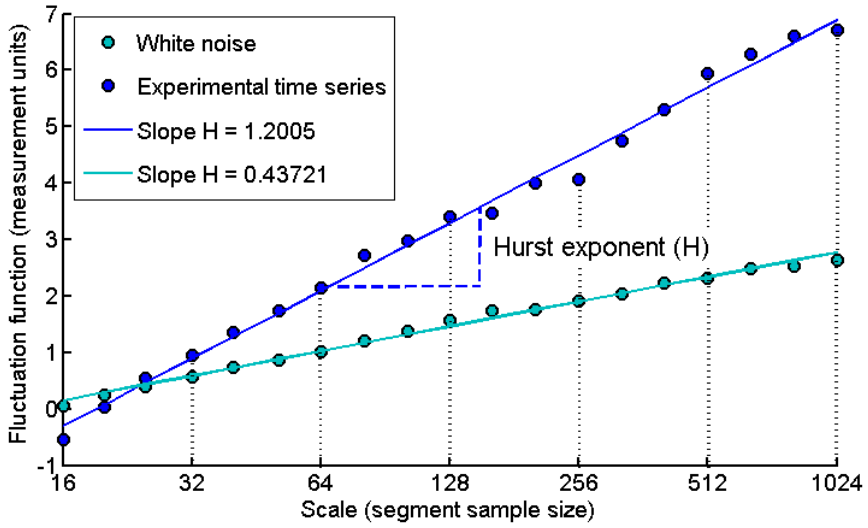


Figure 5.15. Log-log plot of the local fluctuations and overall RMS versus multiple scales.

The Hurst exponent (H) is defined as the slope of the regression line. It indicates the fractal structure of time series in a single dimension. Its value measures the local fluctuation by how fast the overall RMS grows with an increasing segment sample size. In Figure 5.15, the overall RMS is grows with the increase in the segment sample size. The growth is fast in the experimental time series compared to the white noise.

Moreover, there is a continuum between random walk like and noise like time series as represented by H. Extracted from Ihlen [9], Figure 5.16 illustrates the fractal structures with different Hurst exponents.

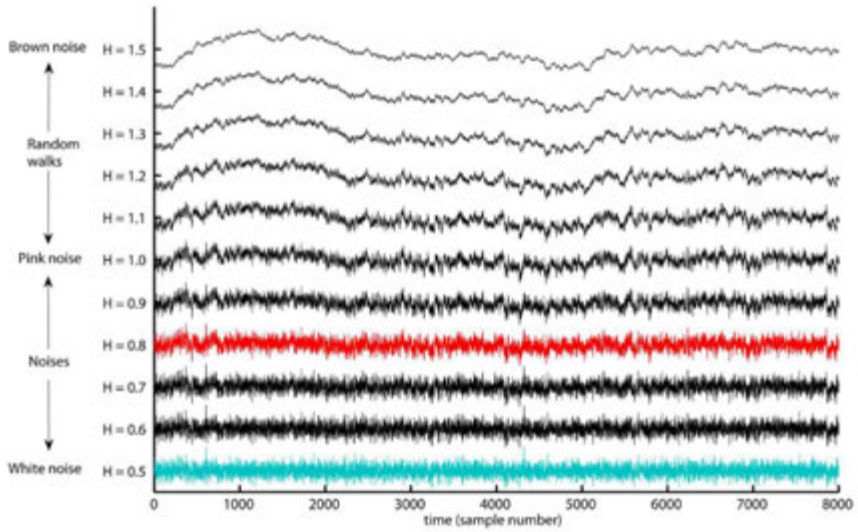


Figure 5.16. Fractal structures with different Hurst exponents.

When H falls in the range between 0 and 1, the time series is said to have a noise-like structure. If it is above 1, the time series consists of a random walk-like structure. When H is in the range between 0 and 0.5 or between 0.5 and 1, a time series is said to have a long-range dependent structure. In the case of a range between 0.5 and 1, the time series has a correlated structure, whereas the range between 0 and 0.5 is said to have an anticorrelated structure. In particular, when H equals to approximately 0.5, the time series is said to have an independent or short-range dependent structure. The other cases of note have Hurst exponents of 1.0 and

1.5, which correspond to pink noise and Brown noise, respectively. The pink noise separates between noises H < 1 that have more apparent fast evolving fluctuations and random walks H > 1 that have more apparent slow evolving fluctuations. According to the previous log-log fluctuation function plot versus time scale, the white noise has a Hurst exponent close to 0.5, which means that the time series tends to be an independent or short-range dependent structure. The Hurst exponent has a value of 1.2 in the experimental time series, which indicates a random walk-like structure with apparent slow evolving fluctuations.

### 5.1.6. Multifractal Detrended Fluctuation Analysis

From the previous plot on the fluctuation function, the overall RMS variation can be seen increasing when the segment scale increases. This explains the definition of the Hurst exponent. However, within a time series that consists of a multifractal structure, local fluctuations exist in both extremely small and large magnitudes. Because this is not present as a structure of normal distribution, in the case of monofractal time series, a second order statistical moment, for example, variance, cannot be used alone. Consequently, a multiple order statistical moment should be considered. Thus, the q-th order RMS is applied to extract the various magnitude of large and small fluctuations in multifractal DFA.

$$F_q\,(s) = \left\{ \frac{1}{N_s} \sum_{v=1}^{N_s} \left[ F^2\,(s, v\,) \right]^{\frac{q}{2}} \right\}^{\frac{1}{q}}$$

where $F_q(s)$ is the q-th order fluctuation function at time scale s; s is the segment length; $N_s$ is the number of segments in a scale of s; $F^2(s, v)$ is the square of the RMS on the basis of the local trend; and v is the segment 1, … , $N_s$ .

The q-th order varies from negative to positive q; it weights the influence of the segment from a small to large magnitude of fluctuations. Figure 5.17 illustrates the plot of the RMS with a different q-th order ranging from -3 to 3 on the basis of the experimental and monofractal time series.

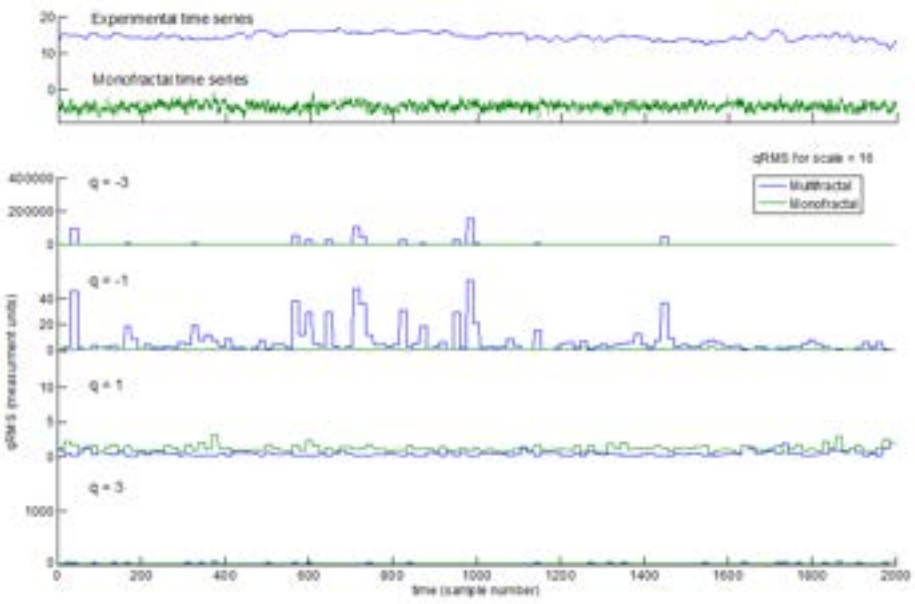


Figure 5.17. RMS plot with a different q-th order ranging from -3 to 3 on the basis of the experimental and monofractal time series.

For a negative q-th order, the qRMS is influenced by a small magnitude of fluctuation. By contrast, a positive q-th order is influenced by a large magnitude of fluctuation. The local variation in a large and small magnitude of the qRMS is graded by the magnitude of the fluctuation in the time series. By comparing the negative q-th order of -1 and -3, the magnitude amplifies the segments with an extremely small RMS. Therefore, the overall q-th order RMS is applicable for distinguishing between the structures of small and large magnitudes of fluctuations.

Within the experimental time series, the large and small magnitudes of fluctuations represent the large and small spinal movement along time. From the perspective of the motor control system in a static posture, the human body tries to stabilize itself in every moment. The spinal movement may be the response action to balance the human body. The large and small movement may then be the scale of how much the human body tends to stabilize itself. Furthermore, this might also reveal how unstable the human body is at that particular moment. Larger movement might mean a more unstable situation.

In the aforementioned case of the experimental and monofractal time series, both have a similar larger magnitude of fluctuation when the q-th order is set at 3. For a large magnitude, the monofractal time series has more peaks than the experimental time series does when q-th is set at 1. This can be observed in the original time series, with the monofractal time series having more up and down fluctuation compared to the experimental one. Because the magnitude of those fluctuations is

not considerably large, this can only be noticed when the q-th order equals to 1 and not 3.

On the positive side of the q-th order, there are many peaks in the experimental time series, whereas there are hardly any in the monofractal time series. This can be explained by the appearance of the two time series of which the experimental one has more segments with a small magnitude of fluctuation compared to the monofractal one. When the q-th order is reduced from -1 to -3, only those segments with a smaller magnitude of fluctuation appear.

With the introduction of the q-th order RMS, the q-th order Hurst exponent can then be defined. It represents the slopes ($H_q$) of regression lines for each q-th order RMS. Figure 5.18 illustrates the plot on the basis of the experimental time series.

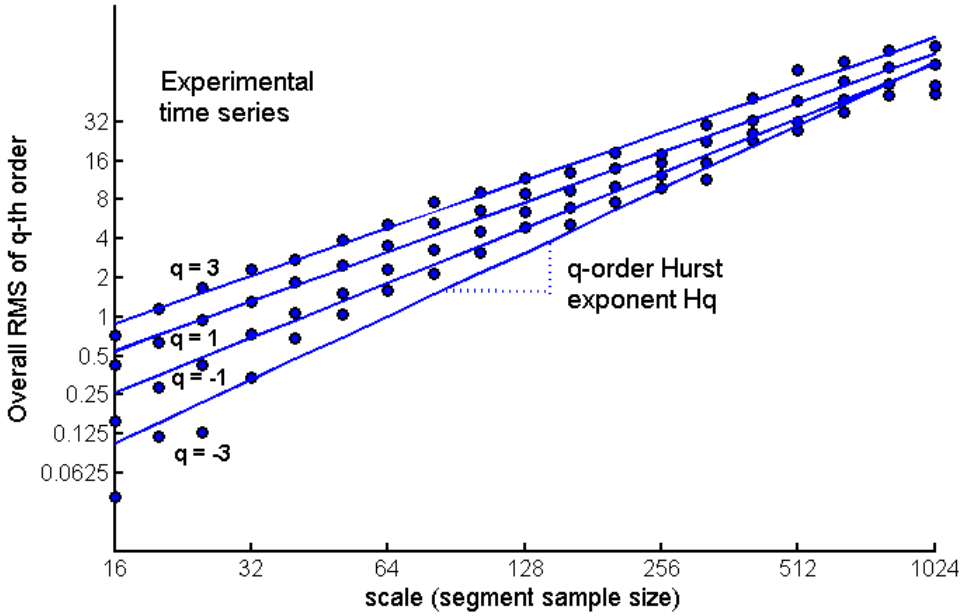


Figure 5.18. Regression lines for different q-th order RMS.

There are multiple values of H when the q-th order varies. How about compared to the monofractal time series and white noise? Figures 5.19 and 5.20 illustrate the plots on the basis of the monofractal time series and white noise.

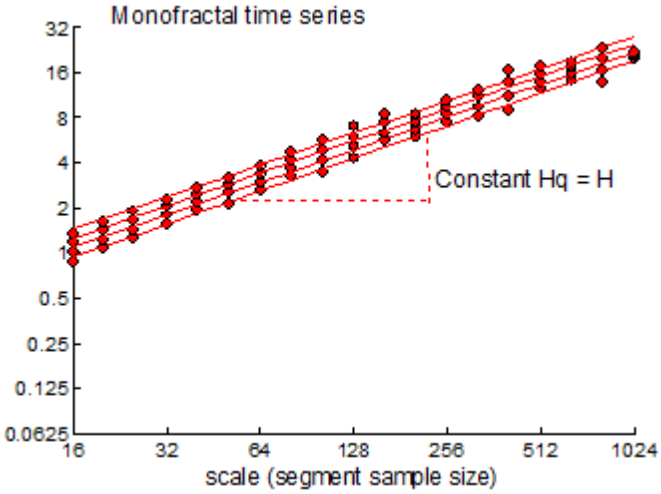


Figure 5.19. Plots on the basis of the monofractal time series.

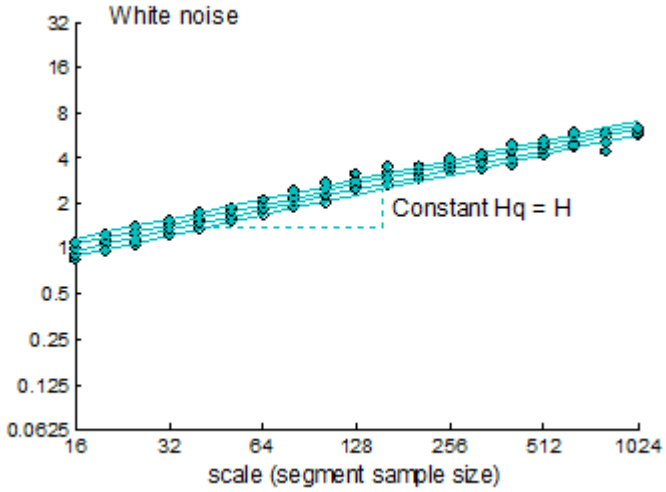


Figure 5.20. Plots on the basis of the white noise.

As shown, there is dependency between the slopes $H_q$ of the regression lines and the q-th order in the case of the experimental time series. When comparing the small and large segments, there is a difference between the qRMS for the positive and negative q-th order. Local fluctuation with either a large or small magnitude can be distinguished using small segments. The scale on the magnitude of local fluctuation can be revealed by positive and negative q-th values corresponding to large and small magnitudes, respectively. In the case of large segments, the fluctuations go across several large and small magnitudes. Therefore, the local fluctuations are averaged by each other, and hence appear to have convergence with large segments.

In the case of the monofractal time series, there is similar difference for positive and negative q-th orders at small and large segments. This explains the phenomenon that there are no distinguished peak values in the qRMS when the q-th order varies from -3 to 3. In this case, the q-th order RMS of the experimental time series can be distinguished from that of the monofractal time series by using the various $H_q$ values when the q-th order varies. Hence, it shows the fundamental structural difference between multifractal and monofractal time series, with different orders of fractal structures.

The white noise shows a similar appearance when compared to the monofractal time series. Both of them have a similar difference of variation in both small and large segments. The distinguished feature between these two plots is that the slopes as noted by $H_q$ are different. In the case of monofractal time series, the value

of $H_q$ is approximately 0.76, whereas it is approximately 0.46 in white noise. This shows the phenomenon that there is no multifractal structure in both monofractal time series and white noise. When the q-th order varies, the $H_q$ shows a consistent value that defines the fundamental nature in the continuum of fractal structures with the range of Hurst exponents. White noise appears to have H values of approximately 0.5. When H is between 0.5 and 1, the time series has a correlated structure.

When the q-th order is plotted against different $H_q$ , Figure 5.21 clearly shows the difference between the three time series. The experimental time series has varying $H_q$ values with a difference order of q. This distinguishes the existence of a multifractal structure in the experimental time series. According to the previous Hurst exponent continuum, there is a random walk-like structure when the value of H is between 1 and 1.5. The variation of H shows the structural differences in fluctuation embedded in the time series, which is the multifractal feature. The monofractal time series has a constant $H_q$ value of approximately 0.76. There is no distinguished variation in $H_q$ , meaning that along the whole time series, there only appears one fractal structure corresponding to the specific H value in the Hurst exponent continuum. A similar structural feature is found in the white noise, which has an $H_q$ value of approximately 0.46.

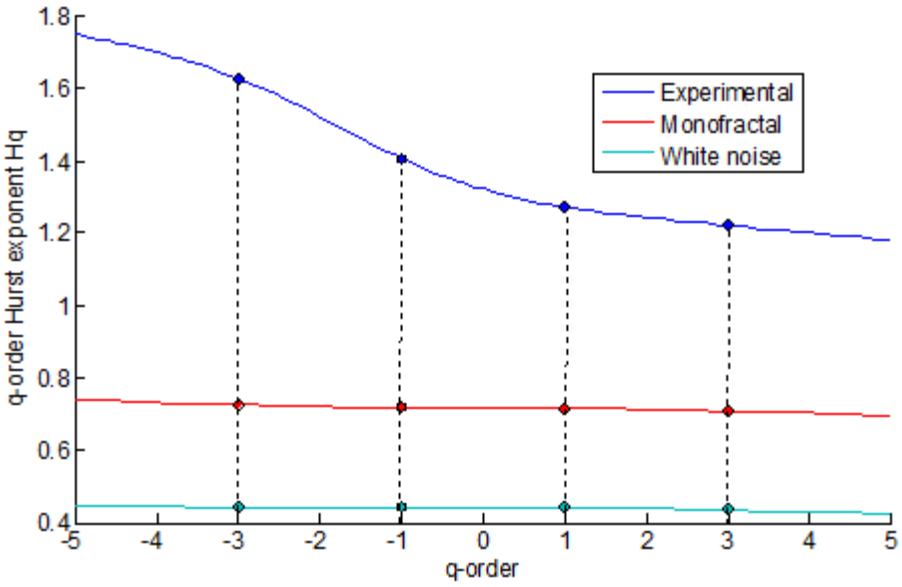


Figure 5.21. Difference between the experimental time series, monofractal time series and white noise.

At this moment, the experimental time series shows the fractal structure and indicates multifractal dimensions. There are multiple strategies used by the motor control in response to unstable human body posture.

### 5.1.7. Multifractal Spectrum

The aforementioned q-th order Hurst exponent $H_q$ is one of the several scaling exponents to reveal the multifractal structure of time series. According to Kantelhardt [45], there are other parameters derived from $H_q$ to illustrate other aspects of the multifractal structure. The $H_q$ is first converted to the q-th order mass exponent $t_q$ and is calculated as

$$t_q = q \cdot H_q - 1$$

The plot against q is illustrated in Figure 5.22. In monofractal time series, the long-range correlation is characterized by $t_q$ by a linearly dependent q-th order with a single $H_q$.

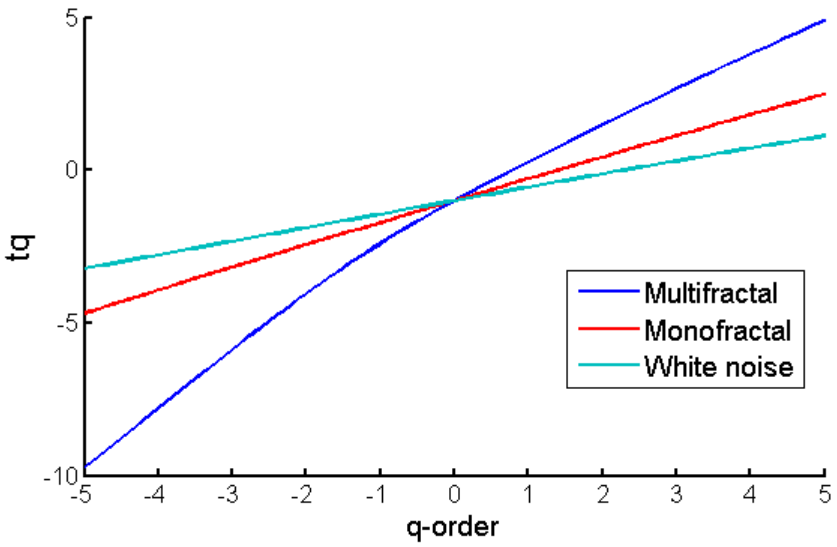


Figure 5.22. Plot of the q-th order mass exponent.

Thereafter, the mass exponent ($t_q$) is converted to the q-th order singularity exponent ($h_q$) by using the following equation:

$$h_q = H_q + q \cdot H'_q$$

where $h_q$ is the singularity strength and the tangent slop of $t_q$. The plot against q is illustrated in Figure 5.23.

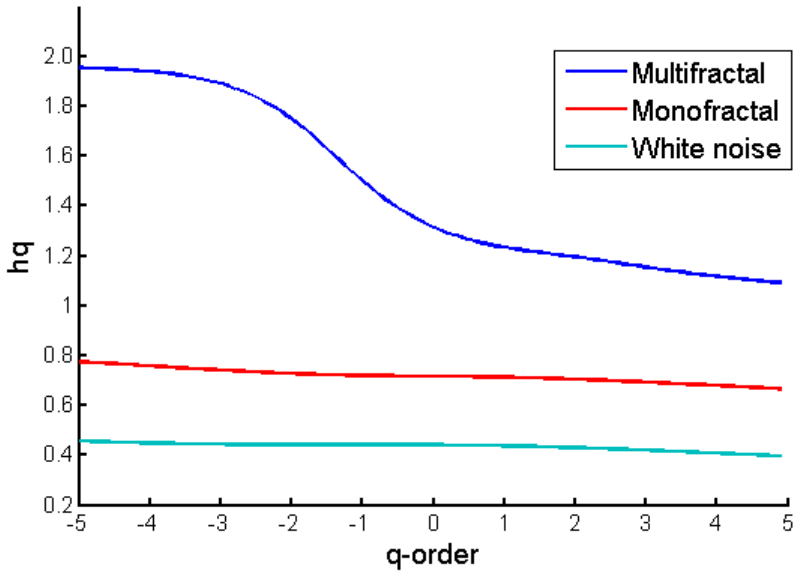


Figure 5.23. Plot of the q-th order singularity exponent against q.

The q-th order singularity dimension ($D_q$) is then defined by

$$D_q \equiv \frac{t_q}{q-1} = \frac{q \cdot h_q - 1}{q-1}$$

$D_q$ is the generalized multifractal dimensions that are used instead of $t_q$ in some research. In both cases, they depend on q. When q = 0, $D_0 = -t_0 = -1$. The plot of $D_q$ against q is illustrated in Figure 5.24.

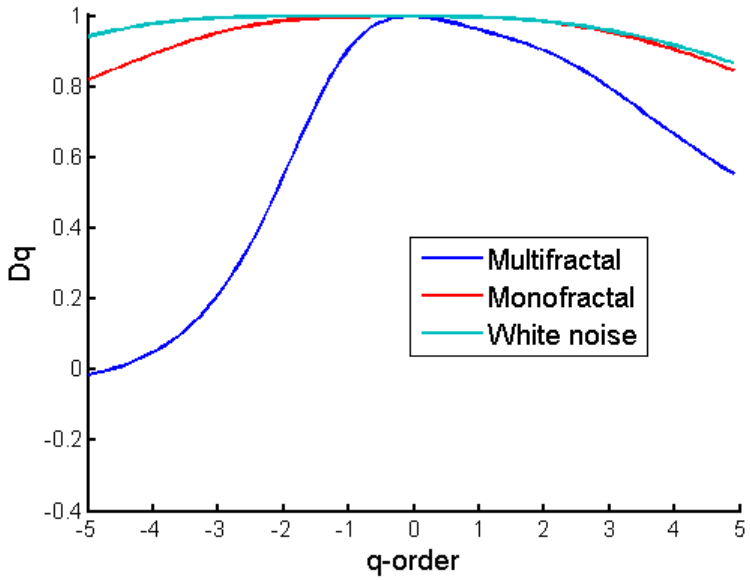


Figure 5.24. Plot of the q-th order singularity dimension ($D_q$) against q.

When plotting the singularity dimension ($D_q$) against the singularity exponent ($h_q$), the multifractal spectrum is reduced into a small arc for the time series of monofractal and white noise. As illustrated in Figure 5.25, in the case of the multifractal time series, a large arc is resulted in which the difference between the maximum and minimum $h_q$ is called the multifractal spectrum width, W.

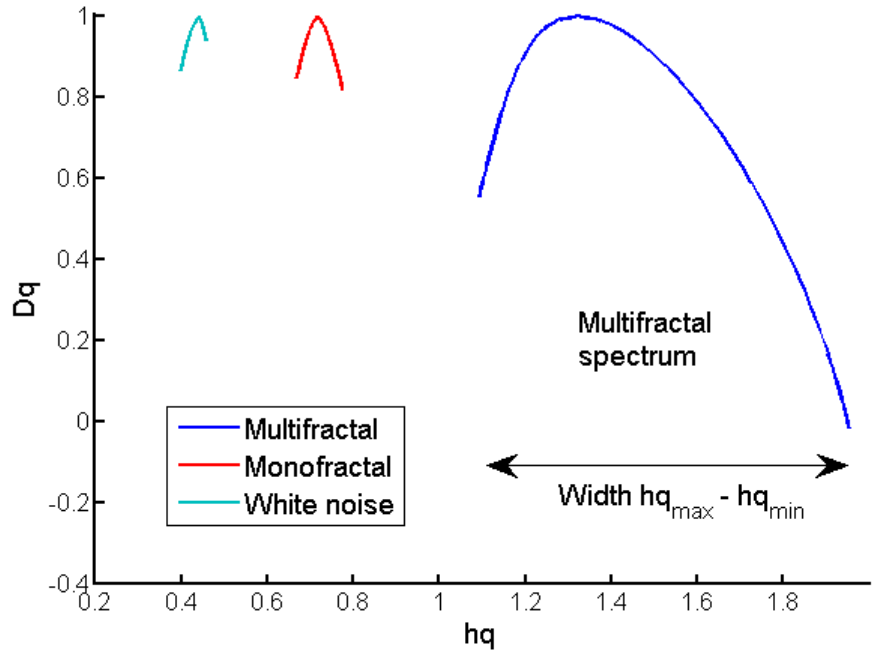


Figure 5.25. Plot of the singularity dimension ($D_q$) against singularity exponent ($h_q$).

The multifractal spectrum width (W) is approximately zero if the time series are monofractal or white noise. In the case of the multifractal time series, W increases with the spectrum of the multifractal structure.

The autocorrelation exponent (γ) can be estimated [45] using the following equation

$$\gamma = 2 - 2\,h(q = 2)$$

where h(q = 2) is the singularity exponent when the q-th order equals to 2. For uncorrelated or short-range correlated data, h(2) is expected to have a value of 0.5, whereas a value greater than 0.5 is expected for long-range correlations. Therefore, for uncorrelated data, γ has a value of 1, and the lower the value is, the more correlated the data are.

## 5.2. Analysis of Results

The positional motion capture data of each participant were computed to obtain the spinal curvature angles at each vertice: M3, M4, M5, and M6. All the time series then underwent analysis on the basis of MFDFA. Selected multifractal parameters were then computed to identify an overview on the basis of the time series.

### 5.2.1. Multifractality Structure

The plot of the Hurst exponent ($H_q$) is illustrated in Figure 5.26, which is based on $H_q$ against the q-th order. The $H_q$ was calculated by computing the mean and extracting the minimum and maximum of all the time series in accordance with each value of q. There are altogether 100 values of the q-th order divided in equal intervals between -5 and 5 inclusively. The numerical values of the data are also recorded in Table 5.3. The minimum and maximum values of $H_q$ produce a tunnel that illustrates a decreasing trend of the q-th order from -5 to 5.The time series follow a regular pattern without any outlier. As an indication of long-range correlation, the mean value as computed from the means of $H_q$ is 1.190. This falls into the definition of a random walk structure. In addition, the range of the means of $H_q$ is 0.414. This indicates that all the time series do not behave as a monofractal structure; instead,

there is a range of multifractality. This can be further ascertained using other fractal parameters.

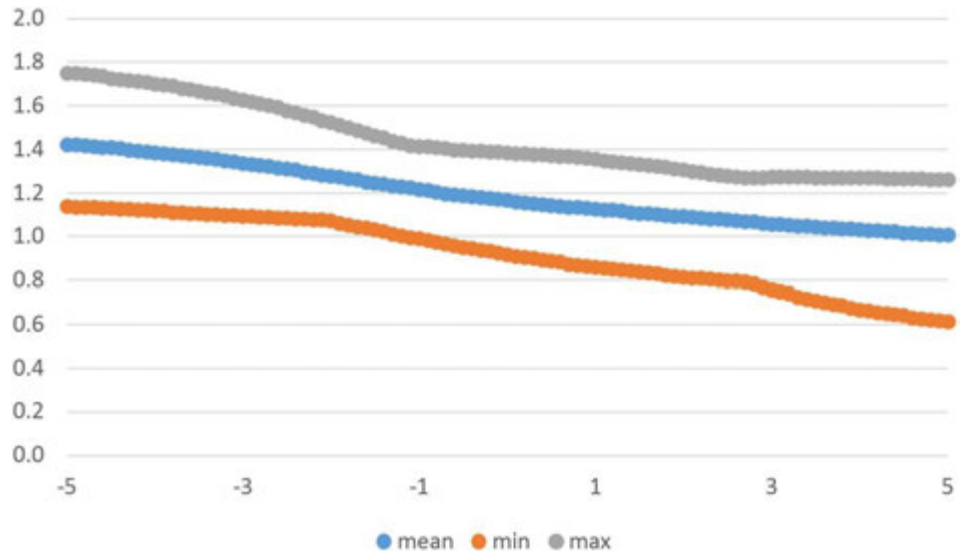


Figure 5.26. Plot of the Hurst exponent $H_q$ against the q-th order according to the mean, minimum, and maximum of each time series.

Table 5.3. Numerical values of the Hurst exponent $H_q$ against the q-th order according to the mean, minimum, and maximum of each time series.

| | **Mean** | **Standard Deviation** | **Minimum** | **Maximum** | **Range** |
|---|---|---|---|---|---|
| **Mean of $H_q$** | 1.190 | 0.131 | 1.008 | 1.422 | 0.414 |
| **Minimum of $H_q$** | 0.916 | 0.165 | 0.614 | 1.138 | 0.524 |
| **Maximum of $H_q$** | 1.436 | 0.163 | 1.259 | 1.750 | 0.491 |

The plot of the mass exponent ($t_q$) is illustrated in Figure 5.27, which is based on the $t_q$ against the q-th order. The $t_q$ is also calculated by computing the mean and extracting the minimum and maximum of all the time series in accordance with each value of q. The numerical values of the data are also recorded in Table 5.4. The

range on the means of $t_q$ has a value of 12.147, which shows an obvious difference from the monofractal and white noise as illustrated in the previous section on the definition of $t_q$. The standard deviation and range among the means, minimums, and maximums both have similar values of approximately 3.5 and 12, respectively. This indicates that the slope is approximately consistent across the q value from -5 to 5, which illustrates a consistency of having the multifractality structure.

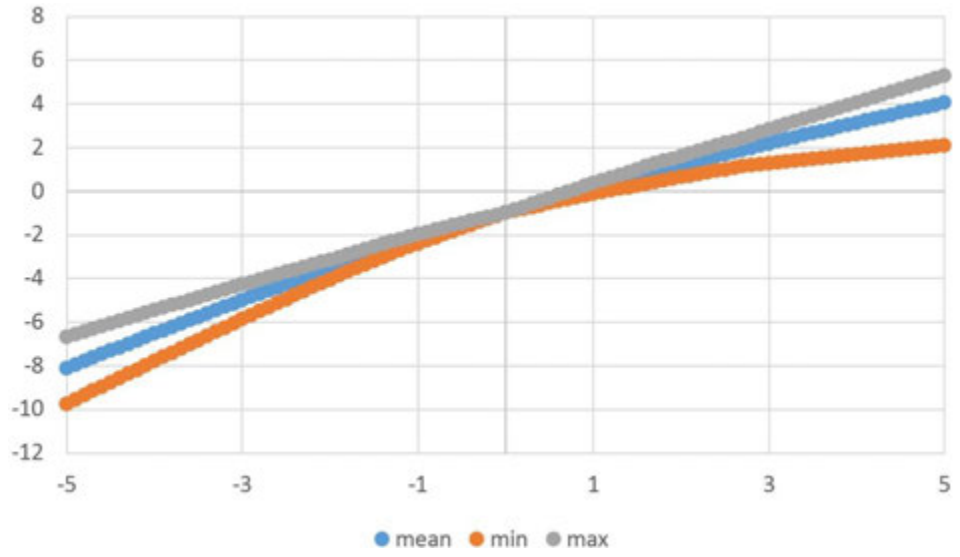


Figure 5.27. Plot of the mass exponent $t_q$ against the q-th order according to the mean, minimum, and maximum of each time series.

Table 5.4. Numerical values of the mass exponent $t_q$ against the q-th order according to the mean, minimum, and maximum of each time series.

| | **Mean** | **Standard Deviation** | **Minimum** | **Maximum** | **Range** |
|---|---|---|---|---|---|
| **Mean of $t_q$** | -1.377 | 3.545 | -8.109 | 4.038 | 12.147 |
| **Minimum of $t_q$** | -2.162 | 3.575 | -9.751 | 2.071 | 11.822 |
| **Maximum of $t_q$** | -0.768 | 3.490 | -6.689 | 5.296 | 11.984 |

The singularity exponent ($h_q$) is then evaluated. It indicates the singularity strength of the time series. The plot of $h_q$ against the q-th order is shown in Figure 5.28 and the statistics of corresponding numerical values are shown in Table 5.5. The range of the value 0.672 on the means of $h_q$ provides an initial estimation of the width on the multifractal spectrum as an average across the entire participant set. Compared to those of monofractal and white noise, which have an approximate value of zero, the value of 0.672 indicates the existence of multifractality in the participant set.

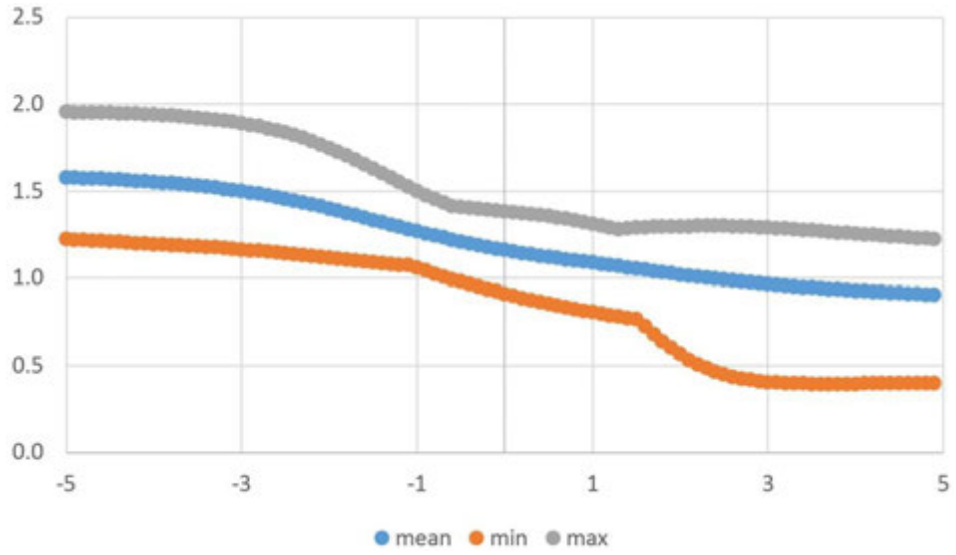


Figure 5.28. Plot of the singularity exponent $h_q$ against the q-th order according to the mean, minimum, and maximum of each time series.

Table 5.5. Numerical values of the singularity exponent $h_q$ against the q-th order according to the mean, minimum, and maximum of each time series.

| | **Mean** | **Standard Deviation** | **Minimum** | **Maximum** | **Range** |
|---|---|---|---|---|---|
| **Mean of $h_q$** | 1.215 | 0.235 | 0.905 | 1.577 | 0.672 |
| **Minimum of $h_q$** | 0.847 | 0.315 | 0.394 | 1.221 | 0.827 |

| | | | | | |
|---|---|---|---|---|---|
| **Maximum of $h_q$** | 1.523 | 0.274 | 1.224 | 1.953 | 0.729 |

The singularity dimension ($D_q$) is then computed to prepare for the illustration of the multifractal spectrum width. The plot of $D_q$ against the q-th order is illustrated in Figure 5.29. The statistics of the corresponding numerical values are shown in Table 5.6. Figure 5.30 plots the relationship between $D_q$ and $h_q$.

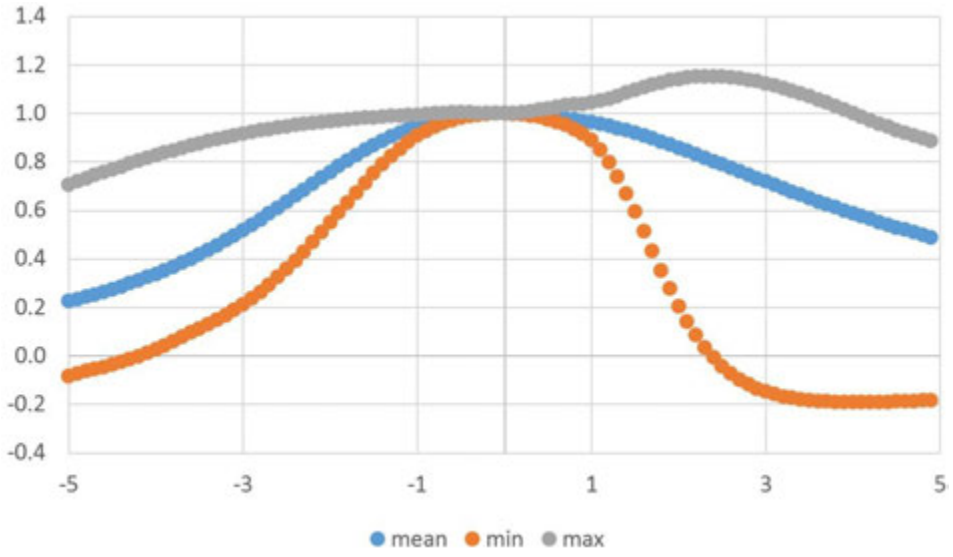


Figure 5.29. Plot of the singularity dimension $D_q$ against the q-th order according to the mean, minimum, and maximum of each time series.

Table 5.6. Numerical values of the singularity dimension $D_q$ against the q-th order according to the mean, minimum, and maximum of each time series.

| | **Mean** | **Standard Deviation** | **Minimum** | **Maximum** | **Range** |
|---|---|---|---|---|---|
| **Mean of $D_q$** | 0.704 | 0.238 | 0.225 | 1.000 | 0.775 |
| **Minimum of $D_q$** | 0.333 | 0.444 | -0.191 | 1.000 | 1.191 |

| | | | | | |
|---|---|---|---|---|---|
| **Maximum of $D_q$** | 0.983 | 0.110 | 0.707 | 1.153 | 0.446 |

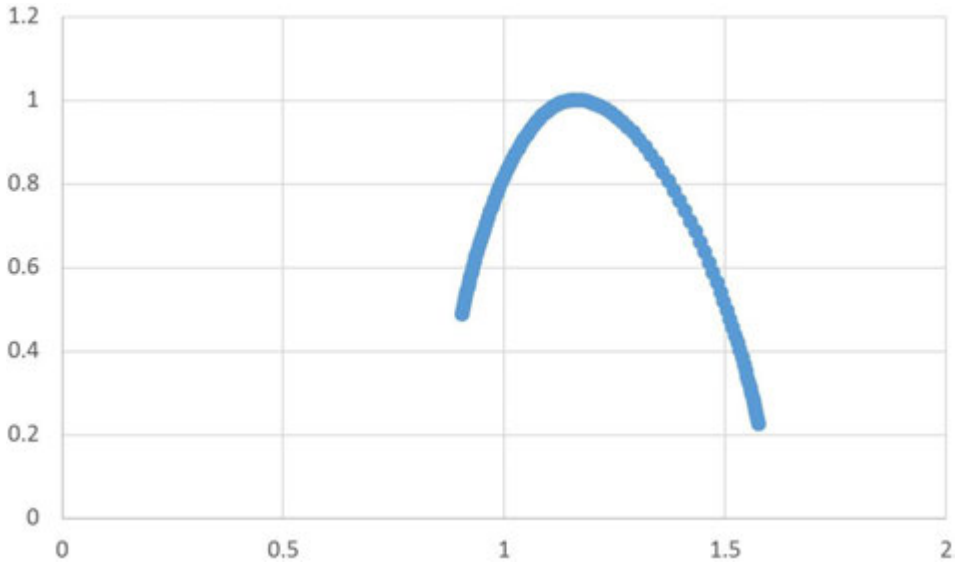


Figure 5.30. Plot of the singularity dimension $D_q$ against the singularity strength $h_q$ according to the mean of each time series.

To conclude the aforementioned statistical results, some of the multifractal parameters are selected in Table 5.7. These are the mean and standard deviation of the overall means across all the time series of all participants. For comparison, Table 5.8 provides a preview of the set of multifractal parameters extracted from the shuffled data, which is described in a subsequent section. Briefly, the shuffled data are based on the random placement of the original time series. The aim is to prove that the multifractal properties extracted from the original time series exist only in their original form, but not the shuffled data series, in which the multifractal properties are deconstructed.

Table 5.7. Selected multifractal parameters from participant data series.

| | Mean | Standard Deviation |
|---|---|---|
| **Mean of $h_q$** | 1.215 | 0.102 |
| **Width of $h_q$** | 0.673 | 0.141 |
| **Mean of $D_q$** | 0.704 | 0.067 |
| **Height of $D_q$** | 0.824 | 0.138 |

Table 5.8. Selected multifractal parameters from shuffled data series.

| | Mean | Standard Deviation |
|---|---|---|
| **Mean of $h_q$** | 0.507 | 0.026 |
| **Width of $h_q$** | 0.116 | 0.084 |
| **Mean of $D_q$** | 0.953 | 0.041 |
| **Height of $D_q$** | 0.206 | 0.141 |

The across participant mean of $h_q$ is 1.215 from the original data series, which is defined as a random walk series, compared to the shuffled series of 0.507, which is defined as white noise. Because the data are calculated across all participants in the set, there is a standard deviation of 0.102, showing the variation between participants across the set. The width of $h_q$ defines the multifractality of the data series. The wider the $h_q$ is, the higher the level of multifractality in the data is. Between the original and shuffled data, the width of $h_q$ has a difference of 0.673 and 0.116, respectively. Again, the standard deviation on the width of $h_q$ denotes the variation between participants across the set.

The across participant means of $D_q$ between the original and shuffled data are similar in value. The main difference can be observed when comparing the heights of $D_q$ . The original data set has a value of 0.824, whereas the shuffled one has a

value of 0.206. Because $D_q$ is another indicator of multifractality, it again ascertains that the original data have a multifractality structure.

## 5.3. Difference between Participants

In the previous section, the analysis ascertains that a multifractality structure exists in the spinal curvature of the cervical region in the experimental set of the upright sitting posture. This is an analysis on the basis of the summary across all participants within the experiment set. In this section, the investigation involves details about whether there is a difference between participants and how the various multifractal parameters differ when comparing across participants. Four multifractal parameters are compared, namely the Hurst exponent, mass exponent, singularity exponent, and singularity dimension. In addition, the plot of the singularity exponent is plotted against the singularity dimension.

### 5.3.1. Comparison between Participant Sequences

The first parameter to be compared across participants is the mean value of the Hurst exponent ($H_q$). The mean is computed based on the time series of all trials and vertices of each participant. To indicate the difference between participants, the $H_q$ values are sorted according to their values in ascending order, as shown in Figure

5.31. The minimum and maximum means of $H_q$ are 1.133 and 1.265, respectively. Both of these values indicate that the time series has the random walk-like structure. They also indicate a range of 0.133 difference between the minimum and maximum values. Comparing to the spectrum, which defines the range of Hurst exponents into a continuum of fractal structures, between 0.5 (as white noise) to 1.5 (as Brown noise of random walk), a 0.138 difference indicates 13.3% of the maximum range variation in the fractal structure across participants.

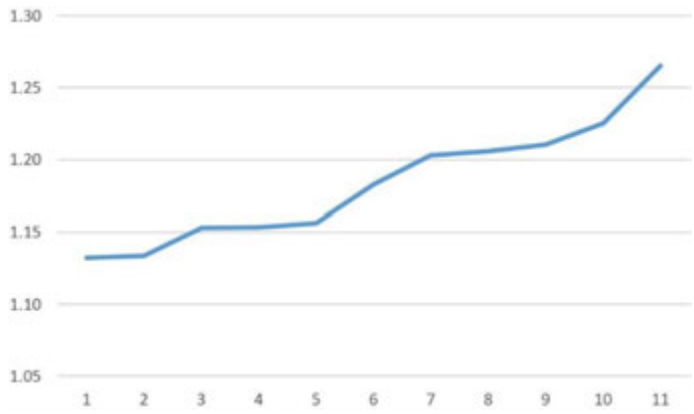


Figure 5.31. Plot of the participant mean Hurst exponent ($H_q$) in ascending order of values.

The order of the participants here is S10, S07, S11, S05, S01, S09, S02, S04, S06, S03, and S08.

The range on $H_q$ according to each participant is also plotted in Figure 5.32. The order is based again on the participant sequence in the previous plot of the mean $H_q$. The plot illustrates that the range of difference across all participants is approximated within 0.4 and 0.5. Most of the values are within half of the standard

deviation. The mean and standard deviation values are shown in Table 5.9. The values range between 0.411 and 0.440. There are only four values that exceed that: 0.369, 0.393, 0.446, and 0.485. This means the range of $H_q$ within each participant is about consistent. The two extreme values 0.369 and 0.485 are outliers, beyond the range of two standard deviations, either positive or negative. Because the calculation between the negative and positive values of the q-th order is based on the small and large fluctuations of the time series, the variation on the fractal structure between small and large fluctuations indicates a consistency in the random walk structure. This leads to the consistency of the motor control mechanism generating these values in the cervical region.

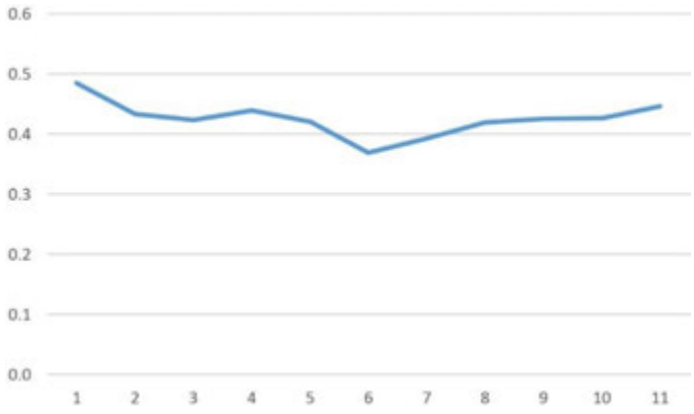


Figure 5.32. Plot of the participant range of the Hurst exponent ($H_q$) in the order according to ascending values of $H_q$ .

Table 5.9. Mean and standard deviation values in the range of $H_q$ .

| -2 S.D. | -1 S.D. | -0.5 S.D. | Mean | +0.5 S.D. | +1 S.D. | +2 S.D. |
|---|---|---|---|---|---|---|
| 0.367 | 0.296 | 0.411 | 0.425 | 0.440 | 0.454 | 0.483 |

The second parameter to investigate is the mass exponent ($t_q$). Again, the values are computed based on the overall means of $t_q$ in each trial and vertex of each participant. Subsequently, the values are sorted according to the ascending order. The plot is illustrated in Figure 5.33. The minimum and maximum means of $t_q$ are -1.442 and -1.319, respectively, producing a range of 0.124. This indicates that in the participant group, there exists the variation in values of $t_q$ . However, there is one outlier at the end of the sequence. The mean value is -1.319, which is less than two times the standard deviation from the mean. The order of the participant here is S10, S08, S05, S07, S01, S04, S06, S03, S11, S02, and S09. The comparison of the participant order is conducted later in this section.

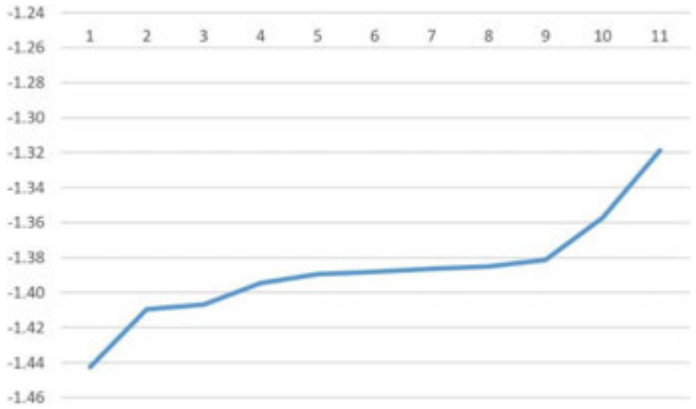


Figure 5.33. Plot of the participant mean mass exponent ($t_q$) in ascending order of values.

Next is the multifractal parameter on the singularity exponent ($h_q$). The computation process of retrieving the mean values is similar to the aforementioned. The mean is computed based on the time series of all trials and vertices of each participant. To

indicate the difference between participants, the $h_q$ values are sorted according to their values in ascending order. Figure 5.34 shows the sorted order of $h_q$ values. The minimum and maximum values are 1.142 and 1.296, respectively. This is a range of 0.155. There is one outlier within the data that exceeds two standard deviations: the maximum value, 1.296. The sequence of the participant here is S10, S07, S05, S01, S11, S09, S06, S02, S04, S03, and S08.

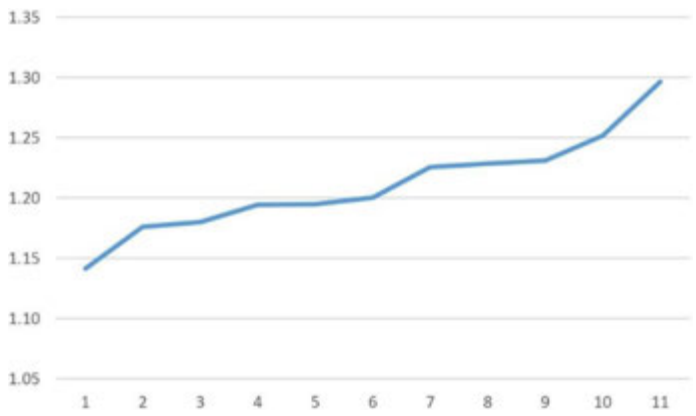


Figure 5.34. Plot of the participant mean singularity exponent ($h_q$) in ascending order of values.

In relation to the multifractal parameter of $h_q$, the width of the multifractal spectrum (W) is indicated by the width of $h_q$, which is the value between the maximum and minimum of $h_q$. Similarly, for each trial and vertex on each participant, W is computed based on the difference between minimum and maximum $h_q$ values. Subsequently, the mean is computed from the set of W obtained for each participant. The plot sorted in ascending order is illustrated in Figure 5.35. There is one outliner at the maximum value, 0.767, which is more than

two standard deviations from the mean. The participant sequence here is S09, S02, S04, S01, S11, S06, S07, S03, S05, S08, and S10.

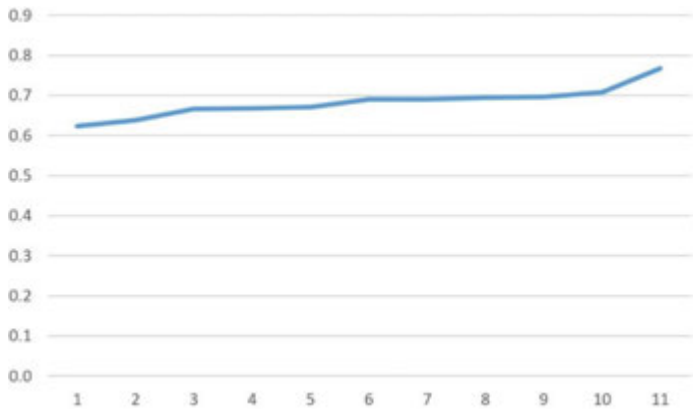


Figure 5.35. Plot of the participant mean on the width of the multifractal spectrum (W) in ascending order of values.

Next, the singularity dimension ($D_q$) is analyzed. The computation process is similar to the aforementioned. The $D_q$ is calculated based on each time series regarding the trials and vertices per participant. These mean values are then averaged to obtain a value for each participant. To show the variation between participants, these values are then sorted in ascending order. The plot is shown in Figure 5.36. The minimum and maximum values are 0.657 and 0.720, respectively. This is a range of 0.063. However, from the plot, there is obviously an outlier at the minimum side. The value is 0.657, which is approximately 2.5 standard deviations less than the mean. Excluding the outlier, the overall range is 0.029, which is approximately 1.6 times the standard deviation and only approximately 0.8 times the standard deviation at each side, positive and negative. In other words, the value of $D_q$ is quite consistent across

the participant set. This indicates that the singularity dimension is of similar values in the healthy participant set. The participant sequence here is S10, S03, S08, S06, S07, S05, S11, S01, S04, S09, and S02.

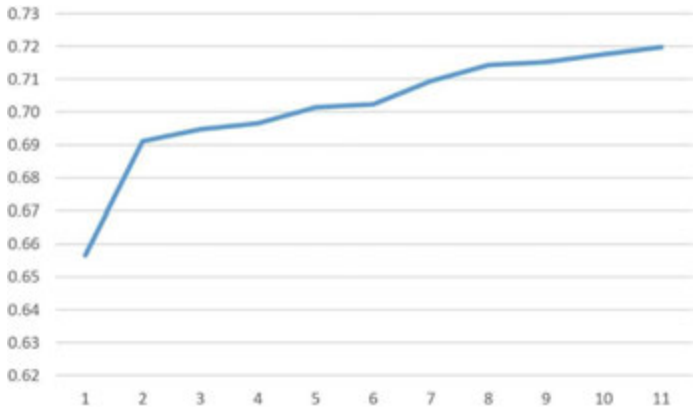


Figure 5.36. Plot of the participant mean singularity dimension ($D_q$) in ascending order of values.

In relation to $D_q$, the height of the singularity dimension is indicated by the difference between the maximum and minimum values of $D_q$. The mean on the $D_q$ values can also be computed from the means of the trials and vertices per participant, and then sorted in ascending order to obtain the participant variation. Figure 5.37 illustrates the plot on $D_q$ in ascending order of values on the basis of the participant sequence. There is no obvious outlier within the data sequence. The minimum and maximum values are 0.759 and 0.897, respectively, which is a range of 0.138. This value is approximately three times the standard deviation, which is approximately 1.5 times at both the positive and negative side from the mean. In other words, the multifractal parameters can also be considered consistent across

the healthy participants. The sorted participant sequence here is S02, S04, S06, S05, S03, S08, S01, S09, S10, S11, and S07.

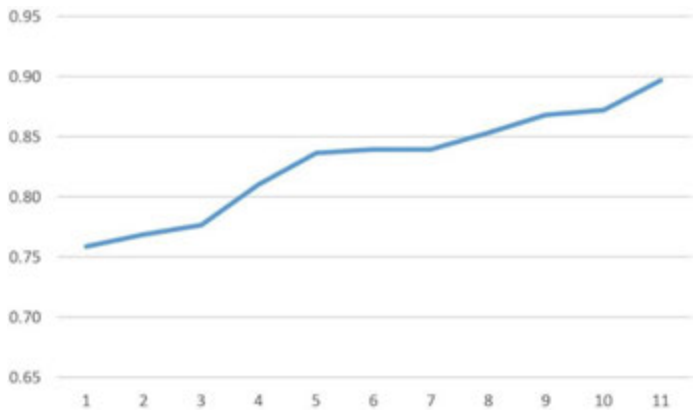


Figure 5.37. Plot of the participant mean on the height of the singular dimension in ascending order of values.

On the basis of the previous orders, the participant sequence is shown in Table 5.10 according to different multifractal parameters. The outliers are highlighted in the table. By excluding the outliers, the variation among participants for each multifractal parameter can further be analyzed and visualized. The final graph is often used to indicate the multifractality plot of $D_q$ against $h_q$. On the basis of the previous sorted results, different plots can be constructed to illustrate the participant variation.

Table 5.10. Ascending order of the participant sequence with respect to each multifractal parameter, with outliers highlighted.

| **Mean of $H_q$** | S10 | S07 | S11 | S05 | S01 | S09 | S02 | S04 | S06 | S03 | S08 |
|---|---|---|---|---|---|---|---|---|---|---|---|
| **Range of $H_q$** | S09 | S02 | S04 | S01 | S11 | S06 | S03 | S07 | S05 | S08 | S10 |

| | | | | | | | | | | | |
|---|---|---|---|---|---|---|---|---|---|---|---|
| **Mean of $t_q$** | S10 | S08 | S05 | S07 | S01 | S04 | S06 | S03 | S11 | S02 | S09 |
| **Mean of $h_q$** | S10 | S07 | S05 | S01 | S11 | S09 | S06 | S02 | S04 | S03 | S08 |
| **Width of $h_q$** | S09 | S02 | S04 | S01 | S11 | S06 | S07 | S03 | S05 | S08 | S10 |
| **Mean of $D_q$** | S10 | S03 | S08 | S06 | S07 | S05 | S11 | S01 | S04 | S09 | S02 |
| **Height of $D_q$** | S02 | S04 | S06 | S05 | S03 | S08 | S01 | S09 | S10 | S11 | S07 |

#### 5.3.1.1 Correlation Analysis on Participant Sequences

To further evaluate the relationship between these participant sequences, a correlation test is applied to extract the correlation relationship. The Spearman rank correlation test is applied for the analysis [59] by using SPSS v20 (IBM, USA). To adapt this correlation test, several requirements must be checked and data must be prepared before the test is conducted. This correlation test is a nonparametric test that is used to measure the degree of association between two variables. In the data set, there are seven variables. The objective of the correlation test is to extract the association that possibly exists between any two variables. Therefore, altogether there are 21 possible associations as bivariate sets for investigation. The other requirement for the correlation test is to assess the distribution of data. Assessments such as Pearson r assume a normal distribution in the data set. In the data set, the data do not have a normal distribution. Because they exist as a list with respect to various variables, they are evenly distributed. The Spearman rank correlation test does not have any assumptions about the distribution of data. This test is appropriate for this case. The last requirement is about the characteristics of

the variables. The variables should be measured on a scale that is at least ordinal. Because the data here exist as lists of participants, transformation is needed to fulfill the requirement on the characteristics of variables.

On the basis of the lists in Table 5.11, a numeric value on ranking is assigned to each position along the list. These values are a monotonic increasing sequence from 1 and to 11. The number is associated with the participant ID with respect to each variable, as illustrated in Table 5.12. Then, the sequences are sorted according to the participant ID. The data can then be organized to observe the result from each variable according to each individual participant. For example, regarding participant S01, the set of data associated is (5, 4, 5, 4, 4, 8, 7) with respect to variables (mean of $H_q$, range of $H_q$, mean of $t_q$, mean of $h_q$, width of $h_q$, mean of $D_q$, height of $D_q$). After this transformation of the participant sequence, the variables are now numeric on a scale measurement. This fulfills the requirement for the correlation test.

Table 5.11. Rank associated with the participant sequence with respect to each multifractal parameter.

| **Mean of $H_q$** | **Range of $H_q$** | **Mean of $t_q$** | **Mean of $h_q$** | **Width of $h_q$** | **Mean of $D_q$** | **Height of $D_q$** |
|---|---|---|---|---|---|---|
| S10 : 1 | S09 : 1 | S10 : 1 | S10 : 1 | S09 : 1 | S10 : 1 | S02 : 1 |
| S07 : 2 | S02 : 2 | S08 : 2 | S07 : 2 | S02 : 2 | S03 : 2 | S04 : 2 |
| S11 : 3 | S04 : 3 | S05 : 3 | S05 : 3 | S04 : 3 | S08 : 3 | S06 : 3 |
| S05 : 4 | S01 : 4 | S07 : 4 | S01 : 4 | S01 : 4 | S06 : 4 | S05 : 4 |
| S01 : 5 | S11 : 5 | S01 : 5 | S11 : 5 | S11 : 5 | S07 : 5 | S03 : 5 |
| S09 : 6 | S06 : 6 | S04 : 6 | S09 : 6 | S06 : 6 | S05 : 6 | S08 : 6 |
| S02 : 7 | S03 : 7 | S06 : 7 | S06 : 7 | S07 : 7 | S11 : 7 | S01 : 7 |

| | | | | | | |
|---|---|---|---|---|---|---|
| S04 : 8 | S07 : 8 | S03 : 8 | S02 : 8 | S03 : 8 | S01 : 8 | S09 : 8 |
| S06 : 9 | S05 : 9 | S11 : 9 | S04 : 9 | S05 : 9 | S04 : 9 | S10 : 9 |
| S03 : 10 | S08 : 10 | S02 : 10 | S03 : 10 | S08 : 10 | S09 : 10 | S11 : 10 |
| S08 : 11 | S10 : 11 | S09 : 11 | S08 : 11 | S10 : 11 | S02 : 11 | S07 : 11 |

Table 5.12. Sorted sequence according to participant ID.

| **Mean of $H_q$** | **Range of $H_q$** | **Mean of $t_q$** | **Mean of $h_q$** | **Width of $h_q$** | **Mean of $D_q$** | **Height of $D_q$** |
|---|---|---|---|---|---|---|
| S01 : 5 | S01 : 4 | S01 : 5 | S01 : 4 | S01 : 4 | S01 : 8 | S01 : 7 |
| S02 : 7 | S02 : 2 | S02 : 10 | S02 : 8 | S02 : 2 | S02 : 11 | S02 : 1 |
| S03 : 10 | S03 : 7 | S03 : 8 | S03 : 10 | S03 : 8 | S03 : 2 | S03 : 5 |
| S04 : 8 | S04 : 3 | S04 : 6 | S04 : 9 | S04 : 3 | S04 : 9 | S04 : 2 |
| S05 : 4 | S05 : 9 | S05 : 3 | S05 : 3 | S05 : 9 | S05 : 6 | S05 : 4 |
| S06 : 9 | S06 : 6 | S06 : 7 | S06 : 7 | S06 : 6 | S06 : 4 | S06 : 3 |
| S07 : 2 | S07 : 8 | S07 : 4 | S07 : 2 | S07 : 7 | S07 : 5 | S07 : 11 |
| S08 : 11 | S08 : 10 | S08 : 2 | S08 : 11 | S08 : 10 | S08 : 3 | S08 : 6 |
| S09 : 6 | S09 : 1 | S09 : 11 | S09 : 6 | S09 : 1 | S09 : 10 | S09 : 8 |
| S10 : 1 | S10 : 11 | S10 : 1 | S10 : 1 | S10 : 11 | S10 : 1 | S10 : 9 |
| S11 : 3 | S11 : 5 | S11 : 9 | S11 : 5 | S11 : 5 | S11 : 7 | S11 : 10 |

The following formula is used to calculate the Spearman rank correlation:

$$\rho = 1 - \frac{6 \sum_{i=1}^{n} {d_i}^2}{n\,(n^2 - 1)}$$

where ρ is the Spearman rank correlation, $d_i$ is the difference between the ranks of corresponding values $X_i$ and $Y_i$ , and n is the number of values in each data set. $d_i$ can further be defined as follows:

$$d_i = rank\ (X_i) - rank\ (Y_i)$$

where rank( ) is the function to extract the ranking order of a particular data i from the data set.

The results of the Spearman rank correlation analysis are shown in Table 5.13. The first to consider regarding the correlation results is the direction of the relationship between the variables. It is determined by the sign in front of the correlation coefficient value. A positive correlation between the two variables means that there is a positive relationship between the two; in other words, a high score on one variable is associated with a high score on the other. By contrast, a negative correlation between the two variables (a negative sign in front of the correlation coefficient value) means that there is a negative relationship between the two; in other words, a high score on one variable is associated with a low score on the other. In the data set, there are a few bivariate sets with a positive relationship, namely (mean of $H_q$, mean of $t_q$), (mean of $H_q$, mean of $h_q$), (range of $H_q$, width of $h_q$), (range of $H_q$, height of $D_q$), (mean of $t_q$, mean of $h_q$), (mean of $t_q$, mean of $D_q$), (mean of $h_q$, mean of $D_q$), and (width of $h_q$, height of $D_q$). Regarding the negative relationship set, they are (mean of $H_q$, range of $H_q$), (mean of $H_q$, width of $h_q$), (mean of $H_q$, mean of $D_q$), (mean of $H_q$, height of $D_q$), (range of $H_q$, mean of $t_q$), (range of $H_q$, mean of $h_q$), (range of $H_q$, mean of $D_q$), (mean of $t_q$, width of $h_q$), (mean of $t_q$, height of $D_q$), (mean of $h_q$, width of $h_q$), (mean of $h_q$, height of $D_q$), (width of $h_q$, mean of $D_q$), and (mean of $D_q$, height of $D_q$). Those bivariate sets, namely (mean of $H_q$, mean of $H_q$), (range of $H_q$, range of $H_q$), (mean of $t_q$, mean of $t_q$), (mean of $h_q$, mean of $h_q$), (width of $h_q$, width of $h_q$), (mean of $D_q$, mean of $D_q$),

and (height of $D_q$ , height of $D_q$), have 1.00 correlation values because each variable is wholly correlated.

Table 5.13. Results of the Spearman rank correlation analysis on multifractal parameters.

| | **Mean of $H_q$** | **Range of $H_q$** | **Mean of $t_q$** | **Mean of $h_q$** | **Width of $h_q$** | **Mean of $D_q$** | **Height of $D_q$** |
|---|---|---|---|---|---|---|---|
| **Mean of $H_q$** | 1.00 | -0.18 | 0.24 | 0.95 | -0.11 | -0.02 | -0.64 |
| **Range of $H_q$** | -0.18 | 1.00 | -0.86 | -0.27 | 0.99 | -0.88 | 0.31 |
| **Mean of $t_q$** | 0.24 | -0.86 | 1.00 | 0.35 | -0.82 | 0.64 | -0.21 |
| **Mean of $h_q$** | 0.95 | -0.27 | 0.35 | 1.00 | -0.20 | 0.09 | -0.58 |
| **Width of $h_q$** | -0.11 | 0.99 | -0.82 | -0.20 | 1.00 | -0.91 | 0.25 |
| **Mean of $D_q$** | -0.02 | -0.88 | 0.64 | 0.09 | -0.91 | 1.00 | -0.30 |
| **Height of $D_q$** | -0.64 | 0.31 | -0.21 | -0.58 | 0.25 | -0.30 | 1.00 |

The next consideration regarding the correlation coefficient is the size of values. The size is bounded from -1.00 to 1.00. This indicates the strength on the relationship between the two variables. A correlation of -1.0 indicates a perfect negative correlation. A value of 0.0 indicates no relationship. A perfect positive relationship has a correlation value of 1.0. For the numerical values in between, the interpretation by Cohen [60] suggests the guidelines of having a small correlation when the values are between 0.10 and 0.29, a medium correlation between 0.30

and 0.49, and a large correlation between 0.50 and 1.00. On the basis of this guideline, the respective correlations are shown in Tables 5.14 to 5.17. It can be observed that only two bivariate sets, namely (mean of $H_q$, mean of $D_q$) and (mean of $h_q$, mean of $D_q$), have a minimal correlation value lower than 0.1. For the small correlation relationship, there are seven bivariate sets. Approximately half the total number of bivariate sets within minimal and small correlation groups involves a mean of $H_q$. In the medium correlation group, there are three bivariate sets, in which two involve a height of $D_q$. Altogether among three of the correlation groups, there are 11 out of 21 bivariate sets. In the large correlation relationship group, there are nine bivariate sets. By navigating each row within the table, it can be observed that there are three variables, namely the mean of $H_q$, mean of $h_q$, and height of $D_q$, with two correlated variables. The other four variables, namely range of $H_q$, mean of $t_q$, width of $h_q$, and mean of $D_q$, have two correlated variables. Because these variables are defined as multifractal parameters and valued by the participant sequence of sorted order, as a summary, the sequence of the participant has a considerable relationship between these multifractal parameters. In other words, the participant list in this experimental set has a consistency across various multifractal parameters, and they exhibit a certain variation in a consistent order.

Table 5.14. Minimal correlation results on multifractal parameters.

| | **Mean of $H_q$** | **Range of $H_q$** | **Mean of $t_q$** | **Mean of $h_q$** | **Width of $h_q$** | **Mean of $D_q$** | **Height of $D_q$** |
|---|---|---|---|---|---|---|---|

| | | | | | | | |
|---|---|---|---|---|---|---|---|
| **Mean of $H_q$** | | | | | | 0.02 | |
| **Range of $H_q$** | | | | | | | |
| **Mean of $t_q$** | | | | | | | |
| **Mean of $h_q$** | | | | | | 0.09 | |
| **Width of $h_q$** | | | | | | | |
| **Mean of $D_q$** | 0.02 | | | 0.09 | | | |
| **Height of $D_q$** | | | | | | | |

Table 5.15. Small correlation results on multifractal parameters.

| | **Mean of $H_q$** | **Range of $H_q$** | **Mean of $t_q$** | **Mean of $h_q$** | **Width of $h_q$** | **Mean of $D_q$** | **Height of $D_q$** |
|---|---|---|---|---|---|---|---|
| **Mean of $H_q$** | | 0.18 | 0.24 | | 0.11 | | |
| **Range of $H_q$** | 0.18 | | | 0.27 | | | |
| **Mean of $t_q$** | 0.24 | | | | | | 0.21 |
| **Mean of $h_q$** | | 0.27 | | | 0.20 | | |
| **Width of $h_q$** | 0.11 | | | 0.20 | | | 0.25 |
| **Mean of $D_q$** | | | | | | | |
| **Height of $D_q$** | | | 0.21 | | 0.25 | | |

Table 5.16. Medium correlation results on multifractal parameters.

| | Mean of $H_q$ | Range of $H_q$ | Mean of $t_q$ | Mean of $h_q$ | Width of $h_q$ | Mean of $D_q$ | Height of $D_q$ |
|---|---|---|---|---|---|---|---|
| **Mean of $H_q$** | | | | | | | |
| **Range of $H_q$** | | | | | | | 0.31 |
| **Mean of $t_q$** | | | | 0.35 | | | |
| **Mean of $h_q$** | | | 0.35 | | | | |
| **Width of $h_q$** | | | | | | | |
| **Mean of $D_q$** | | | | | | | 0.30 |
| **Height of $D_q$** | | 0.31 | | | | 0.30 | |

Table 5.17. Large correlation results on multifractal parameters.

| | Mean of $H_q$ | Range of $H_q$ | Mean of $t_q$ | Mean of $h_q$ | Width of $h_q$ | Mean of $D_q$ | Height of $D_q$ |
|---|---|---|---|---|---|---|---|
| **Mean of $H_q$** | 1.00 | | | 0.95 | | | 0.64 |
| **Range of $H_q$** | | 1.00 | 0.86 | | 0.99 | 0.88 | |
| **Mean of $t_q$** | | 0.86 | 1.00 | | 0.82 | 0.64 | |
| **Mean of $h_q$** | 0.95 | | | 1.00 | | | 0.58 |
| **Width of $h_q$** | | 0.99 | 0.82 | | 1.00 | 0.91 | |
| **Mean of $D_q$** | | 0.88 | 0.64 | | 0.91 | 1.00 | |
| **Height of $D_q$** | 0.64 | | | 0.58 | | | 1.00 |

Given the values of correlation, the coefficient of determination can be calculated. That is the indicator of how much variance the two variables share. The computation is simply a square on the correlation value and then converts it to a percentage of variance. For example, a correlation value of 0.2 has a 4% variance. In that case, there is no substantial overlapping between the two variables. A correlation of 0.5 has a 25% shared variance. Table 5.18 shows the percentage of variance in the variable set. Except those with a considerably small variance, each of the variables has a consistently shared variance related to two to three other variables. The percentages have a considerable amount of variance explained. In other words, the sorted order of the participant list has a considerable amount of shared characteristics. Hence, the experimental set and the participants group both have the profile of common characteristics and distinguished variation. An assumption in the data set here is that it is based on the experimental participant group. Hence, the percentages of variance may vary from experiment to experiment.

Table 5.18. Percentage of variance on multifractal parameters.

| | **Mean of $H_q$** | **Range of $H_q$** | **Mean of $t_q$** | **Mean of $h_q$** | **Width of $h_q$** | **Mean of $D_q$** | **Height of $D_q$** |
|---|---|---|---|---|---|---|---|
| **Mean of $H_q$** | 100% | 3% | 6% | 89% | 1% | 0% | 40% |
| **Range of $H_q$** | 3% | 100% | 73% | 7% | 98% | 78% | 10% |
| **Mean of $t_q$** | 6% | 73% | 100% | 12% | 67% | 40% | 4% |

| | | | | | | | |
|---|---|---|---|---|---|---|---|
| **Mean of $h_q$** | 89% | 7% | 12% | 100% | 4% | 1% | 34% |
| **Width of $h_q$** | 1% | 98% | 67% | 4% | 100% | 83% | 6% |
| **Mean of $D_q$** | 0% | 78% | 40% | 1% | 83% | 100% | 9% |
| **Height of $D_q$** | 40% | 10% | 4% | 34% | 6% | 9% | 100% |

The significance level must also be considered. The level of statistical significance indicates the confidence of the results obtained. Although the significance is strongly influenced by the size of the sample, a common practice is to consider $p < 0.05$ as reaching statistical significance. Table 5.19 shows the significance level of the variable set. Combining the table of variance and the significance (Table 5.20) provides a conclusion on how these variables are confidently correlated to each other. There are four variables, namely range of $H_q$, mean of $t_q$, width of $h_q$, and mean of $D_q$, with a shared variance with three other variables. There is one variable, namely the mean of $H_q$, which has a shared variance with two other variables. Finally, there are two variables, namely the mean of $h_q$ and height of $D_q$, with a shared variance with only one variable. By observing the relationship of the shared variance, it can be found that among the seven variables, there are two clusters of variables with a stronger relationship with each other compared to the other cluster. The two clusters are (mean of $H_q$, mean of $h_q$, height of $D_q$) and (range of $H_q$, mean of $t_q$, width of $h_q$, mean of $D_q$). Moreover, on the basis of the significance level, there is another bivariate set of note. It is (mean of $H_q$, mean of $D_q$). It has a

significance level of 0.96 in terms of correlation. This means the two variables significantly do not have a correlation relationship with each other. Hence, they have the percentage of variance of 0%.

Table 5.19. Significance level on multifractal parameters.

| | **Mean of $H_q$** | **Range of $H_q$** | **Mean of $t_q$** | **Mean of $h_q$** | **Width of $h_q$** | **Mean of $D_q$** | **Height of $D_q$** |
|---|---|---|---|---|---|---|---|
| **Mean of $H_q$** | 0.00 | 0.59 | 0.48 | 0.00 | 0.75 | 0.96 | 0.04 |
| **Range of $H_q$** | 0.59 | 0.00 | 0.00 | 0.42 | 0.00 | 0.00 | 0.36 |
| **Mean of $t_q$** | 0.48 | 0.00 | 0.00 | 0.30 | 0.00 | 0.04 | 0.54 |
| **Mean of $h_q$** | 0.00 | 0.42 | 0.30 | 0.00 | 0.56 | 0.79 | 0.06 |
| **Width of $h_q$** | 0.75 | 0.00 | 0.00 | 0.56 | 0.00 | 0.00 | 0.45 |
| **Mean of $D_q$** | 0.96 | 0.00 | 0.04 | 0.79 | 0.00 | 0.00 | 0.37 |
| **Height of $D_q$** | 0.04 | 0.36 | 0.54 | 0.06 | 0.45 | 0.37 | 0.00 |

Table 5.20. Percentage of variance on multifractal parameters.

| | **Mean of $H_q$** | **Range of $H_q$** | **Mean of $t_q$** | **Mean of $h_q$** | **Width of $h_q$** | **Mean of $D_q$** | **Height of $D_q$** |
|---|---|---|---|---|---|---|---|
| **Mean of $H_q$** | 100% | 3% | 6% | 89% | 1% | 0% | 40% |
| **Range of $H_q$** | 3% | 100% | 73% | 7% | 98% | 78% | 10% |
| **Mean of $t_q$** | 6% | 73% | 100% | 12% | 67% | 40% | 4% |
| **Mean of $h_q$** | 89% | 7% | 12% | 100% | 4% | 1% | 34% |

| | | | | | | | |
|---|---|---|---|---|---|---|---|
| **Width of $h_q$** | 1% | 98% | 67% | 4% | 100% | 83% | 6% |
| **Mean of $D_q$** | 0% | 78% | 40% | 1% | 83% | 100% | 9% |
| **Height of $D_q$** | 40% | 10% | 4% | 34% | 6% | 9% | 100% |

#### 5.3.1.2 Participant Variation on Multifractal Parameters

First, the mean value of $h_q$ can be illustrated in Figure 5.38. This is a plot between s10 and s03. The mean value of $h_q$ is from 1.142 to 1.252. This means there is a 0.11 difference between these two participants, with minimum and maximum values. This range shows the variation in the participant set.

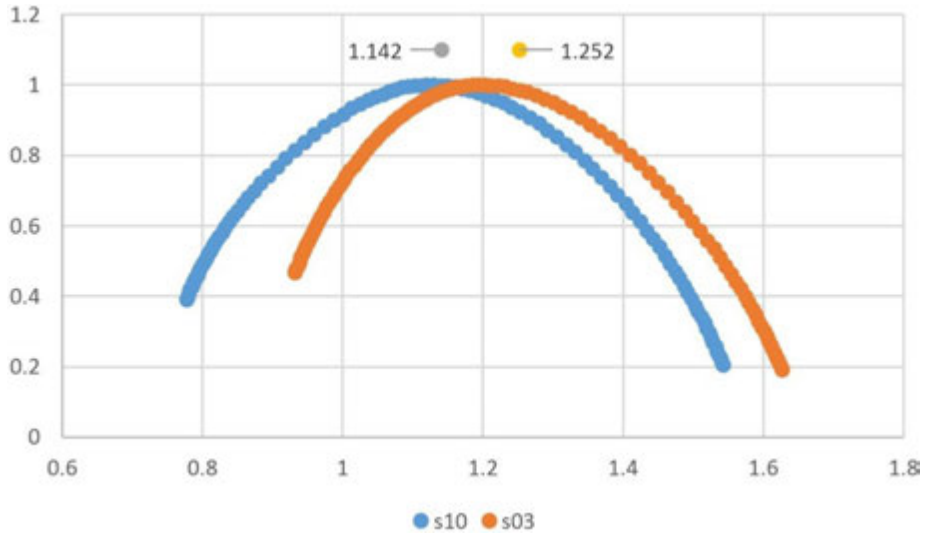


Figure 5.38. Plot of the singularity exponent ($h_q$) against the singularity dimension ($D_q$), illustrating the mean of $h_q$ between participants s10 and s03.

In relation to the mean value of $h_q$ , there is the width of $h_q$ , which is the width of the multifractal spectrum of the participant. The plot is illustrated in Figure 5.39. The value difference between these two participants is 0.622 and 0.708 for participants of minimum and maximum values, respectively. The indicative range of variation in the participant set is 0.085.

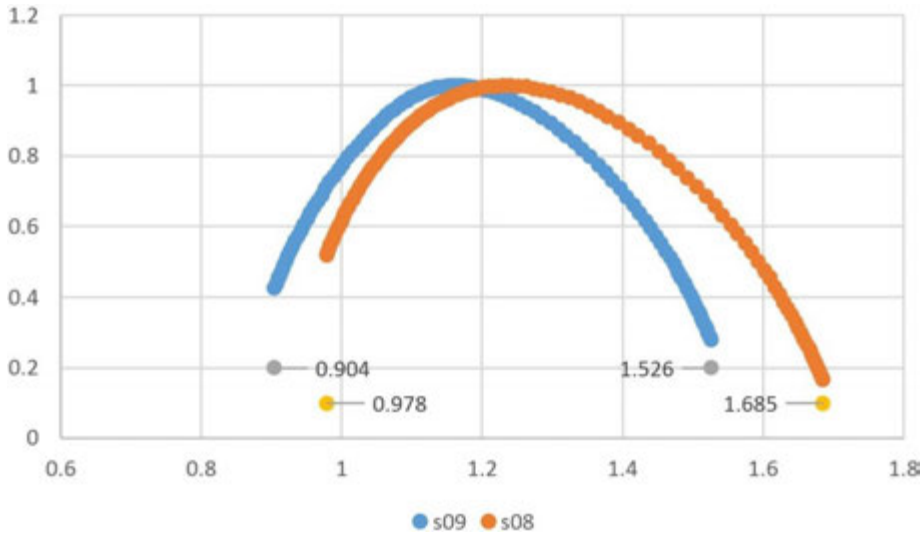


Figure 5.39. Plot of the singularity exponent ($h_q$) against the singularity dimension ($D_q$), illustrating the width of $h_q$ between participants s09 and s08.

The other major multifractal parameter is the mean of $D_q$ . Figure 5.40 shows the difference between the two participants S03 and S02. These two participants contain the minimum and maximum on the mean of $D_q$ . The values are from 0.691 to 0.720, which result in a range of 0.029. Clearly, there is no substantial variation indicated by this parameter for different participants.

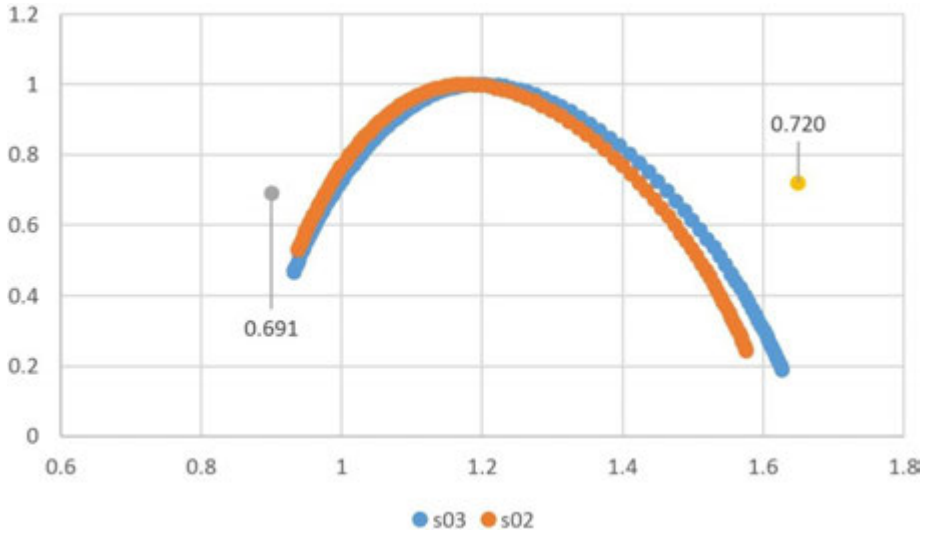


Figure 5.40. Plot of the singularity exponent ($h_q$) against the singularity dimension ($D_q$), illustrating the mean of $D_q$ between participants s03 and s02.

In relation to $D_q$, there is the height of $D_q$, which is the difference between the maximum and minimum of $D_q$. Figure 5.41 illustrates the difference between participants S02 and S07. The resulting values between these two participants are 0.756 and 0.887 for the minimum and maximum height, respectively. This means the range indicating the participant variation is 0.131.

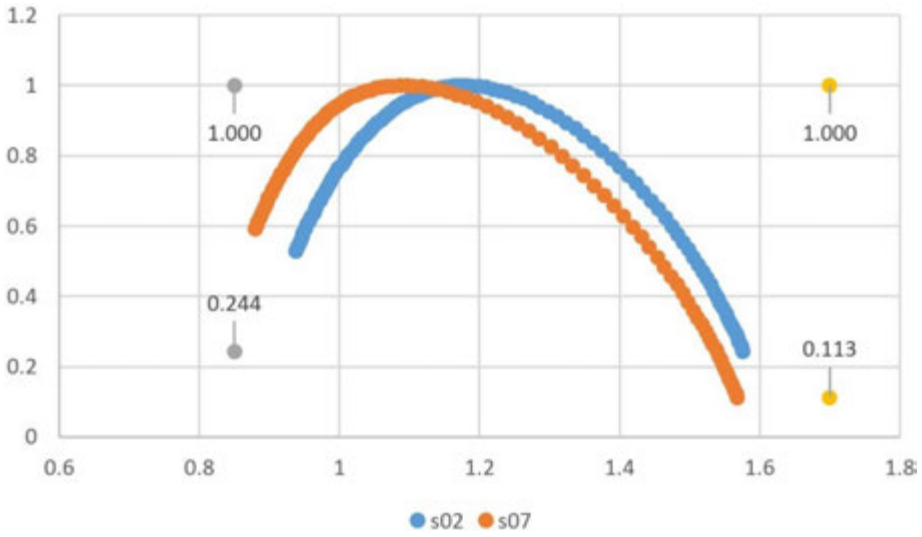


Figure 5.41. Plot of the singularity exponent ($h_q$) against the singularity dimension ($D_q$), illustrating the height of $D_q$ between participants s02 and s07.

In sum, the variation on various multifractal parameters that indicates the difference in the participant set provides the preliminary findings for the subsequent section regarding the correlation between the multifractal parameters of participants and neck pain information. From the variation on the range extracted, the mean of $D_q$ cannot be used as an indicator because it defines the minimum and maximum participant values as too small to observe the variation. By observation, the other three parameters can be used for correlation analysis.

## 5.4. Comparison between Support Groups

In the previous section, the analysis ascertains that a multifractality structure exists in the spinal curvature of the cervical section in the experimental set of the upright sitting posture. Furthermore, during the experiment, there were two sitting conditions arranged. One required the participants to sit on a seat with low back support; the other condition required them to sit without the support. The two conditions are compared to observe any major difference in terms of the multifractal parameters. Four multifractal parameters are compared, namely the Hurst exponent, mass exponent, singularity exponent, and singularity dimension. In addition, the plot of the singularity exponent is plotted against the singularity dimension.

First, we have the Hurst exponent ($H_q$) compared. Figure 5.42 shows the comparison of the mean, minimum, and maximum values of the plot with $H_q$ against the q-th order. The plot at the top shows the condition when there is no low back support, whereas the bottom one is the condition of having low back support. Table 5.21 shows the corresponding numerical values.

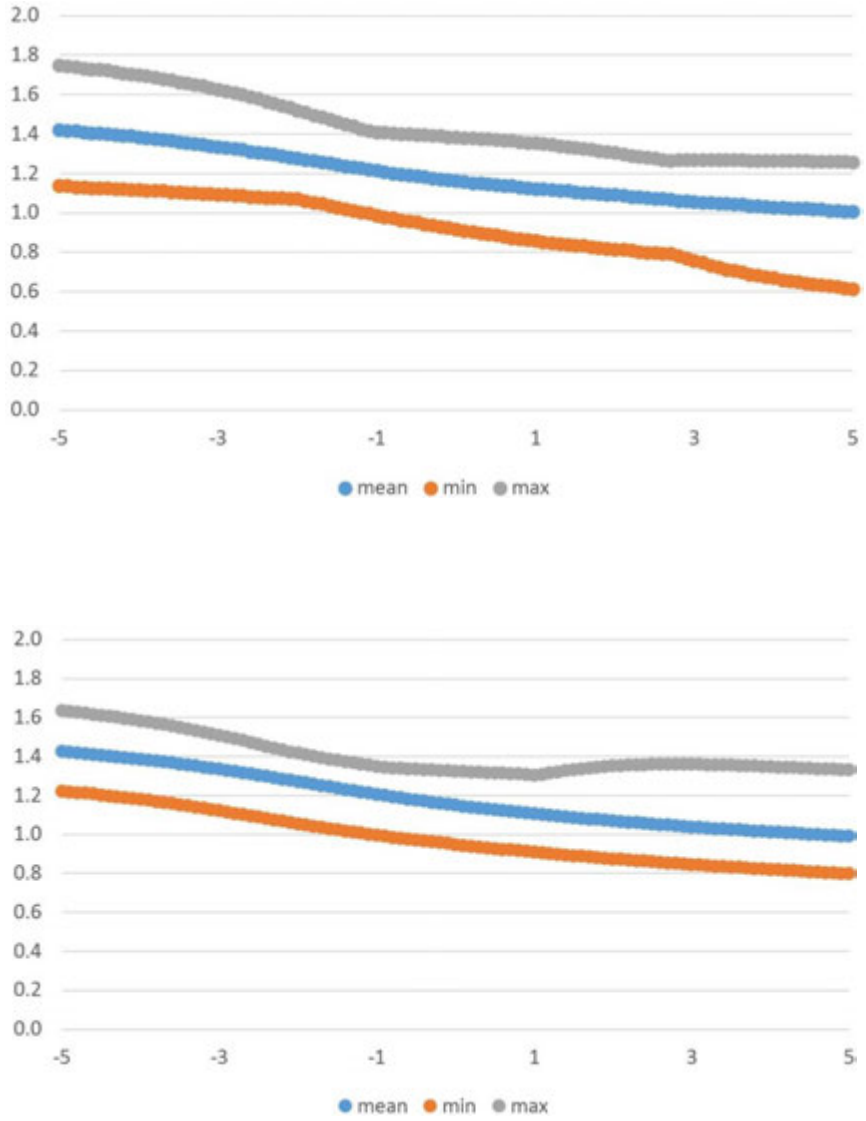


Figure 5.42. Plot of the Hurst exponent ($H_q$) against the q-th order according to the mean, minimum, and maximum of each time series between conditions of without low back support (up) and with low back support (down).

Table 5.21. Numerical values of the Hurst exponent $H_q$ against the q-th order according to the mean, minimum, and maximum of each time series between conditions of without low back support and with low back support.

| **Without low back support** | | | | | |
|---|---|---|---|---|---|
| | **Mean** | **Standard Deviation** | **Minimum** | **Maximum** | **Range** |
| **Mean of $H_q$** | 1.190 | 0.131 | 1.008 | 1.422 | 0.414 |

| | | | | | |
|---|---|---|---|---|---|
| **Minimum of $H_q$** | 0.916 | 0.165 | 0.614 | 1.138 | 0.524 |
| **Maximum of $H_q$** | 1.436 | 0.163 | 1.259 | 1.750 | 0.491 |
| **With low back support** | | | | | |
| | **Mean** | **Standard Deviation** | **Minimum** | **Maximum** | **Range** |
| **Mean of $H_q$** | 1.177 | 0.139 | 0.990 | 1.424 | 0.433 |
| **Minimum of $H_q$** | 0.975 | 0.132 | 0.797 | 1.221 | 0.424 |
| **Maximum of $H_q$** | 1.403 | 0.100 | 1.304 | 1.633 | 0.330 |

The plots show that the mean value curve is more or less the same between the two conditions. The difference involves the minimum and maximum curves. The range of the minimum of $H_q$ is from 0.524 (without low back support) to 0.424 (with low back support). Similarly, the range of the maximum of $H_q$ is from 0.491 to 0.330. Moreover, under the condition of having low back support, the minimum curve has a shift to a higher value compared to without low back support. By contrast, the maximum curve has the maximum value shifting down under the condition of having low back support. These narrow the space between the minimum and maximum curves in the case of having low back support condition. This may imply a more stable spinal curvature condition when there is low back support. In other words, there is a more balanced state with less need to control the motion.

The second parameter to compare is the mass exponent ($t_q$). The plots in Figure 5.43 illustrate the comparison between the condition of having no low back support and having low back support, whereas Table 5.22 shows the corresponding numerical values.

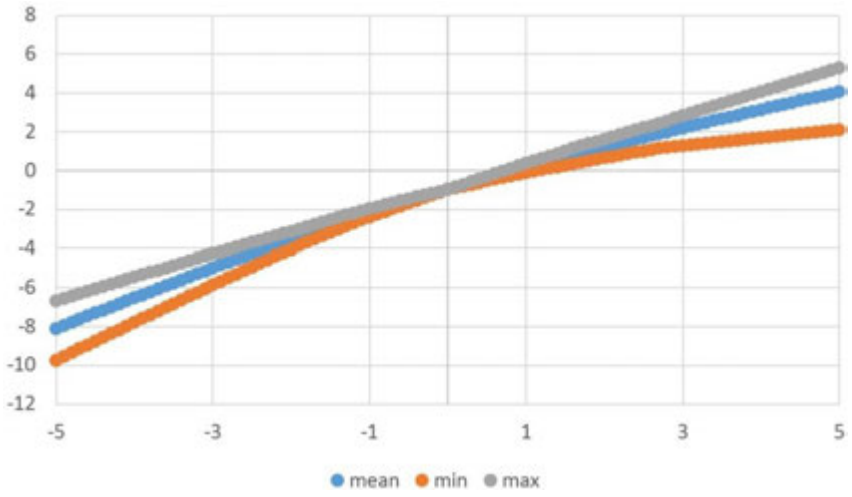


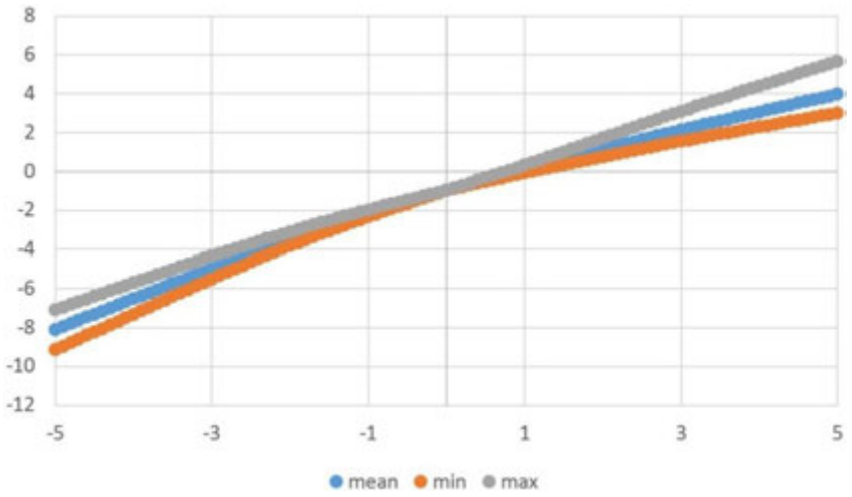


Figure 5.43. Plot of the mass exponent ($t_q$) against the q-th order according to the mean, minimum, and maximum of each time series between the conditions of without low back support (up) and with low back support (down).

Table 5.22. Numerical values of the mass exponent $t_q$ against the q-th order according to the mean, minimum, and maximum of each time series between the conditions of without low back support and with low back support.

| **Without low back support** | | | | | |
|---|---|---|---|---|---|
| | **Mean** | **Standard Deviation** | **Minimum** | **Maximum** | **Range** |
| **Mean of $t_q$** | -1.377 | 3.545 | -8.109 | 4.038 | 12.147 |

| | | | | | |
|---|---|---|---|---|---|
| **Minimum of $t_q$** | -2.162 | 3.575 | -9.751 | 2.071 | 11.822 |
| **Maximum of $t_q$** | -0.768 | 3.490 | -6.689 | 5.296 | 11.984 |
| **With low back support** | | | | | |
| | **Mean** | **Standard Deviation** | **Minimum** | **Maximum** | **Range** |
| **Mean of $t_q$** | -1.398 | 3.516 | -8.119 | 3.952 | 12.071 |
| **Minimum of $t_q$** | -1.872 | 3.552 | -9.167 | 2.985 | 12.152 |
| **Maximum of $t_q$** | -0.739 | 3.673 | -7.107 | 5.649 | 12.756 |

By comparing the curves between the two conditions, it can be found again that the space in between the minimum and maximum is narrower under the condition of having low back support, although the difference in this case is not significant. By contrast, the mean value curve is again similar in both of the conditions.

After the mass exponent, there is the singularity exponent ($h_q$). Figure 5.44 shows the plots of the two conditions and Table 5.23 shows the corresponding numerical values. Again, the main difference is the space between the minimum and maximum curves. It shows that the space is narrower under the condition of having low back support.

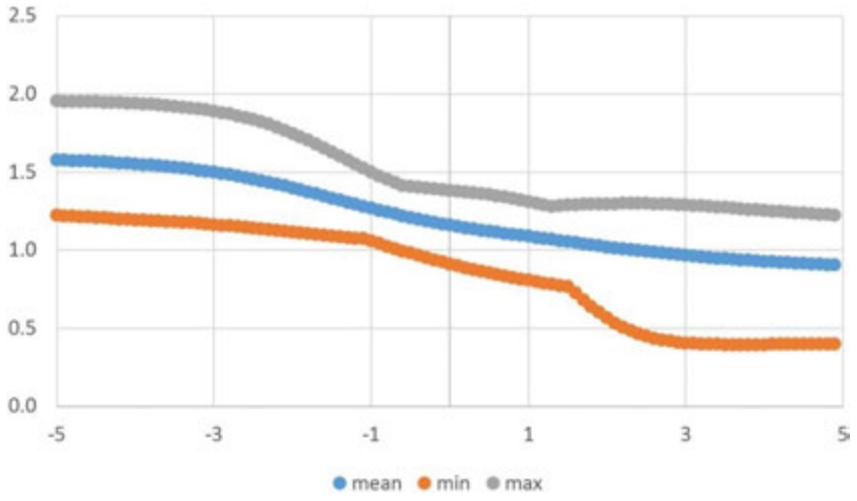

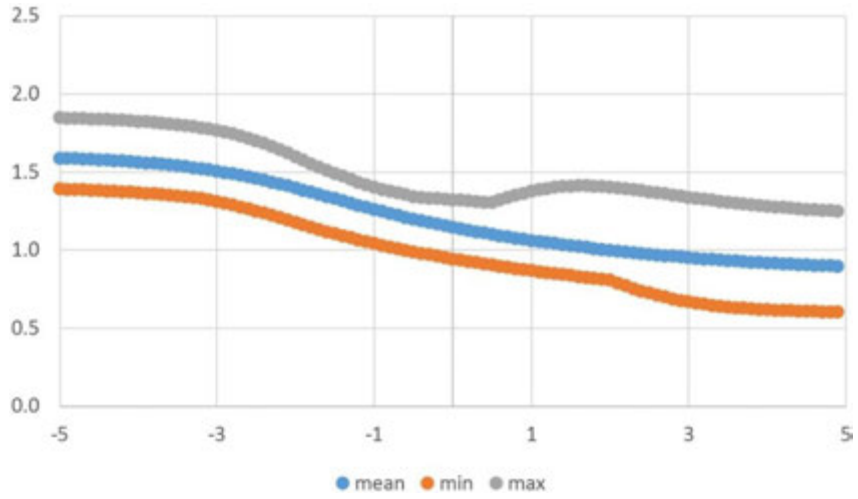


Figure 5.44. of the singularity exponent ($h_q$) against the q-th order according to the mean, minimum, and maximum of each time series between the conditions of without low back support (up) and with low back support (down).

Table 5.23. Numerical values of the singularity exponent $h_q$ against the q-th order according to the mean, minimum, and maximum of each time series between the conditions of without low back support and with low back support.

| **Without low back support** | | | | | |
|---|---|---|---|---|---|
| | **Mean** | **Standard Deviation** | **Minimum** | **Maximum** | **Range** |
| **Mean of $h_q$** | 1.215 | 0.235 | 0.905 | 1.577 | 0.672 |
| **Minimum of $h_q$** | 0.847 | 0.315 | 0.394 | 1.221 | 0.827 |
| **Maximum of $h_q$** | 1.523 | 0.274 | 1.224 | 1.953 | 0.729 |
| **With low back support** | | | | | |
| | **Mean** | **Standard Deviation** | **Minimum** | **Maximum** | **Range** |
| **Mean of $h_q$** | 1.207 | 0.245 | 0.895 | 1.588 | 0.693 |
| **Minimum of $h_q$** | 0.982 | 0.272 | 0.603 | 1.390 | 0.787 |
| **Maximum of $h_q$** | 1.488 | 0.207 | 1.249 | 1.847 | 0.597 |

The singularity dimension ($D_q$) is then computed to compare the results from the two conditions. Figure 5.45 illustrates the plots and Table 5.24 shows the numerical values. By comparing the two plots, there is a downward shift on the plots toward the -5-th order from without low back support to with low back support. At the other side toward the 5-th order, the maximum and mean curves are approximately the same in both conditions, whereas the minimum curve has an upward shift in the low back support condition. This makes the space toward this side narrower. The unsymmetrical changes toward the two sides of the q-th order can be a basis for the meaning of the positive and negative of the q-th order. The negative side of the q-th order denotes the sensitivity to local fluctuations with small magnitudes. By contrast, the positive side of the q-th order is sensitive to local fluctuations with large magnitudes.

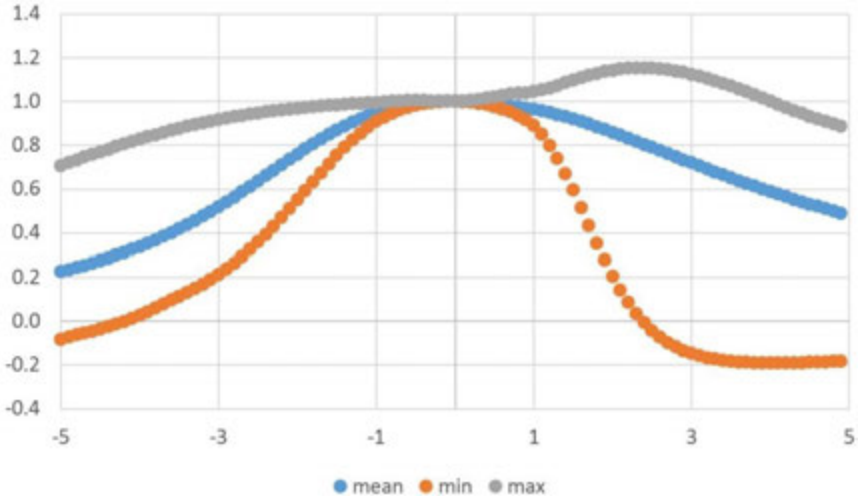

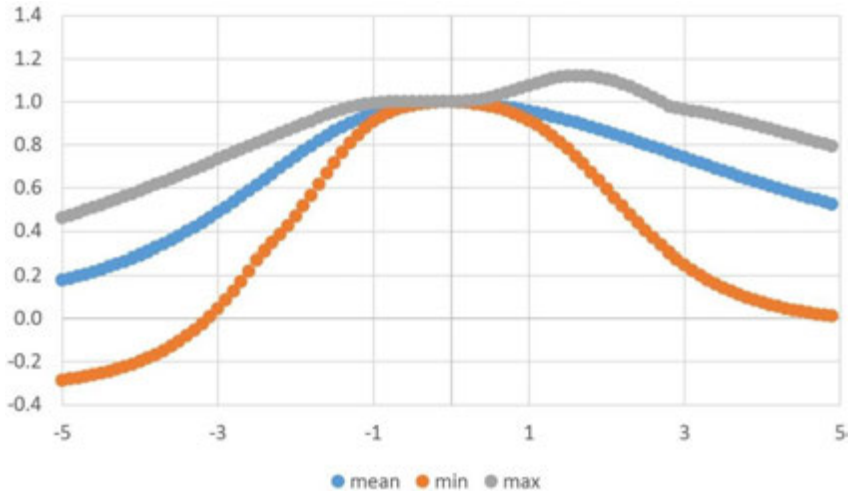


Figure 5.45. Plot of the singularity dimension ($D_q$) against the q-th order according to the mean, minimum, and maximum of each time series between the conditions of without low back support (up) and with low back support (down).

Table 5.24. Numerical values of the singularity dimension $D_q$ against the q-th order according to the mean, minimum, and maximum of each time series between the conditions of without low back support and with low back support.

| **Without low back support** | | | | | |
|---|---|---|---|---|---|
| | **Mean** | **Standard Deviation** | **Minimum** | **Maximum** | **Range** |
| **Mean of $D_q$** | 0.704 | 0.238 | 0.225 | 1.000 | 0.775 |
| **Minimum of $D_q$** | 0.333 | 0.444 | -0.191 | 1.000 | 1.191 |
| **Maximum of $D_q$** | 0.983 | 0.110 | 0.707 | 1.153 | 0.446 |
| **With low back support** | | | | | |
| | **Mean** | **Standard Deviation** | **Minimum** | **Maximum** | **Range** |
| **Mean of $D_q$** | 0.699 | 0.250 | 0.177 | 1.000 | 0.823 |
| **Minimum of $D_q$** | 0.392 | 0.432 | -0.286 | 1.000 | 1.286 |
| **Maximum of $D_q$** | 0.885 | 0.180 | 0.463 | 1.121 | 0.658 |

Figure 5.46 plots the singularity dimension ($D_q$) against the singularity exponent ($h_q$) of the two low back support conditions and Table 5.25 shows the mean and

standard deviation of selected multifractal parameters corresponding to the two conditions. From both the plots and table, there is not much difference between the two conditions.

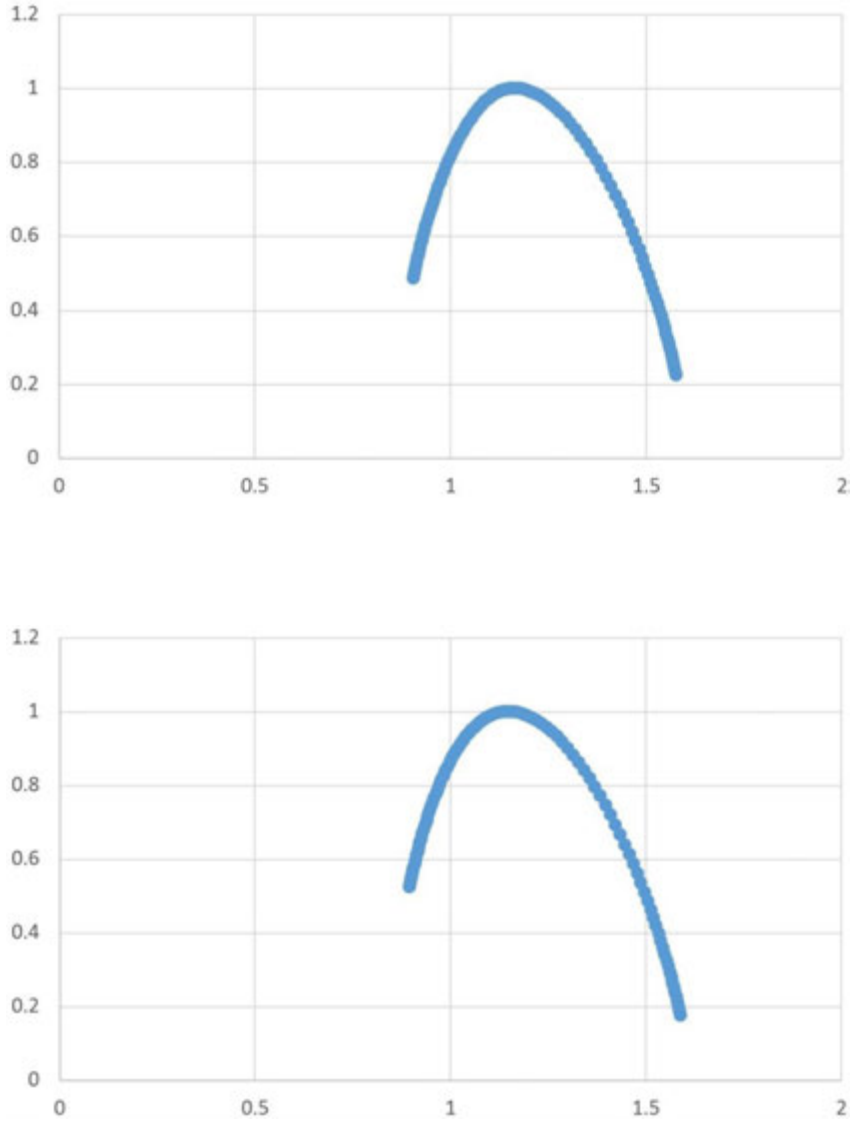


Figure 5.46. Plot of the singularity dimension ($D_q$) against the singularity exponent ($h_q$) according to the mean, minimum, and maximum of each time series between the conditions of without low back support (up) and with low back support (down).

Table 5.25. Selected multifractal parameters under the two support conditions.

| | Without low back support | | With low back support | |
|---|---|---|---|---|
| | **Mean** | **Standard Deviation** | **Mean** | **Standard Deviation** |
| **Mean of $h_q$** | 1.215 | 0.102 | 1.207 | 0.074 |
| **Width of $h_q$** | 0.673 | 0.141 | 0.693 | 0.132 |
| **Mean of $D_q$** | 0.704 | 0.067 | 0.699 | 0.055 |
| **Height of $D_q$** | 0.824 | 0.138 | 0.834 | 0.143 |

## 5.5. Comparison between Vertices

In this section, the data series are prepared by grouping together respective vertices to investigate the consistency. For each participant, each data series is computed for the mean value. The mean values are then averaged for different trials on the basis of the same condition. There are two conditions considered here. One is whether there is low back support. The other condition is the vertex of focus; here, there are four vertices to be considered, namely M3, M4, M5, and M6. Altogether, the four multifractal parameters are again computed, namely the Hurst exponent, mass exponent, singularity exponent, and singularity dimension. The mean and range values are considered for comparison.

The Hurst exponent ($H_q$) is considered here. There are three plots prepared for comparison. The first one is the overall condition, including both with and without low back support. The second one is the condition with low back support. The last one is that without support. Figure 5.47 illustrates the plots of the three conditions

on the basis of the M3, M4, M5, and M6 vertices. On the left-hand side are the mean values of $h_q$ as a summary of all participants, whereas on the right-hand side are the range values. From the mean value plots, it can be seen that M5 and M6 in general have higher values than M3 and M4. The values between M5 and M6 are approximately the same. Regarding the range values of $H_q$, M5 and M6 also describe a similar value relationship. Investigating further into the details of the numerical values, a statistical summary is provided in Table 5.26 and 5.27 for the mean and range values, respectively. The tables show the percentages on the changes of numerical values when comparing between vertices. The change is either increase or decrease comparing one vertex to another.

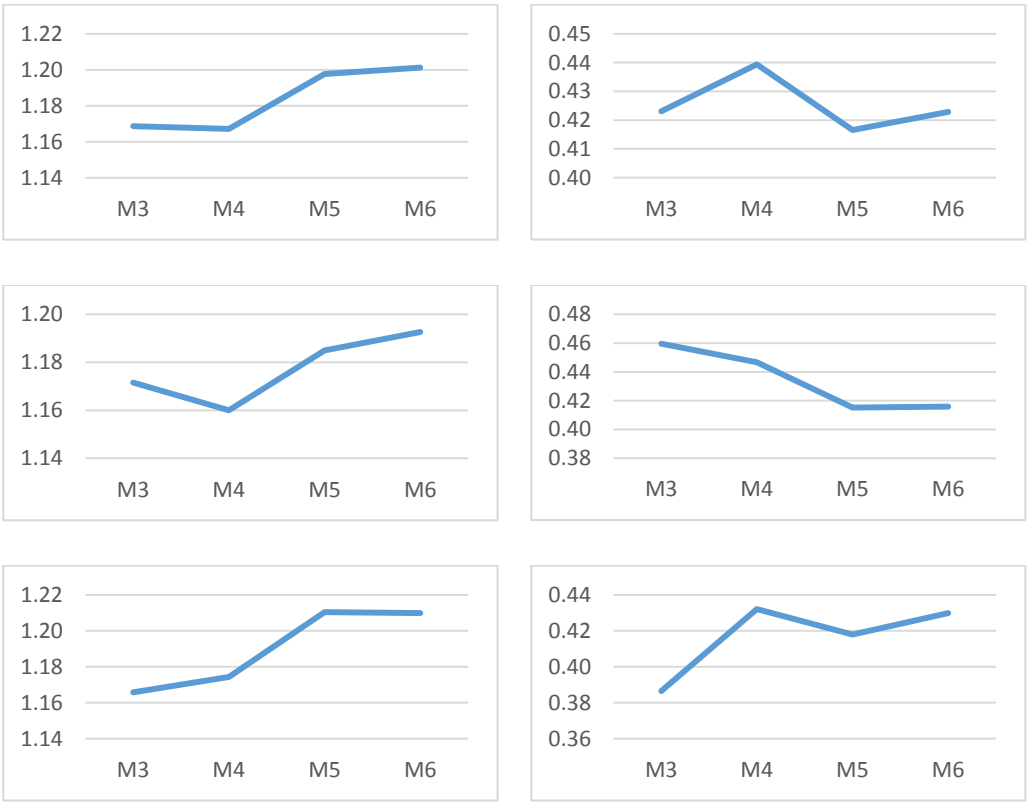

Figure 5.47. Comparison on the mean (left) and range (right) of Hq on the basis of vertices under the following conditions: (i) with and without low back support (top); (ii) with low back support (middle); (iii) without low back support (bottom).

Table 5.26. Statistical summary on the percentages indicating the change between individual vertices regarding the mean values of $H_q$ .

| | | **M3 > M4** | **M3 > M5** | **M3 > M6** | **M4 > M5** | **M4 > M6** | **M5 > M6** |
|---|---|---|---|---|---|---|---|
| **Overall** | **Increase** | 45% | 36% | 36% | 68% | 59% | 59% |
| | **Decrease** | 55% | 64% | 64% | 32% | 41% | 41% |
| **With Support** | **Increase** | 36% | 45% | 45% | 64% | 64% | 45% |
| | **Decrease** | 64% | 55% | 55% | 36% | 36% | 55% |
| **Without Support** | **Increase** | 55% | 27% | 27% | 73% | 55% | 73% |
| | **Decrease** | 45% | 73% | 73% | 27% | 45% | 27% |

Table 5.27. Statistical summary on the percentages indicating the change between individual vertices regarding the range values of $H_q$ .

| | | **M3 > M4** | **M3 > M5** | **M3 > M6** | **M4 > M5** | **M4 > M6** | **M5 > M6** |
|---|---|---|---|---|---|---|---|
| **Overall** | **Increase** | 59% | 59% | 50% | 45% | 50% | 64% |
| | **Decrease** | 41% | 41% | 50% | 55% | 50% | 36% |
| **With Support** | **Increase** | 45% | 73% | 73% | 45% | 45% | 64% |
| | **Decrease** | 55% | 27% | 27% | 55% | 55% | 36% |
| **Without Support** | **Increase** | 73% | 45% | 27% | 45% | 55% | 64% |
| | **Decrease** | 27% | 55% | 73% | 55% | 45% | 36% |

The mass exponent ($t_q$) is computed. Similarly, the plots on the mean and range values are illustrated in Figure 5.48 on the left- and right-hand sides, respectively. The two plots on the top illustrate the overall condition. Those in the middle illustrate the condition with low back support. The two plots at the bottom show the one without support. From the mean value plots, the values between M5 and

M6 are approximately the same. M4 are, in general, lower than M5 and M6. Regarding the range plots, there is an upward trend across M4, M5, and M6. At the other end, M3 and M4 are more or less the same in values. As a further reference to the relationship, Tables 5.28 and 5.29 show the statistical percentages when comparing the individual values among any two of the vertices regarding the mean and range values, respectively. The statistics are based on changes, either increase or decrease, when comparing one vertex to another.

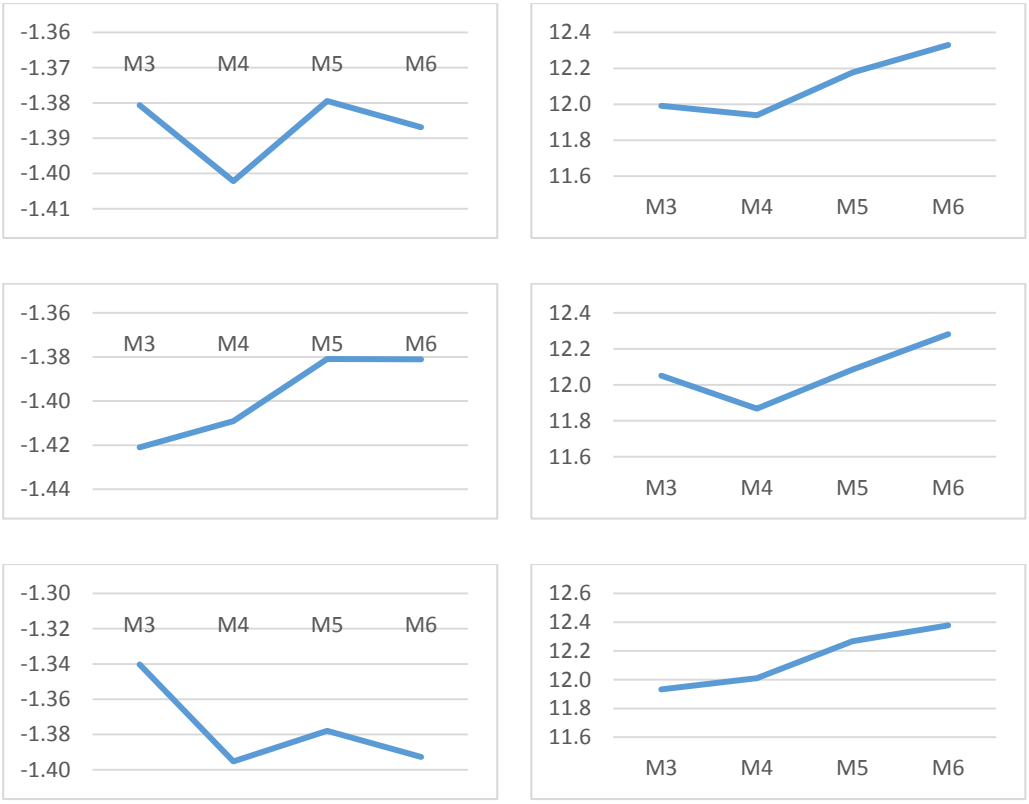


Figure 5.48. Comparison on the mean (left) and range (right) of $t_q$ on the basis of vertices under the following conditions: (i) with and without low back support (top); (ii) with low back support (middle); (iii) without low back support (bottom).

Table 5.28. Statistical summary on the percentages indicating the change between individual vertices regarding the mean values of $t_q$ .

| | | M3 > M4 | M3 > M5 | M3 > M6 | M4 > M5 | M4 > M6 | M5 > M6 |
|---|---|---|---|---|---|---|---|
| **Overall** | **Increase** | 41% | 41% | 50% | 55% | 55% | 41% |
| | **Decrease** | 59% | 59% | 50% | 45% | 45% | 59% |
| **With Support** | **Increase** | 55% | 27% | 36% | 55% | 55% | 36% |
| | **Decrease** | 45% | 73% | 64% | 45% | 45% | 64% |
| **Without Support** | **Increase** | 27% | 55% | 64% | 55% | 55% | 45% |
| | **Decrease** | 73% | 45% | 36% | 45% | 45% | 55% |

Table 5.29. Statistical summary on the percentages indicating the change between individual vertices regarding the range values of $t_q$ .

| | | M3 > M4 | M3 > M5 | M3 > M6 | M4 > M5 | M4 > M6 | M5 > M6 |
|---|---|---|---|---|---|---|---|
| **Overall** | **Increase** | 45% | 41% | 41% | 55% | 64% | 64% |
| | **Decrease** | 55% | 59% | 59% | 45% | 36% | 36% |
| **With Support** | **Increase** | 36% | 55% | 55% | 55% | 73% | 55% |
| | **Decrease** | 64% | 45% | 45% | 45% | 27% | 45% |
| **Without Support** | **Increase** | 55% | 27% | 27% | 55% | 55% | 73% |
| | **Decrease** | 45% | 73% | 73% | 45% | 45% | 27% |

The singularity exponent ($h_q$) is then computed. Figure 5.49 illustrates the means (left) and ranges (right) across the vertices of the cervical region as a summary on the participant group. Again, the top two plots illustrate the overall condition, the middle ones illustrate the one with low back support, and the bottom two illustrate the condition without low back support. From the mean value plots, there is an upward trend across M4, M5, and M6 vertices, whereas M3 and M4 are approximately the same in values. Regarding the range value plots, M5 and M6 have similar values among all the three conditions. Investigating further into the details in

the numerical values, a statistical summary is provided in Tables 5.30 and 5.31 for the mean and range values, respectively. The tables show the percentages on the changes of numerical values when comparing between vertices. The change is either increase or decrease comparing one vertex to another.

So far, among the parameters $H_q$ , $t_q$ , and $h_q$ , there is a hint that the vertices of M5 and M6 are consistent across different conditions, both in the mean values and the ranges, whereas M3 and M4 have a similar relationship in some of the plots. Between the groups M3–M4 and M5–M6, there is a jump, either upward or downward, in some plots. The other type of relationship that can be found is a general trend across vertices. These relationships can be further ascertained by investigating the remaining multifractal parameters.

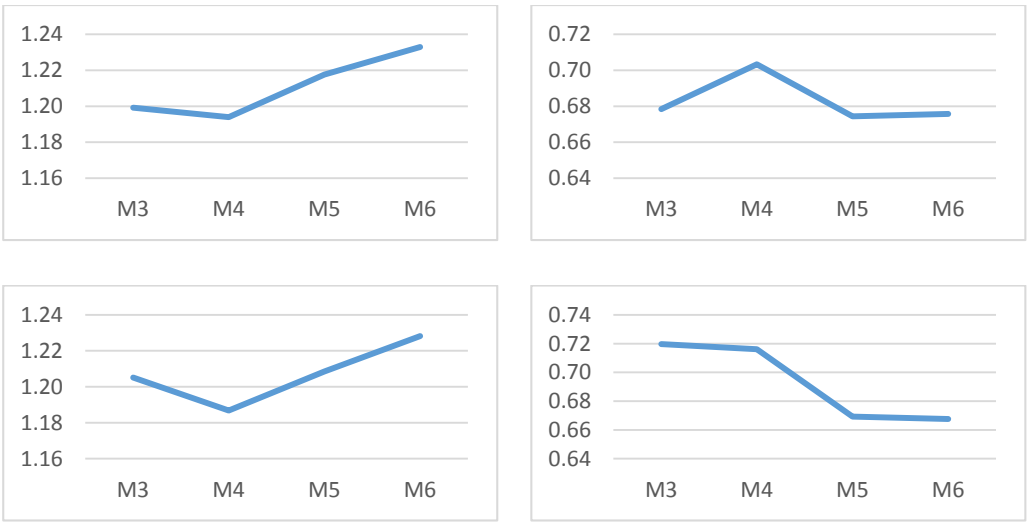

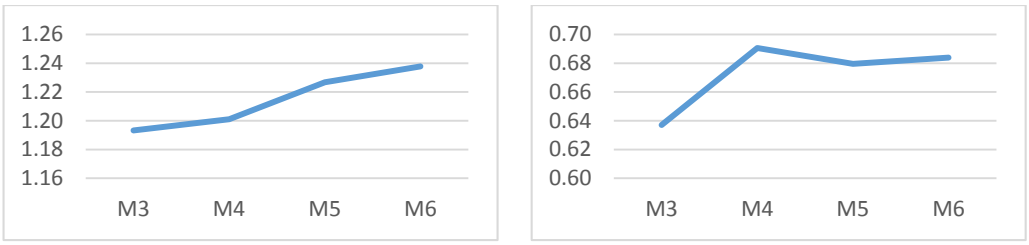


Figure 5.49. Comparison on the mean (left) and range (right) of $h_q$ on the basis of vertices under the following conditions: (i) with and without low back support (top); (ii) with low back support (middle); (iii) without low back support (bottom).

Table 5.30. Statistical summary on the percentages indicating the change between individual vertices regarding the mean values of $h_q$ .

| | | **M3 > M4** | **M3 > M5** | **M3 > M6** | **M4 > M5** | **M4 > M6** | **M5 > M6** |
|---|---|---|---|---|---|---|---|
| **Overall** | **Increase** | 45% | 41% | 41% | 55% | 64% | 64% |
| | **Decrease** | 55% | 59% | 59% | 45% | 36% | 36% |
| **With Support** | **Increase** | 36% | 55% | 55% | 55% | 73% | 55% |
| | **Decrease** | 64% | 45% | 45% | 45% | 27% | 45% |
| **Without Support** | **Increase** | 55% | 27% | 27% | 55% | 55% | 73% |
| | **Decrease** | 45% | 73% | 73% | 45% | 45% | 27% |

Table 5.31. Statistical summary on the percentages indicating the change between individual vertices regarding the range values of $h_q$ .

| | | **M3 > M4** | **M3 > M5** | **M3 > M6** | **M4 > M5** | **M4 > M6** | **M5 > M6** |
|---|---|---|---|---|---|---|---|
| **Overall** | **Increase** | 64% | 59% | 45% | 41% | 50% | 59% |
| | **Decrease** | 36% | 41% | 55% | 59% | 50% | 41% |
| **With Support** | **Increase** | 55% | 73% | 64% | 36% | 45% | 55% |
| | **Decrease** | 45% | 27% | 36% | 64% | 55% | 45% |
| **Without Support** | **Increase** | 73% | 45% | 27% | 45% | 55% | 64% |
| | **Decrease** | 27% | 55% | 73% | 55% | 45% | 36% |

Subsequently, we have the multifractal parameter on the singularity dimension ($D_q$). Figure 5.50 illustrates the plots at different conditions. The plots on the left-hand side are the mean values, whereas the right ones are the ranges. Three conditions are again illustrated in the top, middle, and bottom for the combination of both with and without low back support, with low back support, and without low back support, respectively. It can be observed that M5 and M6 are approximately the same in mean values. M3 and M4 are approximately the same in range values. There is a general increase in values in the mean value plots from M4 to M5 and M6. Regarding the range value plots, M5 features a valley among M3, M4, and M6 in all the conditions. As a further reference to the relationship, Tables 5.32 and 5.33 show the statistical percentages when comparing the individual values among any two of the vertices regarding the mean and range values, respectively. The statistics are based on changes, either increase or decrease, when comparing one vertex to another.

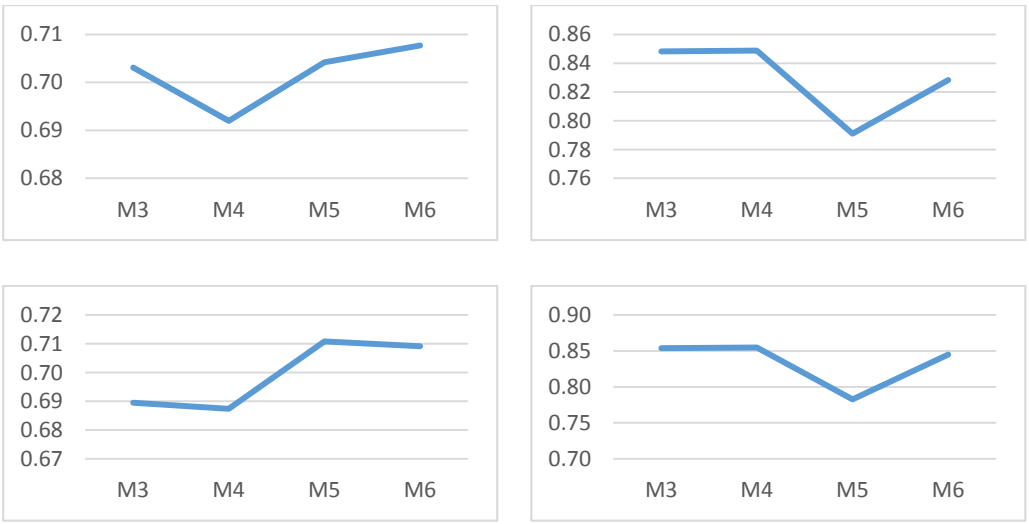

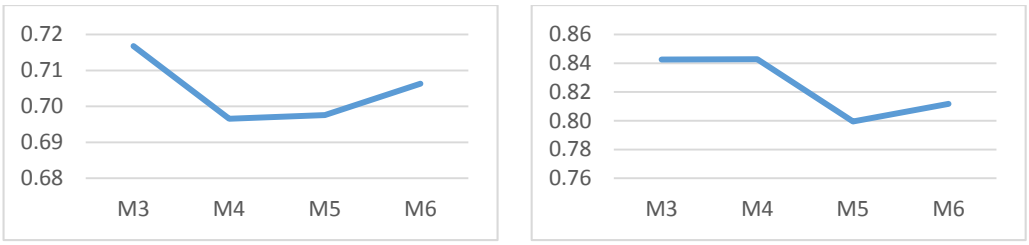


Figure 5.50. Comparison on the mean (left) and range (right) of $D_q$ on the basis of vertices under the following conditions: (i) with and without low back support (top); (ii) with low back support (middle); (iii) without low back support (bottom).

Table 5.32. Statistical summary on the percentages indicating the change between individual vertices regarding the mean values of $D_q$ .

| | | **M3 > M4** | **M3 > M5** | **M3 > M6** | **M4 > M5** | **M4 > M6** | **M5 > M6** |
|---|---|---|---|---|---|---|---|
| **Overall** | **Increase** | 32% | 45% | 59% | 59% | 59% | 41% |
| | **Decrease** | 68% | 55% | 41% | 41% | 41% | 59% |
| **With Support** | **Increase** | 36% | 36% | 45% | 64% | 64% | 45% |
| | **Decrease** | 64% | 64% | 55% | 36% | 36% | 55% |
| **Without Support** | **Increase** | 27% | 55% | 73% | 55% | 55% | 36% |
| | **Decrease** | 73% | 45% | 27% | 45% | 45% | 64% |

Table 5.33. Statistical summary on the percentages indicating the change between individual vertices regarding the range values of $D_q$ .

| | | **M3 > M4** | **M3 > M5** | **M3 > M6** | **M4 > M5** | **M4 > M6** | **M5 > M6** |
|---|---|---|---|---|---|---|---|
| **Overall** | **Increase** | 45% | 68% | 68% | 36% | 45% | 59% |
| | **Decrease** | 55% | 32% | 32% | 64% | 55% | 41% |
| **With Support** | **Increase** | 55% | 73% | 64% | 27% | 55% | 64% |
| | **Decrease** | 45% | 27% | 36% | 73% | 45% | 36% |
| **Without Support** | **Increase** | 36% | 64% | 73% | 45% | 36% | 55% |
| | **Decrease** | 64% | 36% | 27% | 55% | 64% | 45% |

To illustrate the findings when comparing the fractal parameters under different mean and range values, Table 5.34 shows a summary of the relationship between different cervical section vertices. As a general observation, M3 and M4 can be seen as a group of the movement behaviour, whereas M5 and M6 is another group. This may imply that the motor control mechanism has a difference between the upper and lower regions under various balancing and movement conditions. There are some general trends in selected parameters when considering the vertices across M4, M5, and M6. This may provide a hint on the magnitude of control along the spinal region. If the head is seen as the end point of mass along the cervical region and the body is the base, the movement can be controlled by various vertices along the spine. When the vertex is farther away from the point of mass and nearer to the base, a small fluctuation in movement can initiate a larger movement in angle than those nearer to the point of mass. This could be the reason for having M5 and M6 in a larger magnitude at a large time scale range, compared to M3 and M4, which appear more in a smaller magnitude at a small time scale range. The lower cervical region could be under the mechanism of coarse control, whereas the upper region is for fine control.

Table 5.34. Summary of comparison on fractal parameters among vertices.

| | **M3** | **M4** | **M5** | **M6** |
|---|---|---|---|---|
| **Mean of $H_q$** | Similar values | | Similar values | |
| **Range of $H_q$** | | | Similar values | |

| | | | | |
|---|---|---|---|---|
| **Mean of $t_q$** | | Lower than M5 and M6 | Similar values | |
| **Range of $t_q$** | | Increase upward | | |
| | Similar values | | | |
| **Mean of $h_q$** | | Increase upward | | |
| | Similar values | | | |
| **Range of $h_q$** | | | Similar values | |
| **Mean of $D_q$** | | | Similar values | |
| | | Increase from M4 to M5 and M6 | | |
| **Range of $D_q$** | Similar values | | A valley among M3, M4 and M6 | |

## 5.6. Validation Tests

In this section, a number of tests is described in the experimental set and data series. The aim is to provide evidence that the analysis and its results have the confidence level as a valid research output findings. The first evaluation is based on the shuffled series from the original time series. It is to provide evidence that a multifractality structure exists only in its original data form, and is destroyed after a shuffling process.

### 5.6.1. Evaluation of the Shuffled Series

The multifractality of the time series can be determined by analyzing the randomly shuffled series from the same data set. The process of shuffling places the data into a random order. The aim is to eliminate all correlations. Therefore, the long-range correlations within the multifractal structure disappear and then become nonfractal scaling. By contrast, the time series are said to originate based on the probability density if $H_q$ is approximately the same before and after the shuffle. If the multifractal structure is present in both the original and shuffled time series, the multifractality appears weaker in the shuffled series [58].

After the shuffling process, the random walk plot is from the scale of the absolute maximum value of approximately 2000 (Figure 5.51) to approximately 150 (Figure 5.52).

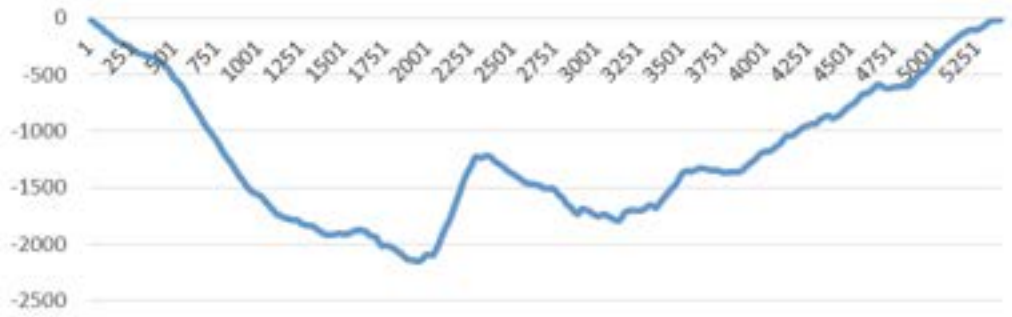


Figure 5.51. Random walk plot of the original time series.

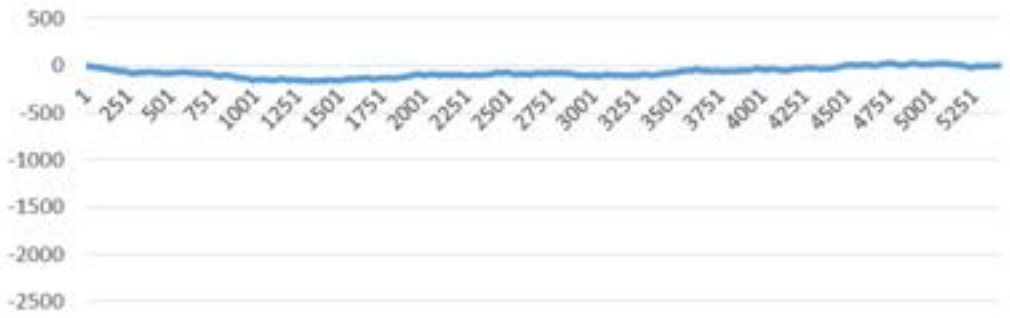


Figure 5.52. Random walk plot of the shuffled time series.

To discover the multifractality of the time series, the original and shuffled time series are compared and analyzed. The variation of the values of $H_q$ vs. q, $t_q$ vs. q, $h_q$ vs. q, $D_q$ vs. q, and $D_q$ vs. $h_q$ is shown in Figures 5.53 to 5.62. It is obvious that the plot of the original data is largely different from that of the shuffled data. Compared to the plots from the previous section on the difference between the multifractal, monofractal data and noise, the following figures show similar differences in plots. This shows that the original data correspond to the multifractal data, and the shuffled data correspond to the noise. In particular, the plot of $D_q$ vs. $h_q$ illustrates the multifractality structure between a large arc of the original data and small arc of the shuffled data. In other words, the shuffling process largely reduces the multifractal spectrum width.

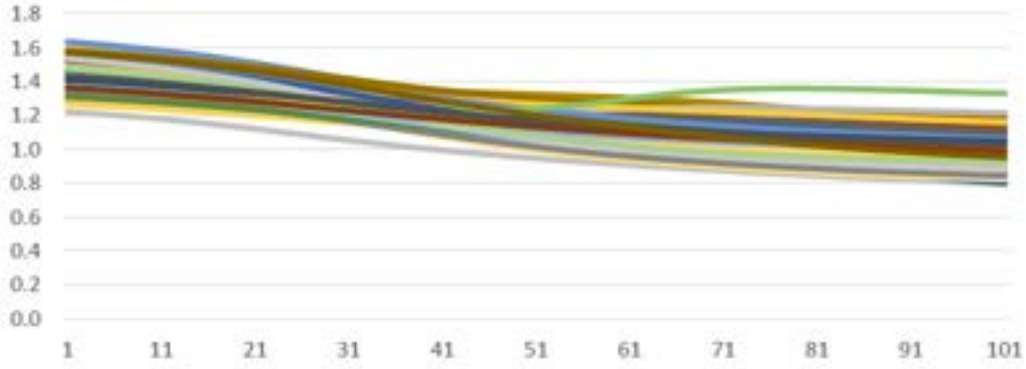


Figure 5.53. Plot of $H_q$ against the q-th order of the original time series.

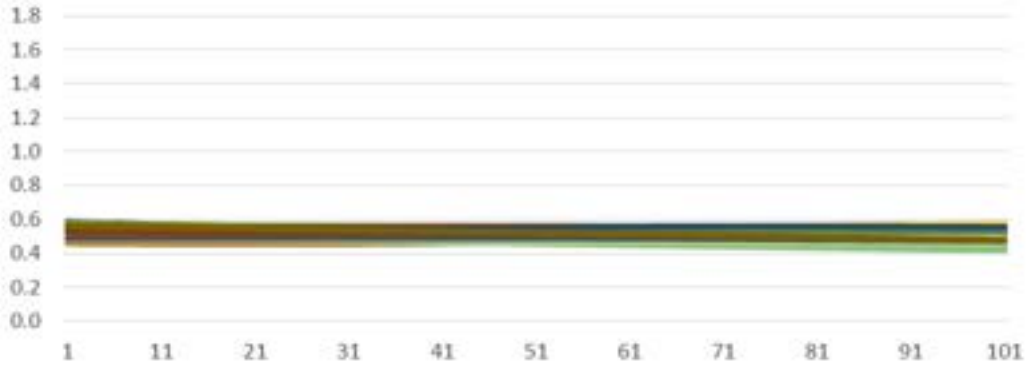


Figure 5.54. Plot of $H_q$ against the q-th order of the shuffled time series.

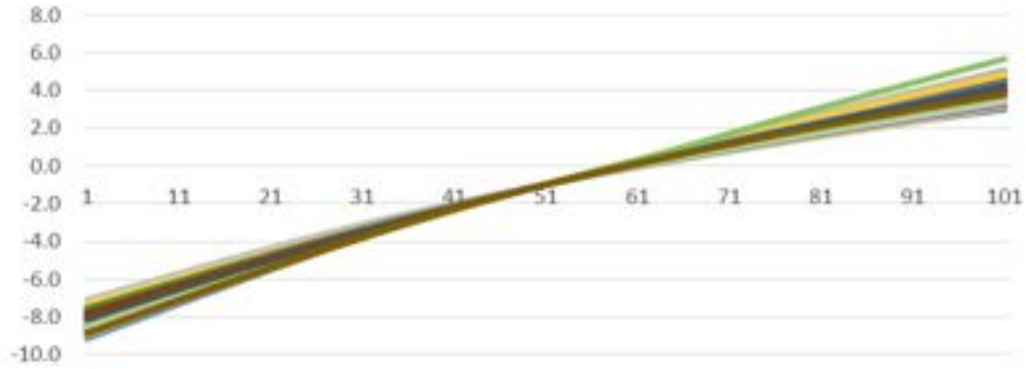


Figure 5.55. Plot of $t_q$ against the q-th order of the original time series.

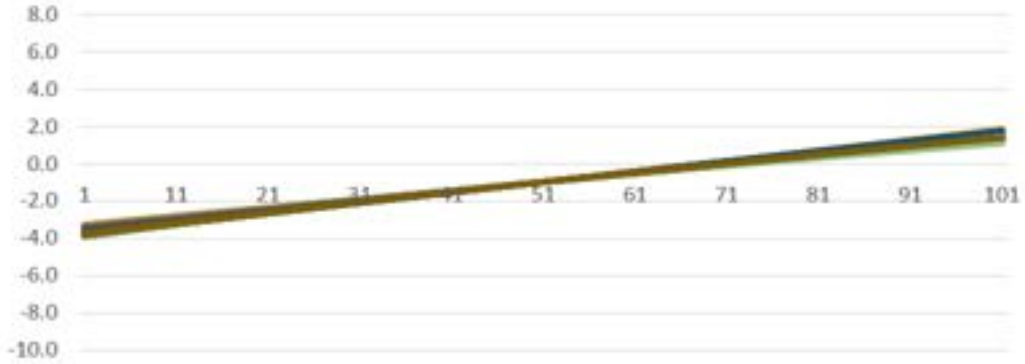


Figure 5.56. Plot of $t_q$ against the q-th order of the shuffled time series.

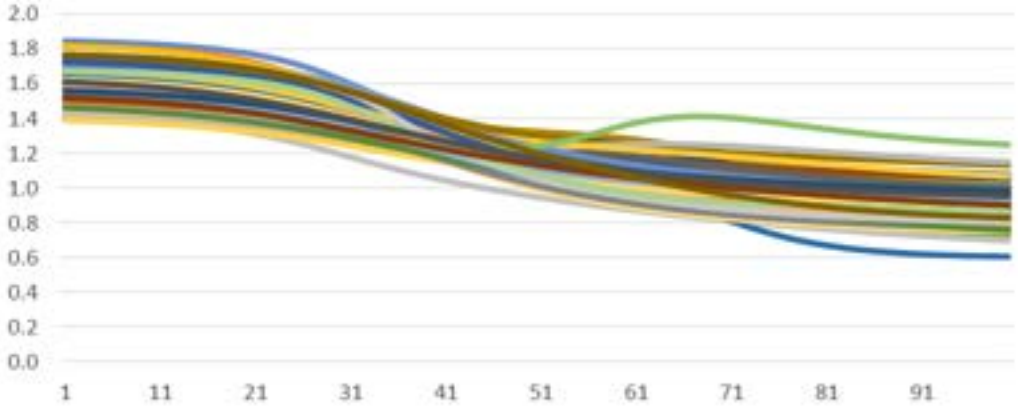


Figure 5.57. Plot of $h_q$ against the q-th order of the original time series.

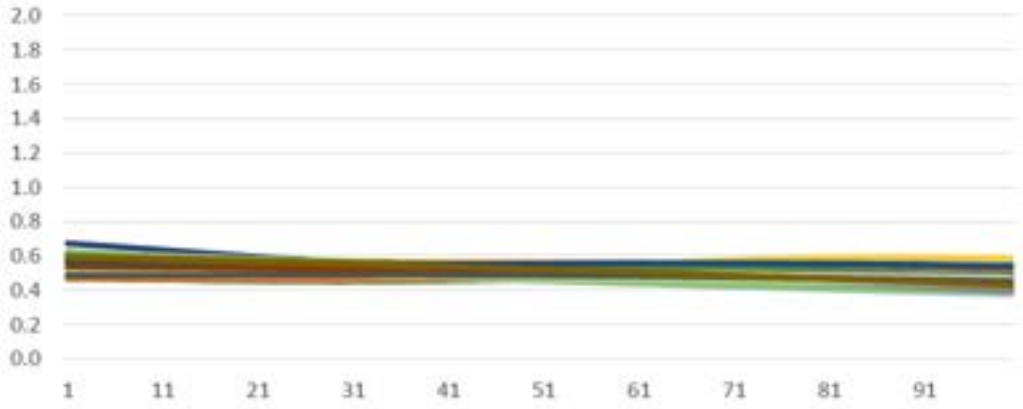


Figure 5.58. Plot of $h_q$ against the q-th order of the shuffled time series.

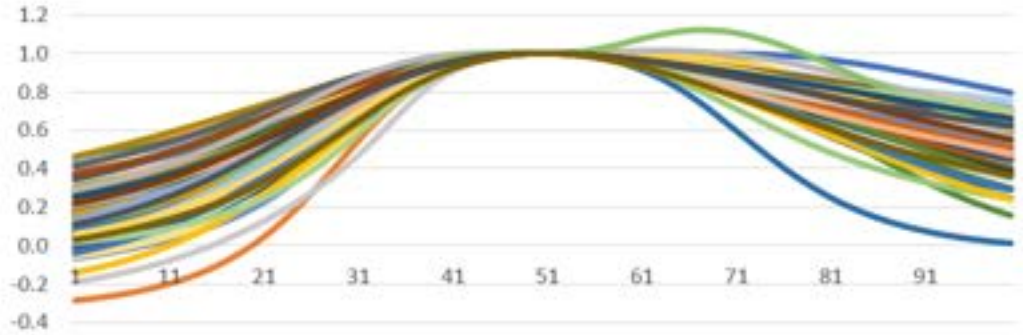


Figure 5.59. Plot of $D_q$ against the q-th order of the original time series.

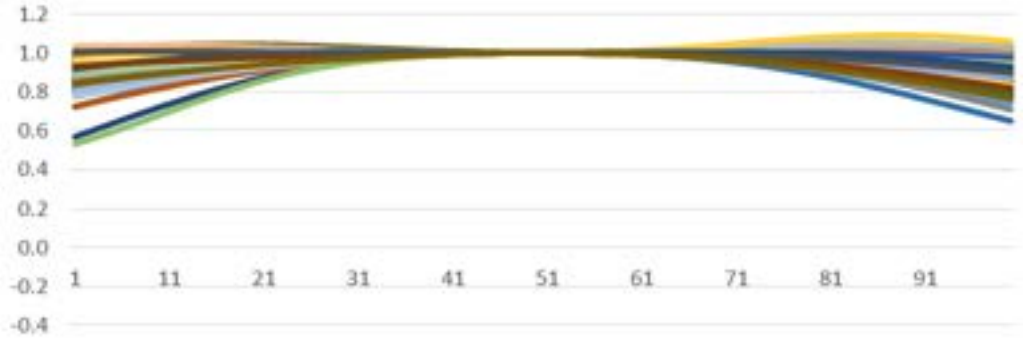


Figure 5.60. Plot of $D_q$ against the q-th order of the shuffled time series.

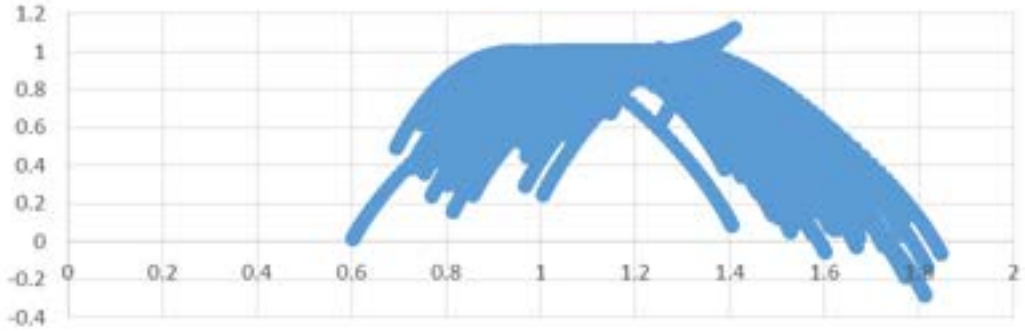


Figure 5.61. Plot of $D_q$ against $h_q$ of the original time series.

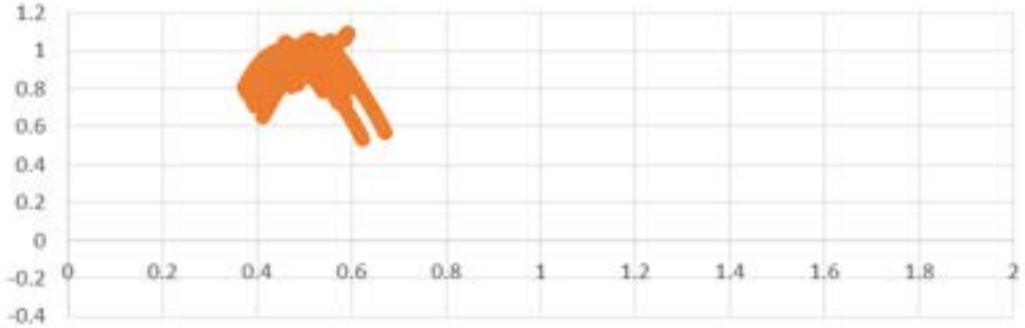


Figure 5.62. Plot of $D_q$ against $h_q$ of the shuffled time series.

Table 5.35 shows the values of $h_q$, W, and γ compared between the original and shuffled data. Together with the previous figures, it suggests that multifractality is due to both the probability distribution and long-range correlation. However, the long-range correlation is dominant as suggested by the large reduction in the multifractal width. Values of γ in the shuffled data are quite close to 1, whereas those of the original data have lower values. This is as expected because the correlations are destroyed in the shuffling process. This result demonstrates the fact

that the multifractality in spinal curvature is predominantly due to long-range correlations.

Table 5.35. Values of the singularity exponent, multifractal width, and autocorrelation coefficient between original and shuffled data.

| | $hq_{min}$ | $hq_{max}$ | W | Γ |
|---|---|---|---|---|
| **Original data** | 0.90 ± 0.11 | 1.59 ± 0.10 | 0.69 ± 0.13 | 0.00 ± 0.20 |
| **Shuffled data** | 0.46 ± 0.04 | 0.55 ± 0.04 | 0.09 ± 0.05 | 1.01 ± 0.06 |

## 5.7. Adoption of MFDFA to Spine Movement

In the previous section, the calculation and results on the basis of MFDFA are described. The analysis follows the computation process in general in the analysis signals of time series. In most of the steps, the application of MFDFA is similar. However, similar to all other fractal analysis methods, MFDFA requires careful consideration of signal properties, parameter settings, and the interpretation of results, and cannot be applied blindly without understanding the characteristics of the signals. It is particularly crucial to plot and carefully inspect the time series. Careful investigation should be conducted on the resultant plots to ensure that the apparent signal properties match the obtained results. In addition, statistical validation must be conducted to provide the confidence in the results. In this

section, several points are discussed with regard to the adoption of cervical spine signals into the MFDFA.

Before taking the first step to conduct the MFDFA analysis, investigation on the signal time series must be conducted. In the case of the cervical spine, the original captured signal is provided on a time basis. By plotting the signal along the time dimension, the structure of the signal is similar to noise. This seems to fulfill the noise-like characteristic of the signal in time series. However, with regard to the physiological properties of the signal, the positional data captured do not conform substantially to the motor control mechanism. Although the spinal movement is definitely generated by the motor control mechanism, the positional data are only part of a small numerical element that cannot describe the movement of the spine as a whole in each segment. Therefore, the positional signals are transformed into signals on spinal angles. The angles can represent the output of the motor control mechanism as a whole in describing the movement for each spinal segment.

After ascertaining that the signals are of suitable physiological meaning for analysis, the time series can then be plotted for inspection. By visual inspection, the signal must exhibit a structure similar to noise. However, it can be difficult to visually differentiate between random walk- and noise-like time series. A possible solution is to run a monofractal DFA [121]. The time series are noise-like if the Hurst exponent (H) is between 0.2 and 0.8. The time series are random walk-like if H is between 1.2 and 1.8. The time series in the case of the cervical spine as described in the previous sections are random walk series, with H between 1.2 and 1.8.

The local fluctuation in the time series is computed as a local RMS. This local RMS within the biomedical time series cannot be close to zero. The time series must contain fluctuation in a noisy manner. Local fluctuation can become zero if the trend fitting is approximately perfect to fit into the original time series. That means there are not many fluctuations that can alter the value of the local RMS. The reason why that should not be zero local fluctuation can be explained further by the mathematics in the computation. There is a logarithmic function at the time when the Hurst exponent is first attempted. This logarithmic function takes into account the local RMS values. If the parameter inside a logarithmic function is zero, the return value becomes infinitely small. An extremely large Hurst exponent results in a negative q-th order. Consequently, a local RMS close to zero leads to large right tails for the multifractal spectrum. As an example from the previous sections, in one selected trial of a participant of cervical spine curvature with a total of 5400 frames, the average local RMS is approximately 50 units when the segment length is set to 600 frames.

There are other reasons that can lead to the local fluctuation in the RMS to become zero. It happens when the local fluctuation is calculated from small sample sizes. In that case, the local trend line of the time series can fit the original time series well. The two lines can be highly similar to each other. Hence, the residual can be close to zero. The sample size of the smallest segment should therefore be substantially larger than the polynomial order to prevent an over-fitted trend. As described in previous sections, the smallest segment size in the computation is selected to be 16

frames. In the case when the q-th order is computed at a low value, -5, the local fluctuation, RMS, is approximately 1.

Local fluctuations often appear in various sizes. If that does not happen in the biomedical time series, the RMS plot might be smooth with little apparent variation, resulting in little local fluctuation for some orders. Particularly for observable local fluctuations, if they cannot be found, the value of the smallest scale can be increased and then the local fluctuations must be check carefully.

Because MFDFA is a technique of fractal analysis, by definition, the biomedical time series must have fractal behavior. In other words, when considering the time series, the signals must exhibit a similar noise-like feature. Moreover, this phenomenon must exist for a certain level of detailed investigation. There is a particular concept in the mathematical term: the biomedical time series are scale invariant. That means the logarithmic plot between the q-th order and local fluctuation yields a linear relationship between the two variables. There is also the relationship on the logarithmic plot between the q-th order and local fluctuation, resulting in a slight curve or S shape. This behavior can be visually confirmed using the plot. A nonlinear relation in this plot might originate from the phenomenon recorded in the biomedical time series. One example is about studying the respiratory frequency in the time series of [122]. At the end of the fast fluctuations, there are distinct oscillations of the heart rate variability. This causes the scale invariance to break down at the smallest scales. Variation of the COP is also a common example in evaluating the postural sway of humans. Two distinct scaling regions are identified

from the variation. They have been thought to represent the human balance control in two distinct modes [29].

This is similar to the experiment in this study. Both of the biomedical time series capture the variation caused by postural sway. The COP and the movement of spinal curvature share a similar characteristic of attempting to control the human balance. Both of them result in a random walk structure. This could be the reason why both SDA and MFDFA reveal the multifractal structure representing distinct modes of motor control.

## 5.8. Discussion

In this chapter, the computational procedure of MFDFA is introduced. The experiment was set up to capture the feature points in the cervical spinal region by using the optical motion capture system in a laboratory environment. Healthy participants without distinctive neck pain disease were recruited for the experiment. They were asked to sit upright under two conditions during the capture. One condition is to have low back support from a seat, and the other condition is to sit without the low back support. During the capture, body sway is observed and captured in balancing the body around the static posture. The other crucial experimental parameter is the number of feature points. These feature

points are attached to the cervical region from C2 to C7, with four distinctive points in between, named as M3, M4, M5, and M6.

The fundamental aim for introducing the computational procedure is to investigate whether the biomedical time series captured exhibit a multifractality structure. This multifractality structure is hypothesized to describe various discharges of neural activity in motor control to balance the static posture through body sway. From the previous sections, it is shown that the data are consistent in having multifractality structures in both small and large time scale ranges. From the investigation of a few selected multifractal parameters extracted, the findings consistently describe various components within the multifractality structure. The parameters indicate the multifractality. In particular, the parameters on the singularity exponent and singularity dimension combine to define the width of the multifractal spectrum. This ascertains that the original time series has the multifractality structure.

Several previous studies reported that healthy human behavior that is coordinated and stable reveals a strong long-range correlated structure than pathological behaviors [77, 123]. Furthermore, several reports have suggested that the behavioral signal decorrelates with increases in sources of external variation [124]. Thus, results from fractal analysis of human performance suggest that less correlated variation reflects less coordinated behavior in the presence of external variation and pathological conditions. However, the multifractal formalisms of motor control open for the possibility that coordination behavior is intermittent in time and vary along with the demands of the task and variations in the

environment. It also reflects the potential of healthy, versus pathological, behavior to adapt to possible variation in the environment. The selected human performance of static sitting posture in this study attempts to eliminate the external variation. On the other hand, human performance is likely to have periods with large and counter-adjusted increments reflecting critical transitions to adapt to multiple sources of external variation. In the case of sitting, the body has to adjust itself to reflect the counter balancing mechanism in adapting the imbalance condition due to various physiological functioning happens constantly all at the same time. This can be observed from the random walk plot of the cervical spine movement.

The large and counter-adjusted increments of the performance variables result in a locally impersistent structure. It can be observed in the adjustment made to counter-adjust the imbalance state while sitting during the experiment. The impersistent structure can be defined and described by small local singularity exponents within the various multifractal parameters. It is also associated with the left-tail side of the multifractal spectrum. In addition, the performance variable is likely to contain periods of small variation as well that fixes the performance due to the variations in a heterogeneous environment. The heterogeneous environment has been designed and attempted to set a minimal influence to the participant during the sitting capture and experiment. In this case, the maintenance of the present state of the performance variable is reflected in less counter adjustments and, consequently, results in a more persistent structure. By contrast, the persistent structure is defined and described by a large local singularity exponent within the

various multifractal parameters. It is also associated with the right-tail side of the multifractal spectrum. The large deviations of the local singularity exponent are significantly influenced by multiplicative interactions between temporal scales. Thus, the healthy adaption of performance to several sources of external variation as well as the potential of the motor system for such adaption can be reflected by multiplicative interactions between temporal scales.

In consideration of distinguishing the participant sequence across various multifractal parameters, it is shown that there exists correlation between various sequences with respect to various multifractal parameters. Because the multifractality structure is hypothesized to describe the activity in motor control, the participant sequence can provide a trace on the difference in neural activity across the participant group. There exists variation in patterns on the basis of various multifractal parameters and difference in time scales. These can be related to the local and global neural interconnectivity. Because the propagation of neural signals is finite, time scales may reflect local and progressively longer neighborhoods of neural interaction, within and outside the given spinal region.

The analysis of the time series on the participant variation indicates that the properties of multifractal spectrum, for example, width, have variation between various participants. From the previous table showing the percentage of variance on multifractal parameters in combination with the significance level, it can be found that the variation, to be specific, on the basis of the ordered sequence, of participants can be an estimation of the multifractal spectrum correlation for

various parameters within the participant group. Because the participant group here is limited to the number of participants, the deviation can be further ascertained by the larger group of participants. In sum, the results indicate that the scale invariant structure exists in the biomedical time series fluctuations. The movement performance, that is, the body sway in static posture here, is definitely different from monofractal noise. It provides evidence that the movement performance is multifractal behavior, which can be associated with the multiple strategy behind the motor control and neural activities. However, it is not conclusive: the series of stimulus–response interactions and intervals that integrate to construct the distributions of movement variation still require validation.

In another study, the multifractal structure of the interbeat intervals can identify pathological conditions of the human heart [125]. The rhythm exhibits multifractal properties both in healthy and pathological cases. The difference is that the degree of multifractality is greater in normal persons compared to persons with neurodegenerative diseases. In this study, instead of inviting a pathological participant group for comparison to the healthy participant group, an attempt is made to investigate whether there is any significant difference under the variation of the environment, which is the condition of whether there is low back support when sitting upright. From the previous sections, in the analysis of various multifractal parameters under the two conditions, there exist traces of difference, particularly regarding the standard deviation under descriptive statistics. These differences are consistent across the various parameters. However, in terms of

whether the results significantly distinguish the two sets of conditions, the evidence is not strong enough to prove the confidence. Thus, after the multifractal analysis comparing the two conditions, there are only hints for altering the multifractal behaviors under different conditions within the healthy participant group; however, further investigation is needed to confirm this.

Multifractal analysis that can be applied directly on the raw neural discharge data appears to be highly effective in differentiating the two structures inside the brain [126]. The neural firings are consistent with a multifractal process over a certain time scale range. The generalized singularity dimension within the multifractal spectrum effectively differentiates the two brain areas for both intra- and interpatient groups. During the capture of participants, there are six feature points attached to the cervical region, whereas the inner four are entered into the analysis. This is an attempt to investigate whether there is any significant difference at various positions along the spine. A major difference from the previous study is that the points of analysis here are all along the same movement structure and can be said to be interrelated with each other. From the previous sections, in the analysis of various multifractal parameters under the four feature points of focus, there are noticeable differences when compared with all the points of focus. Particularly for the matrix on the summary between the multifractal parameters and feature points, it can be found that the upper and lower parts of the cervical region are distinguishable in several cases. Although the difference in value between these two parts are not strongly significant, it gives an evidence in considering the features

points along a human movement structure, and, importantly, the results are about consistent with the previous study.

# Chapter 6.
# Results on Correlation between Survey and Multifractal Analysis

The previous chapter shows that the captured data from cervical spine curvature exhibit the multifractality structure. This structure can be found across all participants in the experimental set and is distinguishable by using various multifractal parameters from the monofractal and noise data. The values extracted using the multifractal parameters also show the trace of variation in the experimental set. In this chapter, the neck pain assessment instrument is used to compare and identify the correlation and consistency in between multifractal parameters and NPAD scores.

In the first section, the correlation in the NPAD score factors is analyzed. Initially, the correlation in the NPAD scale score factors is analyzed. It can be found that there exists a significant level of correlation between sets of bivariate. In a similar manner, the correlation within multifractal parameters is analyzed. Results also show that there are correlated bivariate sets between the multifractal parameters. In sum, the results of these correlation indicate that the parameters selected for analysis are related and consistent.

In the second section, the data on the basis of the results of multifractal parameters and NPAD scores of various factors are combined for correlation analysis. The aim is to extract any possible relationship between subjective neck pain issues and the fractal analysis parameters. This shows evidence that neck pain issues can be extracted in relation to the multifractality structure on spinal curvature movement. The multifractality structure can then be associated with the motor control research to the extent on the behavior and degree of spinal movement.

In the third section, the physiological meanings are discussed and associated to illustrate the findings extracted from the analysis. Limitations are also considered for the extension of analysis.

## 6.1. Analysis on the Instruments

### 6.1.1. Correlation in NPAD Score Factors

The NPAD scores are investigated to check the correlations across different factors. In this analysis, SPSS v20 is used to compute the correlation. To prepare the data, five variables are set in the data editor view. The five variables are set according to the factors on NPAD scores. The measurements are all set as a numeric type on a scale. Spearman rank correlation is used for the analysis [59]. It is a nonparametric test that is used to measure the degree of association between two variables. In this case, we have five variables in the data editor view; the bivariate test is executed on each of the two sets of variables. This creates a matrix of five times five correlation test results, minus those five that are self-correlated. That means there are 20 correlation results that are appropriately used for analysis. By contrast, the test does not have any assumptions regarding the distribution of the data. That is, the assumption and observation on the NPAD scores. From the previous chapters, the scores are computed to observe the variation between participants. The results

show that the distribution of the experiment participant set is evenly spread across. Some other correlation tests, for example, Pearson r, assume a normal distribution in the data set, which is inappropriate for use in this case. The other requirement for using Spearman rank correlation is that the variables should be measured on a scale that is at least ordinal. The data here are a numeric type on a scale, which fulfills the requirement. The following formula is used to calculate the Spearman rank correlation:

$$\rho = 1 - \frac{6 \sum_{i=1}^{n} {d_i}^2}{n\,(n^2 - 1)}$$

where ρ is the Spearman rank correlation, $d_i$ is the difference between the ranks of corresponding values $X_i$ and $Y_i$ , and n is the number of values in each data set. $d_i$ can further be defined as follows:

$$d_i = rank\ (X_i) - rank\ (Y_i)$$

where rank( ) is the function to extract the ranking order of a particular data i from the data set.

The results of the Spearman rank correlation analysis are shown in Table 6.1. For convenient notation, the variables on the various factors are defined as follows: OV as the overall NPAD score, PA as the “pain” factor, DI as the “disability” factor, NS as the “neck-specific function” factor, and EC as the “emotion and cognitive influences” factor.

The first to consider regarding the correlation results is the direction of the relationship between the variables. It is determined by the sign in front of the

correlation coefficient value. A positive correlation between the two variables means that there is a positive relationship between the two; in other words, a high score on one variable is associated with a high score on the other. By contrast, a negative correlation between the two variables (a negative sign in front of the correlation coefficient value) means that there is a negative relationship between the two; in other words, a high score on one variable is associated with a low score on the other. In the data set, there is only one negative correlation. That is the bivariate set between the overall NPAD score and the “pain” factor.

The size of the correlation coefficient is then considered. This can range from -1.000 to 1.000. This value indicates the strength of the relationship between the two variables. A correlation of zero indicates no relationship at all. A correlation of 1.0 indicates a perfect positive correlation, and a value of -1.0 indicates a perfect negative correlation. For the numerical values in between, Cohen [60] suggested a small correlation when the values are between 0.10 and 0.29, a medium correlation between 0.30 and 0.49, and a large correlation between 0.50 and 1.00. On the basis of this guideline, the respective correlations are shown in Tables 6.2 to 6.5. Only one bivariate set has a minimal correlation, which is the relationship between OA and PA. For the small correlation, again, there is only one bivariate set in relation to OA and NS. For the medium correlation, there are two bivariate sets, namely OA to DI and OA to EC. From the minimal to medium correlation, the bivariate sets all involve the variable OA. However, OA is actually the overall NPAD score. This may imply that because of the multiple dimensions regarding the overall NPAD score, the

correlation between the factors and the overall score is diluted by the orthogonal properties. The remaining bivariate sets all have a large correlation. This implies that they are all related to each other to a certain extent with a strong strength of correlation.

Table 6.1. Results of the Spearman rank correlation analysis on the NPAD score factors.

| | **OV** | **PA** | **DI** | **NS** | **EC** |
|---|---|---|---|---|---|
| **OV** | 1.000 | -0.014 | 0.310 | 0.247 | 0.399 |
| **PA** | -0.014 | 1.000 | 0.840 | 0.743 | 0.712 |
| **DI** | 0.310 | 0.840 | 1.000 | 0.799 | 0.874 |
| **NS** | 0.247 | 0.743 | 0.799 | 1.000 | 0.668 |
| **EC** | 0.399 | 0.712 | 0.874 | 0.668 | 1.000 |

Table 6.2. Minimal correlation results on the NPAD score factors.

| | **OV** | **PA** | **DI** | **NS** | **EC** |
|---|---|---|---|---|---|
| **OV** | | -0.014 | | | |
| **PA** | -0.014 | | | | |
| **DI** | | | | | |
| **NS** | | | | | |
| **EC** | | | | | |

Table 6.3. Small correlation results on the NPAD score factors.

| | **OV** | **PA** | **DI** | **NS** | **EC** |
|---|---|---|---|---|---|
| **OV** | | | | 0.247 | |
| **PA** | | | | | |
| **DI** | | | | | |
| **NS** | 0.247 | | | | |
| **EC** | | | | | |

Table 6.4. Medium correlation results on the NPAD score factors.

| | OV | PA | DI | NS | EC |
|---|---|---|---|---|---|
| **OV** | | | 0.310 | | 0.399 |
| **PA** | | | | | |
| **DI** | 0.310 | | | | |
| **NS** | | | | | |
| **EC** | 0.399 | | | | |

Table 6.5. Large correlation results on the NPAD score factors.

| | OV | PA | DI | NS | EC |
|---|---|---|---|---|---|
| **OV** | 1.000 | | | | |
| **PA** | | 1.000 | 0.840 | 0.743 | 0.712 |
| **DI** | | 0.840 | 1.000 | 0.799 | 0.874 |
| **NS** | | 0.743 | 0.799 | 1.000 | 0.668 |
| **EC** | | 0.712 | 0.874 | 0.668 | 1.000 |

Given the values of correlation, the coefficient of determination can be calculated. This is the indicator of how much variance the two variables share. The computation is simply a square on the correlation value and then converted to a percentage of variance. For example, a correlation value of 0.2 has 4% of the variance. In that case, there is no substantial overlapping between the two variables. A correlation of 0.5 has a 25% shared variance. Table 6.6 shows the percentage of variance in the variable set. Except for those related to the OV, the remaining variable set has considerable amount of variance explained when compared with a lot of the research conducted in the social sciences. An assumption is that the data set used here is based on the experimental participant group. This means that these percentages of variance may vary from experiment to experiment. However, this

correlation analysis concludes that these selected factors have a strong strength of relationships in the data set.

Table 6.6. Percentage of variance on the NPAD score factors.

| | **OV** | **PA** | **DI** | **NS** | **EC** |
|---|---|---|---|---|---|
| **OV** | 100% | 0% | 10% | 6% | 16% |
| **PA** | 0% | 100% | 71% | 55% | 51% |
| **DI** | 10% | 71% | 100% | 64% | 76% |
| **NS** | 6% | 55% | 64% | 100% | 45% |
| **EC** | 16% | 51% | 76% | 45% | 100% |

The next to consider is the significance level. The level of statistical significance indicates the confidence of the results obtained. Although the significance is strongly influenced by the size of the sample, a common practice is to consider $p < 0.05$ as reaching statistical significance. Table 6.7 shows the significance level of the variable set. To conclude, the factors on PA, DI, NS, and EC have a strong correlation between each other at a significance level, whereas all the bivariate correlations in relation to OA do not have significant results.

Table 6.7. Significance level on the NPAD score factors.

| | **OV** | **PA** | **DI** | **NS** | **EC** |
|---|---|---|---|---|---|
| **OV** | 0.00 | 0.95 | 0.16 | 0.27 | 0.07 |
| **PA** | 0.95 | 0.00 | 0.00 | 0.00 | 0.00 |
| **DI** | 0.16 | 0.00 | 0.00 | 0.00 | 0.00 |
| **NS** | 0.27 | 0.00 | 0.00 | 0.00 | 0.00 |
| **EC** | 0.07 | 0.00 | 0.00 | 0.00 | 0.00 |

After combing the percentage of variance and significance level on the NPAD score factors, Table 6.8 indicates the significant bivariate set and the corresponding percentage of variance. The factors are correlated with each other to a certain extent.

Table 6.8. Percentage of variance at the significance level on the basis of the NPAD score factors.

| | **OV** | **PA** | **DI** | **NS** | **EC** |
|---|---|---|---|---|---|
| **OV** | 100% | | | | |
| **PA** | | 100% | 71% | 55% | 51% |
| **DI** | | 71% | 100% | 64% | 76% |
| **NS** | | 55% | 64% | 100% | 45% |
| **EC** | | 51% | 76% | 45% | 100% |

### 6.1.2. Correlation within Multifractal Parameters

The multifractal parameters, namely the mean of $h_q$, width of $h_q$, mean of $D_q$, and height of $D_q$, are investigated to validate the correlations across. The analysis is conducted using SPSS v20 to compute the correlation. To prepare the data, four variables are set in the data editor view. The four variables are set according to the multifractal parameters. The measurements are all set as a numeric type on a scale. Spearman rank correlation is again used for the analysis [59]. In this case, we have four variables in the data editor view; a bivariate test is executed on each of the two sets of variables. This produces a matrix of four times four correlation test results,

minus those four that are self-correlated. That means there are 12 correlation results that are appropriately used for analysis. By contrast, the test does not hold any assumptions about the distribution of the data. However, to test for normality, the Shaprio-Wilk test was used. This assesses the normality of the distribution of scores. A nonsignificant result, with a significance value of more than 0.05, indicates normality. By contrast, a significance value of lower than 0.05 suggests the violation of the assumption on normality. Table 6.9 shows the significance value on the basis of the results of the Shaprio-Wilk test. The results show that the mean of $h_q$ and height of $D_q$ exhibit the normal distribution, whereas width of $h_q$ and mean of $D_q$ do not.

Table 6.9. Results from the test of normality.

| | **Mean of $h_q$** | **Width of $h_q$** | **Mean of $D_q$** | **Height of $D_q$** |
|---|---|---|---|---|
| **Significance Value** | 0.25 | 0.04 | 0.00 | 0.39 |

The other requirement for using the Spearman rank correlation is that the variables should be measured on a scale that is at least ordinal. The data here are a numeric type on a scale, which fulfills the requirement. The results of the Spearman rank correlation analysis are shown in Table 6.10.

Table 6.10. Results of the Spearman rank correlation analysis on the multifractal parameters.

| | **Mean of $h_q$** | **Width of $h_q$** | **Mean of $D_q$** | **Height of $D_q$** |
|---|---|---|---|---|
| **Mean of $h_q$** | 1.00 | -0.05 | 0.00 | 0.09 |

| | | | | |
|---|---|---|---|---|
| **Width of $h_q$** | -0.05 | 1.00 | -0.94 | 0.56 |
| **Mean of $D_q$** | 0.00 | -0.94 | 1.00 | -0.65 |
| **Height of $D_q$** | 0.09 | 0.56 | -0.65 | 1.00 |

The first to consider regarding the correlation results is the direction of the relationship between the variables. It is determined by the sign in front of the correlation coefficient value. A positive correlation value between the two variables indicates that there is a positive relationship between the two. By contrast, a negative sign in front of the correlation coefficient value means there is a negative relationship between the two. In the data set, there are three negative correlations. That is the bivariate set on (mean of $h_q$, width of $h_q$), (width of $h_q$, mean of $D_q$), and (mean of $D_q$, height of $D_q$).

The size of the correlation coefficient is then considered. The numerical value indicates the strength of the relationship between the two variables. A small correlation exists when the value is between 0.10 and 0.29, a medium correlation is between 0.30 and 0.49, and a large correlation is between 0.50 and 1.00. The strength of correlations are shown in Tables 6.11 and 6.12.

There are three bivariate sets with a minimal correlation, which is the relationship between (mean of $h_q$, width of $h_q$), (mean of $h_q$, mean of $D_q$), and (mean of $h_q$, height of $D_q$). There is no bivariate set with a small or medium correlation. For the minimal correlation relationship, the bivariate sets all involve the variable mean of $h_q$. The remaining bivariate sets all have a large correlation relationship. This implies

that they are all related to each other to a certain extent with a strong strength of correlation.

Table 6.11. Minimal correlation results on the multifractal parameters.

| | **Mean of $h_q$** | **Width of $h_q$** | **Mean of $D_q$** | **Height of $D_q$** |
|---|---|---|---|---|
| **Mean of $h_q$** | | -0.05 | 0.00 | 0.09 |
| **Width of $h_q$** | -0.05 | | | |
| **Mean of $D_q$** | 0.00 | | | |
| **Height of $D_q$** | 0.09 | | | |

Table 6.12. Large correlation results on the multifractal parameters.

| | **Mean of $h_q$** | **Width of $h_q$** | **Mean of $D_q$** | **Height of $D_q$** |
|---|---|---|---|---|
| **Mean of $h_q$** | 1.00 | | | |
| **Width of $h_q$** | | 1.00 | -0.94 | 0.56 |
| **Mean of $D_q$** | | -0.94 | 1.00 | -0.65 |
| **Height of $D_q$** | | 0.56 | -0.65 | 1.00 |

Given the values of correlation, the coefficient of determination can be calculated. That is the indicator of the amount of variance the two variables share. The computation is simply a square on the correlation value and then converted to a percentage of variance. Table 6.13 shows the percentage of variance in the variable set. Except for those related to the mean of $h_q$, the remaining variable set has a considerable amount of variance explained. The results conclude that the selected multifractal parameters have a strong strength of relationships in the data set, except for the mean of $h_q$.

Table 6.13. Percentage of variance on the NPAD score factors.

| | **Mean of $h_q$** | **Width of $h_q$** | **Mean of $D_q$** | **Height of $D_q$** |
|---|---|---|---|---|
| **Mean of $h_q$** | 100% | 0% | 0% | 1% |
| **Width of $h_q$** | 0% | 100% | 89% | 31% |
| **Mean of $D_q$** | 0% | 89% | 100% | 42% |
| **Height of $D_q$** | 1% | 31% | 42% | 100% |

The next to consider is the significance level. The level of statistical significance indicates the confidence of the results obtained. A common practice is to consider $p < 0.05$ as reaching statistical significance. Table 6.14 shows the significance level of the variable set. To conclude, the multifractal parameters on width of $h_q$, mean of $D_q$, and height of $D_q$ have a strong correlation between each other at a significance level, whereas all the bivariate correlations in relation to mean of $h_q$ do not have significant results obtained.

Table 6.14. Significance level on the multifractal parameters.

| | **Mean of $h_q$** | **Width of $h_q$** | **Mean of $D_q$** | **Height of $D_q$** |
|---|---|---|---|---|
| **Mean of $h_q$** | | 0.50 | 0.96 | 0.22 |
| **Width of $h_q$** | 0.50 | | 0.00 | 0.00 |
| **Mean of $D_q$** | 0.96 | 0.00 | | 0.00 |
| **Height of $D_q$** | 0.22 | 0.00 | 0.00 | |

## 6.2. Correlation Analysis to Extract Relationship

In this section, the data are combined from both the NPAD instrument and multifractal parameters. The aim is to extract possible relationships between subjective neck pain issues and the fractal analysis parameters. This can help to understand possible neck pain issues on the basis of the numerical data captured and computed. It can further serve as a foundation of design and a technical guideline for developing methods to capture using wearable devices. The objective is to obtain a relationship between these two sets of variables. Each individually identified correlation value and significance value can be used to define the priority on the importance or the weighting of each variable within the parameter set. Moreover, the correlation values across various variables can indicate the relationship and also the weighting factors for the extraction of subjective variables, that is, the trace of neck pain issues. These are related to how the system can be defined and designed for the purpose of movement-monitoring by using wearable devices.

The analysis is conducted using SPSS v20 to compute the correlation. The first step is to prepare the data for the analysis. Within the NPAD instrument, the overall NPAD score and all the four factors, namely “pain”, “disability”, “neck-specific function” and “emotion and cognitive influences”, are prepared. For convenient notation, the variables are defined as follows: OV as the overall NPAD score, PA as the “pain” factor, DI as the “disability” factor, NS as the “neck-specific function” factor, and EC as the “emotion and cognitive influences” factor. For the multifractal parameters, four variables are prepared, namely the mean of the singularity exponent ($h_q$), width

of $h_q$ , mean of the singular dimension ($D_q$), and height of $D_q$ . In the data editor view, altogether there are nine variables defined. All of them are set as a numeric type on scale measurement.

On the basis of the analysis conducted in previous sections, the data can be grouped using two classifiers. One is whether or not there is low back support, noted as “w/ LBS” and “w/o LBS,” respectively. The other one is the various vertices along the cervical region, namely M3, M4, M5, and M6, which are the marker point of data captured.

Spearman rank correlation is again used for the analysis [59]. In this case, we have nine variables altogether; a bivariate test is conducted on each of the two sets of variables. This produces a matrix of nine times nine correlation analysis results, minus those nine that are self-correlated. That means there are 72 correlation results that are appropriately used for analysis. Considering the symmetrical order within the correlation matrix between the upper right and lower left quadrants, there are 36 correlation results extracted. The test does not hold any assumptions about the distribution of the data. As from the previous sections, the variable set contains both normal and evenly distributed data. The other requirement for using the Spearman rank correlation is that the variables should be measured on a scale that is at least ordinal. The data here are a numeric type on a scale, which fulfills the requirement.

The results of the Spearman rank correlation analysis are shown in the following tables. On the basis of the preparation of data, Tables 6.15 to 6.22 are grouped by

whether there is low back support and the various vertices. In addition, the tables focus on the relationship between the two data sets.

Table 6.15. Results of the Spearman rank correlation analysis on the M3 vertex without low back support.

| **M3 – w/o LBS** | | | | | |
|---|---|---|---|---|---|
| | **OV** | **PA** | **DI** | **NS** | **EC** |
| **Mean of $h_q$** | 0.04 | 0.39 | 0.38 | 0.47 | 0.39 |
| **Width of $h_q$** | 0.01 | -0.44 | -0.41 | -0.59 | -0.41 |
| **Mean of $D_q$** | -0.10 | 0.41 | 0.37 | 0.52 | 0.30 |
| **Height of $D_q$** | 0.00 | -0.14 | 0.02 | -0.08 | 0.06 |

Table 6.16. Results of the Spearman rank correlation analysis on the M3 vertex with low back support.

| **M3 – w/ LBS** | | | | | |
|---|---|---|---|---|---|
| | **OV** | **PA** | **DI** | **NS** | **EC** |
| **Mean of $h_q$** | -0.03 | 0.34 | 0.34 | 0.38 | 0.28 |
| **Width of $h_q$** | -0.11 | 0.29 | 0.31 | 0.07 | 0.28 |
| **Mean of $D_q$** | 0.09 | -0.25 | -0.26 | -0.03 | -0.29 |
| **Height of $D_q$** | -0.37 | 0.13 | 0.05 | 0.01 | 0.06 |

Table 6.17. Results of the Spearman rank correlation analysis on the M4 vertex without low back support.

| **M4 – w/o LBS** | | | | | |
|---|---|---|---|---|---|
| | **OV** | **PA** | **DI** | **NS** | **EC** |
| **Mean of $h_q$** | -0.03 | 0.34 | 0.34 | 0.38 | 0.28 |
| **Width of $h_q$** | -0.11 | 0.29 | 0.31 | 0.07 | 0.28 |
| **Mean of $D_q$** | 0.09 | -0.25 | -0.26 | -0.03 | -0.29 |
| **Height of $D_q$** | -0.37 | 0.13 | 0.05 | 0.01 | 0.06 |

Table 6.18. Results of the Spearman rank correlation analysis on the M4 vertex with low back support.

| **M4 – w/ LBS** | | | | | |
|---|---|---|---|---|---|
| | **OV** | **PA** | **DI** | **NS** | **EC** |
| **Mean of $h_q$** | -0.10 | -0.02 | -0.16 | -0.03 | 0.01 |
| **Width of $h_q$** | 0.50 | -0.20 | 0.03 | 0.03 | 0.13 |
| **Mean of $D_q$** | -0.50 | 0.12 | -0.02 | -0.18 | -0.08 |
| **Height of $D_q$** | 0.54 | -0.12 | 0.10 | -0.03 | 0.27 |

Table 6.19. Results of the Spearman rank correlation analysis on the M5 vertex without low back support.

| **M5 – w/o LBS** | | | | | |
|---|---|---|---|---|---|
| | **OV** | **PA** | **DI** | **NS** | **EC** |
| **Mean of $h_q$** | -0.03 | -0.13 | -0.11 | 0.14 | -0.09 |
| **Width of $h_q$** | 0.34 | 0.18 | 0.18 | 0.21 | 0.03 |
| **Mean of $D_q$** | -0.29 | -0.08 | -0.04 | -0.08 | 0.01 |
| **Height of $D_q$** | -0.26 | 0.02 | 0.02 | -0.15 | -0.10 |

Table 6.20. Results of the Spearman rank correlation analysis on the M5 vertex with low back support.

| **M5 – w/ LBS** | | | | | |
|---|---|---|---|---|---|
| | **OV** | **PA** | **DI** | **NS** | **EC** |
| **Mean of $h_q$** | 0.05 | 0.43 | 0.30 | 0.39 | 0.39 |
| **Width of $h_q$** | 0.08 | -0.06 | 0.12 | -0.10 | 0.09 |
| **Mean of $D_q$** | -0.10 | 0.06 | -0.07 | 0.07 | -0.03 |
| **Height of $D_q$** | -0.06 | 0.25 | 0.28 | 0.12 | 0.27 |

Table 6.21. Results of the Spearman rank correlation analysis on the M6 vertex without low back support.

| **M6 – w/o LBS** | | | | | |
|---|---|---|---|---|---|
| | **OV** | **PA** | **DI** | **NS** | **EC** |
| **Mean of $h_q$** | -0.25 | -0.19 | -0.20 | -0.29 | -0.16 |

| | | | | | |
|---|---|---|---|---|---|
| **Width of $h_q$** | 0.07 | 0.00 | 0.07 | 0.18 | 0.17 |
| **Mean of $D_q$** | -0.09 | 0.02 | -0.08 | -0.15 | -0.16 |
| **Height of $D_q$** | -0.15 | 0.11 | 0.13 | -0.04 | 0.19 |

Table 6.22. Results of the Spearman rank correlation analysis on the M6 vertex with low back support.

| **M6 – w/ LBS** | | | | | |
|---|---|---|---|---|---|
| | **OV** | **PA** | **DI** | **NS** | **EC** |
| **Mean of $h_q$** | 0.40 | -0.16 | -0.01 | -0.13 | 0.27 |
| **Width of $h_q$** | 0.40 | 0.04 | 0.05 | -0.02 | 0.07 |
| **Mean of $D_q$** | -0.35 | 0.01 | 0.02 | 0.05 | 0.01 |
| **Height of $D_q$** | 0.22 | -0.29 | -0.29 | -0.27 | -0.23 |

### 6.2.1. Statistical Results on the Minimal Correlation Strength

To interpret the correlation results, the size of the correlation coefficient is considered. The numerical value indicates the strength of the relationship between the two variables. A small correlation is indicated when the value is between 0.10 and 0.29, a medium correlation is between 0.30 and 0.49, and a large correlation is between 0.50 and 1.00. The strength of correlations are shown in Tables 6.23 to 6.30 for minimal correlation.

Table 6.23. Minimal correlation results on the M3 vertex without low back support.

| **M3 – w/o LBS** | | | | | |
|---|---|---|---|---|---|
| | **OV** | **PA** | **DI** | **NS** | **EC** |

| | | | | | |
|---|---|---|---|---|---|
| **Mean of $h_q$** | 0.04 | - | - | - | - |
| **Width of $h_q$** | 0.01 | - | - | - | - |
| **Mean of $D_q$** | - | - | - | - | - |
| **Height of $D_q$** | 0.00 | - | 0.02 | -0.08 | 0.06 |

Table 6.24. Minimal correlation results on the M3 vertex with low back support.

| **M3 – w/ LBS** | | | | | |
|---|---|---|---|---|---|
| | **OV** | **PA** | **DI** | **NS** | **EC** |
| **Mean of $h_q$** | -0.03 | - | - | - | - |
| **Width of $h_q$** | - | - | - | 0.07 | - |
| **Mean of $D_q$** | 0.09 | - | - | -0.03 | - |
| **Height of $D_q$** | - | - | 0.05 | 0.01 | 0.06 |

Table 6.25. Minimal correlation results on the M4 vertex without low back support.

| **M4 – w/o LBS** | | | | | |
|---|---|---|---|---|---|
| | **OV** | **PA** | **DI** | **NS** | **EC** |
| **Mean of $h_q$** | -0.02 | -0.04 | - | 0.07 | - |
| **Width of $h_q$** | 0.04 | - | - | - | - |
| **Mean of $D_q$** | - | - | - | - | - |
| **Height of $D_q$** | - | - | - | - | - |

Table 6.26. Minimal correlation results on the M4 vertex with low back support.

| **M4 – w/ LBS** | | | | | |
|---|---|---|---|---|---|
| | **OV** | **PA** | **DI** | **NS** | **EC** |
| **Mean of $h_q$** | -0.10 | -0.02 | - | -0.03 | 0.01 |
| **Width of $h_q$** | - | - | 0.03 | 0.03 | - |
| **Mean of $D_q$** | - | - | -0.02 | - | -0.08 |
| **Height of $D_q$** | - | - | - | -0.03 | - |

Table 6.27. Minimal correlation results on the M5 vertex without low back support.

| **M5 – w/o LBS** |
|---|

| | OV | PA | DI | NS | EC |
|---|---|---|---|---|---|
| **Mean of $h_q$** | -0.03 | - | - | - | -0.09 |
| **Width of $h_q$** | - | - | - | - | 0.03 |
| **Mean of $D_q$** | - | -0.08 | -0.04 | -0.08 | 0.01 |
| **Height of $D_q$** | - | 0.02 | 0.02 | - | -0.10 |

Table 6.28. Minimal correlation results on the M5 vertex with low back support.

| **M5 – w/ LBS** | | | | | |
|---|---|---|---|---|---|
| | **OV** | **PA** | **DI** | **NS** | **EC** |
| **Mean of $h_q$** | 0.05 | - | - | - | - |
| **Width of $h_q$** | 0.08 | -0.06 | -- | -0.10 | 0.09 |
| **Mean of $D_q$** | -0.10 | 0.06 | -0.07 | 0.07 | -0.03 |
| **Height of $D_q$** | -0.06 | - | - | - | - |

Table 6.29. Minimal correlation results on the M6 vertex without low back support.

| **M6 – w/o LBS** | | | | | |
|---|---|---|---|---|---|
| | **OV** | **PA** | **DI** | **NS** | **EC** |
| **Mean of $h_q$** | - | - | - | - | - |
| **Width of $h_q$** | 0.07 | 0.00 | 0.07 | - | - |
| **Mean of $D_q$** | -0.09 | 0.02 | -0.08 | - | - |
| **Height of $D_q$** | - | - | - | -0.04 | - |

Table 6.30. Minimal correlation results on the M5 vertex with low back support.

| **M6 – w/ LBS** | | | | | |
|---|---|---|---|---|---|
| | **OV** | **PA** | **DI** | **NS** | **EC** |
| **Mean of $h_q$** | - | - | -0.01 | - | - |
| **Width of $h_q$** | - | 0.04 | 0.05 | -0.02 | 0.07 |
| **Mean of $D_q$** | - | 0.01 | 0.02 | 0.05 | 0.01 |
| **Height of $D_q$** | - | - | - | - | - |

Several bivariate sets have a minimal correlation. Briefly, there are more entries in the M5 and M6 tables. The statistics are shown in Table 6.31. The first group of percentages corresponds to each table. The individual percentage ranges from 20% to 55%. The second group of percentages is combined based on individual vertices. It ranges from 33% to 53%. The third group of percentages is combined based on low back support. It ranges from 34% to 45%. The final group is the overall percentages with minimal correlation within the data set. It has a percentage of 39%. On the basis of this statistical summary, it can be observed that a certain proportion of data is in the minimal correlation relationship. Especially for those involving M5 and M6, they have higher percentages compared to M3 and M4.

Table 6.31. Statistical percentage on the minimal correlation results.

| | |
|---|---|
| **M3 – w/o LBS** | 30% |
| **M3 – w/ LBS** | 35% |
| **M4 – w/o LBS** | 20% |
| **M4 - w/ LBS** | 45% |
| **M5 – w/o LBS** | 50% |
| **M5 – w/ LBS** | 55% |
| **M6 – w/o LBS** | 35% |
| **M6 – w/ LBS** | 45% |
| | |
| **M3 (combined)** | 33% |
| **M4 (combined)** | 33% |
| **M5 (combined)** | 53% |
| **M6 (combined)** | 40% |
| | |
| **w/o LBS (combined)** | 34% |
| **w/ LBS (combined)** | 45% |

| | |
|---|---|
| **Overall** | 39% |

The other way to investigate the relationship is to statistically calculate the percentage of each bivariate set. Table 6.32 shows the statistical percentage of each bivariate set on the basis of the minimal correlation results. The method to interpret the percentages is to identify those bivariate sets with high percentages; these bivariate sets possibly do not have a substantial relationship. Specifically, the bivariate sets are (OV, mean of $h_q$) and (DI, mean of $D_q$).

Table 6.32. Statistical percentage of each bivariate set on the basis of the minimal correlation results.

| | **OV** | **PA** | **DI** | **NS** | **EC** |
|---|---|---|---|---|---|
| **Mean of $h_q$** | 75% | 25% | 13% | 25% | 25% |
| **Width of $h_q$** | 50% | 38% | 38% | 50% | 38% |
| **Mean of $D_q$** | 38% | 50% | 63% | 50% | 50% |
| **Height of $D_q$** | 25% | 13% | 38% | 50% | 38% |

### 6.2.2. Statistical Results on the Small Correlation Strength

The correlation results with small correlation relationships are shown in Tables 6.33 to 6.40. There is a number of bivariate sets with a small correlation relationship.

Table 6.33. Small correlation results on the M3 vertex without low back support.

| M3 – w/o LBS | | | | | |
|---|---|---|---|---|---|
| | **OV** | **PA** | **DI** | **NS** | **EC** |
| **Mean of $h_q$** | - | - | - | - | - |
| **Width of $h_q$** | - | - | - | - | - |
| **Mean of $D_q$** | -0.10 | - | - | - | - |
| **Height of $D_q$** | - | -0.14 | - | - | - |

Table 6.34. Small correlation results on the M3 vertex with low back support.

| M3 – w/ LBS | | | | | |
|---|---|---|---|---|---|
| | **OV** | **PA** | **DI** | **NS** | **EC** |
| **Mean of $h_q$** | - | - | - | - | 0.28 |
| **Width of $h_q$** | -0.11 | 0.29 | - | - | 0.28 |
| **Mean of $D_q$** | - | -0.25 | -0.26 | - | -0.29 |
| **Height of $D_q$** | - | 0.13 | - | - | - |

Table 6.35. Small correlation results on the M4 vertex without low back support.

| M4 – w/o LBS | | | | | |
|---|---|---|---|---|---|
| | **OV** | **PA** | **DI** | **NS** | **EC** |
| **Mean of $h_q$** | - | - | -0.21 | - | -0.11 |
| **Width of $h_q$** | - | - | -0.12 | -0.10 | -0.10 |
| **Mean of $D_q$** | -0.19 | - | 0.19 | 0.19 | 0.27 |
| **Height of $D_q$** | -0.13 | - | - | -0.17 | - |

Table 6.36. Small correlation results on the M4 vertex with low back support.

| M4 – w/ LBS | | | | | |
|---|---|---|---|---|---|
| | **OV** | **PA** | **DI** | **NS** | **EC** |
| **Mean of $h_q$** | - | - | -0.16 | - | - |
| **Width of $h_q$** | - | -0.20 | - | - | 0.13 |
| **Mean of $D_q$** | - | 0.12 | - | -0.18 | - |
| **Height of $D_q$** | - | -0.12 | 0.10 | - | 0.27 |

Table 6.37. Small correlation results on the M5 vertex without low back support.

| **M5 – w/o LBS** | | | | | |
|---|---|---|---|---|---|
| | **OV** | **PA** | **DI** | **NS** | **EC** |
| **Mean of $h_q$** | - | -0.13 | -0.11 | 0.14 | - |
| **Width of $h_q$** | - | 0.18 | 0.18 | 0.21 | - |
| **Mean of $D_q$** | -0.29 | - | - | - | - |
| **Height of $D_q$** | -0.26 | - | - | -0.15 | - |

Table 6.38. Small correlation results on the M5 vertex with low back support.

| **M5 – w/ LBS** | | | | | |
|---|---|---|---|---|---|
| | **OV** | **PA** | **DI** | **NS** | **EC** |
| **Mean of $h_q$** | - | - | - | - | - |
| **Width of $h_q$** | - | - | 0.12 | - | - |
| **Mean of $D_q$** | - | - | - | - | - |
| **Height of $D_q$** | - | 0.25 | 0.28 | 0.12 | 0.27 |

Table 6.39. Small correlation results on the M6 vertex without low back support.

| **M6 – w/o LBS** | | | | | |
|---|---|---|---|---|---|
| | **OV** | **PA** | **DI** | **NS** | **EC** |
| **Mean of $h_q$** | -0.25 | -0.19 | -0.20 | -0.29 | -0.16 |
| **Width of $h_q$** | - | - | - | 0.18 | 0.17 |
| **Mean of $D_q$** | - | - | - | -0.15 | -0.16 |
| **Height of $D_q$** | -0.15 | 0.11 | 0.13 | - | 0.19 |

Table 6.40. Small correlation results on the M5 vertex with low back support.

| **M6 – w/ LBS** | | | | | |
|---|---|---|---|---|---|
| | **OV** | **PA** | **DI** | **NS** | **EC** |
| **Mean of $h_q$** | - | -0.16 | - | -0.13 | 0.27 |
| **Width of $h_q$** | - | - | - | - | - |
| **Mean of $D_q$** | - | - | - | - | - |
| **Height of $D_q$** | 0.22 | -0.29 | -0.29 | -0.27 | -0.23 |

Briefly, the statistics are shown in Table 6.41. The first group of percentages corresponds to each individual table. The individual percentage ranges from 10% to 65%. The second group of percentages is combined based on individual vertices. It ranges from 25% to 53%. The third group of percentages is combined based on low back support. It ranges from 36% to 44%. The final group is the overall percentages with a minimal correlation within the data set. It has a percentage of 40%. On the basis of this statistical summary, there is a certain proportion of data that have the small correlation relationship. Combined with the previous percentage on the minimal correlation, this is approximately 79% of the overall results. The highest percentage groups are those involving M4 and M6. Combined with the previous findings on the minimal correlation results, M6 possibly does not have a substantial correlation between the two variable sets.

Table 6.41. Statistical percentage on small correlation results.

| | |
|---|---|
| **M3 – w/o LBS** | 10% |
| **M3 – w/ LBS** | 40% |
| **M4 – w/o LBS** | 55% |
| **M4 - w/ LBS** | 40% |
| **M5 – w/o LBS** | 45% |
| **M5 – w/ LBS** | 25% |
| **M6 – w/o LBS** | 65% |
| **M6 – w/ LBS** | 40% |
| | |
| **M3 (combined)** | 25% |
| **M4 (combined)** | 48% |
| **M5 (combined)** | 35% |
| **M6 (combined)** | 53% |

| | |
|---|---|
| **w/o LBS (combined)** | 44% |
| **w/ LBS (combined)** | 36% |
| | |
| **Overall** | 40% |

Similarly, the statistical calculation on the percentage of each bivariate set is conducted. Table 6.42 shows the statistical percentage of each bivariate set on the basis of small correlation results. Because this is a group with a small correlation relationship, those bivariate sets with high percentages possibly have a weak relationship. The highest percentage is the bivariate set at (PA, height of $D_q$). In addition, if the combination of both minimal and small correlation groups has a high percentage, there may be a weak relationship. There is one with 100% combined at (NS, height of $D_q$).

Table 6.42. Statistical percentage of each bivariate set on the basis of small correlation results.

| | **OV** | **PA** | **DI** | **NS** | **EC** |
|---|---|---|---|---|---|
| **Mean of $h_q$** | 13% | 38% | 50% | 38% | 50% |
| **Width of $h_q$** | 13% | 38% | 38% | 38% | 50% |
| **Mean of $D_q$** | 38% | 25% | 25% | 38% | 38% |
| **Height of $D_q$** | 50% | 75% | 50% | 50% | 50% |

### 6.2.3. Statistical Results on the Medium Correlation Strength

The correlation results with medium correlation relationships are shown in Tables 6.43 to 6.50. Compared to the previous two correlation groups, there are fewer bivariate sets with the medium correlation relationship, especially those involving M5 and M6.

Table 6.43. Medium correlation results on the M3 vertex without low back support.

| **M3 – w/o LBS** | | | | | |
|---|---|---|---|---|---|
| | **OV** | **PA** | **DI** | **NS** | **EC** |
| **Mean of $h_q$** | - | 0.39 | 0.38 | 0.47 | 0.39 |
| **Width of $h_q$** | - | -0.44 | -0.41 | - | -0.41 |
| **Mean of $D_q$** | - | 0.41 | 0.37 | - | 0.30 |
| **Height of $D_q$** | - | - | - | - | - |

Table 6.44. Medium correlation results on the M3 vertex with low back support.

| **M3 – w/ LBS** | | | | | |
|---|---|---|---|---|---|
| | **OV** | **PA** | **DI** | **NS** | **EC** |
| **Mean of $h_q$** | - | 0.34 | 0.34 | 0.38 | - |
| **Width of $h_q$** | - | - | 0.31 | - | - |
| **Mean of $D_q$** | - | - | - | - | - |
| **Height of $D_q$** | -0.37 | - | - | - | - |

Table 6.45. Medium correlation results on the M4 vertex without low back support.

| **M4 – w/o LBS** | | | | | |
|---|---|---|---|---|---|
| | **OV** | **PA** | **DI** | **NS** | **EC** |
| **Mean of $h_q$** | - | - | - | - | - |
| **Width of $h_q$** | - | -0.38 | - | - | - |
| **Mean of $D_q$** | - | 0.46 | - | - | - |
| **Height of $D_q$** | - | -0.43 | -0.34 | - | -0.37 |

Table 6.46. Medium correlation results on the M4 vertex with low back support.

| **M4 – w/ LBS** | | | | | |
|---|---|---|---|---|---|
| | **OV** | **PA** | **DI** | **NS** | **EC** |
| **Mean of $h_q$** | - | - | - | - | - |
| **Width of $h_q$** | - | - | - | - | - |
| **Mean of $D_q$** | -0.50 | - | - | - | - |
| **Height of $D_q$** | - | - | - | - | - |

Table 6.47. Medium correlation results on the M5 vertex without low back support.

| **M5 – w/o LBS** | | | | | |
|---|---|---|---|---|---|
| | **OV** | **PA** | **DI** | **NS** | **EC** |
| **Mean of $h_q$** | - | - | - | - | - |
| **Width of $h_q$** | 0.34 | - | - | - | - |
| **Mean of $D_q$** | - | - | - | - | - |
| **Height of $D_q$** | - | - | - | - | - |

Table 6.48. Medium correlation results on the M5 vertex with low back support.

| **M5 – w/ LBS** | | | | | |
|---|---|---|---|---|---|
| | **OV** | **PA** | **DI** | **NS** | **EC** |
| **Mean of $h_q$** | - | 0.43 | 0.30 | 0.39 | 0.39 |
| **Width of $h_q$** | - | - | - | - | - |
| **Mean of $D_q$** | - | - | - | - | - |
| **Height of $D_q$** | - | - | - | - | - |

Table 6.49. Medium correlation results on the M6 vertex without low back support.

| **M6 – w/o LBS** | | | | | |
|---|---|---|---|---|---|
| | **OV** | **PA** | **DI** | **NS** | **EC** |
| **Mean of $h_q$** | - | - | - | - | - |
| **Width of $h_q$** | - | - | - | - | - |
| **Mean of $D_q$** | - | - | - | - | - |
| **Height of $D_q$** | - | - | - | - | - |

Table 6.50. Medium correlation results on the M5 vertex with low back support.

| **M6 – w/ LBS** | | | | | |
|---|---|---|---|---|---|
| | **OV** | **PA** | **DI** | **NS** | **EC** |
| **Mean of $h_q$** | 0.40 | - | - | - | - |
| **Width of $h_q$** | 0.40 | - | - | - | - |
| **Mean of $D_q$** | -0.35 | - | - | - | - |
| **Height of $D_q$** | - | - | - | - | - |

Briefly, the statistics are shown in Table 6.51. The first group of percentages corresponds to each individual table. The individual percentage ranges from 0% to 50%. The second group of percentages is combined based on individual vertices. It ranges from 8% to 38%. The third group of percentages is combined based on low back support. It ranges from 16% to 20%. The final group is the overall percentages with a minimal correlation within the data set. It has a percentage of 18%. On the basis of this statistical summary, M3 possibly has the highest correlation within the bivariate sets. M4 then follows. Because M5 has a high percentage in the minimal correlation group and a moderate percentage in the small correlation group, it also may have a weak correlation.

Table 6.51. Statistical percentage on medium correlation results.

| | |
|---|---|
| **M3 – w/o LBS** | 50% |
| **M3 – w/ LBS** | 25% |
| **M4 – w/o LBS** | 25% |
| **M4 - w/ LBS** | 5% |
| **M5 – w/o LBS** | 5% |
| **M5 – w/ LBS** | 20% |
| **M6 – w/o LBS** | 0% |

| | |
|---|---|
| **M6 – w/ LBS** | 15% |
| | |
| **M3 (combined)** | 38% |
| **M4 (combined)** | 15% |
| **M5 (combined)** | 13% |
| **M6 (combined)** | 8% |
| | |
| **w/o LBS (combined)** | 20% |
| **w/ LBS (combined)** | 16% |
| | |
| **Overall** | 18% |

Similarly, the statistical calculation on the percentage of each bivariate set is conducted. Table 6.52 shows the statistical percentage of each bivariate set on the basis of medium correlation results. Because this is a group with a medium correlation relationship, those bivariate sets with high percentages have a high possibility of a correlation relationship. The bivariate sets with high percentages here are (PA, mean of $h_q$), (DI, mean of $h_q$), and (NS, mean of $h_q$).

Table 6.52. Statistical percentage of each bivariate set on the basis of medium correlation results.

| | **OV** | **PA** | **DI** | **NS** | **EC** |
|---|---|---|---|---|---|
| **Mean of $h_q$** | 13% | 38% | 38% | 38% | 25% |
| **Width of $h_q$** | 25% | 25% | 25% | 0% | 13% |
| **Mean of $D_q$** | 25% | 25% | 13% | 0% | 13% |
| **Height of $D_q$** | 13% | 13% | 13% | 0% | 13% |

### 6.2.4. Statistical Results on the Large Correlation Strength

Finally, the correlation results with large correlation relationships are shown in Tables 6.53 to 6.60. Compared to the previous two correlation groups, there are only several bivariate sets with a large correlation relationship.

Table 6.53. Large correlation results on the M3 vertex without low back support.

| **M3 – w/o LBS** | | | | | |
|---|---|---|---|---|---|
| | **OV** | **PA** | **DI** | **NS** | **EC** |
| **Mean of $h_q$** | - | - | - | - | - |
| **Width of $h_q$** | - | - | - | -0.59 | - |
| **Mean of $D_q$** | - | - | - | 0.52 | - |
| **Height of $D_q$** | - | - | - | - | - |

Table 6.54. Large correlation results on the M3 vertex with low back support.

| **M3 – w/ LBS** | | | | | |
|---|---|---|---|---|---|
| | **OV** | **PA** | **DI** | **NS** | **EC** |
| **Mean of $h_q$** | - | - | - | - | - |
| **Width of $h_q$** | - | - | - | - | - |
| **Mean of $D_q$** | - | - | - | - | - |
| **Height of $D_q$** | - | - | - | - | - |

Table 6.55. Large correlation results on the M4 vertex without low back support.

| **M4 – w/o LBS** | | | | | |
|---|---|---|---|---|---|
| | **OV** | **PA** | **DI** | **NS** | **EC** |
| **Mean of $h_q$** | - | - | - | - | - |
| **Width of $h_q$** | - | - | - | - | - |
| **Mean of $D_q$** | - | - | - | - | - |
| **Height of $D_q$** | - | - | - | - | - |

Table 6.56. Large correlation results on the M4 vertex with low back support.

| **M4 – w/ LBS** | | | | | |
|---|---|---|---|---|---|
| | **OV** | **PA** | **DI** | **NS** | **EC** |
| **Mean of $h_q$** | - | - | - | - | - |
| **Width of $h_q$** | 0.50 | - | - | - | - |
| **Mean of $D_q$** | - | - | - | - | - |
| **Height of $D_q$** | 0.54 | - | - | - | - |

Table 6.57. Large correlation results on the M5 vertex without low back support.

| **M5 – w/o LBS** | | | | | |
|---|---|---|---|---|---|
| | **OV** | **PA** | **DI** | **NS** | **EC** |
| **Mean of $h_q$** | - | - | - | - | - |
| **Width of $h_q$** | - | - | - | - | - |
| **Mean of $D_q$** | - | - | - | - | - |
| **Height of $D_q$** | - | - | - | - | - |

Table 6.58. Large correlation results on the M5 vertex with low back support.

| **M5 – w/ LBS** | | | | | |
|---|---|---|---|---|---|
| | **OV** | **PA** | **DI** | **NS** | **EC** |
| **Mean of $h_q$** | - | - | - | - | - |
| **Width of $h_q$** | - | - | - | - | - |
| **Mean of $D_q$** | - | - | - | - | - |
| **Height of $D_q$** | - | - | - | - | - |

Table 6.59. Large correlation results on the M6 vertex without low back support.

| **M6 – w/o LBS** | | | | | |
|---|---|---|---|---|---|
| | **OV** | **PA** | **DI** | **NS** | **EC** |
| **Mean of $h_q$** | - | - | - | - | - |
| **Width of $h_q$** | - | - | - | - | - |
| **Mean of $D_q$** | - | - | - | - | - |

| | | | | | |
|---|---|---|---|---|---|
| **Height of $D_q$** | - | - | - | - | - |

Table 6.60. Large correlation results on the M5 vertex with low back support.

| **M6 – w/ LBS** | | | | | |
|---|---|---|---|---|---|
| | **OV** | **PA** | **DI** | **NS** | **EC** |
| **Mean of $h_q$** | - | - | - | - | - |
| **Width of $h_q$** | - | - | - | - | - |
| **Mean of $D_q$** | - | - | - | - | - |
| **Height of $D_q$** | - | - | - | - | - |

Briefly, the statistics are shown in Table 6. 61. Only M3 and M4 have percentages here. Combined with the previous findings of M3 and M4 with a high possibility of correlation within the bivariate set, the results are consistent across.

Table 6.61. Statistical percentage on large correlation results.

| | |
|---|---|
| **M3 – w/o LBS** | 10% |
| **M3 – w/ LBS** | 0% |
| **M4 – w/o LBS** | 0% |
| **M4 - w/ LBS** | 10% |
| **M5 – w/o LBS** | 0% |
| **M5 – w/ LBS** | 0% |
| **M6 – w/o LBS** | 0% |
| **M6 – w/ LBS** | 0% |
| | |
| **M3 (combined)** | 5% |
| **M4 (combined)** | 5% |
| **M5 (combined)** | 0% |
| **M6 (combined)** | 0% |
| | |
| **w/o LBS (combined)** | 3% |

| | |
|---|---|
| **w/ LBS (combined)** | 3% |
| | |
| **Overall** | 3% |

The statistical calculation on the percentage of each bivariate set is conducted. Table 6.62 shows the statistical percentage of each bivariate set on the basis of large correlation results. Because this is a group with a large correlation relationship, those bivariate sets with high percentages have a high possibility of a correlation relationship. The bivariate sets with high percentages here are (OV, width of $h_q$), (OV, height of $D_q$), (NS, width of $h_q$), and (NS, mean of $D_q$).

Table 6.62. Statistical percentage of each bivariate set on the basis of large correlation results.

| | **OV** | **PA** | **DI** | **NS** | **EC** |
|---|---|---|---|---|---|
| **Mean of $h_q$** | 0% | 0% | 0% | 0% | 0% |
| **Width of $h_q$** | 13% | 0% | 0% | 13% | 0% |
| **Mean of $D_q$** | 0% | 0% | 0% | 13% | 0% |
| **Height of $D_q$** | 13% | 0% | 0% | 0% | 0% |

### 6.2.5. Percentage of Variance between Variables

Given the values of correlation, the coefficient of determination can be calculated. That is the indicator of the amount of variance that the two variables share. The computation is simply a square on the correlation value and then converted to a

percentage of variance. To combine the results on the basis of the two classifiers on low back support and vertices, the percentages of variance are averaged across various groups. Table 6.63 shows the percentages of variance in the variable set. The interpretation can be achieved by highlighting those bivariate sets with a high percentage of variance and then eliminating those with a low percentage of variance. The bivariate sets are consistently interpreted by comparing the previous findings on statistical percentages integrating various correlation groups. The overall scores (OV) and neck-specific function (NS) have improved variance with the multifractal parameters. Regarding the multifractal parameters, the mean of the singularity exponent ($h_q$) has the highest variance with various NPAD factors. Next are the width of $h_q$ and mean of singularity dimension $D_q$ .

Table 6.63. Percentage of variance of each bivariate set.

| | **OV** | **PA** | **DI** | **NS** | **EC** |
|---|---|---|---|---|---|
| **Mean of $h_q$** | 3% | 7% | 6% | 8% | 6% |
| **Width of $h_q$** | 7% | 6% | 4% | 6% | 4% |
| **Mean of $D_q$** | 7% | 6% | 3% | 5% | 4% |
| **Height of $D_q$** | 7% | 5% | 4% | 2% | 5% |

## 6.3. Discussion

Regarding the NPAD factors, OV and NS have improved variance with the multifractal parameters. Regarding the multifractal parameters, the mean of the singularity exponent ($h_q$) has the highest variance with various NPAD factors. Next are the width of $h_q$ and mean of singularity dimension $D_q$. Among those multifractal parameters, the one that is hypothesized to be the most important is the width of $h_q$ . It provides the width of the multifractal spectrum. This could be related to the possible level of motor control in the participant for controlling the movement of cervical spinal curvature. Because the means of $h_q$ and $D_q$ are the average within the multifractal spectrum, this could provide a hint on the probability of the moving trend regarding the human movement performance, and hence, the motor control mechanism.

Investigation on the difference in the correlation with respect to the feature points reveals a general trend. At the lowest end of the correlation relationship, that is, the minimal correlation group, higher percentages are found at M5 and M6. In the small correlation group, higher percentages are found at M4 and M5. M5 and M6 have a weak correlation between the NPAD factor and multifractal parameters. By contrast, at the higher end of the correlation relationship, that is, the large and medium correlation groups, a high percentage can be found at M3, and then at M4. Summarizing the findings, there is a general trend from high to low correlation when traversing from M3 to M6.

From the discussion in the previous chapter, under the multifractal analysis, the whole cervical spine can be observed to have the upper and lower region. The

upper region could be related to the small magnitude time scale associated with fine spinal curvature movement. The lower region could be related to the large magnitude time scale associated with coarse spinal curvature movement. On the basis of the correlation analysis on feature points, the upper region, that is, M3 and M4, has a comparatively stronger correlation to both the NPAD scores and multifractal parameters. This result provides evidence for the design criteria mentioned previously regarding the wearable devices. One of the aims in this study is to provide evidence for design criteria in monitoring spinal curvature movement, which can eventually improve the understanding of movement performance or preventive measures. The findings provided an association for the design criteria of wearable devices. The feature points or points of capture would be more obvious if they are in the upper cervical region. The data points captured can be computed to provide an overview about the multifractal parameters, which in turn could be correlated to the NPAD scores and factors. Although this study shows evidence in the design application and criteria of relationships, further investigation is needed to generalize the findings.

This study has several limitations that require consideration. First, the number of participants in the experimental group is relatively small, which diminished the statistical power of the study and its ability to detect correlations. The participants recruited are in general healthy. Although some had higher scores in the NPAD instrument, the spectrum between healthy and pathological participants is relatively narrow. In addition, the NPAD scores are subjective to the participant's

instantaneous feeling and interpretation of the questionnaire. Although the instrument has been validated for accuracy and reliability, the variety of background of the participants and, most importantly, they do not have the gold standard in giving the answers to the scales. The validation of scores can increase in confidence if there are objective instruments to cross-correlate the scores. Nonetheless, the research findings conclude that positive correlation relationships exist between the NPAD instrument scores and multifractal parameters. This correlation relationship exists from the perspectives of NPAD scores, multifractal parameters, and feature points in the cervical region.

# Chapter 7.
# Summary and Discussion on Findings and Applications

In the previous chapter, results show that there are correlated relationships between various neck pain factors of NPAD scores and parameters extracted from the multifractality structure. This provides hints on possible neck pain issues on the basis of the numerical data captured and computed. In this chapter, the implication on the design criteria of wearable devices for health is explored.

In the first section, the research findings from the computation of spinal curvature on the basis of SDA are summarized. Results show that dynamic features exist and can be extracted. These features exhibit under the condition of body sway at the static posture of sitting upright. The outcome of the analysis provides a nonanalytical approach to understanding the motor control mechanism that governs the human movement.

In the second section, the research findings from the computation of the cervical spinal are summarized based on MFDFA. Results show that there are correlated relationships between the NPAD and MFDFA.

The third section is a summary of key features as a part of the design strategy for wearable technology and apps for healthcare. With the sensing capability and seamless connection with mobile phones, wearable devices are an upcoming trend. However, the expected feature requirement from the consumer side is also increasing. Some of these major keywords are described here, together with an introduction of a prerelease neck wearable device.

The fourth section focuses on the specific and crucial issues within the design space for developing a wearable computing system. The concerns are placed on the active

relationship between wearable devices and the human form. A number of aspects are considered and defined in the design guidelines.

In the fifth section, on the basis of the identified correlations and significance in features, these features are used to define the priority on the importance or the weighting of each variable within the parameter set. These findings help to obtain the weighting factors for the extraction of participant variables, that is, the trace of neck pain issues, for the purpose of a definite set of design criteria and movement monitoring by using wearable devices. The criteria on sensing movement are also illustrated by examples and findings from the market.

The final section summarizes the other challenges in wearable technology, such as the interface and interactive experience. These include the user interface, cognitive model, contextual awareness, and adaptation to tasks.

## 7.1. Findings from SDA

By using SDA, the spinal curvature is modeled to determine whether the dynamic features exist under the condition of body sway at the static posture of sitting upright. The outcome of the analysis could give an association and a nonanalytic approach to understanding the motor control mechanism that governs human movement. Data were captured along spinal segments from the cervical to sacrum region. The spinal curvatures, measured as angles in degree, were calculated based

on various feature points and data intervals between ordered markers. There were altogether 49 angles extracted. After a series of computational processes for SDA, results on dynamic features were extracted.

From the 49 angles calculated, there were 47 angles with a critical time. The results were significant with a score of 96%. The results were further ascertained by entering the dummy capture into the computational processes for SDA. None of the data trials from the dummy were found to have a critical time. This provided strong evidence that the dynamic features extracted were due to human movement instead of noise characteristics from motion capture data.

Regarding the parameters describing the control mechanism, that is, the persistency of open- and closed-loop behavior, the data also showed positive and consistent results across. Because 96% of the data were found with a critical time, there was a difference in the diffusion coefficient of the short term ($D_s$) and long term ($D_l$). The literature reveals that in the case of exhibiting control behavior, $D_s$ is larger than $D_l$. From the analysis, results found that 100% of the data, from those with a critical time, followed this evidence of control behavior. There are two outliers on the parameter $D_s$ and one on $D_l$ .

In relation to the diffusion coefficient, also 100% of the data were found with distinguished values on the Hurst exponent in both the short term ($H_s$) and long term ($H_l$). The $H_s$ was found consistently between 0.675 and 0.868, which denoted the open-loop region exhibiting a persistent and positively correlated control behavior. The values of $H_l$ were found having a mean of 0.231 and a standard

deviation of 0.148. This was consistent with the literature findings on closed-loop behavior. Table 7.1 shows the summary of findings from the analysis.

Table 7.1. Summary of findings on extracted dynamic parameters.

| **Dynamic Parameters** | **Features** | **Outcome Measurement** |
|---|---|---|
| Critical Time (Δt) | Identified | 96% |
| Diffusion Coefficient | Distinguishable between short and long term | 100% (based on Δt identified) |
| Short-term Diffusion Coefficient ($D_S$) | Smaller than $D_l$ | 100% (based on Δt identified, with 2 outliers) |
| Long-term Diffusion Coefficient ($D_l$) | Larger than $D_s$ | 100% (based on Δt identified, with 1 outlier) |
| Hurst Exponent | Distinguishable between short and long term | 100% (based on Δt identified) |
| Short-term Hurst Exponent ($H_s$) | Smaller than 0.5 | 100% (based on Δt identified) |
| Long-term Hurst Exponent ($H_s$) | Larger than 0.5 | 98% (based on Δt identified) |

After the development of the analysis model and assessment of the protocol, the methodology was applied to two situations on the basis of the hypothesis that participants who had different characteristics would exhibit different dynamic features in control.

The first experiment was conducted to distinguish the features of spinal control in the cervical region between patients and normal participants. The same SDA was computed on the captured data of both patients and normal participants. On the basis of the hypothesis from the literature review, the results are summarized in

Table 7.2. In conclusion, the difference between patients and normal participants was successfully identified using the variations in dynamic parameters.

Table 7.2. Results of dynamic parameters compared between patients and normal participants.

| **Dynamic Parameters** | **Patient** | **Normal** | **Outcome Measurement** |
|---|---|---|---|
| Critical Time | Identified | Identified | 100% |
| Critical Time | Longer | Shorter | 100% |
| Diffusion Coefficient | Distinguishable | Distinguishable | 100% |
| Diffusion Coefficient (short-term) | Smaller than long-term | Smaller than long-term | 100% |
| Diffusion Coefficient (long-term) | Larger than short-term | Larger than short-term | 100% |
| Diffusion Coefficient (short- and long-term) | Larger | Smaller | 75% |
| Hurst Exponent (short-term) | > 0.5 | >0.5 | 100% |
| Hurst Exponent (short-term) | Smaller | Larger | 100% |
| Hurst Exponent (long-term) | < 0.5 | < 0.5 | 100% |

The second experiment was conducted to explore the dynamic features of spinal postural control by using SDA for the effects of age and gender in relation to the development of children. The same SDA was computed on the captured data of all male and female students aged 11 and 15 years. On the basis of the hypothesis from the literature review, the results are summarized in Table 7.3. In conclusion, the difference between 11 and 15 year-old children was successfully identified using the variations in dynamic parameters.

Table 7.3. Results of dynamic parameters compared between 11 and 15 year old children.

| **Dynamic Parameters** | **11 years old** | **15 years old** | **Outcome Measurement** |
|---|---|---|---|
| Critical Time | Identified | Identified | 100% |
| Critical Time | Longer | Shorter | 83% |
| Diffusion Coefficient | Distinguishable | Distinguishable | 100% |
| Diffusion Coefficient (short-term) | Smaller than long-term | Smaller than long-term | 100% |
| Diffusion Coefficient (long-term) | Larger than short-term | Larger than short-term | 100% |
| Diffusion Coefficient (short- and long-term) | Larger | Smaller | 96% |
| Mean Square Angle | Larger | Smaller | 100% |
| Hurst Exponent (short-term) | > 0.5 | > 0.5 | 100% |
| Hurst Exponent (short-term) | Smaller | Larger | 58% |
| Hurst Exponent (long-term) | < 0.5 | < 0.5 | 100% |

## 7.2. Findings from MFDFA

The experiment was set up to study the cervical spine movement on the basis of the assessment and six feature points from C2 to C7. The participants were a healthy participant group aged from 19 to 25 years. The whole experiment was divided into two parts. One is the neck pain assessment on the basis of the NPAD instrument. The other part is the optical motion capture of the feature points. The participants were asked to finish the questionnaire and then to sit upright for 30 seconds during the capture for various trials.

The total NPAD score is calculated from all the questions answered. The higher the score is, the less favorable the neck pain and disability is. Regarding the NPAD score, the questions can be categorized into a few factors, namely “pain”, “disability”, “neck-specific function”, and “emotion and cognitive influences”. These various factors are the basis for the correlation test on fractal analysis. From the healthy participant group recruited, on the basis of the descriptive statistics analysis, there exists a spectrum of variation among the participants. To ascertain the consistency in the assessment, the participant list was arranged into a sorted order according to various factors. The participant list resulted in a consistent sorted order as shown in Table 7.4. Along the horizontal axis starting from left to right, an increase in scores considering all the factors is indicated. The vertical axis indicates the percentages of occurrence in various ranked orders, starting with the ranking of the lowest score at the top. With this ranking in order, the results of fractal analysis can then be correlated with this list to explore the relationship in between.

Table 7.4. Sorted order on the sequence of participant in ascending order (from left to right) in consideration of occurrence among different factors.

| **S01** | **S09** | **S11** | **S02** | **S04** | **S07** | **S05** | **S03** | **S08** | **S06** | **S10** |
|---|---|---|---|---|---|---|---|---|---|---|
| 60% | 40% | | | | | | | | | |
| 40% | 40% | | | 20% | | | | | | |
| | | 80% | 20% | | | | | | | |
| | | | 80% | 20% | | | | | | |
| | 20% | 20% | | 20% | 20% | 20% | | | | |
| | | | | 20% | 60% | | 20% | | | |
| | | | | | 20% | 60% | | 20% | | |
| | | | | 20% | | | 40% | 20% | 20% | |

| | | | | | | | | | | |
|---|---|---|---|---|---|---|---|---|---|---|
| | | | | | | 20% | 20% | 60% | | |
| | | | | | | | 20% | | 80% | |
| | | | | | | | | | | 100% |

On the basis of the motion capture data of feature points from the participant group, the computation for MFDFA was conducted. Most of the steps in the application of MFDFA are similar to those described in the literature. However, like all other fractal analysis methods, MFDFA requires the careful consideration of signal properties, parameter settings, and the interpretation of results.

1. In this study, the motion capture data are transformed into angles that can represent the output of the motor control mechanism as a whole in describing the movement for each spinal segment.
2. To investigate the time series, monofractal DFA is conducted, and the Hurst exponent (H) value is used to determine the nature of the noise. From the plots, H is between 1.2 and 1.8, which describes the cervical spine movement as random walk.
3. The local fluctuation in the time series is computed as a local RMS; it cannot be close to zero within the biomedical time series. If that is the case, an extremely large H results for the negative q-th order, which leads to large right tails in the multifractal spectrum.
4. By contrast, the time series should exist with local fluctuations. If those cannot be found, the local trend line can fit the original time series well, resulting in RMS values close to zero.

5. The other situation arising from not having substantial observable local function is that the RMS plots might be smooth without apparent variation, particularly at the lower order end. Therefore, the value of the smallest scale needs to be checked carefully.

From the MFDFA results on the multifractality structure, some of the multifractal parameters are particularly selected for illustration. These include the mean of the singularity exponent ($h_q$), width of $h_q$ , mean of the singular dimension ($D_q$), and height of $D_q$ . To ascertain the existence of the multifractality structure as extracted from the physiological signal, instead of a general property arising from noise signal, a shuffling process on time series was conducted and tested for multifractality structure. Table 7.5 shows the difference in statistical results between the original and shuffled time series. From the sample test on significance, all the four multifractal parameters are significantly different between the original and shuffled time series. That means the multifractality structure is found from the behavior of the physiological signal, and hence, the cervical spine movement.

Table 7.5. Difference on the multifractal parameters between original and shuffled data series.

| | **Original Time Series** | | **Shuffled Time Series** | | **Significance on Sample Test** |
|---|---|---|---|---|---|
| | **Mean** | **Standard Deviation** | **Mean** | **Standard Deviation** | |
| **Mean of $h_q$** | 1.215 | 0.102 | 0.507 | 0.026 | 0.00 |
| **Width of $h_q$** | 0.673 | 0.141 | 0.116 | 0.084 | 0.00 |
| **Mean of $D_q$** | 0.704 | 0.067 | 0.953 | 0.041 | 0.00 |
| **Height of $D_q$** | 0.824 | 0.138 | 0.206 | 0.141 | 0.00 |

The analysis confirms that the multifractality structure exists in the spinal curvature of the cervical region in the experimental set of the sitting upright posture. Investigation is then conducted on whether there is a difference between participants and how the various multifractal parameters differ when comparing across participants. The participants are ranked according to various multifractal parameters. The correlation analysis is conducted afterward on the basis of the ranked participant list. Table 7.6 shows the large correlation results across the selected multifractal parameters. The corresponding significance level is shown in Table 7.7. By observing the relationship, it can be found that among the seven variables, there are two clusters of variables with a stronger relationship with each other than those in the other cluster. The two clusters are (mean of $H_q$, mean of $h_q$, height of $D_q$) and (range of $H_q$, mean of $t_q$, width of $h_q$, mean of $D_q$). Moreover, on the basis of the significance level, there is another bivariate set worth mentioning. That is (mean of $H_q$, mean of $D_q$). It has a significance level of 0.96 in terms of correlation. That means the two variables are significantly not correlated with each other. Hence, they have a percentage of variance equal to 0%.

Table 7.6. Large correlation results on the multifractal parameters.

| | **Mean of $H_q$** | **Range of $H_q$** | **Mean of $t_q$** | **Mean of $h_q$** | **Width of $h_q$** | **Mean of $D_q$** | **Height of $D_q$** |
|---|---|---|---|---|---|---|---|
| **Mean of $H_q$** | 1.00 | | | 0.95 | | | 0.64 |

| | | | | | | | |
|---|---|---|---|---|---|---|---|
| **Range of $H_q$** | | 1.00 | 0.86 | | 0.99 | 0.88 | |
| **Mean of $t_q$** | | 0.86 | 1.00 | | 0.82 | 0.64 | |
| **Mean of $h_q$** | 0.95 | | | 1.00 | | | 0.58 |
| **Width of $h_q$** | | 0.99 | 0.82 | | 1.00 | 0.91 | |
| **Mean of $D_q$** | | 0.88 | 0.64 | | 0.91 | 1.00 | |
| **Height of $D_q$** | 0.64 | | | 0.58 | | | 1.00 |

Table 7.7. Significance level on the multifractal parameters.

| | **Mean of $H_q$** | **Range of $H_q$** | **Mean of $t_q$** | **Mean of $h_q$** | **Width of $h_q$** | **Mean of $D_q$** | **Height of $D_q$** |
|---|---|---|---|---|---|---|---|
| **Mean of $H_q$** | 0.00 | 0.59 | 0.48 | 0.00 | 0.75 | 0.96 | 0.04 |
| **Range of $H_q$** | 0.59 | 0.00 | 0.00 | 0.42 | 0.00 | 0.00 | 0.36 |
| **Mean of $t_q$** | 0.48 | 0.00 | 0.00 | 0.30 | 0.00 | 0.04 | 0.54 |
| **Mean of $h_q$** | 0.00 | 0.42 | 0.30 | 0.00 | 0.56 | 0.79 | 0.06 |
| **Width of $h_q$** | 0.75 | 0.00 | 0.00 | 0.56 | 0.00 | 0.00 | 0.45 |
| **Mean of $D_q$** | 0.96 | 0.00 | 0.04 | 0.79 | 0.00 | 0.00 | 0.37 |
| **Height of $D_q$** | 0.04 | 0.36 | 0.54 | 0.06 | 0.45 | 0.37 | 0.00 |

After the investigation of participant variation, the two sitting conditions are compared. One requires the participants to sit on a seat with low back support, and the other condition is without the support. The two conditions are compared to

observe whether there is any major difference in terms of the multifractal parameters. Table 7.8 shows the statistical results between the two conditions according to various multifractal parameters. It can be found that there is no significant difference between the two conditions because all the values are above 0.05.

Table 7.8. Selected multifractal parameters under the two support conditions.

| | **Without low back support** | | **With low back support** | | **Significance on Sample Test** |
|---|---|---|---|---|---|
| | **Mean** | **Standard Deviation** | **Mean** | **Standard Deviation** | |
| **Mean of $h_q$** | 1.215 | 0.102 | 1.207 | 0.074 | 0.571 |
| **Width of $h_q$** | 0.673 | 0.141 | 0.693 | 0.132 | 0.323 |
| **Mean of $D_q$** | 0.704 | 0.067 | 0.699 | 0.055 | 0.581 |
| **Height of $D_q$** | 0.824 | 0.138 | 0.834 | 0.143 | 0.640 |

The analysis shows that the data from cervical spine curvature exhibit the multifractality structure. That is the first major achievement in this study. It also includes the methodology and consideration that the multifractal analysis can be adopted into the particular type of physiological signal of this study. Furthermore, the second achievement is to explore the variation space that the multifractality structure could possibly be given on the basis of this experimental participant set. The consistency of participant ranking shows that the variation space exists in a consistent manner. The next attempt is to explore the correlation between the NPAD instruments for neck pack assessment, and the motion capture for MFDFA

computation. First, analysis is conducted on the two separate sets of variables. The aim is to ascertain that the findings are consistent. Table 7.9 shows the significance level on the NPAD score factors resulting from the Spearman rank correlation analysis. The experiment data are consistent with a number of bivariate sets with $p < 0.05$. Table 7.10 shows the significance level on the multifractal parameters. Again, there are a few bivariate sets with $p < 0.05$. In conclusion, the two separate sets of variables on the basis of the experiment data on NPAD and MFDFA are consistent.

Table 7.9. Significance level on the NPAD score factors.

| | **OV** | **PA** | **DI** | **NS** | **EC** |
|---|---|---|---|---|---|
| **OV** | 0.00 | 0.95 | 0.16 | 0.27 | 0.07 |
| **PA** | 0.95 | 0.00 | 0.00 | 0.00 | 0.00 |
| **DI** | 0.16 | 0.00 | 0.00 | 0.00 | 0.00 |
| **NS** | 0.27 | 0.00 | 0.00 | 0.00 | 0.00 |
| **EC** | 0.07 | 0.00 | 0.00 | 0.00 | 0.00 |

Table 7.10. Significance level on the multifractal parameters.

| | **Mean of $h_q$** | **Width of $h_q$** | **Mean of $D_q$** | **Height of $D_q$** |
|---|---|---|---|---|
| **Mean of $h_q$** | 0.00 | 0.50 | 0.96 | 0.22 |
| **Width of $h_q$** | 0.50 | 0.00 | 0.00 | 0.00 |
| **Mean of $D_q$** | 0.96 | 0.00 | 0.00 | 0.00 |
| **Height of $D_q$** | 0.22 | 0.00 | 0.00 | 0.00 |

The correlation analysis then involves the exploration of the relationship between the two separate sets of variables. The aim is to explore the possible relationship between subjective neck pain issues and the fractal analysis parameters. This

provides hints on possible neck pain issues on the basis of the noninvasive numerical data captured and computed. It can further serve as a foundation for the design and technical guidelines on how the wearable devices can be developed to capture the issues within the cervical region. Table 7.11 shows the percentages of variance in the variable set. The interpretation can be achieved by highlighting those with a high percentage of variance and then eliminating those with a low percentage of variance. Although the values on variance are not significantly high to indicate the close correlation relationship, all the bivariate sets can be consistently interpreted.

Table 7.11. Percentage of variance of each bivariate set.

| | **OV** | **PA** | **DI** | **NS** | **EC** |
|---|---|---|---|---|---|
| **Mean of $h_q$** | 3% | 7% | 6% | 8% | 6% |
| **Width of $h_q$** | 7% | 6% | 4% | 6% | 4% |
| **Mean of $D_q$** | 7% | 6% | 3% | 5% | 4% |
| **Height of $D_q$** | 7% | 5% | 4% | 2% | 5% |

As described in previous chapters, each individually identified correlation value and significance value can be used to define the priority on the importance or the weighting of each variable within the parameter set. Moreover, the correlation values across various variables can indicate the relationship and also the weighting factors for the extraction of subjective variables, that is, the trace of neck pain issues. These are related to how the system can be defined and designed for the purpose of movement monitoring by using wearable devices.

In this study, an experimental pilot was conducted to generate data to explore the feasibility of adopting the analysis method and to guide the design criteria on engineering the wearable devices. It is particularly necessary here because there is no data from previous studies to inform this process. Although the experiment set here is a small sample size pilot, the participants chosen could be representative of the target study population. The participants chosen were also on the basis of the inclusion and exclusion criteria. On the basis of the results from participant space evaluation, the participant group could be representative with a variation ensuring that the key features of the study are preserved in this pilot. Moreover, the data acquisition is conducted blindly in randomized controlled trials. To further extend this study with a sample size, a common formula for obtaining a 95% confidence interval approach for a single proportion is illustrated as follows:

$$C_p = \pm Z_\alpha \left( \sigma_p \right)$$

where $C_p$ is the confidence interval in terms of proportions; $Z_\alpha$ is the Z score for levels of confidence, with the value most commonly set at 1.96 for a 95% confidence level; and $\sigma_p$ is the standard error for a distribution of sample proportions, as follows:

$$\sigma_p = \sqrt{\frac{p\,(1-p)}{n}}$$

where p is the prior estimate of the proportion of interest, and n is the sample size. Solving for n yields the following:

$$n = \left( \frac{Z_\alpha \sqrt{p\,(1-p)}}{C_p} \right)^2$$

A 95% level of confidence and a confidence interval of 10% are applied. These are set for not exceeding the typical values on the basis of the reason that this experimental pilot is the first attempt of this research methodology. With the statistical outliers identified during the analysis, the expected completion rate is estimated to be 75%. The required sample size is therefore at least 73 participants. This would give an estimation for a further study to proof of research findings as for the participant population needed.

## 7.3. Wearable Devices for Health

Although the smartphone remains as the device of choice for everyday life, the advancement of technology is creating and enabling the wearable devices to deliver a variety of benefits to consumers, with a lower cost for healthier lives. A number of different health and wellness applications have been created, together with their corresponding wearable devices. They range from fitness bands that monitor sleep patterns and daily activity to flexible attachments that detect the heat rate, body temperature, hydration level, and more. The wearable devices capture human body data, which in turn enable analytics. The information can then provide feedback to consumers for managing their health and behavior. The improvement of care

services and potential reduction in costs through remote monitoring are also what healthcare entities are interested.

The findings from sections before contribute in a way to give hints on possible neck pain related issues based on the noninvasive numerical data captured and computed. From laboratory experimental environment with specific capturing procedures, moving to wearable devices targeting for movement monitoring purposes, there are definitely other technical difficulties need further research efforts in order to overcome. The current findings can serve as a foundation on the design and technical guidelines on how the wearable devices can be developed and advanced forward to capture the healthcare issues.

Wearable technology has become cheaper in cost and more sophisticated in functionality. Data quality has also improved substantially. The assembled devices and their associated applications are becoming part of the consumer life and ecosystem of health. The demand from consumers is also increasing. Devices must be produced with seamless integration and be interoperable, self-sufficient, and self-enabling at both user and system levels. The software of the wearable devices has been emphasized as much as the hardware. Potential improvement of health is always one of the major criteria for consumers to consider when choosing wearable devices and associated applications.

A crucial part of the design strategy for a wearable system is to maintain consumer engagement beyond the first few weeks of use. Companies would consider user experience and design for novelty, incentives, rewards, and truly actionable insights.

For variability of user experience, wearable devices, applications, and their associated platforms must be flexible enough. At the research side, the algorithms must be developed for sophistication that can transform user data into insights for consumers and/or health organizations. These insights would require a seamless integration into the life of consumers, clinical workers, and health-related entities. In summary, there are a few keywords to describe the features of wearable technology and apps, as shown in Table 7.12 [129].

Table 7.12. Key features of wearable technology and apps.

| | |
|---|---|
| **Intelligent** | Intelligent so they provide user insights |
| **Interoperable** | Interoperable with other devices and apps |
| **Integrated** | Integrated into the consumer's life and into the life cycle of care |
| **Social** | Social so insights can be shared based on user preference |
| **Engaging** | Engaging so they inspire consumers to use them |
| **Outcomes-based** | Outcomes-based for consumer, healthcare practitioner or other healthcare partner |

From the previous literature, a high percentage of the population experience neck pain and associated problems. Probably the most common are individuals with office jobs, which generally involve leaning forward toward the computer monitor and keyboard. There is the need for a device that is worn similarly to a necklace and designed to monitor head and neck movement to improve posture. The Fineck device, currently at the prerelease stage of a start-up business, aims to address neck pain by tracking head movements, identifying bad habits, and suggesting exercises via gaming experience [130]. It claims to be the first wearable device for the neck

that keeps track of continuous neck activity and provides feedback and even warning for unfavorable posture for a prolonged period of time. Currently, the technical details about the analytics of the capture are protected as the intellectual properties of the company. By capturing movement through two device components, one at the front and one at the back, it clearly captures the overall movement in the neck and shoulder region. However, there is a high possibility that it cannot capture the fine movement of the neck on the basis of the spinal segment configuration, which is also one of the research gaps in cervical spine movement analysis.

## 7.4. Design Consideration on Wearable Attributes

According to a study, design for wearability focuses on a specific and important issue within the design space for a developing wearable computing system [127]. It concerns the physical shape of wearable devices and their active relationship with the human form. In relation to that, design guidelines have been developed to address the wearability. The guidelines have been designed to include a few perspectives. The wearable object is the first concern. This involves the exploration of history and cultures regarding numerous topics including clothing, costume, protective wearable devices, and a variety of carried devices. Directly related to the wearable object is the human body. It focuses on the form and dynamics, which

include physiology and biomechanics, as well as the movements of modern dancers and athletes. Regarding the interaction between the wearable object and the human body, the design value is an essential concern. The value is produced from the manner in which people prepare, compromise, and construct themselves with what they wear and carry. The findings involve the research of more than two dozen generations of wearable computers, representing more than 100 person years of research; the results are codified into guidelines for designing wearable systems. The results are summarized in Table 7.13 [127, 128].

Table 7.13. Design for wearability attributes.

| **Attributes** | **Comments** |
|---|---|
| Placement | Identify where the computer should be placed on the body. Issues include identifying areas of similar size across a population, areas of low movement/flexibility, and large surface areas. |
| Humanistic form language | The form of the object should work with the dynamic human form to ensure a comfortable fit. Principles include inside surface being concave to fit body, outside surface being convex to deflect objects, tapering sides to stabilize form on body, and radiusing edges and corners to provide soft form. |
| Human movement | Many elements make up a single human movement: mechanics of joints, shifting of flesh, and flexing and extending of muscles and tendons beneath the skin. Allowing for freedom of movement can be accomplished in one of two ways: by designing around the more active areas of the joints or by creating spaces on the wearable form into which the body can move. |
| Human perception of size | The brain perceives an aura around the body. Forms should stay within the wearer's intimate space, so that perceptually they become a part of the body. (The intimate space is between 0 and 5 inches off the body and varies with position on the body.) |
| Size variations | Wearable devices must be designed to fit many types of users. Allowing for size variations is achieved in two ways: (1) use of static anthropometric data, which detail point-to-point distances on |

| | |
|---|---|
| | different-sized bodies, and (2) consideration of human muscle and fat growth in three dimensions using solid rigid areas coupled with flexible areas. |
| Attachment | Comfortable attachment of a form can be created by wrapping the form around the body, rather than using single-point fastening systems such as clips or shoulder straps. |
| Contents | The system must have sufficient volume to house electronics, batteries, and so on, which in turn constrains the outer form. |
| Weight | The weight of a wearable should not hinder the body's movement or balance. The bulk of the wearable object weight should be close to the center of gravity of the human body, minimizing the weight that spreads to the extremities. |
| Accessibility | Before purchasing a wearable system, one should walk and move with the wearable object to test its comfort and accessibility. |
| Interaction | Passive and active sensory interaction with the wearable should be simple and intuitive. |
| Thermal | The body needs to breathe and is very sensitive to products that create, focus, or trap heat. |
| Aesthetics | Culture and context will dictate shapes, materials, textures, and colors that perceptually fit users and their environment. |

The placement of the wearable device for neck movement monitoring should be located around the neck. For reasons related to the physiological activities involved in capturing the cervical spine movement, the measurement device is recommended to be placed in the upper region of the neck. Because of the differences in the body's shape, however, it is difficult to perform measurements at the exact same location each time.

The form factor of an interactive device is one of the biggest concerns nowadays. It concerns the product design and should also take fashion as one of the major requirements. Fashion accessories in wearable devices usually require features of lightweight, strong durability, and excellent appearance. Particularly when all-day

wearing is concerned, humanistic form language would be defined in parallel with various situations within a whole day-long journey.

Similar to the concern on the differences in the placement of wearable devices according to various body shapes, human movement also occurs in a similar manner. The neck has a large degree of freedom according to the various complicatedly aligned spinal segments in place. The design on how to take the movement into an accurate input and then digitalize the movement into data for analysis is definitely a challenge.

Wearable devices are now gaining image and branding in personal accessories, clothing, and even jewelry. The daily practice for users is to simply wear the device on, in, or around the body. The devices seamlessly incorporate sensors and connect with other electronic technology. Wearable devices on the neck are perceived as a necklace, which is one of the most identifiable accessories. Consumers' high expectation in perception must be met.

To further consider the wearable device as a commercial product, variables in human anthropometric data, for example, body size, proportion, and shape, must be taken into account. Moreover, the concern must be seriously considered if the product is targeted at the global market. According to studies on anthropometry, people of various races have various characteristics. Regarding a sensor on the neck, which, in turn, can affect the acquisition of human movement data because of the sensor position around the neck, power of sensitivity, geometrical alignment, etc. because of the muscle and fat exist around the neck.

Because wearable devices have become a part of clothing that is worn for many hours a day before being taken off, comfortable fitting on the human body is crucial. To acquire the neck movement, the easiest method is to attach sensors such as accelerometers along the cervical spine region. However, attachment is not usually favorable because of the discomfort between the attaching surface and the skin.

As discussed in the previous chapter, the choice of electronic components inside the device is a difficult decision to make. There are numerous concerns such as limited functionality, power consumption, the type of movement-sensing mechanism, and accuracy. If placed around the neck, the wearable device cannot be a huge bulky box.

Weight is another design concern. This study is about neck pain; by introducing the neck wearable device, it should not introduce any negative influence on the neck, especially factors of pain and fatigue.

For any wearable device, it is crucial to consider the degree of freedom on accessibility necessary for the product to be effective and efficient. That is the reason why experiments must be conducted to investigate the kinematic access on the human body. Regarding a wearable device for the neck, the kinematics on and around the neck is the primary concern. Because neck pain can also occur in a radiated manner, upper body movement is part of the concern.

Sensory interaction, either passive or active, is a crucial aspect of a wearable product. Functional features are not possible if the data acquisition process is not

smooth. In addition, a balance between attention and seamless interaction is also a complex design concern. In general, interaction should be simple and intuitive.

There are three thermal aspects of designing objects for the body, namely functional, biological, and perceptual. The body must breathe, especially around the neck and trachea, and is sensitive to products that create, focus, or trap heat.

A crucial aspect of the form and function of any wearable device is aesthetics. Culture and context dictate shapes, materials, textures, and colors that perceptually fit the users, their environment, and various daily situations.

The aforementioned design guidelines include the essential and crucial aspects of designing wearable devices. The concern in relation to the present study of the neck is also described. The guidelines communicate a means to consider all the issues involved when creating a wearable form.

In relation to the previous example on Fineck [130], the device contains sensors, specifically, an accelerometer and a gyroscope, to monitor movement. In addition, there is a motor that vibrates. The housing of electronic components is made of titanium to achieve a lightweight and durable product. Another advantage of using a titanium casing is that the material is approved to be stable for human attachment and also has low risk for allergy. The shape of the curve around the neck is based on human factor analysis for optimum fitting. Because the device is connected to smartphones, through the user interfaces, users can realize their unfavorable habits and play neck-training games. The application can record user activities for constructing a health profile. It warns users of any potential health risks and vibrates

to remind them of proper sitting posture. Similar to other wearable applications, it also allows users to set a target. The Fineck has a battery life of approximately seven days and requires one hour to charge. The retail price is set at RMB 599.

This is a summary and case study of design for wearability attributes. Several aspects from the design guidelines are considered and well defined for a product that is intended for users in the market.

## 7.5. Criteria on Sensing Movement

The design for motion-sensing devices includes the acquisition of the motion characteristics of an object in three-dimensional space. In the case of the acquisition of neck movement in the cervical spine region, the angular relationship between the spinal segments of C2 and C7 must be captured. From the correlation results reported in previous chapters, M3 and M4 feature points have a more favorable correlation relationship for multifractal parameters and neck pain factors. These findings lead to the sensing criteria on the degree of freedom with regard to the mechanism of movement-sensing components. After the previous chapters of analysis, design requirements and criteria can be concluded to reflect the concerns regarding the portable device specifically on the basis of this study.

The term “portable” implies the essential consideration of weight and size. With reference to the Fineck [130], to minimize the weight of the product, the electronic

components are cased in titanium. This metal has a few advantages for the application of wearable devices. Titanium has strength, durability, and vibration-dampening characteristics that make it an ideal material for premium wearable devices. It is often made by an alloy of titanium into seamless, aerospace-grade titanium. Compared to other often used materials such as aluminium, titanium has a high strength-to-weight ratio, making it an ideal lightweight and durable choice for portable purposes. The size often depends on the choice of components. The necessary components here include the accelerometer and gyroscope for sensing and monitoring movement. For feedback purpose, a motor is needed for vibration.

Considering the details of motion sensing, the device must have adequate sensitivity to meet the numerical requirement on the data captured. On the basis of the previous chapters about the measurement of cervical curvature, for static upright sitting, the statistical range of angular movement is approximately $10^{o}$ with a standard deviation of $1.5^{o}$. These numbers imply that the angular resolution of captured data must be significant with one decimal place measured in degree. This is the criteria on the resolution that chosen electronic devices must meet.

In relation to resolution, frequency is another crucial criteria in capture signal along time series. Frequency determines how fast the sensing process must happen. The measurement is usually achieved in frame per second. When preparing the time series data, a Butterworth low pass filter is applied to clean and separate the signal from high-frequency digital noise. Together with the reference on research findings regarding the processing physiological signal of human movement, the cut-off

frequency is set to 10 Hz. This can be the minimum requirement for the wearable device. In addition, on the basis of the concept of the fractal structure, the scale invariant factor can be taken into consideration. It describes the similarity of signal behaviour in relation to the frequency of time sampling. The frequency chosen here for movement acquisition could be lowered, but this is yet to be confirmed by further analysis through experiments.

Accuracy is the criteria that determine the amount of data output that is reliable in measurement. On the basis of the signal measurement in previous chapters, the signal-to-noise ratio of the data from the optical motion capture system has an average of 8.4. That means the measurement of the signal level is eight times more than the noise. This method determines whether the captured signal from an object is reliable.

Cost is an essential parameter for both the device manufacturer and consumers. Motion-sensing products require a large portion of the design budget because precise motion-sensing component choices are limited and traditionally expensive. In addition, the mounting of the device is another concern. To the extent of retrieved research findings, there is no wearable device that can capture the neck movement, except the Fineck [130]. As a result, no price comparison can be conducted. For reference, the online selling price of a Fineck is currently RMB 599. Generally, the price is set near the low end (compared to Figure 7.1, currency in USD) in terms of various wearable devices in the market, regardless of the variety of body locations [153]. The products cover a wide range of variety including locations

on the wrist, legs, torso, and head. At the time of the report, information for 233 wearable devices was collected and analyzed.


Figure 7.1. Wearable device price statistics as of 2014 Q1 and Q2, currency in USD.

The battery-powered portable motion-sensing device must maintain the power consumption of all components at the lowest possible level to maximize the operating time. The device must be wearable for at least a day, with continuous wearing in daily practice. With reference to the Fineck [130], the power consumption criteria are set with a battery life of approximately seven days and it requires one hour to charge. The specification is more favorable than average, as compared to a report conducted on the wearable market [153]. The information was sourced from 233 wearable devices. The products covered a wide range of

variety including locations on the wrist, legs, torso, and head. An average battery life of 3 to 4 days is expected to be the norm. Figure 7.2 [153] shows the statistics on the battery life of wearable devices.

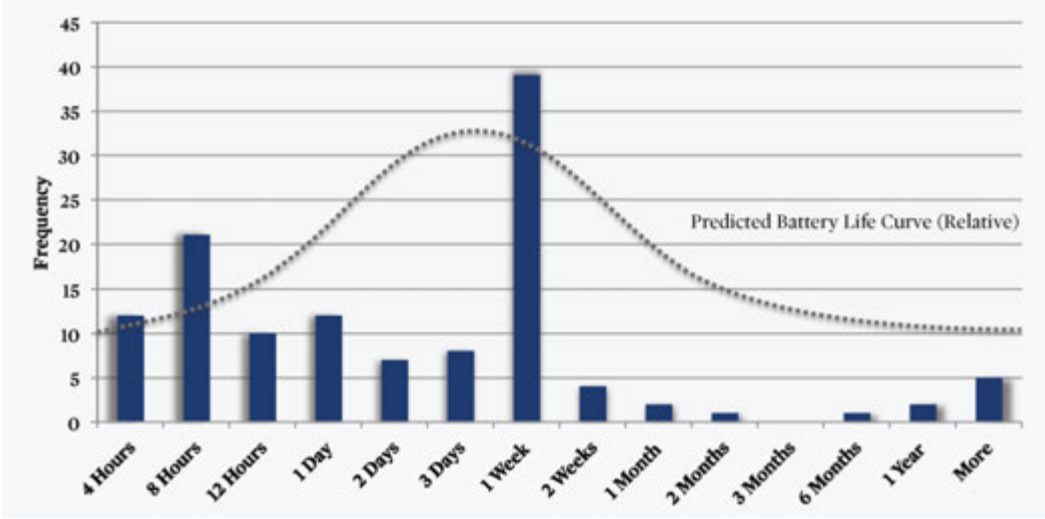


Figure 7.2. Statistics on the battery life of wearable devices as of 2014 Q2.

## 7.6. As a Wearable Interface

Another large challenge in wearable technology is dealing with the human when the computer is fitted in place. This includes the user interface, cognitive model, contextual awareness, and adaptation to tasks.

The user interface model concerns the appropriate set of metaphors for providing mobile access to information. The design development process usually requires a certain amount of time to arrive at a metaphor from the original concept. Extensive

experimentation working with end-user applications is required. With reference to the previous case study, a few screens of the mobile interface are shown in Figure 7.3 [130]. The design approach of the interface is to make the visualization of health data easy to understand. The interfaces put the human movement scenario into a graphical format, thereby allowing a direct association with the situation as perceived by wearers. In addition, the direct metaphoric visualization makes the real-time status easy to understand. The use of graphical icons is usually easy for enabling users to have a quick understanding on the meaning of functions. Figure 7.4 illustrates some of the functions included using icons [130].


Figure 7.3. User interfaces on the mobile device of Fineck.


Figure 7.4. Functional icons of the Fineck.

The cognitive model concerns the input and output capabilities of the human brain. It has been the subject of computer science research for decades. User frustrations result if there are inaccuracies. Given the various portable devices in the market, the convention should be used as the foundation in design. However, there is substantial design space for new, easy-to-use input and output devices, especially for wearable technology, because the form factor varies a lot as compared to the standard, say, mobile phones. One of the major issues in cognitive consideration is when scientific health data meet design and user-friendliness. General users usually do not have the knowledge background to understand the implication of measurements; however, from the point of view of healthcare domain, the measurements may simply be perceived as a common sense. There is usually a knowledge gap. The role of the designer is to take initiative in bringing the general user and professional domain together. For example, regarding the screen in the middle of the figure, wearers might not know the implication of these statistics,

particularly the numerical values. The perception could be more meaningful if there were some points of reference and cases of illustration for possible implications.

When contextual awareness is concerned in designing an application, social and cognitive models are usually taken into account. Regarding wearable technology, one of the concerns is how inputs from multiple sensing sources can be integrated and mapped into user social and cognitive states. Other design concerns include how to anticipate user needs and how to interact with the user. One of the major issues in this study of the cervical spine is that the wearer must be aware of the instantaneous status of the neck position, posture, and movement. An adorable interface and animation could give intuitive feedback of health information to the wearer. Other related features such as enriching with exercise experience and add-ons with motion-sensing games and therapeutic intervention can also increase contextual awareness through interaction design.

Evaluation methodology is another topic of how the design development can be pipelined to take the user testing and feedback into consideration, and highly reflects the adaptation for users. Evaluation on the basis of various fidelity of prototypes is a common practice in evaluating the system for interaction design. Matching the capability with applications is the trade-off between the highest performance capability and the technical capability when the form factor and computing power are concerned. It is common for user feedback to have a high demand on requirement. However, substantial resources and also the actual decrease on the ease of usage should be avoided. This may be caused by the

overloading of information and interfaces for users. The interface and functionality design should focus on the most effective means for information access and resist providing excess capabilities simply because they are available.

# Chapter 8.
# Conclusion

This chapter summarizes the findings related to the aims of this research study that are discussed in Chapter One. One of the major aims of the study is to research the dynamics and statistical measures of the physiological signals on spinal curvature during upright static sitting. The importance of this research is in describing the subtle fluctuations of body movement along the spine. The investigation is essential in demonstrating the strong connection between static postural control and dynamic characteristics. To the extent of research studies found, there are no findings about the fine movement along the spine. In this research, the findings demonstrate the parameters that describe the dynamics of human movement that were captured from the experimental measurements.

The computational study on the dynamics is also about initiating a nonanalytical framework to understand human movement. The study is about the understanding of the complex human movement dynamics that emerged from the captured measurement. A nonanalytical approach is rectified based on computational techniques to extract knowledge from the movement data. The knowledge can be related to the neural and motor control mechanism that thoroughly affects the human perception in the sensation, processing, and activation of movement.

In addition, the knowledge is a practical aspect for the design related to human movement for wearable technology and applications in monitoring movement for healthcare purposes. This is essentially and highly motivated for the future market based on the observed trend. The topic is also of interest for studying because it addresses the importance of academic multidisciplinary studies. This research

effectively forms a foundation that involves the design process of revealing a physiological inspired information-processing model, which is then transformed into design criteria for interactive technology and applications, including wearable sensing devices from the engineering perspective.

The research started from the method and procedure in the collection of experimental human movement on the basis of static upright sitting posture. Subsequently, the data were transformed for analysis. The computational method adopted in this research was based on SDA. The investigation then involved the in-depth analysis of the signals. Results showed that dynamic features existed and could be extracted. These features exhibited under the condition of body sway at the static posture of sitting upright. The research outcomes of the analysis provide a nonanalytical approach of understanding the motor control mechanism that governs the human movement. Investigation and evaluation successfully revealed the dynamic structure on the basis of the noise-like properties.

## 8.1. Conclusion from SDA

The spinal curvatures, measured as angles in degree, were calculated based on various feature points and data intervals between ordered markers. After a series of computational processes for SDA, results on dynamic features were extracted. From the 49 angles calculated, 47 angles were found having a critical time. The research

results were significant in having 96% of angles identified. The outcomes were further ascertained by entering the dummy capture into the computational processes for SDA. None of the data trials from the dummy was found to have a critical time. This provided strong evidence that the dynamic features extracted using SDA were due to human movement instead of noise characteristics from the motion capture system.

Persistency of open- and closed-loop behavior was then identified to describe the control mechanism. The research results show the difference in the diffusion coefficient of the short term ($D_s$) and long term ($D_l$). The research literature shows that in the case of exhibiting control behavior, $D_s$ is larger than $D_l$. The research results showed that all of the data with a critical time followed this evidence of control behavior. There are two outliers on the parameter $D_s$ and one on $D_l$.

In relation to the diffusion coefficient, all the aforementioned data were found to have distinguished values on the Hurst exponent in both the short term ($H_s$) and long term ($H_l$). The $H_s$ were found consistently between 0.675 and 0.868, which denoted the open-loop region exhibiting a persistent and positively correlated control behavior. The values of $H_l$ were found having a mean of 0.231. This showed consistency with the literature findings on closed-loop behavior.

This study had the hypothesis that participants who had different characteristics would exhibit different dynamic features in control. The first experiment was conducted to distinguish the features of spinal control in the cervical region between patients and normal participants. The same SDA was computed. The

research results successfully identified the difference between patients and normal participants by using the variations on dynamic parameters.

The second experiment was conducted to explore the dynamic features of spinal postural control by using SDA for the effects of age and gender in relation to the development of children. The research results successfully identified the difference between 11 and 15 year-old children by using the variations on dynamic parameters.

On the basis of the analysis and experimental results from SDA, this study revealed the existence of a dynamic structure and provided knowledge on the fluctuation of underlying variations in movement performance. This is the first major achievement in this study.

## 8.2. Conclusion from MFDFA

To further explore the fluctuation and variation space, this study adopted MFDFA in the computational process.

The experiment was conducted to study the cervical spine movement on the basis of assessment and six feature points from C2 to C7. The participants were healthy and the participant group was between 19 and 25 years old. The assessment was based on the NPAD instrument, whereas the feature points were captured using the optical motion capture system. The participants were asked to finish the

questionnaire and then to sit upright for 30 seconds during the capture for various trials.

The total NPAD score for each participant was calculated from all the questions answered. The higher the score was, the less favorable the situation was on neck pain and disability. Regarding the score on NPAD, the questions can be categorized into four factors, namely “pain”, “disability”, “neck-specific function”, and “emotion and cognitive influences.”

The analysis started from descriptive statistics on the basis of the NPAD scores; there was a spectrum of variation among the participants. To ascertain the consistency in assessment, the participant list was arranged into sorted order according to various factors. The results demonstrate a consistent sorted order in the participant list.

On the basis of the computation for MFDFA, this research developed careful consideration of signal properties on the basis of the motion data in the context of this study. This process is required to prepare and rectify the data in various stages while conducting the computational analysis.

From the MFDFA results revealing the multifractality structure, some of the multifractal parameters were particularly selected for illustration in this study. These include the mean of the singularity exponent ($h_q$), width of $h_q$ , mean of the singular dimension ($D_q$), and height of $D_q$ .

The research method was followed by ascertaining the existence of the multifractality structure extracted from the physiological signal, instead of a general

property arising from noise signal. A shuffling process on time series was conducted and subjected to test for the multifractality structure. The results demonstrate that all the four multifractal parameters are significantly different. The difference confirms that the multifractality structure arises from the behavior of physiological signals extracted from the cervical spine curvature during the upright sitting condition.

This study then explored variation space. The multifractality structure, that is, the aforementioned parameters, was identified based on the experimental participant set. These parameters are the major findings in this project that describe the variation in the dynamic structure according to the movement performance. These findings were analyzed, compared, and ranked across participants within the experimental set. There was consistency and variation among participants. The consistency suggests the multifractality structure found across participants. The variation is applicable in differentiating various participant characteristics.

On the basis of the consistency of participant ranking, this study revealed the variation space that exists in a consistent manner. After the correlation analysis, there exist groups of properties that are about orthogonal to describe various dimensions. Computational results show that there is a general increasing trend on the strength of correlation when traversing across feature points from M6 to M3, as well as a similarity between the conditions of whether there is low back support. The analysis findings are described in relation to human performance and associated with motor control strategies regarding neural activities. Small and large

local scale fluctuations within the temporal dimension are a major concept developed from this research project in explaining the relationship and the neural control mechanism in spinal movement.

The correlation analysis shows that relationships exist between the NPAD instrument scores and multifractal parameters. First, analysis is conducted on the two separate sets of variables. Given the various factors and parameters, the findings ascertain that they are consistent. The analysis then includes details of the sets of variables. The strength on correlation is relatively stronger with respect to multifractal parameters on the mean and width of the singularity exponent ($h_q$) and NPAD factors on OV and NS. This correlation relationship exists from the perspectives of NPAD scores, multifractal parameters, and feature points in the cervical region.

## 8.3. Conclusion from Design Applications

The aforementioned research findings provide hints on possible neck pain issues on the basis of the noninvasive numerical data captured and computed. From laboratory experimental environment with specific capturing procedures, moving to wearable devices targeting for movement monitoring purposes, there are definitely other technical difficulties need further research efforts in order to overcome. The current research findings can further serve as a foundation for the design and

technical guidelines on how the wearable devices can be developed to capture the issues within the cervical region.

In this study, the implication on the design criteria in relation to wearable devices for health monitoring is explored. Six key features are identified and further illustrated using a recent example, the Fineck. The Fineck is a wearable device on the neck to track the head movement. The device is also able to identify unfavorable habits and suggest various exercises via gaming experience. On the basis of the 12 attributes defined using the fundamental guidelines for designing wearable systems, in-depth design consideration is discussed and the applicability for neck movement monitoring is investigated. Criteria on the motion characteristics for the design on motion-sensing devices are considered through illustrating the analysis results qualitatively by neck movement sensing. Four design challenges from the aspects of the interface and interactive experience in wearable technology are investigated.

In this study, the major and original contribution is the framework developed to investigate the small and large local scale fluctuations within the temporal dimension of physiological signals along the spine. The research findings contribute to the understanding of human movement. This research presents the implication of the technical results on the design on the basis of wearable technology. The implication on design includes the illustration of various interaction design aspects including key features of interactive applications, wearability attributes, and the criteria for sensing and experience in wearable interfaces. This research project develops and consolidates the insights into guidelines on how computational

techniques can be used for the development of a wearable design application, with considerations on both technology and interaction design aspects.

## 8.4. Future Work

Regarding the experimental setup for the analysis, there are several limitations that require future consideration. Because this study is a first attempt as a pilot, the number of participants in the experimental group is relatively small. It diminished the statistical power of the study and its ability to detect correlations. The participants recruited are in general healthy. Regarding the subjective score on the NPAD instrument, although there are some participants who have a higher score on the NPAD instrument, the spectrum of differences between healthy and pathological participants is still relatively narrow. Moreover, the NPAD scores are subjective to the participant's instantaneous feeling and interpretation of the questionnaire. Although the instrument has been validated on the accuracy and reliability, the variety on background profile of the participants and, most importantly, participants may have different perception on the gold standard in giving the answers to the scales.

All in all, a larger sample group of randomized participants with various health and pathological profiles would be the key direction of future work to improve the validity and reliability of the findings.

There are issues in the present argument that the multifractal analysis has limitation subjected to the nature of biomedical time series. The interaction and dominant views of human performance are now constructed by abstract concepts within the black box inside the body to develop the formalism. This black box contains several components such as self-organization, soft ensemble, and meta-stability from an analytic approach on the origin of human behavior. There is the limitation on the multifractal formalism of motor control in providing empirical evidence for these abstract concepts. However, multifractal formalism can provide further suggestion about motor control properties.

Regarding the multifractal formalisms, the second key direction would be to further consolidate and support the concepts in the modeling of motor control by exploration on the association of multifractal parameters with the components in the motor control black box from various aspects, which could help to narrow the knowledge gap.

# Bibliography

[1] Chen, Z., Zhao, Y., Wang, C., Li, M., & Zhu, X. (2011). An adapted Chinese version of neck pain and disability scale: validity and reliability. Spine (Phila Pa 1976), 36(20), E1322-1327.

[2] Wheeler, A. H., Goolkasian, P., Baird, A. C., & Darden, B. V., 2nd. (1999). Development of the Neck Pain and Disability Scale. Item analysis, face, and criterion-related validity. Spine (Phila Pa 1976), 24(13), 1290-1294.

[3] Goolkasian, P., Wheeler, A. H., & Gretz, S. S. (2002). The neck pain and disability scale: test-retest reliability and construct validity. Clin J Pain, 18(4), 245-250.

[4] En, M. C., Clair, D. A., & Edmondston, S. J. (2009). Validity of the Neck Disability Index and Neck Pain and Disability Scale for measuring disability associated with chronic, non-traumatic neck pain. Man Ther, 14(4), 433-438.

[5] Vernon, H., & Mior, S. (1991). The Neck Disability Index: a study of reliability and validity. J Manipulative Physiol Ther, 14(7), 409-415.

[6] Melzack, R. (1987). The short-form McGill Pain Questionnaire. Pain, 30(2), 191-197.

[7] Feise, R. J., & Michael Menke, J. (2001). Functional rating index: a new valid and reliable instrument to measure the magnitude of clinical change in spinal conditions. Spine (Phila Pa 1976), 26(1), 78-86; discussion 87.

[8] Leak, A. M., Cooper, J., Dyer, S., Williams, K. A., Turner-Stokes, L., & Frank, A. O. (1994). The Northwick Park Neck Pain Questionnaire, devised to measure neck pain and disability. Br J Rheumatol, 33(5), 469-474.

[9] Ihlen, E. A. (2012). Introduction to multifractal detrended fluctuation analysis in matlab. Front Physiol, 3, 141.

[10] Important Physiological Signals in the body. (2011). Retrieved March 29, 2015, from http://biomedikal.in/2011/05/important-physiological-signals-in-the-body.

[11] Granata, K. P., & Gottipati, P. (2008). Fatigue influences the dynamic stability of the torso. Ergonomics, 51(8), 1258-1271.

[12] Silfies, S. P., Bhattacharya, A., Biely, S., Smith, S. S., & Giszter, S. (2009). Trunk control during standing reach: A dynamical system analysis of movement strategies in patients with mechanical low back pain. Gait Posture, 29(3), 370-376.

[13] Thomas, J. S., France, C. R., Sha, D., Vander Wiele, N., Moenter, S., & Swank, K. (2007). The effect of chronic low back pain on trunk muscle activations in target reaching movements with various loads. Spine (Phila Pa 1976), 32(26), E801-808.

[14] Van Daele, U., Hagman, F., Truijen, S., Vorlat, P., Van Gheluwe, B., & Vaes, P. (2009). Differences in Balance Strategies Between Nonspecific Chronic Low Back Pain Patients and Healthy Control Subjects During Unstable Sitting. Spine (Phila Pa 1976), 34(11), 1233-1238.

[15] Learman, K. E., Myers, J. B., Lephart, S. M., Sell, T. C., Kerns, G. J., & Cook, C. E. (2009). Effects of spinal manipulation on trunk proprioception in subjects with

chronic low back pain during symptom remission. J Manipulative Physiol Ther, 32(2), 118-126.

[16] Chow, D. H., Leung, K. T., & Holmes, A. D. (2007). Changes in spinal curvature and proprioception of schoolboys carrying different weights of backpack. Ergonomics, 50(12), 2148-2156.

[17] Chow, D. H., Ou, Z. Y., Wang, X. G., & Lai, A. (2010). Short-term effects of backpack load placement on spine deformation and repositioning error in schoolchildren. Ergonomics, 53(1), 56-64.

[18] Hodges, P. W., & Richardson, C. A. (1996). Inefficient muscular stabilization of the lumbar spine associated with low back pain. A motor control evaluation of transversus abdominis. Spine (Phila Pa 1976), 21(22), 2640-2650.

[19] Hodges, P. W. (2001). Changes in motor planning of feedforward postural responses of the trunk muscles in low back pain. Exp Brain Res, 141(2), 261-266.

[20] Silfies, S. P., Squillante, D., Maurer, P., Westcott, S., & Karduna, A. R. (2005). Trunk muscle recruitment patterns in specific chronic low back pain populations. Clin Biomech (Bristol, Avon), 20(5), 465-473.

[21] Silfies, S. P., Mehta, R., Smith, S. S., & Karduna, A. R. (2009). Differences in feedforward trunk muscle activity in subgroups of patients with mechanical low back pain. Arch Phys Med Rehabil, 90(7), 1159-1169.

[22] Anders, C., Wenzel, B., & Scholle, H. C. (2008). Activation characteristics of trunk muscles during cyclic upper-body perturbations caused by an oscillating pole. Arch Phys Med Rehabil, 89(7), 1314-1322.

[23] Cholewicki, J., Panjabi, M. M., & Khachatryan, A. (1997). Stabilizing function of trunk flexor-extensor muscles around a neutral spine posture. Spine (Phila Pa 1976), 22(19), 2207-2212.

[24] Cholewicki, J., Juluru, K., Radebold, A., Panjabi, M. M., & McGill, S. M. (1999). Lumbar spine stability can be augmented with an abdominal belt and/or increased intra-abdominal pressure. European Spine Journal, 8(5), 388-395.

[25] Granata, K. P., & Marras, W. S. (2000). Cost-benefit of muscle cocontraction in protecting against spinal instability. Spine (Phila Pa 1976), 25(11), 1398-1404.

[26] Fitzpatrick, R., Burke, D., & Gandevia, S. C. (1996). Loop gain of reflexes controlling human standing measured with the use of postural and vestibular disturbances. J Neurophysiol, 76(6), 3994-4008.

[27] Morasso, P. G., Baratto, L., Capra, R., & Spada, G. (1999). Internal models in the control of posture. Neural Netw, 12(7-8), 1173-1180.

[28] van der Kooij, H., Jacobs, R., Koopman, B., & Grootenboer, H. (1999). A multisensory integration model of human stance control. Biol Cybern, 80(5), 299-308.

[29] Collins, J. J., & De Luca, C. J. (1993). Open-loop and closed-loop control of posture: a random-walk analysis of center-of-pressure trajectories. Exp Brain Res, 95(2), 308-318.

[30] Chow, C. C., & Collins, J. J. (1995). Pinned polymer model of posture control. Phys Rev E Stat Phys Plasmas Fluids Relat Interdiscip Topics, 52(1), 907-912.

[31] Schultz, S. K. (2001). Principles of neural science, 4th edition. American Journal of Psychiatry, 158(4), 662-662.

[32] Granata, K. P., & England, S. A. (2006). Stability of dynamic trunk movement. Spine (Phila Pa 1976), 31(10), E271-276.

[33] Radebold, A., Cholewicki, J., Polzhofer, G. K., & Greene, H. S. (2001). Impaired postural control of the lumbar spine is associated with delayed muscle response times in patients with chronic idiopathic low back pain. Spine (Phila Pa 1976), 26(7), 724-730.

[34] Prieto, T. E., Myklebust, J. B., Hoffmann, R. G., Lovett, E. G., & Myklebust, B. M. (1996). Measures of postural steadiness: differences between healthy young and elderly adults. IEEE Trans Biomed Eng, 43(9), 956-966.

[35] England, S. A., & Granata, K. P. (2007). The influence of gait speed on local dynamic stability of walking. Gait Posture, 25(2), 172-178.

[36] Li, L., Haddad, J. M., & Hamill, J. (2005). Stability and variability may respond differently to changes in walking speed. Human Movement Science, 24(2), 257-267.

[37] Mandelbrot, B. B. (1983). The fractal geometry of nature. New York: W.H. Freeman.

[38] Bunde, A., Havlin, S., Kantelhardt, J. W., Penzel, T., Peter, J. H., & Voigt, K. (2000). Correlated and uncorrelated regions in heart-rate fluctuations during sleep. Physical Review Letters, 85(17), 3736-3739.

[39] Hausdorff, J. M., Purdon, P. L., Peng, C. K., Ladin, Z., Wei, J. Y., & Goldberger, A. L. (1996). Fractal dynamics of human gait: Stability of long-range correlations in stride interval fluctuations. Journal of Applied Physiology, 80(5), 1448-1457.

[40] Blesic, S., Milosevic, S., Stratimirovic, D., & Ljubisavljevic, M. (1999). Detrended fluctuation analysis of time series of a firing fusimotor neuron. Physica A, 268(3-4), 275-282.

[41] Ossadnik, S. M., Buldyrev, S. V., Goldberger, A. L., Havlin, S., Mantegna, R. N., Peng, C. K., Simons, M., Stanley, H. E. (1994). Correlation Approach to Identify Coding Regions in DNA-Sequences. Biophysical Journal, 67(1), 64-70.

[42] Liu, Y. H., Gopikrishnan, P., Cizeau, P., Meyer, M., Peng, C. K., & Stanley, H. E. (1999). Statistical properties of the volatility of price fluctuations. Physical Review E, 60(2), 1390-1400.

[43] Ashkenazy, Y., Baker, D. R., Gildor, H., & Havlin, S. (2003). Nonlinearity and multifractality of climate change in the past 420,000 years. Geophysical Research Letters, 30(22).

[44] Chen, Z., Ivanov, P. C., Hu, K., & Stanley, H. E. (2002). Effect of nonstationarities on detrended fluctuation analysis. Physical Review E, 65(4).

[45] Kantelhardt, J. W., Zschiegner, S. A., Koscielny-Bunde, E., Havlin, S., Bunde, A., & Stanley, H. E. (2002). Multifractal detrended fluctuation analysis of nonstationary time series. Physica a-Statistical Mechanics and Its Applications, 316(1-4), 87-114.

[46] Telesca, L., Lapenna, V., & Macchiato, M. (2005). Multifractal fluctuations in earthquake-related geoelectrical signals. New Journal of Physics, 7.

[47] Yuan, Y., Zhuang, X. T., & Jin, X. (2009). Measuring multifractality of stock price fluctuation using multifractal detrended fluctuation analysis. Physica a-Statistical Mechanics and Its Applications, 388(11), 2189-2197.

[48] Shang, P. J., Lu, Y. B., & Kamae, S. (2008). Detecting long-range correlations of traffic time series with multifractal detrended fluctuation analysis. Chaos Solitons & Fractals, 36(1), 82-90.

[49] Delignieres, D., Deschamps, T., Legros, A., & Caillou, N. (2003). A methodological note on nonlinear time series analysis: is the open- and closed-loop model of Collins and De Luca (1993) a statistical artifact? J Mot Behav, 35(1), 86-97.

[50] Rosenstein, M. T., Collins, J. J., & De Luca, C. J. (1993). A Practical Method for Calculating Largest Lyapunov Exponents from Small Data Sets. Physica D-Nonlinear Phenomena, 65(1-2), 117-134.

[51] Platisa, M. M., & Gal, V. (2008). Correlation properties of heartbeat dynamics. Eur Biophys J, 37(7), 1247-1252.

[52] Dingwell, J. B., & Cusumano, J. P. (2010). Re-interpreting detrended fluctuation analyses of stride-to-stride variability in human walking. Gait Posture, 32(3), 348-353.

[53] Mandelbrot, B. B., & Van Ness, J. W. (1968). Fractional Brownian motions, fractional noises and applications. SIAM Review, 10, 422-37.

[54] Rougier, P. (1999). Automatic determination of the transition between successive control mechanisms in upright stance assessed by modelling of tee centre of pressure. Archives of Physiology and Biochemistry, 107(1), 35-42.

[55] Treffner, P. J., Kelso, J. A. S. (1995). Functional stabilization on unstable fixed-point. In B.J. Bardy, R.J. Bootsma & Y. Guiard (Eds.), Studies in perception and action III (pp. 83-86). Hillsdale, NY: Erlbaum.

[56] Riley, M. A., Wong, S., Mitra, S., & Turvey, M. T. (1997). Common effects of touch and vision on postural parameters. Exp Brain Res, 117(1), 165-170.

[57] Rougier, P., Burdet, C., Farenc, I., & Berger, L. (2001). Backward and forward leaning postures modelled by an fBm framework. Neuroscience Research, 41(1), 41-50.

[58] Dutta, S., Ghosh, D., & Chatterjee, S. (2013). Multifractal detrended fluctuation analysis of human gait diseases. Front Physiol, 4, 274.

[59] Algina, J., & Keselman, H. J. (1999). Comparing squared multiple correlation coefficients. Examination of a confidence interval and a test of significance. Psychological Methods, 4(1), 76-83.

[60] Cohen, J. (1988). Statistical power analysis for the behavioral sciences. Hillsdale, N.J.: L. Erlbaum Associates.

[61] Wikipedia. (2015). Cervical vertebra. Retrieved March 29, 2015, from http://en.wikipedia.org/wiki/Cervical_vertebrae.

[62] Binder, A. (2007). The diagnosis and treatment of nonspecific neck pain and whiplash. Eura Medicophys, 43(1), 79-89.

[63] Guez, M., Hildingsson, C., Nilsson, M., & Toolanen, G. (2002). The prevalence of neck pain: a population-based study from northern Sweden. Acta Orthop Scand, 73(4), 455-459.

[64] Côté, P., Cassidy, J. D., & Carroll, L. (2003). The epidemiology of neck pain: what we have learned from our population-based studies. J Can Chiropr Assoc., 47(4), 284–290.

[65] Jull, G., Falla, D., Treleaven, J., Hodges, P., & Vicenzino, B. (2007). Retraining cervical joint position sense: the effect of two exercise regimes. J Orthop Res, 25(3), 404-412.

[66] Jull, G. A., Falla, D., Vicenzino, B., & Hodges, P. W. (2009). The effect of therapeutic exercise on activation of the deep cervical flexor muscles in people with chronic neck pain. Manual Therapy, 14(6), 696-701.

[67] Schafer, R. C. (1987). Clinical biomechanics: musculoskeletal actions and reactions. Baltimore: Williams & Wilkins.

[68] Palatinus, Z., Kelty-Stephen, D. G., Kinsella-Shaw, J., Carello, C., & Turvey, M. T. (2014). Haptic perceptual intent in quiet standing affects multifractal scaling of postural fluctuations. J Exp Psychol Hum Percept Perform, 40(5), 1808-1818.

[69] Morales, C. J., & Kolaczyk, E. D. (2002). Wavelet-based multifractal analysis of human balance. Ann Biomed Eng, 30(4), 588-597.

[70] Thurner, S., Mittermaier, C., Hanel, R., & Ehrenberger, K. (2000). Scaling-violation phenomena and fractality in the human posture control systems. Phys Rev E Stat Phys Plasmas Fluids Relat Interdiscip Topics, 62(3 Pt B), 4018-4024.

[71] Stephen, D. G., Arzamarski, R., & Michaels, C. F. (2010). The role of fractality in perceptual learning: exploration in dynamic touch. J Exp Psychol Hum Percept Perform, 36(5), 1161-1173.

[72] Stephen, D. G., & Hajnal, A. (2011). Transfer of calibration between hand and foot: functional equivalence and fractal fluctuations. Atten Percept Psychophys, 73(5), 1302-1328.

[73] Ihlen, E. A., & Vereijken, B. (2013). Multifractal formalisms of human behaviour. Hum Mov Sci, 32(4), 633-651.

[74] Ihlen, E. A., & Vereijken, B. (2013). Identifying multiplicative interactions between temporal scales of human movement variability. Ann Biomed Eng, 41(8), 1635-1645.

[75] Hausdorff, J. M., Lertratanakul, A., Cudkowicz, M. E., Peterson, A. L., Kaliton, D., & Goldberger, A. L. (2000). Dynamic markers of altered gait rhythm in amyotrophic lateral sclerosis. Journal of Applied Physiology, 88(6), 2045-2053.

[76] Hausdorff, J. M., Mitchell, S. L., Firtion, R., Peng, C. K., Cudkowicz, M. E., Wei, J. Y., & Goldberger, A. L. (1997). Altered fractal dynamics of gait: Reduced stride-interval correlations with aging and Huntington's disease. Journal of Applied Physiology, 82(1), 262-269.

[77] Goldberger, A. L., Amaral, L. A. N., Hausdorff, J. M., Ivanov, P. C., Peng, C. K., & Stanley, H. E. (2002). Fractal dynamics in physiology: Alterations with disease and aging. Proceedings of the National Academy of Sciences of the United States of America, 99, 2466-2472.

[78] Scafetta, N., Moon, R. E., & West, B. J. (2007). Fractal response of physiological signals to stress conditions, environmental changes, and neurodegenerative diseases. Complexity, 12(5), 12-17.

[79] Mosa, A. M., Yoo, I., & Sheets, L. (2012). A Systematic Review of Healthcare Applications for Smartphones. Bmc Medical Informatics and Decision Making, 12, 1-31.

[80] Rueterbories, J., Spaich, E. G., Larsen, B., & Andersen, O. K. (2010). Methods for gait event detection and analysis in ambulatory systems. Medical Engineering & Physics, 32(6), 545-552.

[81] Miller, N., Jenkins, O. C., Kallmann, M., & Mataric, M. J. (2004). Motion capture from inertial sensing for untethered humanoid teleoperation. 2004 4th IEEE/RAS International Conference on Humanoid Robots, Vols 1 and 2, Proceedings, 547-565.

[82] Krishna, S., Boren, S. A., & Balas, E. A. (2009). Healthcare via Cell Phones: A Systematic Review. Telemedicine Journal and E-Health, 15(3), 231-240.

[83] Hopkins, W. G. (2000). Measures of reliability in sports medicine and science. Sports Medicine, 30(1), 1-15.

[84] Hermann, K. M., & Reese, C. S. (2001). Relationships among selected measures of impairment, functional limitation, and disability in patients with cervical spine disorders - Author response. Physical Therapy, 81(3), 914-914.

[85] Strimpakos, N., Sakellari, V., Gioftsos, G., & Oldham, J. (2004). Intratester and intertester reliability of neck isometric dynamometry. Archives of Physical Medicine and Rehabilitation, 85(8), 1309-1316.

[86] Strimpakos, N., Georgios, G., Eleni, K., Vasilios, K., & Jacqueline, O. (2005). Issues in relation to the repeatability of and correlation between EMG and Borg

scale assessments of neck muscle fatigue. Journal of Electromyography and Kinesiology, 15(5), 452-465.

[87] Strimpakos, N., Sakellari, V., Gioftsos, G., Kapreli, E., & Oldham, J. (2006). Cervical joint position sense: an intra- and inter-examiner reliability study. Gait & Posture, 23(1), 22-31.

[88] Nordin, M., Carragee, E. J., Hogg-Johnson, S., Weiner, S. S., Hurwitz, E. L., Peloso, P. M., . . . Haldeman, S. (2008). Assessment of neck pain and its associated disorders - Results of the bone and joint decade 2000-2010 task force on neck pain and its associated disorders. Spine, 33(4), S101-S122.

[89] American Medical Association (AMA). (2004). Guidelines to the evaluation of permanent impairment. 4th ed. Chicago, IL: American Medical Association.

[90] Audette, I., Dumas, J. P., Cote, J. N., & De Serres, S. J. (2010). Validity and Between-Day Reliability of the Cervical Range of Motion (CROM) Device. Journal of Orthopaedic & Sports Physical Therapy, 40(5), 318-323.

[91] Dvir, Z., & Prushansky, T. (2000). Reproducibility and instrument validity of a new ultrasonography-based system for measuring cervical spine kinematics. Clinical Biomechanics, 15(9), 658-664.

[92] Jasiewicz, J. M., Treleaven, J., Condie, P., & Jull, G. (2007). Wireless orientation sensors: Their suitability to measure head movement for neck pain assessment. Manual Therapy, 12(4), 380-385.

[93] Feipel, V., Rondelet, B., Le Pallec, J. P., & Rooze, M. (1999). Normal global motion of the cervical spine: an electrogoniometric study. Clinical Biomechanics, 14(7), 462-470.

[94] Castro, W. H. M., Sautmann, A., Schilgen, M., & Sautmann, M. (2000). Noninvasive three-dimensional analysis of cervical spine motion in normal subjects in relation to age and sex - An experimental examination. Spine, 25(4), 443-449.

[95] Syed, F. I., Oza, A. L., Vanderby, R., Heiderscheit, B., & Anderson, P. A. (2007). A method to measure cervical spine motion over extended periods of time. Spine, 32(19), 2092-2098.

[96] Hagberg, M., & Sundelin, G. (1986). Discomfort and Load on the Upper Trapezius Muscle When Operating a Wordprocessor. Ergonomics, 29(12), 1637-1645.

[97] Borenstein, D. G., Wiesel, S. W., Boden, S. D., & Borenstein, D. G. (2004). Low back and neck pain: comprehensive diagnosis and management. Philadelphia, Pa.: Saunders.

[98] Werne, S. (1957). Studies in spontaneous atlas dislocation. Acta Orthop Scand Suppl, 23, 1-150.

[99] Pomeranz, M. M. (1947). Movement of the normal cervical spine. Bull Hosp Joint Dis, 8(2), 215.

[100] White, A. A., 3rd, Johnson, R. M., Panjabi, M. M., & Southwick, W. O. (1975). Biomechanical analysis of clinical stability in the cervical spine. Clin Orthop Relat Res(109), 85-96.

[101] White, A. A., Panjabi, M. M. (1978). Clinical Biomechanics of the Spine. Philadelphia, JB Lippincott.

[102] White, A. A., 3rd, & Panjabi, M. M. (1978). The basic kinematics of the human spine. A review of past and current knowledge. Spine (Phila Pa 1976), 3(1), 12-20.

[103] Merskey, H., Bogduk, N., & International Association for the Study of Pain. Task Force on Taxonomy. (1994). Classification of chronic pain: descriptions of chronic pain syndromes and definitions of pain terms. Seattle: IASP Press.

[104] Bogduk, N., & McGuirk, B. (2006). Management of acute and chronic neck pain: an evidence-based approach. Pain research and clinical management. Edinburgh ; New York: Elsevier.

[105] Bogduk, N. (1999). Medical Management of Acute Cervical Radicular Pain: an Evidence-based Approach. Newcastle, Newcastle Bone and Joint Institute.

[106] Bogduk, N. (2003). Neck and arm pain. In M.J. Aminoff & R.B. Daroff (Eds), Encyclopedia of the Neurological Sciences, Volume 3 (pp. 390-398). Amsterdam, Academic Press.

[107] Bogduk, N. (2002). Cervical pain. In A.K. Ashbury, G.M. McKhann, W.I. McDonald, P.J. Goadsby & J.C. MacArthur (Eds), Disease of the Nervous System (pp. 742-759). Cambridge, Cambridge University Press.

[108] Grubb, S. A., & Kelly, C. K. (2000). Cervical discography: Clinical implications from 12 years of experience. Spine, 25(11), 1382-1389.

[109] Dwyer, A., Aprill, C., & Bogduk, N. (1990). Cervical Zygapophyseal Joint Pain Patterns .1. A Study in Normal Volunteers. Spine, 15(6), 453-457.

[110] Dreyfuss, P., Michaelsen, M., & Fletcher, D. (1994). Atlantooccipital and Lateral Atlantoaxial Joint Pain Patterns. Spine, 19(10), 1125-1131.

[111] Kellgren, J. H. (1939). On the distribution of pain arising from deep somatic structures with charts of segmental pain areas. Clin Sci, 4: 35-46.

[112] Fukui, S., Ohseto, K., Shiotani, M., Ohno, K., Karasawa, H., Naganuma, Y., & Yuda, Y. (1996). Referred pain distribution of the cervical zygapophyseal joints and cervical dorsal rami. Pain, 68(1), 79-83.

[113] Schellhas, K. P., Smith, M. D., Gundry, C. R., & Pollei, S. R. (1996). Cervical discogenic pain - Prospective correlation of magnetic resonance imaging and discography in asymptomatic subjects and pain sufferers. Spine, 21(3), 300-311.

[114] Porterfield, J. A., & DeRosa, C. (1995). Mechanical Neck Pain: Perspectives in Functional Anatomy. PA, W.B. Saunders.

[115] Gower, W. E., & Pedrim, V. (1969). Age related variation in protein polysaccharides from human nucleus pulposus, annulus fibrosus, and costal cartilage. J Bone Joint Surg [Am], 51A: 1154-1162.

[116] Hirsch, C., Paulson, S., Sylven, B. & Snellman, O. (1953). Biophysical and physiological investigation on cartilage and other mesenchymal tissues; characteristics of human nuclei pulposi during aging. Acta Orthop Scand, 22: 175-183.

[117] Hattori, S., Oda, H., & Kawai, S. (1981). Cervical Intra-Discal Pressure in Movements and Traction of the Cervical-Spine. Zeitschrift Fur Orthopadie Und Ihre Grenzgebiete, 119(6), 568-569.

[118] Hu, J., Gao, J. B., & Wang, X. S. (2009). Multifractal analysis of sunspot time series: the effects of the 11-year cycle and Fourier truncation. Journal of Statistical Mechanics-Theory and Experiment, P02066.

[119] Gao, J. B., Sultan, H., Hu, J., & Tung, W. W. (2010). Denoising Nonlinear Time Series by Adaptive Filtering and Wavelet Shrinkage: A Comparison. IEEE Signal Processing Letters, 17(3), 237-240.

[120] Riley, M. A., Bonnette, S., Kuznetsov, N., Wallot, S., & Gao, J. (2012). A tutorial introduction to adaptive fractal analysis. Front Physiol, 3, 371.

[121] Eke, A., Herman, P., Bassingthwaighte, J. B., Raymond, G. M., Percival, D. B., Cannon, M., . . . Ikrenyi, C. (2000). Physiological time series: distinguishing fractal noises from motions. Pflugers Archiv-European Journal of Physiology, 439(4), 403-415.

[122] Stein, P. K., & Kleiger, R. E. (1999). Insights from the study of heart rate variability. Annual Review of Medicine, 50, 249-261.

[123] Goldberger, A. L. (1996). Non-linear dynamics for clinicians: Chaos theory, fractals, and complexity at the bedside. Lancet, 347(9011), 1312-1314.

[124] Kello, C. T., Beltz, B. C., Holden, J. G., & Van Orden, G. C. (2007). The emergent coordination of cognitive function. Journal of Experimental Psychology-General, 136(4), 551-568.

[125] Wang, G., Huang, H., Xie, H. B., Wang, Z. Z., & Hu, X. (2007). Multifractal analysis of ventricular fibrillation and ventricular tachycardia. Medical Engineering & Physics, 29(3), 375-379.

[126] Zheng, Y., Gao, J., Sanchez, J. C., Principe, J. C., & Okun, M. S. (2005). Multiplicative multifractal modeling and discrimination of human neuronal activity. Physics Letters A, 344(2-4), 253-264.

[127] Gemperle, F., Kasabach, C., Stivoric, J., Bauer, M., & Martin, R. (1998). Design for wearability. Second International Symposium on Wearable Computers - Digest of Papers, 116-122.

[128] Siewiorek, D. P. (2002). New frontiers of application design. Communications of the ACM, 45(12), 79-82.

[129] PricewaterhouseCoopers LLP. (2014). Health wearables: Early days. Retrieved March 29, 2015, from http:// www.pwc.com/us/healthcare-new-entrants.

[130] Veari. (2014). Fineck. Retrieved March 29, 2015, from http://www.fineck.com.

[131] Shea, C. H., Shebilske, W., & Worchel, S. (1993). Motor learning and control. Englewood Cliffs, N.J.: Prentice Hall.

[132] Schmidt, R. A., & Wrisberg, C. A. (2008). Motor learning and performance: a situation-based learning approach. Champaign, IL: Human Kinetics.

[133] Military Disability Made Easy. (2013). The spine. Retrieved March 29, 2015, from http://www.militarydisabilitymadeeasy.com/thespine.html.

[134] Johansson, R., Magnusson, M., & Akesson, M. (1988). Identification of Human Postural Dynamics. IEEE Transactions on Biomedical Engineering, 35(10), 858-869.

[135] Loram, I. D., Maganaris, C. N., & Lakie, M. (2005). Human postural sway results from frequent, ballistic bias impulses by soleus and gastrocnemius. Journal of Physiology-London, 564(1), 295-311.

[136] Kiemel, T., Oie, K. S., & Jeka, J. J. (2002). Multisensory fusion and the stochastic structure of postural sway. Biological Cybernetics, 87(4), 262-277.

[137] Park, S., Horak, F. B., & Kuo, A. D. (2004). Postural feedback responses scale with biomechanical constraints in human standing. Experimental Brain Research, 154(4), 417-427.

[138] Collins, J. J., & De Luca, C. J. (1995). Upright, Correlated Random-Walks - a Statistical-Biomechanics Approach to the Human Postural Control-System. Chaos, 5(1), 57-63.

[139] Hines, T. (2013). Anatomy of the spine. Retrieved March 29, 2015, from http://www.mayfieldclinic.com/PE-AnatSpine.htm.

[140] Panjabi, M. M. (1992). The Stabilizing System of the Spine .2. Neutral Zone and Instability Hypothesis. Journal of Spinal Disorders, 5(4), 390-397.

[141] Panjabi, M. M. (1992). The Stabilizing System of the Spine .1. Function, Dysfunction, Adaptation, and Enhancement. Journal of Spinal Disorders, 5(4), 383-389.

[142] Moore, D. E., Feurer, I. D., Holzman, M. D., Wudel, L., Strickland, C., Gorden, D. L., . . . Pinson, C. W. (2004). Long-term detrimental effect of bile duct injury on health-related quality of life. Archives of Surgery, 139(5), 476-481.

[143] Jackson, R. P., & Mcmanus, A. C. (1994). Radiographic Analysis of Sagittal Plane Alignment and Balance in Standing Volunteers and Patients with Low-Back-Pain Matched for Age, Sex, and Size - a Prospective Controlled Clinical-Study. Spine, 19(14), 1611-1618.

[144] Frymoyer, J. W., & Selby, D. K. (1985). Segmental Instability - Rationale for Treatment. Spine, 10(3), 280-286.

[145] Pope, M. H., & Panjabi, M. (1985). Biomechanical definitions of spinal instability. Spine (Phila Pa 1976), 10(3), 255-256.

[146] Ivanov, P. C., Amaral, L. A. N., Goldberger, A. L., Havlin, S., Rosenblum, M. G., Struzik, Z. R., & Stanley, H. E. (1999). Multifractality in human heartbeat dynamics. Nature, 399(6735), 461-465.

[147] Oswiecimka, P., Kwapien, J., & Drozdz, S. (2006). Wavelet versus detrended fluctuation analysis of multifractal structures. Physical Review E, 74(1).

[148] Blackburn, J. T., Riemann, B. L., Myers, J. B., & Lephart, S. M. (2003). Kinematic analysis of the hip and trunk during bilateral stance on firm, foam, and multiaxial support surfaces. Clinical Biomechanics, 18(7), 655-661.

[149] van Emmerik, R. E. A., & van Wegen, E. E. H. (2002). On the functional aspects of variability in postural control. Exercise and Sport Sciences Reviews, 30(4), 177-183.

[150] Glass, L., & Mackey, M. C. (1988). From clocks to chaos: The rhythms of life. Princeton, NJ: Princeton University Press.

[151] Schoner, G., Haken, H., & Kelso, J. A. (1986). A stochastic theory of phase transitions in human hand movement. Biol Cybern, 53(4), 247-257.

[152] Kelso, J. A. S. (1995). Dynamic patterns: the self-organization of brain and behaviour. Cambridge, Mass.: MIT Press.

[153] Vandrico Inc. (2014). Wearables market insights. Retrieved from http://vandrico.com/subscribe/report.

[154] Peters, E. E. (1994). Fractal market analysis: applying chaos theory to investment and economics. Wiley finance editions. New York: J. Wiley & Sons.

[155] Nickolaenko, A. P., Price, C., & Iudin, D. D. (2000). Hurst exponent derived for natural terrestrial radio noise in Schumann resonance band. Geophysical Research Letters, 27(19), 3185-3188.

[156] Hoop, B., Kazemi, H., & Liebovitch, L. (1993). Rescaled range analysis of resting respiration. Chaos, 3(1), 27-29.

[157] Yamada, N. (1995). Nature of Variability in Rhythmical Movement. Human Movement Science, 14(3), 371-384.

[158] DiGiovine, C. P., Cooper, R. A., DiGiovine, M. M., Boninger, M. L., & Robertson, R. N. (1998). Digital filtering of kinematics of racing wheelchair propulsion. Proceedings of the 20th Annual International Conference of the IEEE Engineering in Medicine and Biology Society, Vol 20, Pts 1-6, 20, 2714-2716.

[159] Shiel, W. C. (2015). Neck pain. MedicineNet. Retrieved March 29, 2015, from http://www.medicinenet.com/neck_pain/article.htm.

[160] Hong Kong Spine Centre. (2012). Neck Pain. Retrieved March 29, 2015, from http://www.spinecentre.com.hk/thumbnail-list-layout-en/neck-pain.

[161] International Association for the Study of Pain. (1973). Retrieved March 29, 2015, from http://www.iasp-pain.org.